Attenuation of botulinum toxin mediated blockade of exocytosis at neuromuscular junctions by viral vector mediated gene transfer into spinal motor neurons

by

Arvind Raghunath

International Centre for Neurotherapeutics,

Dublin City University,

Dublin – 9,

Ireland.

December, 2008

A dissertation submitted under the supervision of Prof. Oliver Dolly to fulfil the requirements for award of the degree of Ph.D. from Dublin City University.

Declaration

I hereby certify that this material, which I now submit for assessment on the programme of study leading to the award of **Ph.D** is entirely my own work, that I have exercised reasonable care to ensure that the work is original, and does not to the best of my knowledge breach any law of copyright, and has not been taken from the work of others save and to the extent that such work has been cited and acknowledged within the text of my work.

Signed: _____

(Candidate) ID No.: 53155173

Date: 18th December 2008

Abstract

Botulinum neurotoxin type A (BoNT/A) is implicated in a majority of human cases of botulism and causes long-lasting neuromuscular paralysis due to the persistence in nerve endings of its light chain protease that cleaves synaptosomal-associated protein of 25 kDa (S25). This highly debilitating and, often fatal, neuroparalytic condition cannot be adequately treated by traditional pharmacological methods due to difficulties in efficiently accessing either the pre-synaptic terminals or the cell body of the supplying spinal motor neurons and because of the lack of efficient drugs that can block or reverse the paralysis.

A viral vector mediated gene delivery technique was therefore utilised to confer protection against toxin-induced blockade of exocytosis by the expression of cleavage-resistant S25 (S25-R198T) in susceptible cells. Recombinant adeno-associated viral (AAV) vectors expressing a His_6-tagged S25-R198T (AAV-S25-R198T) were initially used to obtain proof-of-principle of this approach in chromaffin cell cultures, neuroendocrine cells that mimic the exocytotic pathway found in neurons. Stereotaxic injection of AAV-S25-R198T into anterior horns of rat spinal cords resulted in substantial protection against a subsequent challenge by BoNT/A injected into the soleus muscle. Interestingly, intra-muscular injection of this virus also resulted in protection against neuroparalytic action of a subsequently injected toxin.

In order to obtain more efficient neuronally-targeted, peripherally-deliverable viral vectors – which would also confer great utility in the treatment

of genetic diseases affecting the spinal cord – the more versatile lentiviral vectors (LV) were used. Biotinylated LVs were attached to targeting agents, different core-streptavidin (CS) tagged protease-inactive BoNT/E (BoTIM) mutants, and applied to cerebellar granule neuron cultures. These targeting molecules substantially reduced the viral infection of non-neuronal cultures with only minimal effects on the transfection of neurons.

The results obtained in this study demonstrate the applicability of gene therapy to ameliorate the neuroparalytic effects of botulism. In addition, the novel tools and techniques developed, especially in the targeted, peripheral, delivery of viral vectors, could also be adapted to treat genetic disorders of motor neurons.

Acknoledgements

It is my pleasure to thank the many people who made this thesis possible.

First of all, I would like to thank my supervisor, Prof. J. O. Dolly. Without his advice, enthusiasm and encouragement this dissertation would not have reached fruition. I particularly value the detailed scientific discussions we had over the course of this project and, especially, during the grant and paper writing process. The two most important attributes that I hope to have gained from my stay here are his atitudes on positive thinking and of always moving forward (be it in science or rugby!).

I would like to sincerely thank all current, and past, members of ICNT for their help and assistance, especially Francesc, Gary, Valerie, Macdara, Maxim and Roman. Without their advice and support this study would have have never have been feasible. I would like to acknowledge and thank the endless support extended by Rita, Carolyn and Frank throughout my stay here.

I would also like to express my gratitude to USAMRIID and DTRA for providing me with a research assistantship during my PhD.

Finally, I would like to thank my family back home in India for all their love and understanding. Without them I would not have been here and certainly would not have the means or courage to undertake this adventure in science!

Table of contents

Abbreviations used

A-488/546/568	alexa-fluor 488/546/568 nm
AA	amino acid
ANS	autonomic nervous system
ACh	acetylcholine
AAV	adeno-associated virus
BoNT	botulinum neurotoxin
BoTIM	BoNT protease inactive mutant
BSA	bovine serum albumin
α-BuTx	alpha bungarotoxin
CMV	cytomegalovirus
CNS	central nervous system
CNT	clostridial neuro-toxins
CS	core-streptavidin
ChAT	choline acetyltransferase
dNTP	deoxynucleotide triphosphate
DAS	digit abduction score
DC	di-chain
DβH	dopamine β-hydroxylase
DMEM	Dulbecco's modified Eagle's medium
DNA	deoxyribonucleic acid
EF-1α	elongation factor 1α
ECL	enhanced chemiluminescence
EDTA	ethylenediamine tetra-acetic acid
ENT	efficiency of neuromuscular transmission
EP	end-plate
FCS	foetal calf serum
GFP	green fluorescent protein
HEK-293	human embryonic kidney cell line
hrGFP	humanised *Renilla* green fluorescent protein
His$_6$	six-histidine tagged
HBS	hepes-buffered saline

HBSS	Hank's buffered saline solution
HC	heavy chain
HRP	horseradish peroxidase
HIV	human immunodeficiency virus
IRES	internal ribosome entry site
IMAC	immobilised metal affinity chromatography
ITR	inverted terminal repeats
kDa	kilo Dalton
LC	light chain
LDCV	large dense core vesicle
LISM	low ionic strength medium
LV	Lentivirus
LTR	long terminal repeats
MOI	multiplicity of infection
NMJ	neuromuscular Junction
NS	normal saline
NSF	N-ethylmaleimide sensitive factor
PAGE	poly-acrylamide gel electrophoresis
PBS	phosphate buffered saline
PCR	polymerase chain reaction
PNS	peripheral nervous system
RIMs	Rab3-interacting molecules
RNA	ribonucleic acid
SC	single chain
VAMP	synaptobrevin
SDS	sodium dodecyl sulphate
S25	synaptosomal-associated protein of 25 kDa
$S25_A$	BoNT/A-truncated SNAP-25
$S25_E$	BoNT/E-truncated SNAP-25
SNAP	soluble N-ethylmaleimide-sensitive factor attachment protein
SNARE	SNAP receptor
STX	Syntaxin
SYT	Synaptotagmin

SV	synaptic vesicle
TBS	Tris-buffered saline
TeNT	tetanus toxin
t-SNARE	target SNARE
v-SNARE	vesicular SNARE
VAMP	vesicle-associated membrane protein
VSV-G	vesicular stomatitis virus glycoprotein
WPRE	woodchuck post-transcriptional regulatory element

List of figures and tables

1.   Introduction

1.1. Brief overview of neuromuscular transmission in man

Signals from neurons in the motor cortex (Brodmann's area 4 – pre-central gyrus) travel down through the lateral cortico-spinal tract and set up excitatory post-synaptic potentials (EPSPs) in dendrites of motor neurons in anterior horns of the spinal cord. These EPSPs summate and induce action potentials in axons of these neurons which travel down through the anterior roots, and via various nerves, to terminate at the pre-synaptic terminals over the muscle fibers. Arrival of an action potential to these motor nerve endings opens voltage-sensitive Ca^{2+} channels and the resulting influx of Ca^{2+} activates the putative Ca^{2+} sensor, synaptotagmin, triggering into action a complex machinery of proteins. These include the 3 SNAREs (SNAP receptor) – SNAP-25, syntaxin and synaptobrevin, inducing fusion of synaptic vesicles containing the neurotransmitter, acetylcholine (ACh). The released ACh traverses the synaptic cleft and binds to nicotinic ACh receptors (AChR) on the muscle. These ligand-gated ion channels open upon binding ACh and let in cations, predominantly an influx of Na^+, thereby, setting up an end-plate (EP) potential in the underlying muscle fibre. This then causes the rapid activation of the surrounding voltage-gated Na^+ channels, causing an action potential to be setup and propagated through the T-tubule network in the muscle fibre. Subsequent release of Ca^{2+} from stores in the sarcoplasmic reticulum elicits the contraction of the muscle fibres through a sliding filament model of actin-myosin, with troponin-tropomysin acting as the Ca^{2+} sensors.

19

Perturbation of this process at any of the above steps, especially in vital respiratory muscles, i.e. the diaphragmatic or intercostal muscles leads to serious morbidity and mortality. This can be caused by agents such as the botulinum neurotoxin (BoNT – which inhibits the release of ACh) or curare (which blocks the AChR), in genetic disorders like Amyotrophic Lateral Sclerosis (ALS – caused by the degeneration of motor neurons) and Duchenne muscular dystrophy (causing degeneration of muscle fibres) or due to immunological conditions such as myasthenia gravis (caused by production of auto-antibodies against AChR) and Lambert-Eaton syndrome (auto-antibodies against pre-synaptic Ca^{2+} channels) .

1.2. The microscopic architecture of a NMJ

The NMJ is an area where part of the motor nerve specialized for ACh release (pre-synaptic terminal) comes into contact with the part of the muscle fibre, that is most sensitive to ACh (post-synaptic membrane). Upon contact with the skeletal muscle fibre, the supplying α-motor neuron (MN) axon divides into multiple terminal swellings, called 'boutons', devoid of any myelin sheath and which project into corresponding depressions in the thickened muscle membrane (Sanes and Lichtman, 1999). These circumscribed regions of the muscle EP form 1μm deep clefts called 'junctional folds', rich in ACh receptors, and are mirrored by specialised regions called 'active zones' in the pre-synaptic nerve terminal, rich in ACh containing vesicles (see fig. 1). Schwann cells processes cover and protect the nerve terminal and, also, form myelin sheaths covering the pre-terminal axons. Large numbers of mitochondria are found in

nerve termini and fulfil the energy requirements inherent in ACh production, loading and release. The active zones are specialised for the tethering, docking and, most importantly, in regulated Ca^{2+}-dependent fusion of loaded vesicles with the plasma membrane (Sanes and Lichtman, 1999). They contain electron-dense material consisting of proteins such as Rab3-interacting molecules (RIM), Munc13, Piccolo, Bassoon, liprins, tyrosine phosphatases and other interacting molecules which help to maintain their anatomical and physiological differences from the rest of the pre-synaptic membrane (Lonart, 2002; Schoch and Gundelfinger, 2006).

The crests and sides of the junctional folds are richly endowed with nicotinic AChRs (>10,000/μm^2 – compared to an extra-synaptic density of less than 10/μm^2), with an average human EP estimated to contain about 15-40 million receptors (Salpeter et al., 1988; Shyng and Salpeter, 1989; Salpeter et al., 1993; Salpeter, 1999). These receptors are predominantly found in the tops of the junctional folds with neural cell adhesion molecules (NCAMs) and voltage-gated Na^+ channels found at the bottom – an architecture fashioned by the agrin–MuSK–rapsyn pathway and which has been hypothesized to result in increased efficiency of transmission (MuSK - muscle specific kinase) (McConville and Vincent, 2002).
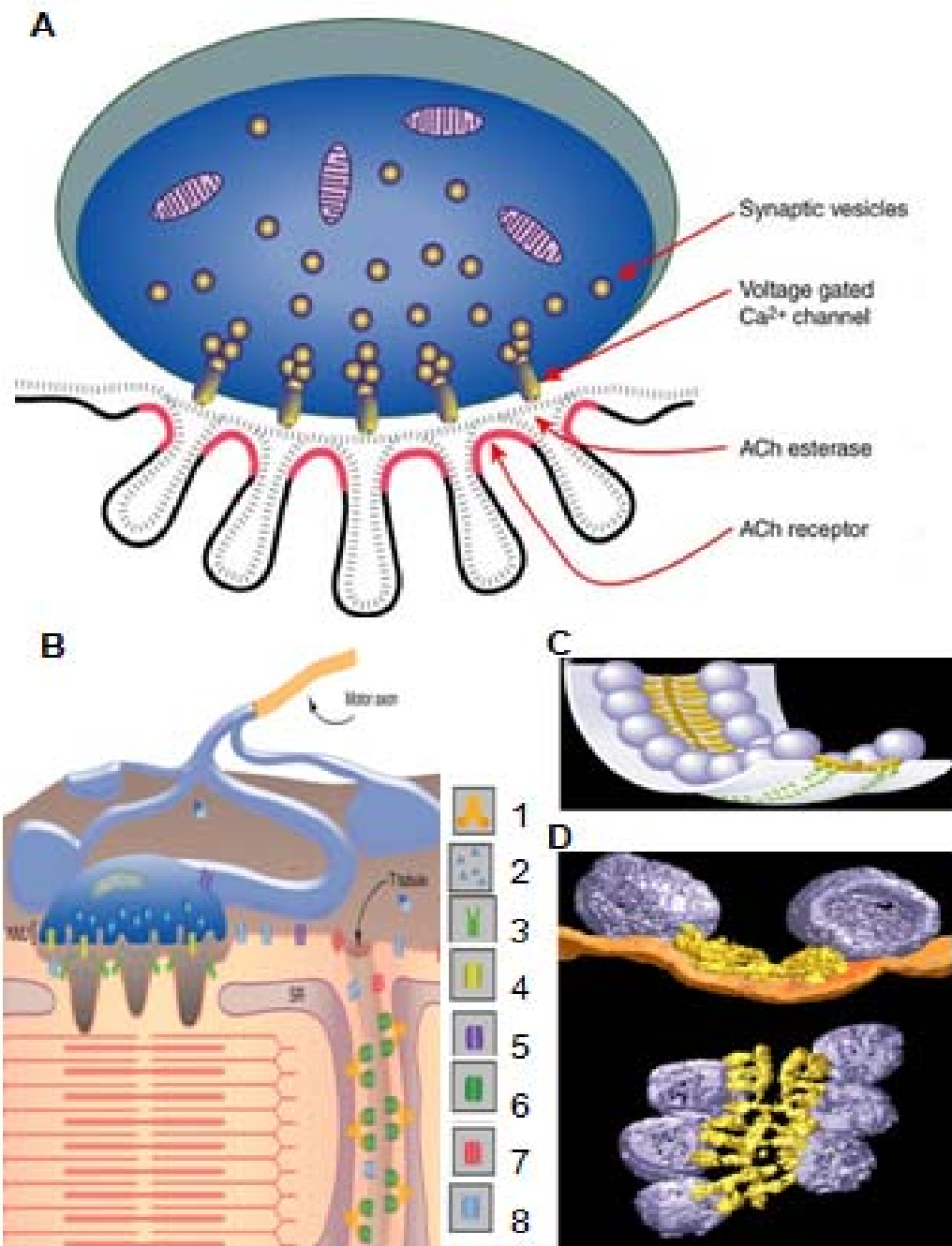
Fig. 1: The microscopic architecture of a NMJ: **A**: Schematic showing the main components of a mammalian NMJ, with the pre-synaptic terminal on top and the post-synaptic in the bottom (Hatched line between the two represents the basal lamina). **B**: Illustration of the architecture of the post-synaptic elements involved in converting end-plate potentials to muscle contraction. The horizontally organised thick and thin filaments are the actin/myosin/troponin/tropomysin contraction machinery. SR represents the sarcoplasmic reticulum (1: SR Ca^{2+} channel, 2: ACh, 3: AChR, 4: Neuronal Ca^{2+} channel, 5: K^+ channel, 6: T-tubule Na^+ channel, 7: Muscle Cl^- channel and 8: Muscle Na^+ channel) **C** & **D**: Ultrastructure of pre-synaptic frog NMJs. D is the reconstruction of multiple electron microscopic images of freeze-fractured active zones. SVs are the blue spheres, the active zone proteins are in gold and the plasma membrane is in orange. C represents a cartoon of the aspects seen in D, with the plasma membrane shown in white. The orderly structure of the active zone is well represented in these images. A & D are adapted from (Squire et al., 2003) and B & C are adapted from (Harlow et al., 2001).

1.2.1. The pre-synaptic apparatus at the NMJ

Mammalian extrafusal skeletal muscle fibres are innervated by axons from α-MNs of the brainstem and spinal cord. These large lower motor neurons, are distinguishable by their size and location from gamma motor neurons, which innervate intrafusal muscle fibers of muscle spindles. The muscle fibres supplied by α-MN forms a motor unit, comprising of biochemically and functionally identical fibres, and the α-MNs supplying a single muscle form a motor neuron pool, whose cell bodies are usually in close proximity to each other in the spinal cord. In the spinal cord, α-MNs are located within the gray matter of the anterior horn and their axons exit in the anterior root to form the motor component of the various spinal nerves (See fig.: 2). These neurons are in turn supplied by upper motor neurons via the corticonuclear, corticospinal, and rubrospinal tracts. The corticonuclear and corticospinal tracts are involved in the control of voluntary movement and end in glutaminergic synapses on α-MNs. In addition, α-MNs receive extensive sensory input from Golgi tendon organs, muscle spindles and other sensory neurons in the periphery and from local inter-neurons in the vicinity, e.g., Renshaw cells. These sensory afferents underlie the several types of reflex circuits of differing complexities, like the monosynaptic knee-jerk reflex. Some of the inputs from the inter-neurons are inhibitory in nature and are involved in the maintenance of proper muscle tone.
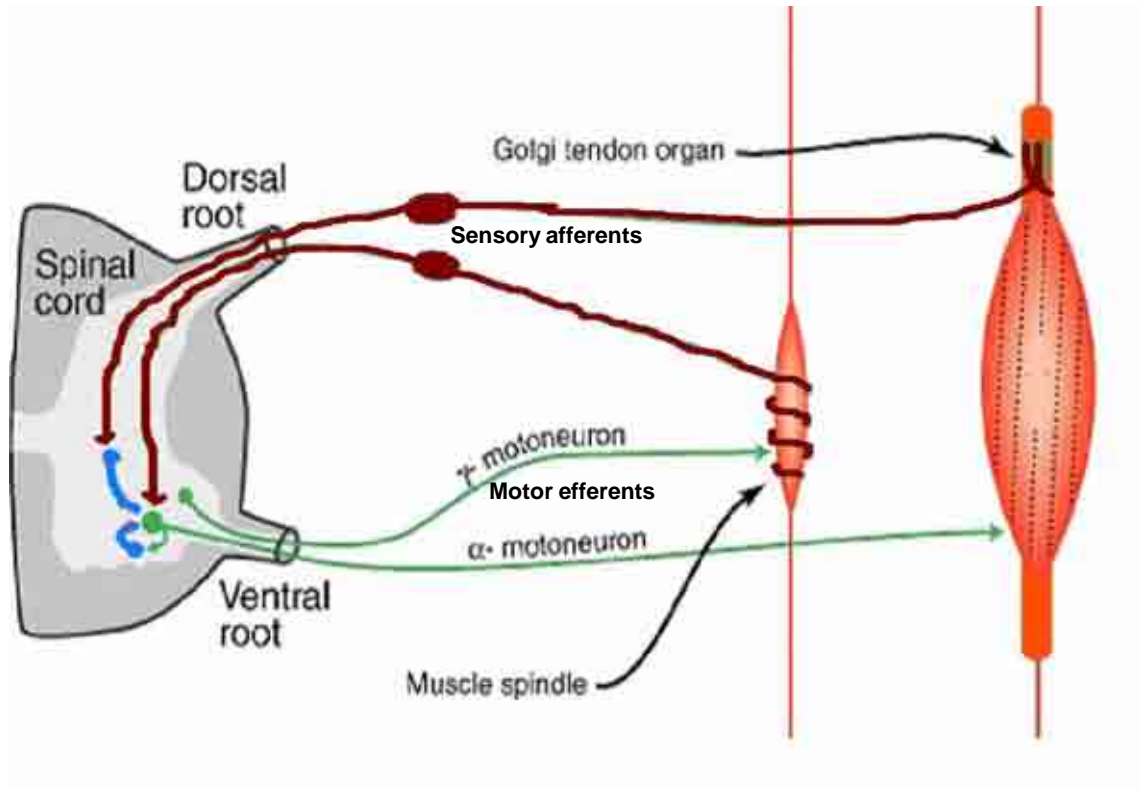
Fig. 2: Spinal control of muscle contraction: Schematic showing the regulatory system controlling muscle contraction. The extra and intra-fusal muscle fibres are shown in orange. The MNs, α and γ, are shown in green, the sensory input in brown and interneurons in blue. Input from the golgi tendon organs and muscle spindles control the excitability of the α MN, while input from the γ MN controls the sensitivity of the muscle spindles. Adapted from (Squire et al., 2003).

Arrival of an action potential at the pre-synaptic terminus, from the supplying α-MN, results in the opening of Ca^{2+} channels, and the ensuing Ca^{2+} influx stimulates a fast (<1 ms), regulated (by a complex cohort of proteins) and spatially accurate (only at the active zones) fusion of synaptic vesicles to the membrane (Katz and Miledi, 1968; Wojcik and Brose, 2007) (See fig.: 3). The trafficking of synaptic vesicles from the cytoplasm to the membrane and back again is termed the "synaptic vesicle cycle" and can be subdivided into sequential steps of vesicle loading, clustering and tethering at the membrane, docking at active zones, priming for release and, finally, release of vesicle contents by fusion with the membrane (Wojcik and Brose, 2007). These vesicles are then recycled and refilled with ACh for repeated rounds of exocytosis, through an intermediate process of acidification by a vacuolar proton pump followed by active transport of the neurotransmitter into the lumen (Sudhof et al., 1993; Sudhof, 2004; Rizzoli and Jahn, 2007). The final steps of fusion and recycling differs in various neuron types and can be classified into a "kiss-and-run" type (Heuser and Reese, 1973), where transient opening and closure occur through a small fusion pore, and "full fusion", where the vesicle completely merges with the plasma membrane and is endocytosed by clathrin-coated pits (Ceccarelli et al., 1973; Hurlbut and Ceccarelli, 1974). Another process of vesicle fusion has also been hypothesized, where the vesicles remain in the readily releasable pool ("kiss-and-stay") and are refilled with neurotransmitters without undocking (Koenig and Ikeda, 1996).
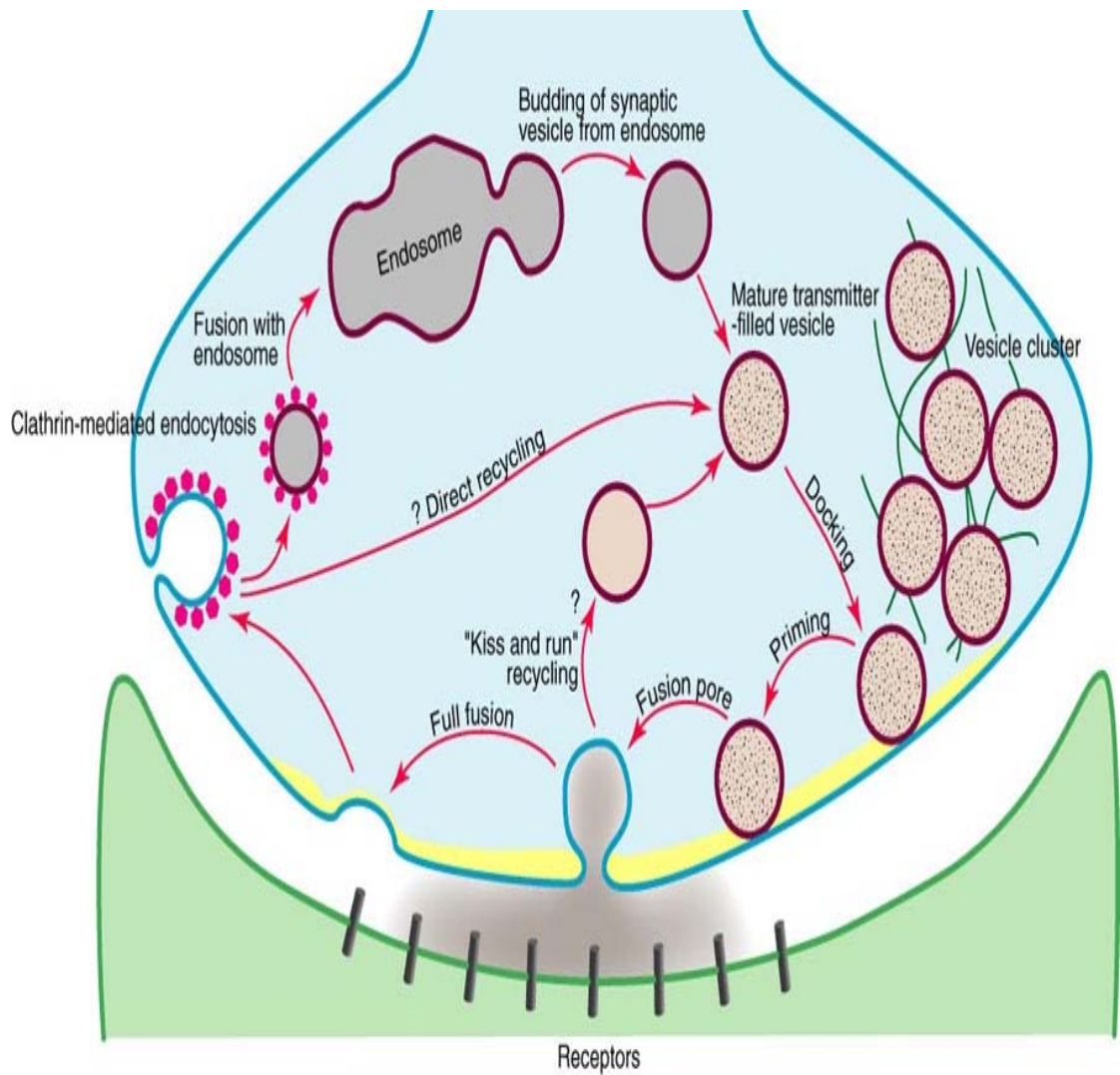
Fig. 3: The synaptic vesicle cycle. SVs bud off from endosomes and are then filled with the specific neurotransmitter. They are then recruited to the active zone, where they go through many intermediate stages before final fusion. Recycling of fused SVs can proceed through different pathways like, the "kiss and run" and clathrin-mediated endocytosis. Adapted from (Squire et al., 2003).

The faster "kiss-and-stay" and "kiss-and-run" methods were thought to be used preferentially at faster synapses thereby avoiding the time- and energy-intensive recycling processes, whereas the slower clathrin-dependent pathway was thought to be more prevalent in slower synapses. However, current evidence does not show any such preference, especially in light of the fact that most neurons only ever undergo exocytosis at a moderate rate and all these three types of recycling are adequate under such circumstances (reviewed in (Rizzoli and Jahn, 2007)). Upon high frequency nerve stimulation, the initial burst of neurotransmitter release is followed by a lower, steady, plateau of vesicle release. The total number of synaptic vesicles at a synapse that participate in these exo-and-endocytotic processes is referred to as the "recycling pool", comprising an initially released burst called the "ready-releasable pool" (~20% of vesicles in mammalian NMJs) and a "reserve pool" that helps to maintain the later steady-state release (the remaining 80%) (Richards et al., 2003; Rizzoli et al., 2003). Some neurons have a third pool of vesicles termed the "resting pool", whose function or absolute number are not yet clear (Sudhof, 2000).

Large dense core vesicles (LDCVs) in neuroendocrine cells such as the adrenaline/noradrenaline-secreting adrenal chromaffin cells or insulin-secreting beta cells in the islet of Langerhans undergo exocytosis by similar mechanisms, differing mainly in the speed of release (up to 20 fold slower) and the lack of specialised active zones (Livett, 1984; Livett et al., 1987).

1.2.2. Organisation of the post-synaptic NMJ

The mature mammalian skeletal NMJ consists of the pre-synaptic nerve terminal of a spinal motor neuron in close apposition with a striated muscle fibre, albeit separated by a thin basal lamina, and is cocooned in Schwann cells (Hughes et al., 2006) (See fig.: 1 and 4). The assembly of this complex apparatus is initiated by signals from the axon as it approaches an immature myotube. While there are many candidates for the actual neuro-chemical signals involved in this process, the heparin-sulphate proteoglycan agrin is most studied and one whose requirement for this process has been proven in null and mutant mice (McConville and Vincent, 2002). Agrin, transported down motor axons and released by the immature pre-synaptic terminal, binds to the basal lamina and activates a transmembrane receptor tyrosine kinase called MuSK on immature muscle cells (Ruegg and Bixby, 1998; Lin et al., 2008). This then activates a series of down-stream steps which leads to the activation of a membrane associated protein – rapsyn – and finally to clustering of AChRs (AChRs), associated 1:1 with rapsyn, and other postsynaptic components like utrophins, ankyrins, Na^+ channels and many cell adhesion and signalling proteins. An immature myotube transcribes α, β, γ and δ AChR genes to form the functional pentamer – $α_2βγδ$ (the adult counterpart has the ε subtype instead of δ). In immature myotubes, the functional AChR protein is found distributed throughout the plasma membrane at a concentration of 1000 per $μm^2$ – upon contact with the motor axon, this density increases to more than 10000 per $μm^2$ at the junctional folds and decreases to less than 10 per $μm^2$ away from them (a process that takes less than 12 h in certain models like

chicken and rat NMJs (Bevan and Steinbach, 1977; Froehner, 1991)). The motor nerve terminal not only controls the clustering of AChR, but also stimulates their local production through a signalling molecule called neuregulin. The innervating motor terminals can also reduce the expression of non-local AChRs by distant myocyte nuclei – by changes in the amount of local and free intracellular Ca^{2+} (Sieburth et al., 2005; Hughes et al., 2006).

The nerve supply to the muscle fibres, while stable, has the property of remodelling in response to alterations in synaptic transmission. This is also reflected in post synaptic modifications in the size, density and location of the AChRs on the muscle fibres. While the molecular signalling mechanisms that govern these changes are not fully known, the defined application of toxins capable of perturbing neurotransmission at the pre-synaptic (BoNT) or post-synaptic level (α bungarotoxin - α-BuTx) can help in studying these processes at morphological and molecular levels. A more in-depth understanding of these processes will not only help in gaining further knowledge of synaptic biology, but also in devising treatments for various muscular and neurological disorders.

The arrival of a nerve impulse at this terminus results in the fusion of ~60 synaptic vesicles per active zone; each containing ~10,000 molecules of ACh. The released ACh then binds to the nicotinic AChRs found in the junctional folds resulting in an influx of Na^+ and depolarisation of the muscle membrane. There is a wide safety margin in the whole process of neuromuscular transmission; the amount of ACh released per impulse being far higher than the number of AChRs and the number of AChRs being higher than that necessary to produce a fully propagated response at the muscle membrane (Ganong,

2003; Squire et al., 2003).
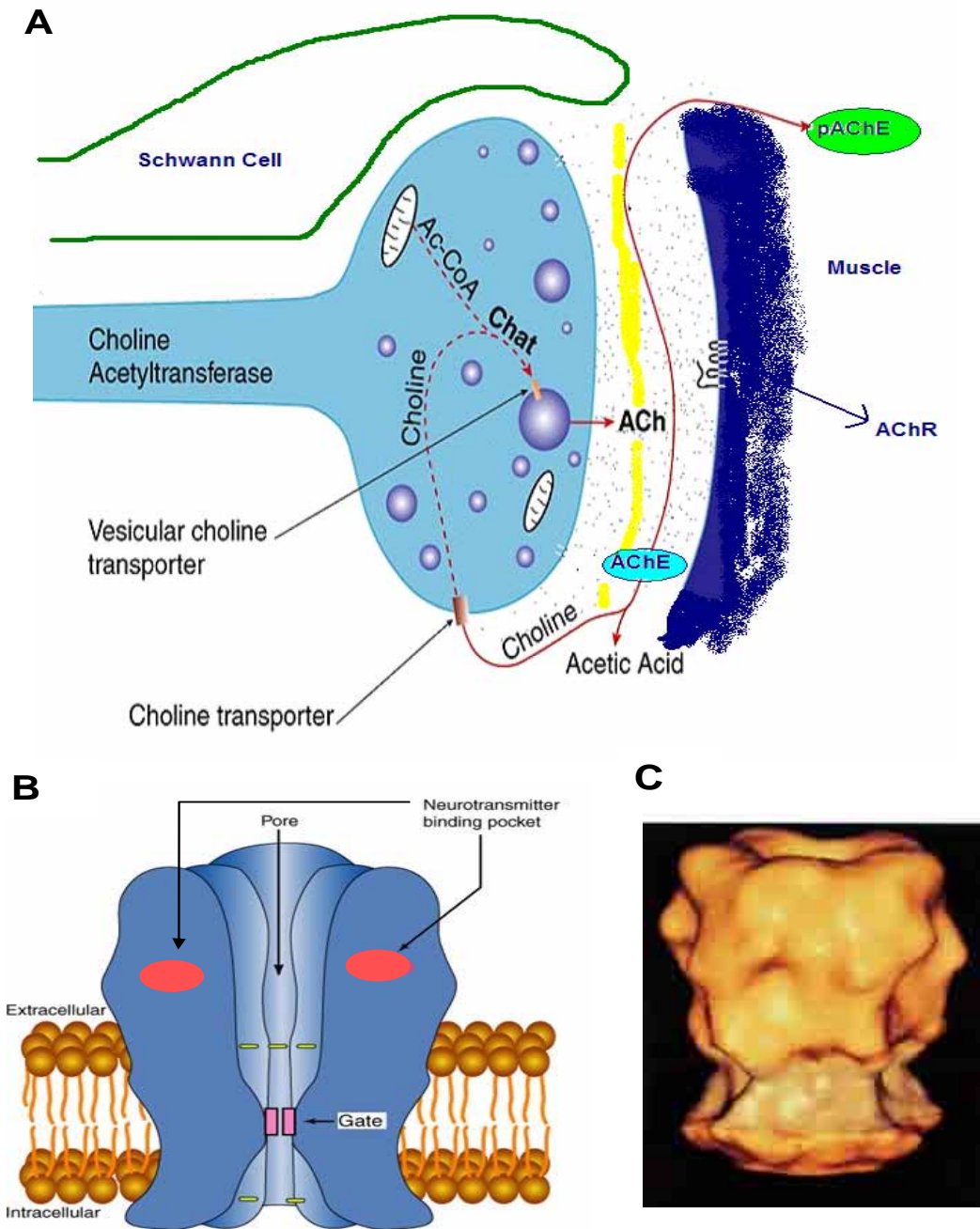
Fig. 4: The Acetylcholine cycle: **A:** Synthesis of ACh. Free choline in the extracellular fluid is taken up and concentrated in the pre-synaptic compartment by a specific choline transporter. The enzyme Choline acetyl-transferase (ChAT), then acetylates this free choline using acetyl-CoA. This is then actively concentrated in the SV by a specific vesicular transporter. Upon release, ACh binds to the post-synaptic AChR, setting up an EPP in the muscle membrane. Excess ACh is destroyed by basal membrane bound Cholinesterase (AChE) or by the plasma pseudo-cholinesterase (pAChE), releasing free choline. **B and C:** Structure of the nicotinic AChR. **B** shows a schematic with the putative structure as exists in intact membranes. It resembles other ligand-gated ion-channel morphology, with a central pore, selectivity filter and an ACh binding pocket. **C** is a three-dimensional computational representation based on electron-density maps. B and C are adapted from (Unwin, 2005)

The excess released ACh is destroyed by cholinesterase found on the basal lamina and by pseudo-cholinesterases in the plasma, priming the apparatus for another action potential (See fig. 4). Repeated trains of stimuli, before the onset of relaxation in the muscle, results in the activation of additional contractile elements and increase in muscle tension in a phenomenon known as 'summation'. With increasing frequency, the tension developed increases proportionally till it reaches a plateau, at tetanic frequency (Preston and Shapiro, 2005).

1.2.3. Other important actors involved in nerve-muscle conduction and its control – Schwann cells, muscle spindles and spinal inter-neurons.

Schwann cells are glia-like cells found along the axons of peripheral motor nerves involved in the creation of a myelin sheath. The myelin sheath of a motor axon is formed of up to 100 layers of the Schwann cell membrane tightly wound around the axon interspersed by the nodes of Ranvier – 1 µm constrictions devoid of any myelin. Terminal Schwann cells, a specialised subset of Schwann cells found near the NMJs, form a closely-fitting cover over the pre-synaptic terminals. Schwann cells are important in initial axon guidance (Mars et al., 2001; Ullian et al., 2004), in the re-establishment of innervation following injury or dismemberment of axons, maintenance and modulation of synaptic terminals and neurotransmission (Hughes et al., 2006) and in the process of nerve sprouting after perturbation of neuromuscular transmission (Son and Thompson, 1995; Son et al., 1996). The portion of the myelin sheath which is in tight contact with itself is composed of extracellular domains of a

31

protein called P_0 (Protein zero). Mutations of this crucial protein can lead to various peripheral neuropathies, especially in certain forms of Charcot-Marie-Tooth disease.

Muscle spindles are an important sensory and calibration system involved in the fine control of muscle contraction (See fig.: 1). Also called intra-fusal fibres, they consist of two morphological distinct, specialised, muscle fibres termed as the nuclear bag and chain fibres. These fibres, innervated separately from the rest of the muscle fibres, have a motor supply from small motor neurons in the lateral horns of the spinal cord via γ efferent axons (along with some innervation from the α motor neurons via β efferent axons). They have terminations of sensory afferents from the dorsal root ganglion through type Ia fibres. The central termination of neurons supplying the muscle spindles end on α motor neurons. Muscle spindles are arranged in parallel to the regular muscle fibres and in the classical stretch reflex, stretching causes the sensory endings on the spindle fibres to start firing. This causes action potentials to be set up in α motor neurons supplying the muscle, thereby, causing its contraction. The spindles are also important in gauging changes in the rate of stretch of the muscle, in reducing tremors, controlling muscle tone and, through inter-neurons in the contralateral side of the spinal cord, in causing relaxation of muscle antagonists (Ganong, 2003; Squire et al., 2003).

The majority of α motor neurons input is from interneuron in the spinal cord, many from those in the same spinal segments. These inter-neurons are in turn connected to muscle spindles (on the same and opposite side), golgi tendon organs, α motor neurons, sensory neurons and upper motor neurons in

the CNS. Inter-neurons act as computational tools that integrate signals from various sensory and central sources and distributes them to α motor neurons and other inter-neurons. They are crucial in relaying sensory and central information to motor neurons that initiate or modulate output and in the formation of rhythmic patterns of muscle contraction (Squire et al., 2003).

1.3. The molecular machinery for fusion of synaptic vesicles with the plasmalemma

Small vesicles, with a phospholipid bilayer and a high protein (>30%) content, predominate at mammalian NMJs. While between 20-50nm in size, they contain all the proteins necessary for acidification, neurotransmitter transport, exocytosis and finally endocytotic recycling (See fig. 5). One of the largest proton on the vesicle is the vacuolar protein pump, most synaptic vesicles can only contain one of these large transmembrane multi-protein complexes containing components responsible for the ATPase activity and proton translocation. The proton gradient setup by this pump is exploited by the 12-transmembrane vesicular ACh transporter to concentrate ACh inside the synaptic vesicles (SVs) – exchanging 2 protons for every ACh molecule (Weihe et al., 1996; Ojeda et al., 2004).
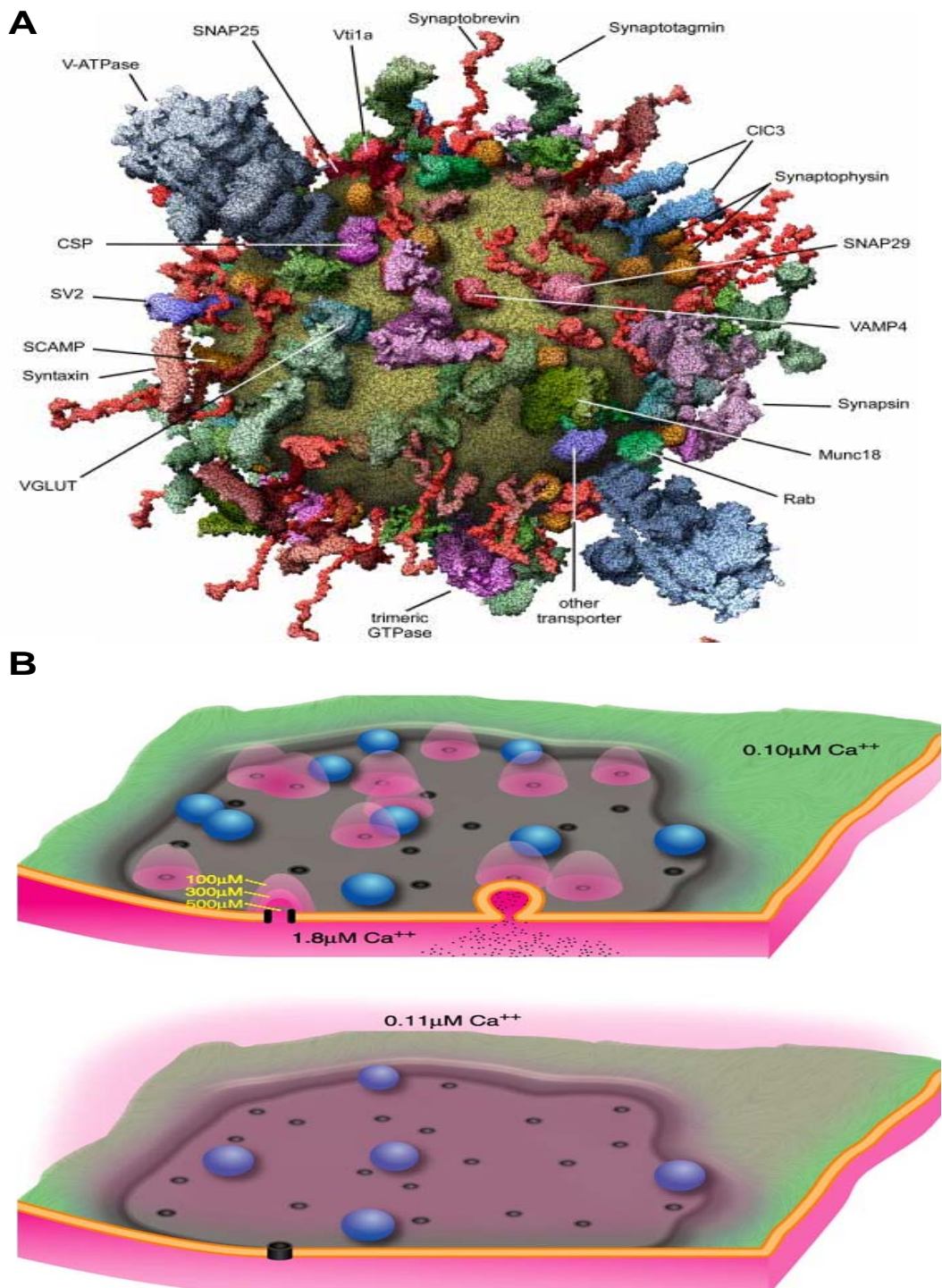
Fig. 5: Synaptic vesicles: **A:** Molecular constituents of an average SV. Computer generated 3D model of all the molecules associated with SVs. The biggest molecule visible is the vesicular ATPase (V-ATPase – in blue) and the most abundant molecule is synaptobrevin (in red). Adapted from (Takamori et al., 2006). **B:** Ca^{2+} microdomains near active zones. The top panel shows the Ca^{2+} concentration upon arrival of an action potential, while the bottom panel shows the dispersal of the ionic gradient a few milliseconds after the end of the action potential (Gradients of pink represent Ca^{2+} concentration – higher extra-cellular concentrations diffuse inwards through open channels in the top panel). The yellow band represents the lipid bi-layer and docked SVs are shown in blue. Adapted from (Squire et al., 2003).

These synaptic vesicles are typically congregated in highly organised regions of the synapse called active-zones. Another of the most important constituents of these active zones are voltage-dependent Ca^{2+} channels – found at a density of more than 100 channels per active zone. These channels are crucial in the excitation-secretion coupling in synapses. The normally low, and strongly buffered, Ca^{2+} concentration inside the synapses undergoes a rapid, <100µs, and massive, >1000 fold, increase in the local concentration of free Ca^{2+} upon arrival of an action potential at the terminal. This high concentration in a spatially localised area is the trigger for synaptic vesicle fusion (Katz and Miledi, 1968; Meinrenken et al., 2003). The high buffering capacity of the terminals also causes the equally rapid reduction in Ca^{2+} concentrations at the end of the action potential. Recent studies have indicated synaptotagmin, with its 5 Ca^{2+} binding sites and micromolar affinity for Ca^{2+}, integrates the Ca^{2+} entry with fast exocytosis (Schneggenburger and Neher, 2000) (See fig. 5).

1.3.1. Molecular mechanisms of SNARE-dependent exocytosis

SNARE proteins found on the vesicles along with their counterparts in the active zone membranes form multi-protein "nano-machines" that mediate membrane fusion responsible for neurotransmitter release. This family of versatile molecules, which despite their widely divergent sequences form similar coiled-coil helical complexes, perform the basic actions of vesicle budding and fusion in all eukaryotes. They are also involved in fusion reactions

necessary for cell growth, membrane repair and movement. A core complex is formed when four characteristic and conserved, 60-70 amino-acid long, SNARE motifs assemble into a parallel four-helical bundle (See fig. 6). The currently accepted molecular model of SNARE-mediated membrane fusion involves the initiation of merger opposing membranes by using energy released during the formation of this bundle. These SNARE motifs are usually, but not always, flanked by a transmembrane domain at the C-terminal and widely variant domains at the N-terminal. Some important exceptions are the synaptobrevins (with no N-terminal domain) and SNAP-25 (with no trans-membrane domain and two SNARE motifs joined by a palmitoylated linker).

While SNAREs were originally classified as v-SNAREs (vesicle-membrane SNAREs) or t-SNAREs (target-membrane SNAREs), the propensity of certain members of this family to act as both v-or-t-SNAREs (Sec22 acting as both v-and-t-SNARE - (McNew et al., 2000) and (Burri et al., 2003)) has resulted in the acceptance of a more refined classification into 4 sub-families. Current classification is based on the detailed analysis of core complexes of four different classes of SNARE motifs – Qa, Qb, Qc and R – based on the identity of highly conserved three glutamine (Q) or one arginine (R) in the central '0' layer of the core complexes.

In vitro SNAREs can interact promiscuously, but *in vivo* they typically only form when a hetero-oligomeric four helical bundle is created containing one SNARE motif from each class (Jahn et al., 2003; Jahn and Scheller, 2006). For example, exocytosis at mammalian NMJs is mediated by the formation of a core complex consisting of the R-SNARE motif from synaptobrevin, the Qa-SNARE

motif from syntaxin 1 and the Qb & Qc-SNARE motifs from SNAP-25 (Söllner et al., 1993; Sollner et al., 1993; Fasshauer et al., 1998). These SNAREs were first identified based on their homology to genes implicated in temperature sensitive trafficking mutations in yeast (Wilson et al., 1989). Their absolute importance to synaptic exocytosis was first established when they were shown to be substrates cleaved by the paralysing botulinum and tetanus neurotoxins (Schiavo et al., 1992b; Schiavo et al., 1992a; Schiavo et al., 1995). While there is continuing controversy as to whether the SNARE complexes are the minimal essential fusion motors or if they are components of a more complex machinery, evidence is increasing for the latter hypothesis being probably more descriptive of the majority of mammalian synapses. VAMP knockout mice, with a severe deficiency in the Ca^{2+} triggered fast exocytotic pathway, still show ~10% of normal release when triggered by other factors such as hypertonic sucrose (Schoch et al., 2001). Similarly, SNAP-25 knockout mice also retain some amount of exocytosis (Washbourne et al., 2002). Only the deletion of Munc18-1/Nsec-1, a syntaxin binding protein from the Sec-Munc (SM) family, eliminated release completely ((Verhage et al., 2000) and reviewed in (Jahn et al., 2003). Munc18 knockout mice died at birth, showed some synapse formation, albeit with early degeneration and demonstrated an absolute lack of spontaneous or evoked fusion.
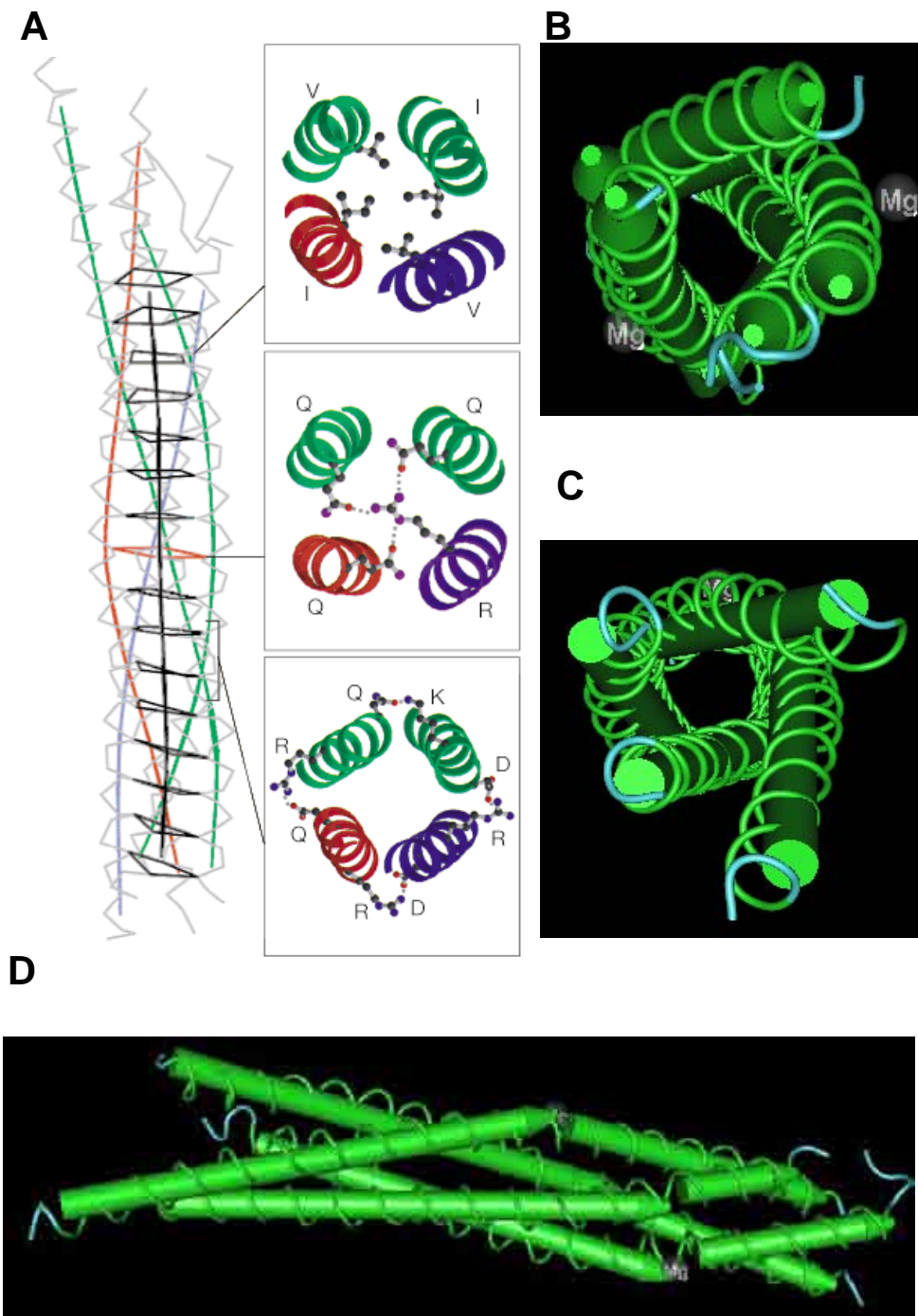
Fig. 6: SNAREs and synaptic exocytosis. **A:** Schematic of the SNARE core complex showing VAMP II (blue – R motif), Stx (red – Qa motif) and SNAP-25 (green – Qb and Qc motifs) in their four-helix bundle configuration. The left panel shows a side-view of the SNARE complex backbone, with the central ionic layer (red) and 15 hydrophobic layers (black) that mediate the core interactions highlighted. The right panel shows top-down views of side-chain interactions, with important amino acid H-bonds and salt bridges indicated. The central layer shows the position of glutamine (Q) or arginine (R) residues that define Q-SNAREs and R-SNAREs, respectively. **B, C and D:** A screen-capture from a Cn-3D rendering of a 2.4Å structure of a mature SNARE-complex, showing the top, bottom and side views respectively – this shows the tight helix-of-helices structure of a core SNARE complex. Adapted from (Chen and Scheller, 2001) and (Sutton et al., 1998).

Initial clues about the organisation of the central SNARE complex was found from *in vitro* studies which showed that SNAP-25, syntaxin 1 and VAMP can form a stable, detergent- and neurotoxin-resistant complex with a 1:1:1 stoichiometric ratio (Hayashi et al., 1994; Pellegrini et al., 1995). This complex dissociates upon addition of NSF and α-SNAP, in the presence of ATP, and renders the components susceptible to cleavage by BoNT and TeNT. The minimal ternary core complex consists of two domains from SNAP-25, spanning residues 1-84 and 143-206, and one domain from syntaxin and VAMP, encompassing residues 199-243 and 27-96, respectively. SNAP-25 domains, which are separated by a long linker region, are organised in a parallel manner in the complex. Furthermore, vesicles containing VAMP were able to fuse with those containing SNAP-25 and syntaxin (Weber et al., 1998), albeit at rates much slower then those observed *in vivo*. While important clues were gained by pull-down assays and cell free systems, the relative abundance of these SNAREs in neurons and their propensity to interact with many different proteins, meant that conclusive evidence was not obtainable by such *in vitro* assays (Jahn and Scheller, 2006). However, based on all accumulated knowledge from yeast homology studies, neurotoxin mediated neuroparalysis and *in vitro* studies, it does appear that membrane fusion is mediated by these SNAREs, in association with other essential proteins like complexins, Stx and Munc-18. The progression of SNARE-mediated fusion can be divided into a step-wise process involving – a) assembly of free SNAREs into an acceptor complex, a process probably mediated by the SM proteins, b) association with VAMP to form a loose trans-SNARE complex and c) creation of tight SNARE complexes,

probably catalysed by complexins and Stx and, finally, fusion with formation of a stable cis-SNARE complex ((Hanson and Jahn, 1997; Lin and Scheller, 1997) and reviewed in (Jahn and Scheller, 2006)). While all these phases can explain the processes involved into bringing the two membranes into close proximity, there is still some ambiguity about the steps involved in actual membrane fusion and lipid mixing. The currently accepted hypothesis is that close membrane apposition is brought about by the 'zippering' of the coil-coil domains of SNAREs, from their N-terminal towards their C-terminal, which clamps the membranes together (Fiebig et al., 1999). The "stalk" hypothesis is the most favoured one to describe the fusion of lipid bi-layers that then takes place. The closely apposed bilayers undergo a transition to a "hemi-fusion" state where the outer membranes are continuous but the inner ones are still separate and there is no aqueous connection. Later, the inner membranes fuse, followed by the release of vesicle contents. After the formation of the hemi-fusion state and before complete fusion, the physical constraints imposed by the close apposition of these membranes probably imposes strong strains on the linker regions that connect the SNAREs to their trans-membrane domains, probably resulting in their C-terminal ends being pulled into the hydrophobic core of the bilayer . This, and the later complete fusion, results in the formation of a cis-SNARE complex – being stable even at 80°C, 8M urea or 2% SDS ((Kozlovsky et al., 2002; Chernomordik and Kozlov, 2003) and reviewed in (Jahn and Grubmuller, 2002)). As yet, how all these complex processes described above fit into the previously described fast and slow, "kiss and run" or "kiss and stay" modes of exo-endocytosis, is as yet unclear.

1.3.1.1.   Recycling of SNAREs for further rounds of exocytosis

After the formation of the cis-SNARE complex, the individual SNAREs need to be redeployed as their free components in the plasma and vesicular membranes in order to catalyse a subsequent round of exocytosis. Indeed, if the particular muscle is receiving stimulation at tetanic frequencies, this needs to happen within milliseconds. While the "reserve pool" of synaptic vesicles helps to maintain the later steady-state release (the remaining 80%) (Richards et al., 2003; Rizzoli et al., 2003), these will soon be exhausted if the vesicles are not quickly and constantly recycled. The cis-SNARE complex, the most energetically stable conformation, needs to be disassembled for them to regain their fusogenic potential. The study of yeast and *Drosophila* temperature-sensitive mutants, that show an accumulation of SNARE cis-complexes at restrictive temperatures, has yielded valuable clues about this process (Littleton et al., 1998). NSF, a hexameric protein of the AAA^+-protein family (ATPases associated with various cellular activities – proteins specialised across many organisms in dismantling protein aggregates), along with co-factors called SNAP (soluble NSF attachment proteins – with three isoforms α, β and γ) are involved in this process (Marz et al., 2003). Three SNAP molecules bind to the cis-SNARE complexes at approximately their 0-layer - one arginine and three glutamines, followed by the activation of NSF (The binding to and importance of the 0-layer is controversial with some studies finding no evidence of its

importance (Lauer et al., 2006)). The ATPase activity of NSF is utilised to generate the energy to separate the highly stable cis-SNARE complex. The exact process of disassembly is still not fully known and might need many cycles of NSF attachment and ATP hydrolysis to bring to completion. This necessity of disassembly, and the absolute dependence on active NSF for *in vitro* fusion, initially lead many into believing that this was an essential step in the process of exocytosis - indeed, while cis-SNARE complex disassembly by NSF is certainly crucial for maintaining fusion competence, fusion can still take place in *Drosophila* mutants at restrictive temperature until all free SNAREs are exhausted (Littleton et al., 1998).

The final part of the recycling story, the recycling of lipids that went into forming the vesicle, has not yet been fully elucidated with two modes proposed – "kiss and run" or "kiss and stay" (reviewed in (Rizzoli and Jahn, 2007)). The latter, with a large amount of data from yeast homologs, involves the fusion and subsequent total collapse of the vesicle into the plasma membrane. This is then retrieved by a clathrin-and-dynamin-mediated retrieval pathway, similar to regular vesicle fusion in eukaryotic cells (Perrais and Merrifield, 2005). Indeed the uptake of neurotoxins and other proteins from the synaptic terminals shows that this process is taking place to a certain extent. However, the speed of exo-endocytosis at fast synapses and the discovery that peptide blockers of endocytosis do not completely inhibit synaptic transmission, implies that this cannot be the predominant mode in all synapses (Zhang, 2003; Jockusch et al., 2005; Granseth et al., 2006). On the other hand, the "kiss and run" mode has the advantages of easy and rapid recycling and conservation of

many essential vesicle proteins. Evidence of such recycling has accumulated from studies examining capacitance flickers at synaptic terminals, from studies using FM1-43 and other hydrophobic fluorescent dyes and through the use of pH sensitive VAMP-GFP chimeric proteins called PHlourins – all these demonstrated recapture and re-acidification of synaptic vesicles with 100-1000ms, a time-scale probably beyond a clathrin-and-dynamin-mediated retrieval pathway (Richards et al., 2003; Rizzoli et al., 2003; Rizzoli and Jahn, 2007). On the other hand, classical imaging studies with electron-micrography have not shown clear visual evidence of such activity and the molecular machinery that could potentially function in such a rapid process has yet to be fully elucidated.

1.3.1.2. SNAP-25

The SNAP-25 family of SNAREs consists of a related group of ~23-25 kDa t-SNARE proteins which contribute the Qb/c-SNARE motifs to a mature SNARE complex (Steegmaier et al., 1998). The two SNARE motifs flank a central, cysteine-rich, membrane targeting/binding domain which is usually palmitoylated. The two neuronal/neuroendocrine specific isoforms, SNAP-25aA and SNAP-25b, are highly homologous (with a difference of ~9 AAs (Bark, 1993; Bark et al., 1995)). The 23 kDa SNAP-23 protein, showing a 60% homology with SNAP-25, has a more ubiquitous tissue distribution and is essential for regulated exocytosis in non-neuronal cells (Ravichandran et al., 1996; Vaidyanathan et al., 2001). The SNAP-25 family also includes the yeast homologues sec9p (Brennwald et al., 1994), spo20 (Neiman, 1998) and vam7p

(Ungermann and Wickner, 1998). SNAP-25 is usually found associated with syntaxin 1 A in neurons.

SNAP-25 is an essential protein and knockout mice die at birth. These mice also show an almost complete absence of evoked fusion with a near-normal quantity of spontaneous fusion events. Palmitoylation, by the palmitoyl-acyl-transferase enzyme, of the cysteine rich central portion is essential for membrane targeting and exocytotic activity of SNAP-25 (Hess et al., 1992; Gonzalo and Linder, 1998). This is a dynamic process with the half-life of acyl groups being shorter than the half-life of the protein (half-life of SNAP-25 is ~8 h and the half-life for its palmitate derivative is ~4 h in PC12 cells; reviewed in (Salaun et al., 2004)). Membrane association is highly dependent on the central cysteines and removal of any of the four cysteine residues reduces palmitoylation and subsequent membrane association (Veit et al., 1996; Lane and Liu, 1997). Presence of a 36-amino-acid sequence containing the cysteine-rich domain, and the 28 amino acids that follow, is sufficient and essential for efficient palmitoylation (Gonzalo and Linder, 1998; Gonzalo et al., 1999). While spontaneous palmitoylation of SNAP-25 has been shown to occur in the presence of syntaxin 1, the functional importance of such a mechanism is as yet unknown (Salaun et al., 2004). The N-terminal SNARE domain is probably involved in the initial formation of a Ca^{2+}-sensitive binary complex with Stx, before VAMP binding and formation of a final SNARE complex (An and Almers, 2004). BoNT/A cleaves SNAP-25 between Gln197-Arg198, /E between Arg180-Ile181 and /C1 between Lys253-Ala254 (Blasi et al., 1993b; Montecucco and

44

Schiavo, 1994; Schiavo et al., 2000).

1.3.1.3. Syntaxin

The Syntaxin family consists of a homologous group of ~35 kDa t-SNARE proteins which contribute the Qa-SNARE motif to a mature SNARE complex. It is anchored at its C-terminal, through a transmembrane domain, to the plasma membrane. The cytosolic N-terminus consists of a conserved SNARE domain and a Munc18 binding domain. Despite differences in their sequence, the tertiary structures of related syntaxins are very similar and consist of an anti-parallel bundle of three α-helices (e.g.: Neuronal Stx, the N-terminal domain of yeast syntaxin homolog Vam3 and the N-terminal domain of syntaxin 6). On their own, SNARE domains of syntaxin (the H3 domain) form a homo-tetramers (Misura et al., 2000, , 2001; Misura et al., 2002). Syntaxins are expressed as multiple isoforms, with numerous splice variants possible for many of them (15 mammalian Stx gene have been identified, with four of them, 1-4, participating in exocytosis (Teng et al., 2001; Wang and Tang, 2006). Syntaxin 1 gets proteolysed by CI (Blasi et al., 1993a); Syntaxin 1A is cleaved between Lys_{253} and Ala_{254}, whereas syntaxin 1B is cleaved between Lys_{252} and Ala_{253}. Syntaxins 1A and 1B are differentially expressed in the peripheral nervous system, with 1B localized to nerve terminals of the NMJ, and 1A to perivascular nerve endings (Aguado et al., 1999; Kalandakanond and Coffield, 2001). BoNT/C1 is unique in that it cleaves both SNAP-25 (Foran et al., 1996; Osen-Sand et al., 1996) and many members of the syntaxin family, including the neuronal isoforms 1A/1B, 2 and 3 (Blasi et al., 1993a; Schiavo et al., 1995).

1.3.1.4. VAMP

Synaptobrevin or vesicle-associated membrane protein (VAMP) is the smallest member of the group of neuronal SNAREs. It consists of a family of ~13 kDa transmembrane proteins located on SVs and large dense core vesicles (LDCV) (Sudhof et al., 1993). Two neuronal isoforms VAMP 1 and 2 and cellubrevin (Cbr), a non-neuronal homologue, have been identified (McMahon et al., 1993; Rossetto et al., 1996; Advani et al., 1998). These v-SNAREs provide the R-SNARE motif for a SNARE complex. VAMP 2 knockout mice die at birth, form synapses with reduced spontaneous fusion and show no evoked exocytosis. It consists of very short C-terminal end which protrudes into the lumen of the vesicle. This is attached to a trans-membrane domain, followed by a conserved SNARE core and is capped by an unstructured, proline-rich and isoform-specific N-terminal in neuronal VAMPs (Cornille et al., 1995). Some non-neuronal synaptobrevin homologs have conserved N-terminal domains called longin domains (Brunger, 2005). These conserved longin domains probably play a role in vacuolar and sub-cellular targeting. TeNT and BoNT/B cleave VAMP 2 and Cbr but not rat Vamp 1 (Volchuk et al., 1994). TeNT and BoNT/B cleave VAMP2 between Gln76-Phe77 and Cbr between Gln59-Phe60; BoNT/D cleaves VAMP1/2 between Lys59-Leu60 and Cbr between Ala67-Asp68 and possibly Lys42-Leu43; and BoNT/F cleaves VAMP1/2 between Gln58-Lys59 and Cbr between Gln41-Lys42 (Schiavo et al., 2000; Aoki, 2004). Clostridial neurotoxins require a 15-20 amino acid recognition/buffer sequence spanning the cleavage site for efficient proteolysis (Foran et al., 1994).

1.3.2. Other important molecular actors in the synaptic vesicle cycle – synaptotagmin, Rab3, Munc18, SV2, etc.

It has been known for a long time that the fast, evoked, release at nerve terminals is strongly tied to an increase in intra-neuronal Ca^{2+} concentration (Katz and Miledi, 1968). Other studies showed that time-scale of exocytotic fusion of vesicles can best be explained in terms of Ca^{2+} binding to a sensor with at least five binding sites of micromolar affinity, thereby, causing downstream activities that result in fusion (Geppert et al., 1994; Li et al., 1995; Catterall, 1999; Lawrence and Dolly, 2002). The group of Ca^{2+}-binding proteins called synaptotagmins (Syt) best fit this role. While more than 14 different isoforms have been identified, Syt 1 and 2 are found in high abundance in neuronal tissues and have the Ca^{2+} binding properties that match the putative sensor (Ullrich et al., 1994). Syt 1 is a transmembrane protein that also contains two Ca^{2+}-binding C2 domains (conserved region-2 of protein kinase C domains) and, when bound to Ca^{2+} can interact with SNAREs and/or membrane phospholipids. Through a putative syn-print motif, Ca^{2+}-channels can interact with Syt 1 (Sheng et al., 1997) and syntaxin1A/B (Keith et al., 2007) – thus filling another blank in the Ca^{2+}-fast-exocytosis puzzle (Catterall, 1999). Syt 1 knockout mice die within 48 h after birth, form synapses with elevated spontaneous fusion and reduced evoked fusion (Geppert et al., 1994). Structurally, Syt 1 contains two cytoplasmic C2 domains - the C2A domain binds three and the C2B domain binds two Ca^{2+} ions (Schneggenburger and Neher, 2000). While the binding affinities of the free C2 domains are very low

47

(0.5–5 mM), this increases >1000-fold upon binding to phospholipids membranes; this corresponds quite accurately with the hypothesized neuronal Ca^{2+}-sensor. In addition, Syt 1 knockout mice show a selective loss of fast, Ca^{2+}-triggered exocytosis in hippocampal synapses and in chromaffin cells with a small elevation of the rate of spontaneous fusion. Mutations affecting Ca^{2+} affinity of Syt 1 corresponded with an identical shift in the Ca^{2+} affinity of fast, evoked, exocytosis (reviewed in (Stevens and Sullivan, 2003; Meldolesi and Chieregatti, 2004; Yoshihara and Montana, 2004)).

Munc18 knockouts, lethal at birth, are the only ones that show a complete absence of fusion activity in synapses – both spontaneous and evoked fusion is abolished in these animals which synaptic degeneration (Verhage et al., 2000). Belonging to the group of Sec1/Munc18 (SM) proteins, they are conserved in many species and play a central role in synaptic and non-synaptic exo-endocytosis. Munc18-1, the isoform predominantly expressed in neuronal and neuroendocrine tissues, interacts and co-localises *in vivo* with monomeric (closed) Stx and with SNARE complexes. Munc18 has been hypothesised in almost all aspects of synaptic fusion – the transport, docking, tethering, priming and fusion of SVs, in the creation of specific and accurate SNARE complexes by reducing promiscuity and, even in synaptic plasticity (Toonen and Verhage, 2007). The synaptic function of Munc18 is correlated with its interaction with Stx1 – initially, it was thought that since Munc18 binds to the closed form of Stx1, its dissociation from Stx must be necessary for SNARE complexes to form and, therefore, Munc18 must act as a negative regulator of exocytosis (Dulubova et al., 1999). But more recent evidence which showed

that Munc18 can also bind SNARE complexes, at physiological concentrations and *in vivo*, has complicated this picture (Dulubova et al., 2007). Further studies, and analysis of Munc18 knockout mice, have revealed that it plays crucial roles in regulating vesicle translocation to active zones, on vesicle preparation (tethering, docking, priming) for fusion and in increasing the fusion rate (reviewed in (Toonen and Verhage, 2007)).

Rab3 proteins, especially Rab3A, are the most abundant of the GTP-binding Rab proteins in the brain. They regulate general intracellular transport and are found on synaptic vesicles. Initial clues about the importance of Rab3 proteins in exo-endocytosis was found when it was discovered that they undergo a cycle of vesicle association-dissociation that parallels exo-endocytosis (Fischer von Mollard et al., 1991). They are attached to synaptic vesicles in the GTP-bound state via covalently-linked geranylgeranyl moieties. After Ca^{2+}-triggered fusion, Rab3A binds to a GDP-dissociation-inhibitor that, by utilising the GTP, dissociates it from the vesicle. This cycling of Rab3A probably has important implications if the finer aspects of synaptic function like synaptic plasticity and memory (Thakker-Varia et al., 2001; Ring et al., 2006).

Synaptic vesicle protein 2 (SV2) is a conserved membrane glycoprotein specifically localized to SVs and neuroendocrine secretory vesicles. The three homologous SV2 isoforms (SV2A, SV2B, and SV2C – 60-80% homology) found in mammals contain 12 potential transmembrane domains, with cytoplasmic N- and C-termini and a large glycosylated loop that protrudes into the vesicle lumen – this loop gets exposed to the extracellular environment upon vesicular fusion (Bajjalieh et al., 1994). The N-terminal half of SV2 shows considerable

homology to a family of eukaryotic carbohydrate transporter proteins, while the C-terminal shows homology to neurotransmitter transporters. The antiepileptic drug, Levetiracetam, has been shown to specifically bind to, and modulate, the function of SV2A (Lynch et al., 2004; Lambeng et al., 2005; Matveeva et al., 2008). The major isoform SV2A, and to a lesser extent SV2B, is widely distributed in the CNS, in peripheral NMJs and in neuroendocrine cells; SV2C has a more unique and restricted pattern of distribution (Bajjalieh et al., 1994). Phenotypically, SV2A and SV2A/SV2B knockout mice exhibited severe seizures and died after birth; the electrophysiological consequence of this deletion was the accumulation of presynaptic Ca^{2+} during consecutive action potentials (Janz et al., 1999). While evidence points to SV2 being a Ca^{2+} transporter in synaptic vesicles, this has not yet been fully corroborated (Xu and Bajjalieh, 2001).

Many other proteins play essential roles in synaptic neurotransmission. Munc13, Rab3-interacting molecule, ELKS/Rab3-interacting molecule, α-liprins, synapsins, sec6/8 tethering complexes, SNAP-25-interacting proteins such as SNAPin and SNIP, synapsins and synaptophysin are just a few of them (Sudhof, 2000, , 2004).

Despite the huge amount of knowledge and experimental data that has accumulated on all these different molecular actors at the synapse, a complete and final picture of evoked vesicle exocytosis and recycling has yet to emerge.

1.4. Etiology and clinical symptoms of human botulism

Botulism is a group of related neuroparalytic diseases caused by the action of neurotoxins produced by the anaerobic bacillus, Clostridium botulinum.

This group of gram-positive, spore-forming bacteria produces one of the seven antigenically distinct neurotoxin serotypes - /A, /B, /E, /F, /C1, /D & /G (Brin, 1997; Dolly and Aoki, 2006). Of these, the first four are implicated in human disease (Sobel et al., 2004) and types /C1 and /D are known to cause similar paralytic conditions in other mammals and birds; type /G is not known to cause any human or animal disease. While rare, some strains of C. butyricum and C. baratii have also been known to produce type /E and type /F, respectively (Simpson, 2004).

The clinical manifestation of botulism, derived from the Latin word for sausage - 'botulus', was first described by the German physician and poet, Justinus Kerner in early 19th century Würrtemberg. The isolation of the Clostridium bacilli and the discovery of its association with the clinical condition of botulism was achieved by Emil Ermengem in Belgium in 1895 (see (Erbguth, 2007) for a more detailed history of botulism). Botulism presents in humans as an acutely developing, symmetric flaccid paralysis that starts usually in cranial nerves and manifest within 18-36 h as diplopia, dysphagia, slurred speech and dryness of the oral mucosa (CDC, 1998; Cherington, 1998; Shapiro et al., 1998; Cherington, 2004; Sobel, 2005). The paralysis then progresses to respiratory muscles, upper and lower limbs and, if untreated, this ultimately leads to respiratory paralysis and death (Arnon et al., 2001). Type /A causes the longest lasting paralysis in humans, mice and rats (Sloop et al., 1997; Dolly, 2003; Foran et al., 2003; Meunier et al., 2003) and is responsible for more than half of all reported human cases in the US. The minimal lethal dose of the toxin varies from less than a microgram in adults to nanograms in infants (extrapolated from

primate studies); type /A, which is the most potent serotype, has a LD_{50} of 0.001 µg/kg (Arnon et al., 2001; Arnon et al., 2006). Botulism can be contracted by ingestion of neurotoxin contaminated food (food botulism), ingestion of Clostridial spores by infants (infant botulism) or by direct bacterial infection of wounds (Shapiro et al., 1998; Sobel et al., 2004). While food-borne botulism is now seldom found, it is an important public health emergency, especially in poorer countries, due to the explosive epidemic nature of occurrences. This form of transmission results from the ingestion of food containing preformed toxin. With the advent of scientific food processing techniques, the most common cause of botulism in rich countries is infant botulism. This is caused by the ingestion of Clostridial spores, which due to the low acidity of gastric mucosa in infants pass unscathed, colonise the intestines and release the toxin after a short germination. While this form of botulism is predominantly found in infants less than 1 year old, it can also rarely be seen in individuals suffering from a natural or iatrogenic deficiency of gastric acid secretion. In general, while botulism is now a relatively rare cause of mortality, the toxin's exquisite potency and lethality means that it poses a considerable threat as a bio-weapon (WHO, 2002).

The closely related Clostridial toxin, tetanus neurotoxin (TeNT), is produced by Clostridium tetani and causes the disease tetanus. First identified by Kitasato, the spores of this strict anaerobe are widely distributed in nature. Upon entry into wounds, the spores germinate, grow and produce TeNT. Following lysis of the bacilli, the released TeNT causes spastic paralysis characteristic of tetanus and which can lead to death, indirectly, from

exhaustion or respiratory/cardiac failure (Schiavo et al., 2000). Tetanus is far more common, and more easily recognised in its milder forms, than botulism. Despite the development of a very efficacious vaccine, tetanus still claims many lives, especially in under-developed countries (Galazka and Gasse, 1995).

The common pathophysiological mechanism underlying the paralytic activity of all these toxins is the irreversible blockade of ACh exocytosis by proteolytic cleavage of one of the three SNARE partners essential for productive fusion of synaptic vesicles at the peripheral neuro-muscular junctions (Schiavo et al., 1993c; Schiavo et al., 1993d; Schiavo et al., 1993b; Schiavo et al., 1995; Verderio et al., 2006) (Described in detail in Section. 2. See also Figure 7. See Dolly et al., 2008 for a detailed review).
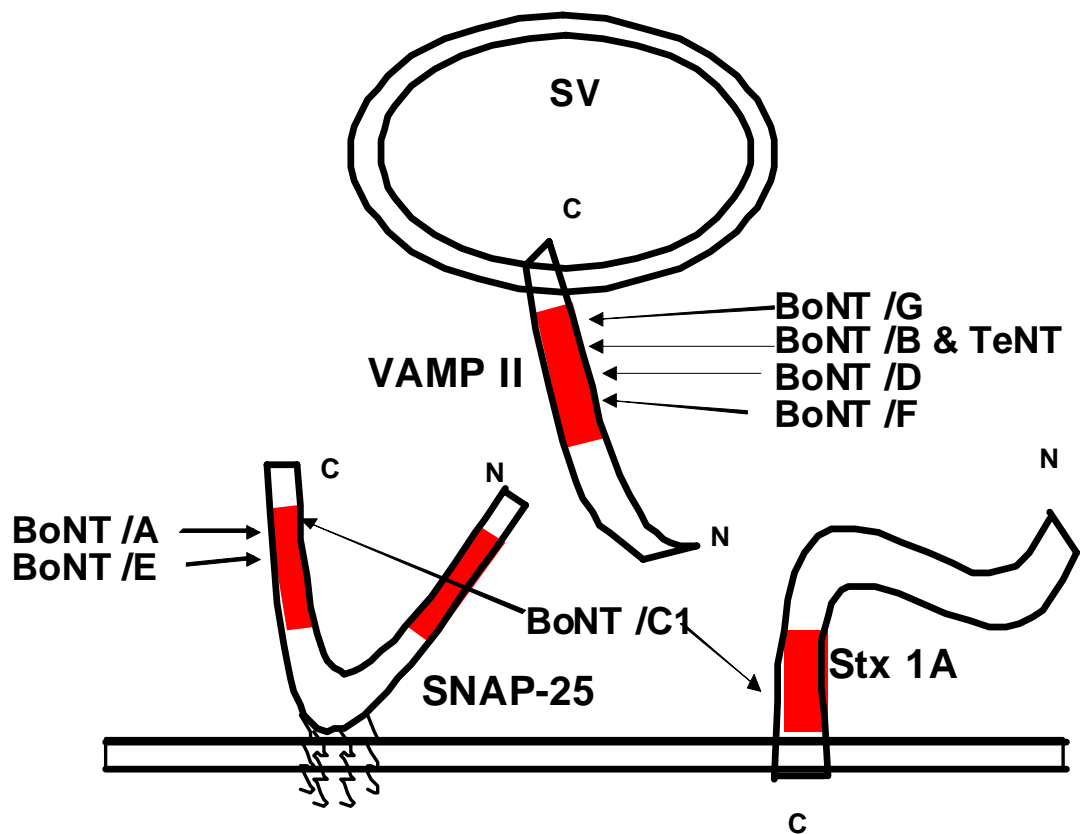
Fig. 7: CNTs inhibit exocytosis in neurons by site-specific cleavage of SNAREs. The SNAREs affected by CNTs are shown in this schematic, with the proteolytic cleavage sites for the different toxins indicated by arrows (BoNT /A, /E and /C1 cleave SNAP-25; BoNT /B, /G, /D, /F and TeNT cleave VAMP II and BoNT /C1 cleaves Stx). The SNARE core domains on the different proteins are indicated in red. N and C refer to the terminals of the different proteins, SV is the synaptic vesicle, P is the plasma membrane and the squiggles represent the palmitoyl groups on SNAP-25.

1.5. Viral vectors for gene therapy

Mammalian post-mitotic neurons are by their very nature incapable of replicating to provide substitutes in case of death or injury of existing neurons. In addition, the extensive macro- and microscopic axo-dendritic network, built up slowly over the life of the animal and which defines the functional capacity of every neuron, cannot be reproduced with other advanced therapies like introduction of stem-cell based substitute neurons. Therefore, a direct approach to manipulate gene expression in the mammalian neurons can lead to the development of novel therapies to treat neurodegenerative diseases or to repair physical, chemical, toxicological, bacterial and even viral injuries in them. This also offers new approaches to probe the patho-physiological basis of neural disorder and to identify new molecular targets for intervention.

Two of the most promising candidates for the role of neuronal gene delivery vectors are the non-enveloped Adeno-Associated Viral vectors (AAVs) and lipid enveloped Lentiviruses (LVs). These vectors, derived from common human viral pathogens, have an outstanding safety profile, show relative ease of production, have been engineered to have a broad tropism and have defined, minimal, genomes. They differ in their transfection rates, target specificity and the timescale and efficiency of transgene production (Kay et al., 2001) (See Table 1 for a comparison of the properties of the two main viral vectors used in gene therapy).

Viruses have evolved efficient strategies over millions of years of

evolution for transferring genes essential to their function and reproduction into mammalian cells. Harnessing this capability, while eliminating their deleterious features has yielded viral vectors that can act as agents for gene delivery for the introduction and expression of genes encoding therapeutic proteins. They can thus be used to rectify phenotypes induced by known genetic mutations or to counteract progressive neurological diseases by introduction of known protective genes. To be useful, viral vectors needs to be replication-deficient (to limit the gene expression in the area of interest and to eliminate cell death that is the usual consequence of replication), non-immunogenic (to prevent the host immune system from mopping up all the introduced viral vectors and to prevent the immune-mediated culling of transfected cells) and non-toxic (by the elimination of non-essential and deleterious proteins found in the viral genome), while still retaining their capability to deliver genetic material to the nucleus of a target cell (thereby ensuring continuous expression of necessary proteins without the necessity of repeated administration). But, an ideal vector system is a difficult task to engineer and all currently used ones involve compromises in one or the other facet. The early candidate vectors used for gene therapy, herpes-virus and adenoviral vectors, contained large fragments of their native genome, expressed non-essential and toxic/immunogenic viral proteins and suffered from immunogenicity and neuronal toxicity. Also, they were occasionally found contaminated with native, and replication-competent, viruses or could recombine with those wild-type viruses that can be often found naturally infecting mammals (Davidson and Breakefield, 2003).

Viral vectors bind to specific receptors on the target cell surface and

undergo internalisation. Non-enveloped, capsid shrouded viruses harness the host cells receptor-mediated endocytosis pathways. Upon endosomal acidification, the capsid breaks down and the DNA or RNA released into the cytoplasm, binds to nucleus-seeking proteins and the genetic material is delivered into the nucleus through the nuclear pore. Some of the capsidated viruses might be transported along the cytoskeleton before nuclear delivery. On the other hand, enveloped virions usually undergo membrane fusion at the cell surface or in endosomes, depending on the nature of the envelope . While there are neurotropic viruses, e.g., herpes, rabies and polioviruses, that specifically bind to pre-synaptic terminals and undergo retrograde transport into neuronal cell bodies, they have their own drawbacks like enhanced toxicity and immunogenicity, The natural binding processes can be exploited to redirect viral tropism by introducing receptor ligands into capsid proteins, by exchanging capsid/lipid-glycoprotein proteins between serotypes, or by using bi-functional neurotoxins or neuron specific antibodies that bind both to the virus and presynaptic targets (e.g., capsid proteins of AAVs and the lipid envelope glycoproteins of lentiviruses) (Schaffer et al., 2008).

Feature	AAV	Lentivirus
Packaging capacity	Low, ~4.9 kb	High, ~8 kb
Host range	Very broad, infects neurons and glia	Very broad, infects neurons and glia
Long-term expression	Yes	Yes
Genomic integration	Yes, 19q11	Yes, random
Bio-safety	Very-high	High, esp. later generations
Size	20-25nm	~100nm
Yield/Titer	Very high	High
Cellular entry	HSPG + co-receptor; receptor-mediated endocytosis	VSV-G mediated fusion of virus followed by entry of genomic content and core
Oncogenesis risk	No (very low)	Yes (depends on MOI and cell type)
Replication competent virus risk	No	Minimal
Immunogenicity	Low	Very low
Envelope	Protein	Lipid with proteins embedded
Retrograde transport	Yes (In CNS and from periphery)	Yes (In CNS, periphery unknown)
Expression onset	Slow	Faster
Purity	Very high	High

Table 1: Comparison of AAV and LV gene delivery systems. (HSPG: Heparan sulphate proteo-glycan)

A
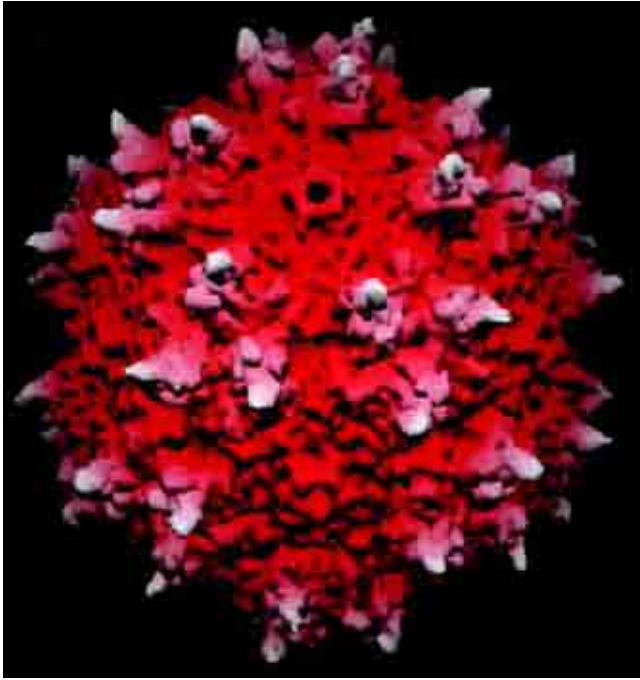
B
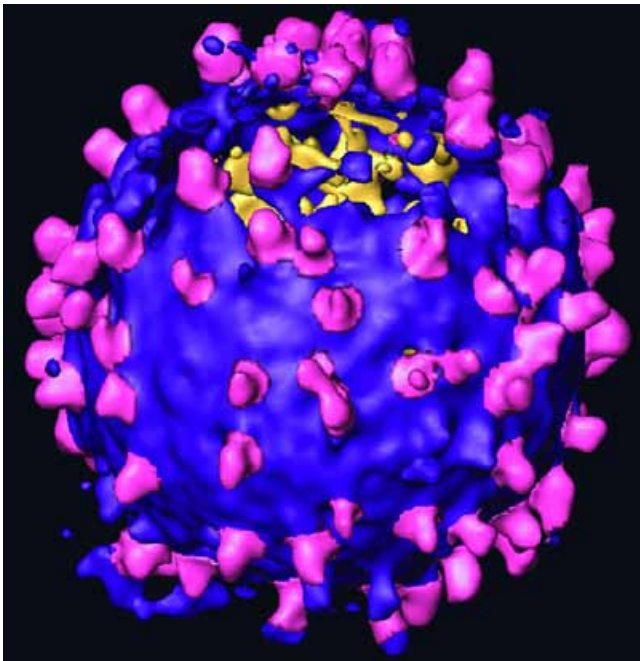
Fig. 8: AAV and LV structure **A:** Computer generated surface topology map of AAV-2. The generated view is colored according to the distance from the center of the AAV. Adapted from (Xie et al., 2002). **B:** Computer generated surface topology map of a model retrovirus. This is a surface rendered tomogram of an individual virion. Proteins on the lipid membrane are represented in magenta and the lipid surface of the virus is shown in purple (Some discontinuities are seen in the lipid membrane exposing the yellow interior). Adapted from (Forster et al., 2005).

1.6. Model systems used to study botulism and to assess the efficacy of various therapies

The gold standard to assess the effects of CNTs is their natural target, the cholinergic NMJ. *In vivo* murine model systems accurately mimic the physiological and anatomic effects of CNT intoxication. But due to the difficulties inherent in this system i.e., the limited amount of tissue and the need for large number of animal subjects, necessitated the use of other *in vitro* and *ex vivo* models systems. The *in vitro* models – protease assays with purified SNAP-25 substrates and permeabalised cell preparations - were used to study enzymatic activity of natural and modified BoNT/A, /E and /C1 on susceptible and cleavage-resistant SNAP-25. These systems, enabled and accurate and high-throughput measurement of the relative cleavage resistance of SNAP-25 mutants and of the innocuousness of toxin mutants. *Ex vivo* models – using bovine chromaffin cells and rat cerebellar granule neurons or mouse hemi-diaphragms – enabled a more physiological measure of the effectiveness of viral delivery of cleavage resistant SNAP-25 genes or of the binding, internalisation and SNARE-cleaving properties of native and mutant BoNT toxins and chimeras. Finally, the benchmark *in vivo* models for studying the effects of toxins and efficacy of the counter-acting therapeutic strategies - mouse LD_{50}, rat/mouse digit abduction scoring and efficiency of neuromuscular transmission (ENT) in rat soleus – enabled a near-accurate mimicking of clinical botulism.

1.7. Principal goals of this study

A major challenge facing gene therapy for motor neuron disorders ‒ a group of rare yet debilitating and ultimately fatal diseases affecting spinal motor neurons ‒ is targeted, minimally-traumatic delivery. Due to the limited number of motor neurons (e.g. rat sciatic nerve has only ~2000 efferents) (Nicolopoulos-Stournaras and Iles, 1983), insults that are merely sub-lethal in other cells can be extremely deleterious (e.g. in superoxide-dismutase mutant mice, which ubiquitously express the damaged protein, motor neurons are the most affected (Bruijn et al., 2004)). Their anatomical structure, with a relatively inaccessible cell body in the spinal column and an elongated axon, complicates therapies including gene transfer by viral vectors. Those that transfect motor neurons (Adeno-associated, Lenti and Herpes viruses) do so most efficiently when in direct contact with the cell body (Mannes et al., 1998). As intra-spinal injection is difficult under clinical conditions, the use of peripherally-deliverable vectors would be desirable; moreover, such an advance requires a model that allows accurate measurement of the graded improvements currently achievable.

An ideal system to evaluate such therapies is the blockade of neuromuscular transmission by botulinum neurotoxin type A (BoNT/A), by specific cleavage of SNAP-25. This toxin is also implicated in the clinical cases of botulism, which, while relatively rare, is a serious condition with no known pharmacological therapies. While some prophylactic vaccines do exist to combat botulism, they are increasingly out of favour due to the recognised therapeutic application of BoNT/A and /B for a variety of neuromuscular

conditions. Furthermore, they only confer a limited period of protection, are not licensed for use in the general population and are ineffective after exposure to the toxin (Shapiro et al., 1998). Anti-toxin serum, especially those generated in humans against multiple toxin serotypes (human botulism immune globulin), is a valuable aid if administered within 24 h of exposure in infants preventing further deterioration of the exposed patient's condition and shortening the duration of hospitalisation, esp. the amount of time spent on mechanical ventilation (Tacket et al., 1984; Arnon et al., 2006). Unfortunately, these anti-toxins have very limited utility after the initial 24 h due to the intracellular action of the toxin's LC and are complicated by factors such as hypersensitivity, for the equine anti-serum (Black and Gunn, 1980), and the currently limited applicability, of the human anti-serum, for any outbreaks in adult populations. The ineffectiveness of current treatments in combating botulism necessitates the development of a refined therapy with the ability to abrogate the prolonged convalescence, high mortality and morbidity associated with this condition. The finding that protection from BoNT/A mediated exocytotic blockade can be achieved by expression of a toxin-resistant S25 mutant gene was an important step in realising this goal (O'Sullivan et al., 1999). Thus the twin goals of developing efficient gene transfer tools to motor neurons and of finding novel therapies for botulism can be simultaneously considered (See fig. 9).

In this study, neuromuscular paralysis by BoNT/A was attenuated using Adeno-associated (AAV) vectors that give long-term expression of a cleavage-resistant S25 mutant (S25-R198T), having all the properties of the wild-type including ability to substitute for truncated S25 and recover exocytosis in

intoxicated chromaffin cells (O'Sullivan et al., 1999). AAV vectors provide an efficient and relatively safe way to ensure prolonged expression of genes in neurons (Burger et al., 2005), and botulism in rats provides a much more valid model for evaluating this gene therapy. Injection of AAVs encoding S25-R198T into the spinal anterior horn innervating the soleus muscle protected neuromuscular transmission from subsequent inhibition by BoNT/A. Moreover, muscles treated in this way showed a decreased amount of nerve sprouting compared to unprotected controls. Finally, administering the therapeutic AAVs directly into the soleus muscle resulted in their retrograde transport to motor cell bodies and a consequential reduction of BoNT/A-mediated blockade of neurotransmission at peripheral synapses. These findings provide the first evidence for the potential applicability of gene therapy to the intractable problems posed by botulism and, possibly in the longer-term, genetic disorders of motor neurons.

The specificity of BoNTs and TeNT for NMJs makes their non-toxic derivatives valuable as transporters for the delivery of therapeutic agents into the motor-neurons (Johnstone et al., 1990). Steps in this direction have been taken through the production of recombinant toxins in which the protease site has been inactivated to create variants that are still able to undergo binding, internalisation and translocation at cholinergic motorneurons (Zhou et al., 1995). The utilisation of such 'cholinergic transporter' molecules might be useful in targeting viral vectors for the prevention of conditions affecting motor neurons. For this purpose, the dichain form of BoTIM was utilized. This has been shown to be essential for productive uptake into motor nerve endings (Dolly et al.,

1994; Daniels-Holgate and Dolly, 1996) while yielding more efficient internalisation than can be achieved with HC alone (Bade et al., 2004). The creation of a core-streptavidin-BoTIM/E chimera (CS-BoTIM) with the targeting properties of BoTIM and the biotin binding properties of CS should yield a versatile molecule that could be attached to biotinylated cargo in the desired stochiometry (Pahler et al., 1987; Sano et al., 1995). The CS-BoTIM also offers the advantage of a smaller conjugate, ease of production, control of positioning of the attachment site and attachment to a single biotin molecule. BoTIM was conjugated at the genomic level to a monomeric streptavidin domain – the minimal streptavidin core (12-16kDa) was cloned into the N-terminus of the His_6BoTIM single chain gene, expressed in *E.coli* and the resultant CS-BoTIM purified using a Ni-NTA column. Retention of neuronal targeting ability by CS-BoTIM was tested after application to rat CGNs and HEK-293s in culture; immuno-histochemical visualization of stronger binding to the former confirmed the neuronal preference of binding. Application of active BoNT/E, conjugated as before to CS at the genomic level, resulted in SNAP-25 cleavage and exocytotic blockade, confirming the binding, internalisation and release of LC.

The next refinement of the gene replacement methodology involved the attempted targeting of lentiviral vectors to neurons by availing of the unique selectivity of CS-BoTIM. This potentially opens up routes of peripheral administration due to the therapeutic becoming concentrated on to the pre-synaptic membrane at the NMJ. Such a targeted virus would have a huge number of applications not just in the treatment of botulism but, also, in hereditary motor neuron diseases (e.g. spinal motor atrophy, amyotrophic

lateral sclerosis) and those caused by viruses, physical and biochemical trauma. A second-generation LV system was exploited to create high titer viruses expressing GFP, which were later biotinylated with a reducible linker interface. Proof of principle for this exciting new strategy was obtained by the successful coupling of the CS-BoTIM protein to the viral vectors, followed by their later application onto CGN and HEK-293 cells. To determine optimal coating conditions, CS-BoTIM was mixed with different ratios of the test and control viruses in order to generate viral particles coated with the targeting agent. The optimally coated viruses, preferentially binding to neuronal terminals, showed a reduction in their promiscuous infectivity to HEK-293 cells, with only a small attenuation of their natural neuronal infectivity.

These devised tools and therapies, targeted initially at botulism, should provide a strong foundation for the later development of sustained motor neuron gene therapies applicable centrally or peripherally.
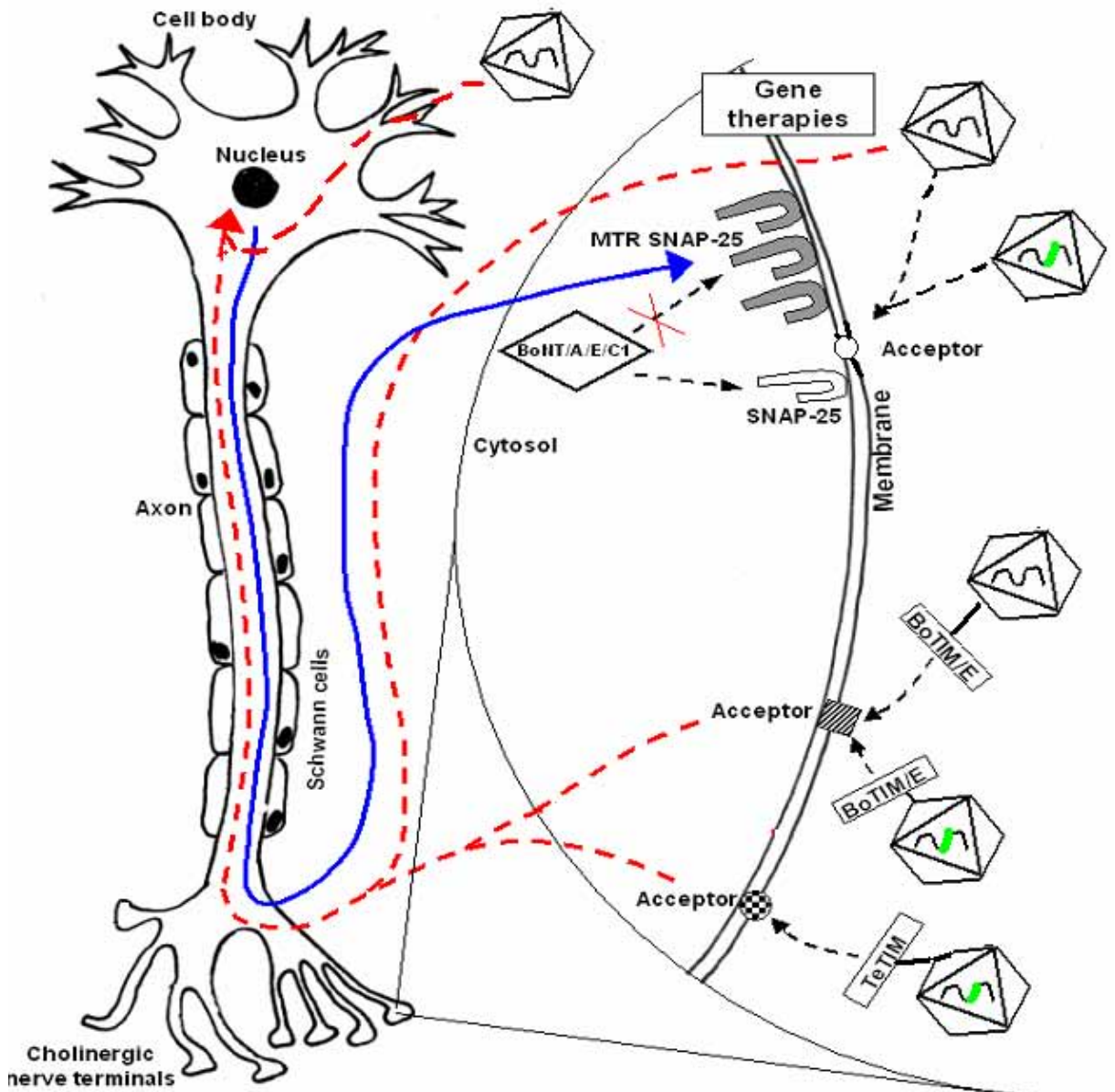
Fig 9: Overview of gene therapy against botulism. A motor neuron, with its nucleus, dendrites, axons and cholinergic terminals is represented here. The hexagonal structures represent viral vectors, clear J-shaped structures - native SNAP-25, shaded J-shaped structures – multi-toxin-resistant SNAP-25 (MTR) and labelled boxes attached to viral particles – targeting agents and the green genomes – specific promoter. The dotted red line represents the path of the virus to the MN nucleus and the solid blue line the path of the SNAP-25 protein. The virus can be delivered spinally or peripherally (in which case it has to undergo retrograde transport). Once in the host nucleus, the viruses start producing cleavage-resistant SNAP-25 mRNA, and thus the protein. Once the MTR SNAP-25 protein is transported down to the cholinergic terminals, they can no longer be inactivated by the introduced CNTs (BoNT A/ E /C1). Thus the treated terminals are able to retain exocytotic activity, in the face of a later challenge with these CNTs, or can retain activity quicker, in the case of a prior treatment with these toxins. Further refinements can be introduced by the addition of targeting molecules (BoTIM/E or TeTIM) and/or by the addition of a cholinergic/neuron-specific promoter.

66

2. Attenuation of BoNT-induced blockade of exocytosis at peripheral NMJs by viral vector mediated gene transfer into spinal motor neurons

The characteristic symptoms of botulism are caused by the BoNT-mediated blockade of neurotransmission in cholinergic nerve terminals, especially NMJs. The processes involved in blockade of neurotransmitter release by Clostridial neurotoxins involve – targeting to the NMJ, binding, internalisation, translocation of light chain to the cytoplasm and, finally, proteolytic cleavage of the requisite SNAREs. The Clostridial neurotoxins share many properties and, upon entry into the bloodstream, target to pre-synaptic nerve terminals. The HCs mediate selectivity by targeting to high-affinity membrane ecto-acceptors located exclusively on cholinergic (motor/autonomic) nerve endings (Dolly et al., 1984a; Black and Dolly, 1986b; Black and Dolly, 1987; Daniels-Holgate and Dolly, 1996). Upon uptake into the target vesicles, the heavy chain helps form a transmembrane pore which allows the light chain to escape into the cytoplasm. Upon intracellular entry, the light chains cleave a defined member of the SNARE family and cause an inhibition of evoked exocytosis (Schiavo et al., 1993a; Schiavo et al., 2000) (The targets and the cleavage sites are described in detail in Section. 1.3). When the rate of synthesis of the new SNARE molecules and/or turnover of the handicapped

SNAREs overwhelms the enzymatic activity of remaining BoNT, normal neuromuscular transmission returns (de Paiva et al., 1999).

2.1.1. Trafficking of Clostridial neurotoxins (CNTs) to their site of action

The Clostridial bacilli producing the different BoNT toxins are quite fastidious anerobes; the growth conditions vary between different serotypes and are sensitive to changes in temperature, pH and oxygenation. Therefore, the usual method of contact with the toxin is through consumption of contaminated food, which already contains previously produced toxin. As the BoNTs are sensitive to the harsh proteolytic conditions found in the gastric lumen, they are packaged with other non-toxic proteins, which protect a proportion of toxin until it reaches the small intestine. Those that protect and contain BoNT/A can be purified as 19 S, 16 S, or 12 S stable complexes. The non-neurotoxic components consist of non-hemagglutinins, with M_r ~120 kDa, and hemagglutinins, consisting of a combination of five different proteins of 52, 35, 20, 19, and 15 kDa (Inoue et al., 1996). In the small intestine, the slightly alkaline pH causes dissociation of the toxin complexes and the free neurotoxin undergoes transcytosis across intestinal epithelial cells and reaches the bloodstream.

The process of migration of CNTs to the extra-cellular space surrounding the NMJ has not yet been completely characterised – a journey that takes the toxin molecule across capillary endothelial and basal laminar barriers while, presumably, evading the body's immune and scavenging systems and

simultaneously preserving its activity for the final target. The clinical importance of this migratory stage, especially in relation to prophylactic treatments such as vaccination or injection of antibodies, is discussed later. Such is the exquisite specificity of the toxin to NMJs that, at physiological doses, the only effect of the toxin is the perturbation of neuromuscular transmission – despite the ready presence of potential substrates in non-neuronal secretory cells. Indeed, in cultured neuroendocrine cells which share the same SNARE targets as the NMJ, permeabalisation or treatment with non-physiological buffers is necessary for the uptake of the toxin. Once near the pre-synaptic motor terminals the toxin undergoes a series of steps that culminates in the delivery of the LC protease to near the SNARE targets. For BoNTs, this process can be divided into a three step model – binding and internalisation of the holo-toxin, pore formation by the HC and, finally, translocation of the LC into the cytoplasm (Dolly et al., 1992; Verderio et al., 2006; Brunger et al., 2007; Fischer and Montal, 2007a, 2007b) (See fig. 10).

The evidence accumulated points to a "dual-receptor", "dual-affinity" mode of entry of BoNTs. The "double specificity" conferred by such an ecto-acceptors can help in explaining the CNT's remarkable specificity for NMJs. Gangliosides, especially the sialylated glycosphingolipids containing N- and O substituted neuraminic acid residues, are hypothesized to act as an intial, accumulatory, ecto-acceptor component for CNTs. The accumulated CNTs then bind to specific protein receptors on the pre-synaptic terminal surface and undergo endocytosis. These two ecto-acceptor families are the most probable candidates for the physico-chemically determined, low–affinity (e.g.:

synaptosomes: K_d ~26 nM, B_{max} ~7.5 fmol/mg protein; presynaptic plasma membrane: K_d ~30 nM, B_{max} ~52 fmol/mg protein for labelled BoNT/A in electric organ of Torpedo) and high-affinity (e.g.: synaptosomes: K_d = 0.11 +/- 0.03 nM, B_{max} = 50 +/- 10 fmol/mg protein; presynaptic plasma membrane: K_d = 0.2 +/- 0.05 nM, B_{max} = 150 +/- 15 fmol/mg protein for labelled BoNT/A in electric organ of Torpedo) receptors (Dolly et al., 1984b; Blasi et al., 1992; Daniels-Holgate and Dolly, 1996).

The ganglioside-binding part of the theory is now well established (See (Simpson and Rapport, 1971; Nishiki et al., 1996; Bullens et al., 2002; Dong et al., 2003; Rummel et al., 2004a; Mahrhold et al., 2006; Rummel et al., 2007) and is reviewed in (Verderio et al., 2006)). The importance of gangliosides on acceptor membranes for the uptake of BoNT and TeNT was confirmed when it was shown that pre-incubation with ganglioside G_{T1} inhibited their uptake in chromaffin cells (Stoeckel et al., 1977), while pre-treatment of cells with the polysialogangliosides G_{D1a}, G_{T1b} and G_{D1b} enhanced the toxin-mediated blockade of exocytosis (Marxen et al., 1991). Also, ganglioside depletion in neuroblastoma cells impairs BoNT/A internalization, treatment with neuraminidase decreases BoNT binding and knockout mice defective in a-series and b-series ganglioside production showed highly reduced sensitivity to BoNT/A and BoNT/B (lacking the complex gangliosides G_{M1}, G_{D1a}, G_{D1b}, G_{T1b} and G_{Q1b} because of disrupted $\beta_{1,4}$-N-acetylgalactosaminyltransferase (G_{M2}/G_{D2} synthase; EC 2.4.1.92) gene) (Bullens et al., 2002, , 2003; Kitamura et al., 2005). The current understanding is that polysialogangliosides, richly distributed on the presynaptic motor nerve terminal, bind BoNTs HC_C, a sub-domain which

shows a high degree of homology to the carbohydrate-binding domain found in plant lectins; BoNT/A and /B has been shown to bind G_{T1b} through a conserved H···SXWY···G peptide motif in this region (Poulain et al., 1989; Miller et al., 2008; Stenmark et al., 2008; Tsukamoto et al., 2008) while binding property of BoNT/C to G_{D1b}, and G_{T1b} and BoNT/D to phosphatidylethanolamine has also been shown to reside in the HC region (Tsukamoto et al., 2005).

However, and complicating matters quite substantially, these same studies showed that ganglioside-binding is not an essential, or the only, pre-requisite for toxin uptake, since the amount of inhibition obtained was not complete when antagonising just the ganglioside part of binding (Stoeckel et al., 1977; Marxen et al., 1991). In addition, neuraminidase treatment of chromaffin cells did not completely abolish CNT activity and ganglioside knockout mutants were still capable of being paralysed by BoNT/A and TeNT, albeit at a far slower rate (Kitamura et al., 1999; Kitamura et al., 2005). So, ganglioside binding alone cannot completely explain the specificity of BoNTs for the cholinergic motoneurons. The best studied protein receptor candidates are Syts and SV2. Studies have shown that binding of BoNT/B to Chinese hamster ovary and PC12 cells is dependent of expression of Syt2 (Dong et al., 2003). *In vitro* pull-down assays have also shown that BoNT/B and /G interact with Syt1 and Syt2 and pre-treatment with peptide fragments corresponding to the luminal domains of these proteins can inhibit toxin-mediated blockade in mouse hemi-diaphragm assays (Rummel et al., 2004b). The binding to BoNT/B was activity dependent, hinting at the luminal region being involved. Truncation analysis of Syt2 revealed that residues adjacent to the transmembrane domain, amino

acids 40–60, are critical for toxin binding. Interestingly, Syt2 binds to gangliosides through residues 61-267, thereby linking the initial binding of CNTs to sialogangliosides and the later binding to Syt2 (there is a high homology between Syt1 and 2 in these regions (Dong et al., 2003)). This finding also explains the frequent finding that CNT uptake in neurons is activity-dependent; the luminal domain of Syt will only be exposed upon fusion of SVs. The dual-receptor hypothesis for CNTs in general and BoNT/B and /G in particular, has been further established by mutation studies that showed a strong and, sometimes, near-complete inactivation of the toxin's activity *in vivo* upon introduced changes in the putative binding regions (Rummel et al., 2007).

The protein receptor for BoNT/A has also been recently identified – the intra-vesicular luminal domain, L4, of SV2 has been shown to be critical for BoNT/A binding (Dong et al., 2006). Proof for this specific interaction has been obtained by pull-down assays with fragments of SV2 (L4- 529-566AA) and by competition assays. BoNT/A binding to hippocampal neurons cultured from SV2B$^{-/-}$ mice was reduced by 28%, by 53% in SV2A^{+}/-SV2B-/- mice and binding was almost completely abolished in SV2A$^{-/-}$SV2B$^{-/-}$ mice (Dong et al., 2006). Uptake was restored by the expression of SV2A in SV2A/2B double knock-out mice. BoNT/A was also shown to bind the least prevalent SV2C isoform as well; indeed, its reported affinity was higher than that for SV2A or 2B (Mahrhold et al., 2006).

Once the ganglioside-protein-receptor-toxin complexes form, they undergo receptor mediated endocytosis, most probably involving clathrin-coated vesicles (the energy- and temperature-dependent uptake of these neurotoxins

is discussed in (Dolly et al., 1984a; Black and Dolly, 1986b, 1986a)). The onset of neuroparalysis induced by CNTs can be shortened under condition of increased SV recycling, a process that is intimately connected with SV fusion [Dolly >>]. While the H_C domains of CNTs have been shown to be essential and sufficient for the internalization into vesicles (Lalli et al., 1999), it is not yet known if they, or other parts of the CNTs, in any way influence the endocytotic process, or if they are mere passengers.

Once internalised, the vesicles containing the CNT-receptor complex are sorted in a TeNT- or BoNT-specific manner, leading to the distinct symptoms associated with each disease. While the cholinergic NMJ is the final target of BoNTs, TeNT undergoes retrograde transport back to the spinal cord, transcytoses across the synaptic junction and targets inhibitory glycinergic inter-neurons in the spinal cord; BoNT/A is >1000 fold more effective than TeNT in blocking release from the peripheral cholinergic nerve endings (Habermann et al., 1980), while the reverse is true at the inter-neurons (Habermann and Erdmann, 1978; Bigalke et al., 1985). The differential sorting of CNTs in the endosomes of NMJs could be a property of the protein/ganglioside receptor or due to a determinant on the HC. The former is supported by studies that show that TeNT co-segregates with p75^{NTR} while the latter model is supported by hybrid toxin studies which show that when the HC of BoNT/A is linked to the LC of TeNT, the hybrid has the binding and sorting features of BoNT/A (Poulain et al., 1991; Weller et al., 1991). The putative mechanism by which TeNT undergoes retrograde axonal transport into the spinal cord is described in the next section.
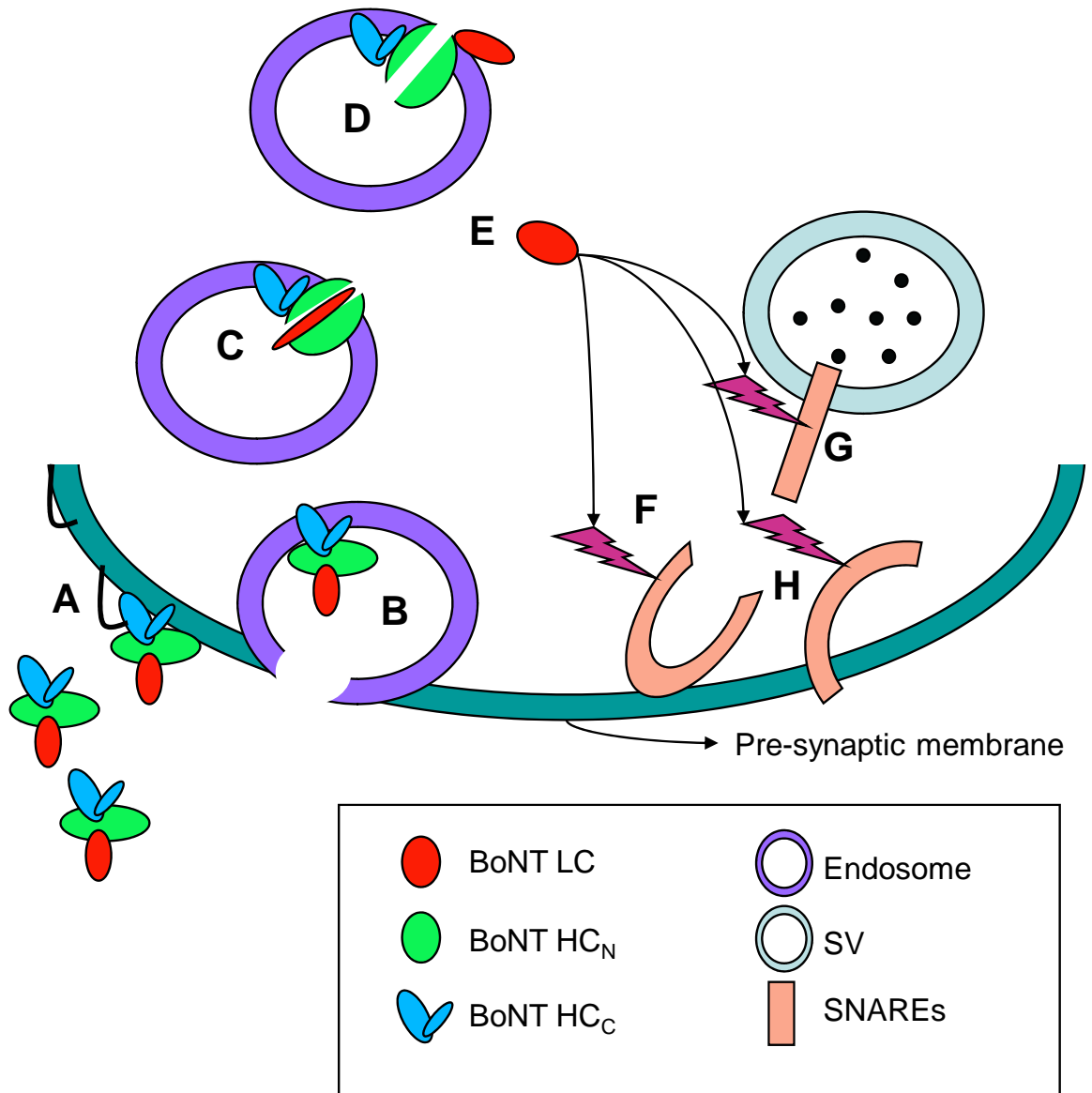
Fig. 10: Mechanism of action of BoNT. The different phases in BoNT action are schematically represented here. After initial binding to specific receptors (A), the holotoxin undergoes internalisation into endosomes (B). Upon endosomal acidification (C), the HC forms a pore through which the LC is extruded into the cytoplasm (D). The LC now targets its specific SNARE substrate, SNAP-25 (F), VAMP (G) or Stx (H).
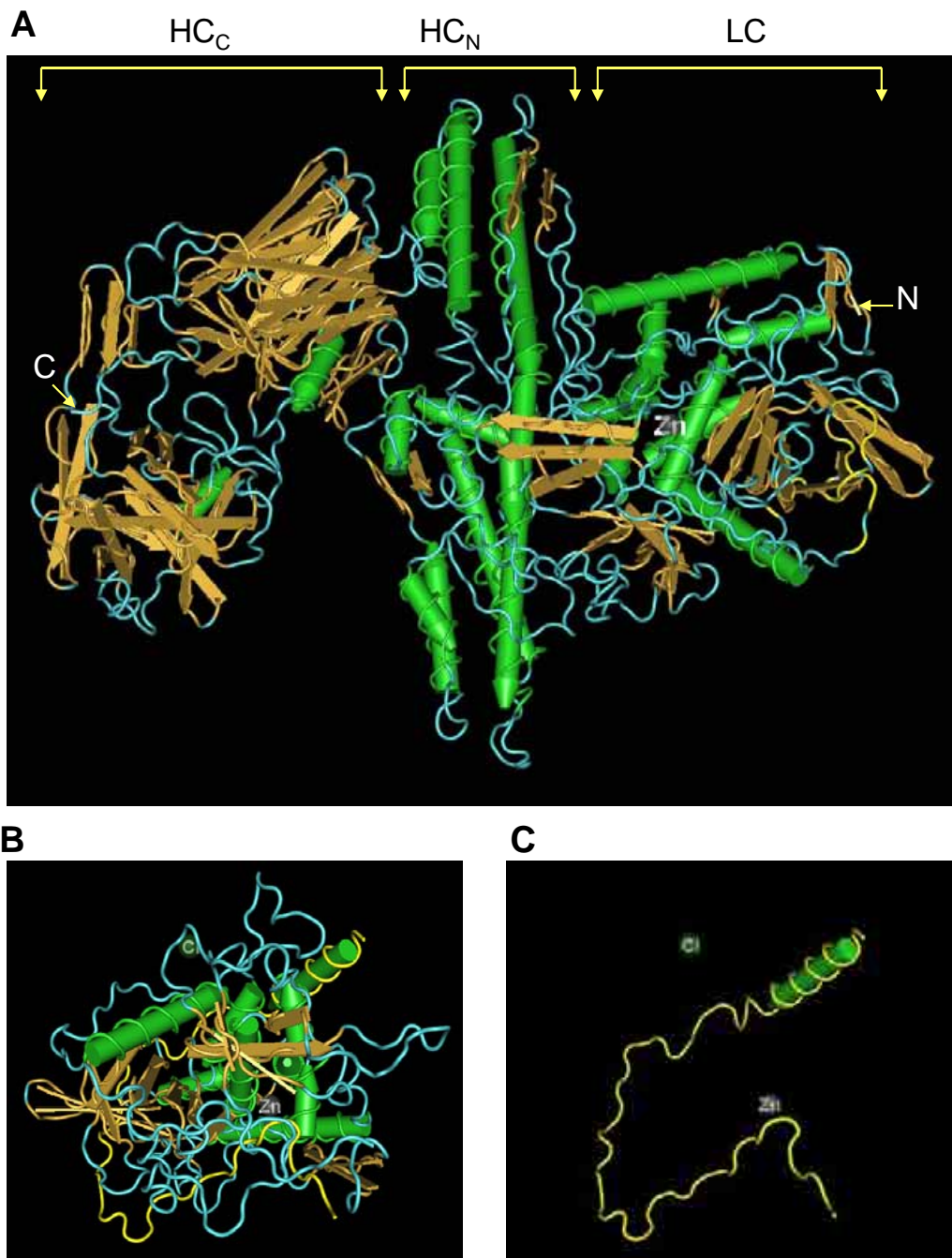
Fig. 11: Crystal structure of BoNT/A. **A:** A screen-shot of a Cn-3D rendering of the determined 3.3Å structure of BoNT/A holotoxin shows the different, biochemically identified, domains. At the C-terminus, comprising mainly of β-sheets, is the HC_C which is involved in specific binding to receptors on cholinergic terminals. This is followed by α-helix rich HC_N and the N-terminus LC. (β-sheets are in gold and α-helices are in green, with intermediate AAs in blue. Also seen is the Zn^{2+} ion at the catalytic site). **B and C:** Structure of BoNT/A LC bound to its SNAP-25 substrate. The complex inter-play between the different α and β exosites on SNAP-25 and the toxin's LC can been seen in this 2.1 Å structure. The LC is shown in gold (β-sheets) and green (α-helices) and the SNAP-25 substrate is shown in yellow (with one α-helix in green). Panel **B** shows both the LC and the substrate, while **C** shows only the substrate for increased clarity. Also seen are the Zn and Cl ions. Based on data from (Lacy et al., 1998) and (Breidenbach and Brunger, 2004).

Since the substrates for the CNTs are in the cytoplasm, the process of transfer of the LC into the cytoplasm is critical to their *in vivo* activity. Extensive clues about this process can be gained by studying similar processes involved in the entry of bacterial and plant toxins, like Shiga, Diptheria and Cholera toxins (Sandvig and van Deurs, 2005). This translocation requires the HC, is triggered by low vesicular pH and requires a reducing environment in the cytoplasm (Boquet and Duflot, 1982). The pH sensitivity of this process has been demonstrated by studies that showed abolition of the toxin's activity upon pre-treatment with drugs such as bafilomycin (inhibitor of the proton pump) or lysosomotropic drugs like chloroquin or methylamine (Simpson, 1982, , 1983; Lawrence et al., 2007). The H_N terminal of BoNT/A consists of two long amphipathic α-helical coil-coil domains, analogous to some viral proteins (Lacy et al., 1998; Lacy and Stevens, 1999). This amphipathic H_N domain of CNTs, exposed under low pH conditions, inserts into the endosomal membrane to form cation-selective conductance channels (Schmid et al., 1993). Simultaneously, the LC which is attached to the HC by a di-sulphide bridge, partially unfolds at low pH and slides into the pore formed by the HC. Upon contact with the reducing environment in the cytoplasm, the di-sulphide bond is reduced and LC liberated (Koriazova and Montal, 2003). If non-reducing conditions or holotoxins, with the LC and HC still attached, are used, the LC does not free itself upon insertion and continues to block the HC pore. Once in the cytoplasm, the free LC now refolds back to its native configuration. The process of translocation has been studied using electrophysiological tools in great detail in Neuro 2a neuroblastoma cells and reconstituted liposomes, mimicking the

natural endosomal environment (Montal et al., 1992; Fischer and Montal, 2007a, 2007b; Fischer et al., 2008). In such conditions, the HC forms channels which open in bursts interspersed between periods of inactivity. These channels are open at negative voltages and show a main conductance of 105 +/- 5 pS or 65 +/- 4 pS in 200 mM CsCl or NaCl, respectively (Fisher and Montal, 2006).

2.1.2. Proteolytic cleavage of specific SNAREs by the LC of CNTs

The protease activity of the CNTs resides in the LC and this alone can mediate the subsequent paralysis of neuromuscular transmission. Direct introduction of the LC, by permeabilisation (Ahnert-Hilger et al., 1989) or by liposomes (de Paiva and Dolly, 1990), results in cessation of synaptic exocytosis identical to that elicited by the whole molecule. The elucidation of the different CNTs amino-acid sequences and solving of their crystal structure, with or without their attached substrates, has enabled a deeper understanding of the mechanisms underlying their enzymatic activity. The LC sequences show a metalo-protease domain with a HExxH^{+}E consensus Zn^{2+}-binding site (Jongeneel et al., 1989; Kurazono et al., 1992). Three residues co-ordinate the catalytic Zn^{2+} in the active site (H222, H226 and E261) while E223 ensures its hydration (Lacy et al., 1998; Lacy and Stevens, 1999). The importance of Zn^{2+} was shown when its removal inactivated the toxin and prevented neuroparalysis (Schiavo et al., 1992b; de Paiva et al., 1993). The identity of their synaptic targets was first revealed when VAMP2 was shown to be the target for BoNT/B and TeNT (Schiavo et al., 1992c) (See section 1.3 for more details about the cleaved SNAREs and their cleavage sites. See also Figure 7). The identification

of critical SNAREs as targets for the different CNTs fits well with the electrophysiological observation that inhibition of SV fusion is a prime consequence of toxin mediated neuroparalysis.

The mechanisms underlying the enzymatic activity of CNTs are now better understood due to recently solved structures of different LCs bound to their substrates (Hanson and Stevens, 2000; Breidenbach and Brunger, 2004, , 2005). Unlike classical metallo-proteases, the LCs, though significantly homologous at their active sites, have no common recognition motif on the SNAREs. While they are generally promiscuous in their requirement for particular side-chains flanking the scissile bond, they do require long stretches of their target SNAREs for optimal efficiency (Foran et al., 1995; Schmidt and Bostian, 1995, , 1997; Breidenbach and Brunger, 2004, , 2005). Also, point mutations in regions remote from the scissile bond can reduce proteolytic efficiency of these LCs. All these clues point to a bi-partite mode of action of the LCs, with regions spatially separated from the scissile bond, exosites, being important in binding and recognising the SNAREs and bringing them into a conformation where the active site can access the scissile bond.

SNAP-25 interacts quite extensively with BoNT/A LC and upon binding abandons its native helical configuration and wraps round most of the LC's circumference (Breidenbach and Brunger, 2004, , 2005). The part of the LC opposite the active site plays an important role in identifying the correct substrate and the C terminus of the correctly bound SNAP-25 probably induces a conformational change in the catalytic motif of the LC, increasing its catalytic efficiency. Thus, while only nine residues from the C-terminus of SNAP-25 are

actually cleaved, 60 residues in the C-terminal are needed for efficient proteolysis, encompassing the structurally-identified a and b exosites on the LC. Truncated forms, with only 40 C-terminal residues, and mutations, including I156E and M167E, substantially decrease the catalytic efficiency by depriving the a-exosite of its binding partner. The b-exosite on the other hand binds at the far C-terminal of SNAP-25; versions of S25 truncated below M202 are cleaved at a very slow rate.

These processes probably occur in a sequential manner – SNAP-25 first binds to BoNT/A at the a-exosite, fastens around the LC molecule, binds at the b-exosite and induces conformational changes at the active site potentiating its catalytic activity. As these disruptions in SNAP-25 structure, caused by the multiple interactions with LC, also bring the Gln197-Arg198 bond near the HExxH$^+$E catalytic domain, allowing efficient and rapid proteolytic cleavage of the terminal 9 residues. This bi-partite multi-site binding strategy can be used to explain the selectivity of CNTs and the necessity of a large extent of substrate for efficient proteolysis. This also explains quite elegantly the finding that proteolysis of SNAP-25 is retarded if it is already incorporated into a ternary SNARE complex (Breidenbach and Brunger, 2004). The identification of these non-scissile substrate binding sites on the surface of BoNT/A, such as the a- and b-exosites, also presents new opportunities for novel peptide inhibitors.

The specific residues flanking the scissile bond influences toxin susceptibility. Amino acids at either the P1 or P'1 site are important for cleavage of VAMP II by BoNT/B (Foran et al., 1994; Regazzi et al., 1996) and SNAP-25 by BoNT/A, /C1 and /E (Schmidt and Bostian, 1997; Schmidt et al., 1998); for

BoNT/E, other sites also contribute to the efficacy of cleavage (P5 to P'3) (Vaidyanathan et al., 1999). The multi-site binding strategy employed by BoNT/A accounts for the extreme selectivity of this enzyme, both in terms of the particular SNARE that is cleaved as well as the particular cleavage site. Due to their high homology, most of the CNT LCs probably use similar mechanisms for substrate recognition (e.g., the similarity between BoNT/A and /B is very high, the overall root mean square deviation between the holotoxins is 2.1 Å, and between the LC active sites is 1.4 Å (Swaminathan and Eswaramoorthy, 2000)).

2.1.2.1. Unique trafficking properties of TeNT

After TeNT enters the motor nerve terminal, it is internalised into a vesicle and transported retrogradely along the axon into the motor neuron cell body, at 7.5mm/H, and to the dendrites and released into the synaptic cleft (Burke et al., 1971). The released TeNT is then taken up by inhibitory inter-neurons where it blocks transmission, tipping the balance between excitatory and inhibitory control of the motor neuron towards the latter, resulting in "tetanic" muscle spasms characteristic of the disease. The differential specificity and targets of TeNT and BoNT is determined by the different vesicles that they enter at the NMJ. TeNT enters non-acidified vesicles undergoing retrograde transport while BoNT enters acidified vesicles and thus remains within the motorneuron presynaptic terminal (Lalli and Schiavo, 2002; Lalli et al., 2003; Bohnert and Schiavo, 2005). An alternate hypothesis is that TeNT could be perverting the course of regular endosomal vesicles and causing them to undergo retrograde axonal transport. An interesting finding is that TeNT uptake

is independent of pre-synaptic activity, unlike BoNT uptake – potentially opening up avenues to target not only active neurons, but also paralysed ones (Deinhardt et al., 2006). The peripheral effects of TeNT are very minimal, unless very high doses are injected. TeNT co-localises with the receptor for NGF (p75^{NTR}), segregates to non-acidified vesicles, requires F-actin, microtubules, dynein, kinesins, V-ATPase and myosin to successfully undergo retrograde transport (Lalli and Schiavo, 2002; Lalli et al., 2003).

2.1.3. The structure of purified CNTs

The solved structures of CNT holotoxins reveal a domain organization consisting of the receptor binding domain (HC$_C$), the translocation domain (HC$_N$), and the light chain (LC) protease domain (Lacy et al., 1998; Lacy and Stevens, 1999) (See fig. 11). The sequence homology and functional similarity between the CNTs is reflected in their structural resemblance as well - the overall root mean squared deviation between /A and /B holotoxins is 2.1 Å, and between the LCs is 1.4 Å. These CNTs are synthesised as single proteins with a molecular weight of 150 kDa and subsequent proteolytic cleavage by endogenous or exogenous proteases creates a C-terminally located heavy chain (HC) and a N-terminally located light chain (LC), with molecular weights of 100 kDa and 50 kDa respectively. Despite cleavage, they persist as a very stable di-chain molecule due to the presence of a disulphide bond and tight non-covalent protein-protein interactions between the chains (Dolly and Aoki, 2006). The solved crystal structure for BoNT/A, accurate to within 3.2 Å , shows that it has an extended structure with dimensions of 45 X 105 X 130 Å in which

the HC_N domain, composed of two 105 Å α-helical domains, separates the L domain from the HC_C domain. The LC domain, a compact structure measuring 55 X 55 X 62 Å, is composed of a mixture of α-helical and β-strands and is linked to the HC_N via a long loop which wraps around the LC (Lacy et al., 1998). Despite the overall similarity, small differences in surface residues probably contribute to the significant substrate specificity of different CNTs. The solved BoNT/A-SNAP-25 complex structure has revealed that the LC depends on an extensive array of exosites to provide the substrate specificity, to orient the scissile peptide bond correctly in relation to the enzyme's catalytic motif and to boost the catalytic efficiency (reviewed in (Breidenbach and Brunger, 2004). See fig. 11).

2.1.4. Recovery of cholinergic transmission at the NMJs after Clostridial toxin poisoning

The speed of recovery from CNT-induced neuromuscular paralysis is strongly serotype dependent. Muscle can remain paralysed for many months after BoNT/A and /C1, while patients exposed to BoNT/B, /D, /E or /F recover from poisoning within a matter of weeks (Cherington, 1998). The response of the pre-synaptic membrane to blockade of exocytosis is proposed to significantly affect the speed and extent of recovery – for example: a higher plasticity and regenerative capacity after injury in younger animals could contribute to the faster recovery compared to adults (Pestronk et al., 1980; Verdu et al., 2000; Chen et al., 2002). At murine muscle endplates, the nerve endings sprout vigorously after exposure to BoNT/A and, in the initial post-

paralytic period, only these sprouts are capable of exocytotic function at newly-formed synapses (Duchen and Strich, 1968; de Paiva et al., 1999). Such sprouting, which has also been detected in juvenile rats (Pestronk and Drachman, 1978b), depends on the amount of toxin introduced and the muscle type; fast muscles show less sprouting and predominantly axonal outgrowths compared to the terminal sprouts seen in slow muscles (Brown et al., 1980). The final phase of recovery involves exocytosis returning to the original synapse and regression of the sprouts. While the stages of this functional recovery have been characterised, it is not known whether the fine control of sprouting and regression are related to the toxin's persistence, its cleavage product (truncated SNAP-25) or if it is controlled solely by the loss of neural stimulation of the muscle resulting from disablement of the SNARE function. The relative importance of the muscle or Schwann cells in either of these complementary processes remains poorly defined (Tam and Gordon, 2003). The up-regulation of synaptic protein production has been observed in paralysed NMJs and could be the key to recovery or merely be a response to an unknown 'switch' for sprouting (Jung et al., 1997). BoNT/A intoxication has also been found to induce the extension of Schwann cell processes, which play important roles in the regeneration by providing paths along which the sprouts extend (Son and Thompson, 1995; Son et al., 1996). However, the matter is complicated by the finding that BoNT/A can cause sprouting in nerve-muscle co-cultures deficient in Schwann cell (Bonner et al., 1994). Hormonal and signalling factors, and their receptors, like insulin-like growth factor (IGF) could also play an important role in sprouting (Caroni and Grandes, 1990; Caroni et al., 1994; Caroni, 1997).

The extended duration of synaptic stasis associated with BoNT/A poisoning causes prolonged convalescence and considerable morbidity. This could be due to the persistence of the toxin LC in the pre-synaptic terminal or the prolonged destabilisation of the SNARE machinery by the cleaved SNAP-25 or due to the time taken to replenish the incapacitated SNAP-25. The latter can be ruled out as BoNT/E, which cleaves the very same substrate as /A, has a very short duration of action (Meunier et al., 2003). The inhibitory effect of the BoNT/A cleavage product of SNAP-25 was demonstrated in chromaffin cells, where over-expression of SNAP-25-197 caused an inhibition of Ba^{2+}-evoked hGH secretion (O'Sullivan et al., 1999). Another important clue to explain the prolonged duration of BoNT/A action was the finding that the BoNT/A-LC is distributed in a punctate manner in the plasma membrane and co-localizes with SNAP-25-197, while BoNT/E LC was predominantly cytoplasmic (Fernandez-Salas et al., 2004a; Fernandez-Salas et al., 2004b). Furthermore, this localisation of BoNT/A-LC to a slow recycling compartment at the plasma membrane may make it less susceptible to degradation or ubiquitination while cytoplasmic BoNT/E-LC could be more accessible to removal, thus, accounting for their different time scales of paralysis. There is also some evidence for the first eight amino acids at the N-terminal of LC/A or a di-leucine motif present at the C-terminal could contain a signal for plasma membrane localization (Fernandez-Salas et al., 2004a; Fernandez-Salas et al., 2004b).

The microscopic manifestation of synaptic re-organisation following intoxication with BoNT/A are well known. Blockade of ACh release for 3 days or more by BoNT serotypes induced nerve sprouting with the formation of

functional extra-junctional synapses whilst the original remains inoperative. Initially, thin amyelinated neuritic processes emanate from their original parent nerve endings (terminal sprouting) or from the last node of Ranvier (nodal sprouting) and extend outside the area occupied by the parent nerve terminal. In time, these sprouts gain the components necessary for a functioning synapse, and the AChR clusters on the opposing muscle surface that go with it, and start to exhibit exo- and endocytosis (de Paiva et al., 1999; Meunier et al., 2003). At their peak, they are much larger than the, currently quiescent, parent synapse, but after 9 weeks, the growth of the sprouts ceases. Activity starts to return to the parent nerve ending and, by 3 months, the sprouts undergo retraction accompanied by complete resumption of the normal level of neuro-exocytosis to the fully-remodelled endplate that is then virtually indistinguishable from the original (de Paiva et al., 1999). This is a very striking and extensive cascade of events which illustrates how such neuronal plasticity can cope with a toxin insult and highlights the role of the activity mediated by the sprouts in allowing and, probably, promoting rehabilitation of the synapse.

2.1.5. Engineering SNAREs resistant to cleavage by CNTs

Extensive work has been undertaken to define the important residues in the SNARE substrates that affect the rate of their cleavage by different CNTs. As with any other enzymatic proteolytic process, substitutions in and around the cleavage site strongly affect the Kd and Vmax of the reaction. For e.g., Q76V, F77W mutations in VAMP2, the P1 and P1' residues respectively, confer resistance to TeNT inhibition of hGH release in PC12 cells and insulin secretion

in HIT-T15 cells (Regazzi et al., 1996; Quetglas et al., 2002). Similarly, Q76V or F77V or F77L mutations of VAMP2 confer resistance to BoNT/B (Shone and Roberts, 1994) and K59R or K59A mutations induce resistance to /F (Schmidt and Stafford, 2005). Mutated SNAP-25 isoforms have been engineered to resist cleavage by BoNT/C1 (R198T or R198E (Vaidyanathan et al., 1999)), /A (R198T (O'Sullivan et al., 1999)) and /E (I181F (Vaidyanathan et al., 1999) or D179K, M182T (Koticha et al., 2002)).

2.1.6. Adeno-associated viruses (AAV)

AAV is a non-pathogenic single-stranded DNA containing replication-deficient parvovirus, with a stringent requirement of co-infection with a helper adenovirus or herpes virus to complete its lytic life-cycle (McLaughlin et al., 1988; Berns and Linden, 1995; Linden et al., 1996; Samulski, 2000; Xie et al., 2002; Burger et al., 2005). While these dependo-viruses are widely prevalent as a latent infection in many mammals, including humans, they rarely cause overt clinical symptoms. AAVs are protein enveloped viruses with a capsid diameter of 26nm. Inside this capsid can be found a single-stranded DNA genome containing all the cis-acting elements needed for AAV replication and packaging and flanked by inverted terminal repeats (ITR). Of the 11 known serotypes, AAV1-5 are the best studied and AAV-2 is widely used in clinical gene therapy (Choi et al., 2005).

The wild-type AAV-2 genome consists of rep and cap genes encoding genes necessary for replication and capsid protein production respectively. Utilizing two promoters and alternative splicing, AAVs generate four rep proteins

- Rep78, Rep 68, Rep 52 and Rep 40. Transcripts from another promoter generates the three structural viral capsid proteins, 1, 2 and 3 (VP1, VP2 and VP3), through alternate splicing and translation start sites (Berns and Linden, 1995; Linden et al., 1996; Linden and Berns, 2000). These differ only in their N-terminals while sharing 533 amino acids in a common C-terminal – generating VP1, VP2 and VP3 proteins of molecular weights 87, 73 and 62 kDA respectively (the former two contain additional N-terminal sequences of 202 and 65 amino acids, respectively). The intact AAV viral particle contains a total of 60 copies of VP1, VP2, and VP3 at a 1:1:20 ratio, arranged in a T=1 icosahedral symmetry (McLaughlin et al., 1988). Wt-AAVs (wildtype AAVs) exist as quiescent integrated forms in the host genome and only replicate in the presence of helper viral infection.

AAVs need to undergo multiple steps prior to synthesizing its genome contents – the introduced AAV first binds to cellular surface receptors (usually heparan sulphate proteoglycans) and is later endocytosed. After uncoating, the viral particle releases the ss-DNA genome which is trafficked to the nucleus. The conversion of the genome from single-stranded to double-stranded DNA is followed by transcription of its constituent proteins in the nucleus. In the absence of the helper virus, wt-AAVs integrate into the host chromosome, usually 19q11, with the assistance of Rep proteins and through the interaction of their ITR with the host chromosome (AAVs replicate epi-chromosomally under replication permissive conditions and integrate into the host genome at a rate of 5–10% under non-permissive conditions (Linden et al., 1996)). The efficiency of infection and the rate of protein production is determined by many

87

factors such as – the abundance of cellular surface receptors for viral attachment and internalization, the effectiveness of release from endosomes and lysosomes, the efficiency of unpacking and nuclear trafficking, the rate of conversion of single-stranded to double-stranded DNA template and, finally, for a sustained long-term expression, the amount of integrated viral genome. All these factors differ between the serotypes and are strongly affected by the host cell, but they might be manipulated to facilitate more efficient or more specific transduction of cells or tissues for gene therapy (Burger et al., 2004; Choi et al., 2005).

The properties of this versatile virus have been exploited to produce recombinant AAV (rAAV) gene delivery vectors. A helper-virus free system for the production of infectious rAAV can be fashioned by removing the two viral genes (rep and cap) and inserting a transgene expression cassette between the two ITRs, with Rep and Cap provided in *trans*. The absence of the constitutively expressed native viral genes reduces the toxicity, eliminates the reproductive capability and lessens the possibility of immune recognition.

A commercially available rAAV helper- free system from Stratagene has been used widely for scientific and pre-clinical applications (Kay et al., 2001) (see Fig. 12). In this system, the stripped down human AAV-2 genome, bereft of all except the ITRs and a coding cassette, is co-transfected into HEK-293 variant (AAV-293) cells with two other plasmids, pHelper and pAAV-RC. The essential helper adenoviral genes, E2A, E4, and VA RNA genes, required for the production of infective AAV particles are supplied in trans (through a co-transfection with the plasmid pHelper). The AAV-293 host cells, which stably

express the adenovirus E1 gene, and the plasmid pAAV-RC, producing the Rep and Cap genes are the other essential requirements supplied in *trans*. The removal of the AAV rep and cap genes also makes space for insertion of a gene of interest, upto 3 kb and driven by a cytomegalovirus (CMV) promoter, in the formed AAVs. In addition, some variants can also be generated to co-express a marker Green Fluorescent protein (GFP) through the use of a bovine Internal Ribosome Entry site (IRES) (with a consequent reduction in the maximum insert size to 1.7kb).

Elimination of live helper virus, removal of all non-*cis* genes from the genome and splitting of the trans components, into two plasmids and one cell line, provides a safer, purer, replication-deficient, recombination-free and more convenient alternative to Herpes and Adenoviral gene delivery systems (Buning et al., 2008). The broad host range, high titer virus production capacity, ability to infect post-mitotic cells and long-term gene transfer potential render them promising tools for gene delivery and expression in neuronal populations (Martinov et al., 2002; Ruitenberg et al., 2002; Burger et al., 2005). There is, however, some evidence to suggest that AAVs have a preference for certain types of neurons, a preference strongly mediated by the serotype used (Burger et al., 2004). There is also strong evidence to suggest that they can undergo retrograde transport from spatially separated pre-synaptic terminals to neuronal nuclei and even from NMJs (Kaspar et al., 2003).

Thus, the positive results obtained from ability of a toxin-resistant SNAP-25 isoform to counteract BoNT/A in chromaffin cells, encouraged the development of gene therapy strategies to achieve a similar goal in neurons, *in*

vitro and *in vivo*. Incorporation of this proven gene into the available AAV system was the first goal of this project. After the creation of such a viral vector, it was tested in chromaffin cells, in CGNs and finally *in vivo*, in rat models of botulism.

2.2. Experimental strategies employed

BoNT/A, purified to a specific neurotoxicity of 1 mouse LD50 = 5 pgs as described previously, was used (Shone and Tranter, 1995). The following reagents were purchased: AAV vector Helper-free plasmids (pAAV-MCS, pIRES-hrGFP, pHelper and pRC) and cell lines (Stratagene), heparin agarose, benzonase, mouse anti-NF200 antibody and basic laboratory chemicals (Sigma-Aldrich), Tissue-tek (Sakura), anti-S25 SMI-81 antibody (Sternberger Monoclonals), mouse anti-His$_6$ antibody (Amersham), α-bungarotoxin (α-BuTx) conjugated to Alexa-488 or rhodamine (Invitrogen), West-Dura ECL developer (Pierce), gel extraction and plasmid purification kits (Qiagen), enzymes for DNA production and purification (NEB), stereotaxic table with rat spinal immobilizers (Stoelting), micro-surgical implements (WPI), micro-syringes and needles (Hamilton). The constituents of the different prepared buffers and solutions can be found in Appendix 1.

2.2.1. Animal husbandry, LD$_{50}$ determination and DAS scoring

Female Wistar rats (8 weeks old, ~200g) and female TO mice (20g) were acquired, under license, from Trinity College Bioresources Unit or Harlan (UK). Animals were housed in certified facilities and handled by trained animal technicians. They were given ad libitum access to water and commercial rodent food. All techniques were approved by the Environmental Health Unit in the Department of Health and Children in Ireland and conformed to relevant EU regulations. Experiments were approved by the University Ethics Committee

and supervised by a consultant veterinary surgeon. Animals that were treated with drugs/toxins, or operated on, were segregated from the normal population. Data sheets were maintained on these animals and details of their weight, feed, excreta, digit abduction scores (DAS) and general condition noted regularly. All potentially painful procedures were done under sedation or anaesthesia. Any animal that seemed to be in pain was given adequate analgesics or, in extreme conditions, euthanized.

The two main procedures involving live animals were LD_{50} determination and viral vector administration (The latter is described in detail in Section 2.2.5). In both cases, every effort was taken to minimise the number of animals by first performing *in vitro* assays to give an approximation of the activity of the toxins or the dose of virus needed. LD_{50} in mice is the only method capable of quantifying the composite activity of the BoNT and TeNT toxins (i.e. extra- and intra-cellular stability in the animal, binding to neuronal acceptors, acceptor-mediated toxin uptake, translocation and enzymatic cleavage of their targets in the conformations existing within neurons). A mouse bioassay is the ultimate, most reliable and, thus, the only internationally-accepted measure of toxin activity for human uses (see (Schantz and Kautter, 1978) and (Schantz and Johnson, 1990)). This entails a single intraperitoneal injection followed by monitoring of generalised neuromuscular paralysis (Union, 2000). The toxin paralyses the respiratory muscles leading to death by asphyxiation; however, the mice were not subjected to prolonged suffering and were euthanised at the onset of confirmed respiratory paralysis. After the injection, they were observed every 3 h during the day, every 6 h at night and more often when symptoms

become evident, for the length of the procedure. The animals were examined for signs of lethargy, which indicates early stages of botulism, and when the animals ceased to "run away" from the handler, the extent of respiratory distress was carefully assessed. Signs of distress include cyanosis in the tail and "drawing in" of its stomach (abdominal contraction). When there was clear evidence that the animal would not survive from respiratory distress, it was humanely killed. In early stages, mice sometimes demonstrated signs of dysphagia and difficulty in accessing food and water and, therefore, the animals were fed with easily accessible water-soaked food pellets. Another checkpoint monitored was body weight; if loss exceeded 20%, the mice were humanely killed.

The speed of onset of the symptoms can differ depending on the dose. The different subtypes of BoNT to be used have distinct patterns and time courses of paralysis. For example, an animal injected with BoNT/A will show serious symptoms on day 1-2 whereas those injected with BoNT/E or other short-acting forms display symptoms on day 2, yet are likely to recover. Four days after toxin injection the experiment was ended and animals were euthanized by cervical dislocation, according to the EU guidelines.

The same monitoring procedures were used for experiments involving the intra-muscular injection of BoNT and viruses.
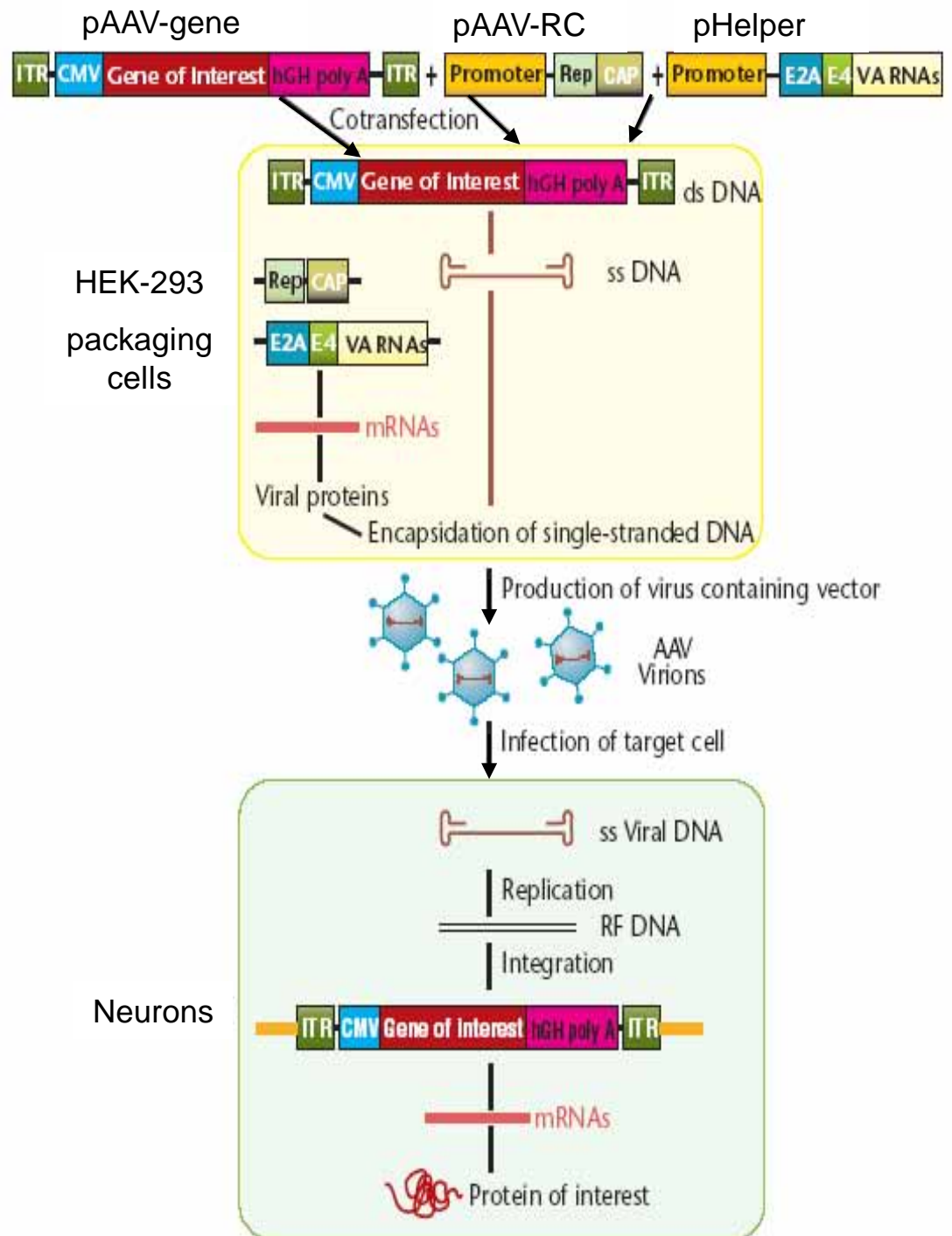
Fig. 12: The AAV vector production process. This flowchart represents the different plasmids and steps involved in the production of a functional virion and the processes implicated in its integration into the target cell. pAAV-gene: the transfer construct containing the expression cassette with the necessary flanking cis-acting promoter and poly-adenylation sequences. pAAV-RC: Containing the Rep and Cap genes of the AAV2 virus (Rep: AAV2 replication genes. CAP: AAV2 capsid genes). pHelper: Containing the E2A, E4 and VA sequences from adenovirus. HEK-293: human embryonic kidney cell line. CMV: cytomegalovirus promoter. hGHpA: human growth hormone polyadenylation sequence. ITR: inverted terminal repeats. E2A, E4 and VA: Adenoviral genes that along with the E1A and E1B genes from HEK-293 enable the successful production of an AAV2 particle.
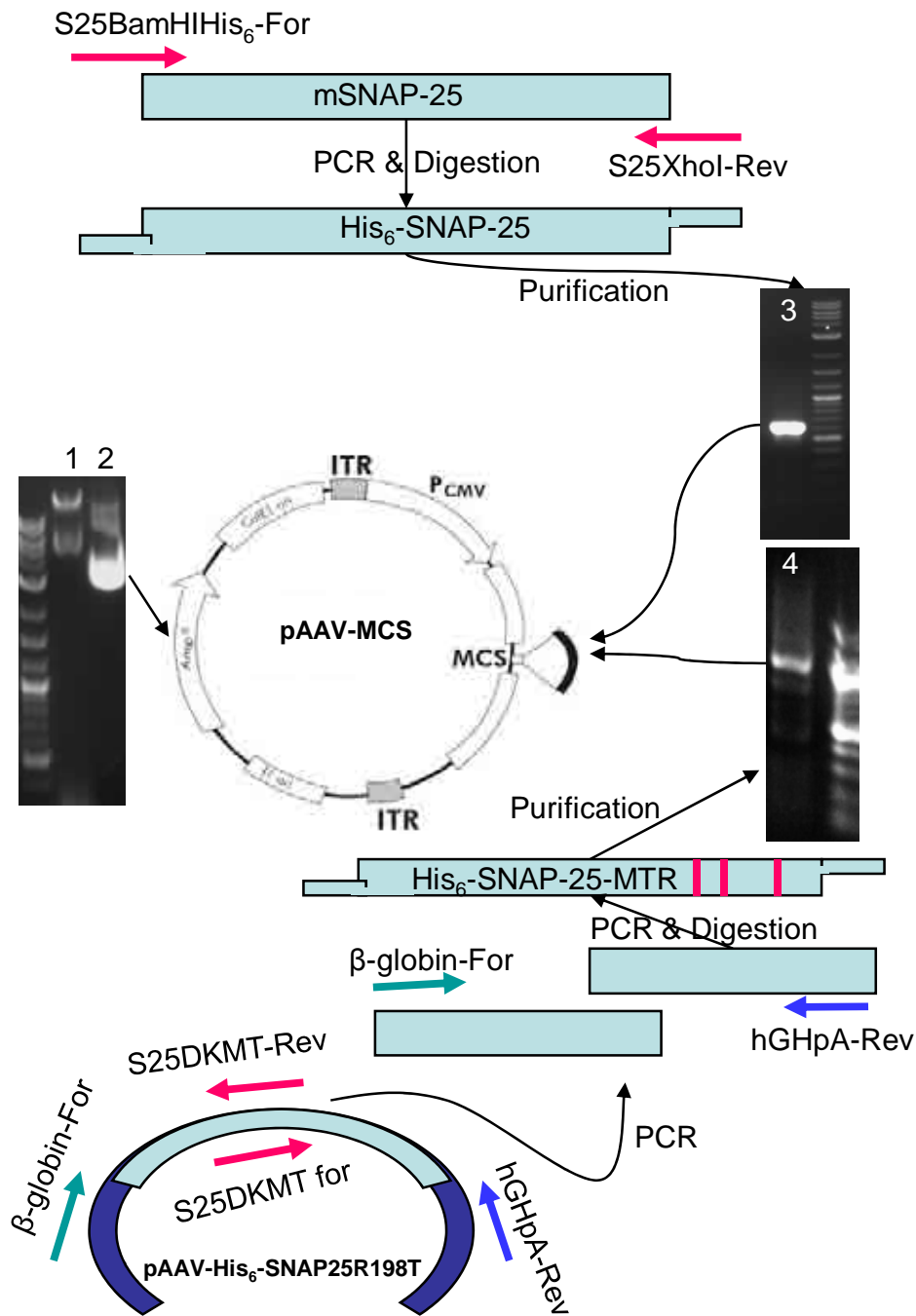
Fig. 13: Cloning of pAAV-His$_6$-S25 and pAAV- His$_6$-S25MTR: The top half of the figure shows the PCR amplification of wild-type S25 using an N-terminal primer containing a BamHI site, 6 repeats of CAT (coding for His) & a start codon, and a C-terminal primer containing a XhoI site with a stop codon. After restriction digestion, the PCR product is inserted into a BamHI and XhoI digested pAAV-MCS vector (Middle). The lower panel shows amplification of the S25R198T gene using two sets of primers (containing the necessary D179K and M182T mutations) resulting in the production of two overlapping PCR products. Using them as templates, PCR with the two initially used outer primers yielded the multiple toxin resistant His$_6$-S25MTR gene which, after digestion with BamHI and XhoI, was inserted into the pre-digested pAAVMCS plasmid. Lane 1 & 2 – undigested & Bam H1/Xho1 digested pAAVMCS; 3 – digested His$_6$-S25 PCR product; 4- digested His$_6$-S25 MTR PCR product.

Name of Primer	Sequences
bGlobulin For	ATTCTGAGTCCAAGCTAGGC
hGH pA Rev	TAGAAGGACACCTAGTCAGA
T3 For	ATTAACCCTCACTAAAGGGA
T7 Rev	TAATACGACTCACTATAGGG
left ITR For	CCTCTGACTTGAGCGTCGAT
right ITR Rev	TACTATGGTTGCTTTGACGT
SNAP-25-XhoI-Rev	ATCCGCTCGAGTTAACCACTTCCCAGC
SNAP-25BamHIHis$_6$For	CGGGATCCATGCATCATCATCATCATGCCGAGGACGCAGACA TGCG
SNAp-25RTXhoIrev	AGATCTCTCGAGTTAACCACTTCCCAGCATCTTTGTTGCAGTTTGG TTGGCTTCATCAATTC
CMV Taqman	5'FAM-CCGCTATCCACGCCCATTGATG-3'TAM
CMV_TFor	TGGAAATCCCCGTGAGTCAA
CMV_TRev	CATGGTGATGCGGTTTTGG
EF-1 short for	TGCCGCCAGAACACAGGTG
WPRE rev	TAGTTAAGAATACCAGTCAATCTTTCAC
EF1-a for	CCATTTCAGGTGTCGTGAGGA
IRES Rev	CATATAGACAAACGCACAC
S25D-K M-T For	AAGAGGATCACAGAGAAGGCTGACTC
S25D-K M-T Rev	TGTGATCCTCTTAATCTGGCGATTCTG
S25T-For	GGCTGATGAGTCCCTGGAAA
S25T-Rev	CGCCTTGCTCATCCAACAT
S25Taqman	5'FAM-AGCTGGTTGAAGAGAGTAAAGATGCTGGC-3'TAMRA
GAPDH For	TGCCAAGTATGATGACATCAAGAAG
GAPDH Rev	TAGCCCAGGATGCCCTTTAGT
GAPDH Taqman	5'FAM-TGGTGAAGCAGGCGGCCGAG-3'TAMRA
b-actin for	AGGGAAATCGTGCGTGACA
b-actin rev	GTCTAGGGCAACATAGCACAGCTT
pQE For	GTATCACGAGGCCCTTTCGTCT
pQE Rev	CATTACTGGATCTATCAACAGGAG
CS-For	ATGATGAGATCTCTCGAGGGTGGC
CS-Rev	GCCGCCAGATCTCTCGAGGGATC
Botim Clon1 For:	ACTGGATCCCCGACCATTAATAGTTTTAATTATAATGATCCTG
Botim Clon1 Rev:	CAGGGATCCACCGGTACGCGTAGAATCGAGACCG
LCE For:	ATTTCAAGTTAAATGTAGGCAAAC
HCE Rev:	CATAATTATTATTTGAAGTTACTGTATC
LCE Rev:	GTACCAATTACATTTCTCTCTGG
HCE For:	TGGAAATAATATTGGGTTGTTAGG

Table 2: Sequences of the different primers used: All sequences are represented 5'-3'. The taqman probe, CMV_Taqman is labeled with the reporter dye FAM (6-carboxy-fluorescein) at its 5' end and the quencher TAMRA (6-carboxy-tetramethyl-rhodamine) at its 3' end.

2.2.2. Construction, production and purification of recombinant AAVs expressing BoNT/A-resistant S25 (S25RT), wild-type S25, markers hrGFP or hrGFP with S25RT

An AAV vector Helper-free system consisting of three plasmids – transfer construct (e.g.: pAAV-hrGFP, pAAV-His$_6$SNAP-25RT etc); pAAV-RC, containing the rep and cap AAV genes and pHelper, expressing the necessary adenoviral-proteins – was used to produce replication-deficient AAV virions (See fig. 12 and 13). PCR, using the S25BamH1His$_6$-For and S25XhoI-Rev primer pair, was undertaken to generate a His$_6$-tagged S25 product from a pcDNA1.1 plasmid containing the mouse S25 gene His$_6$-tagged (see Table 2 for primer sequences). After restriction digestion with Bam HI and Xho I, the product was purified using a Qiagen gel extraction kit and inserted into the pAAV-MCS plasmid, pre-digested with the same enzymes, to yield pAAV-His$_6$-S25 plasmid (see fig. 13 for more information on the cloning process). Confirmation of cloning and correct orientation of the insert was obtained by sequencing, using the β-globin-For and hGHpA-Rev primers.

A similar technique, with the substitution of S25RTXhoI-Rev for S25XhoI-Rev, was used to create pAAV-His$_6$-S25-R198T encoding a functional S25 which is resistant to cleavage by BoNT/A. For generating a S25 gene resistant to cleavage by /A, /C1 and /E splicing by overlap extension PCR was used to introduce two further mutations into the S25R198T gene – D179K and M182T(Koticha et al., 2002). Briefly, PCR using the pAAV-S25R198T plasmid with the two primer pairs, β-globin-For & S25DKMT-Rev and S25DKMT-For &

97

hGHpA-Rev yielded two overlapping fragments of 680 and 200 bps. When purified and mixed together in a PCR reaction with β-globin-For & hGHpA-Rev primers, these generated a full-length 860bp S25 MTR (multi-toxin resistant) containing BamHI and XhoI restriction sites at its 5' and 3' ends. Insertion into the pre-digested pAAV-MCS plasmid yielded the pAAV-His$_6$-S25-MTR plasmid containing the triply-mutated S25 gene – R198T, D179K and M182T (Figure 13). Using the same strategies and cloning methods, a second set of plasmids was created which could co-express these previously described genes along with a hrGFP marker gene, that is driven by an internal ribosome entry site (IRES) sequence (pAAV-His$_6$-S25-IRES-hrGFP, pAAV-His$_6$-S25-R198T-IRES-hrGFP and pAAV-His$_6$-S25-MTR-IRES-hrGFP). Isolation of all these plasmids, along with the pAAV-hrGFP control, to a high purity was then scaled up using a Qiagen Giga-prep kit. These different plasmids, along with the commercial AAV-hrGFP, were used to create their respective AAVs as described in Zolutukhin *et al*, 1999 (Zolotukhin et al., 1999).

The cis-construct plasmids, along with pAAV-RC and pHelper, were transfected into HEK-293 cells using calcium phosphate. An aliquot (10 µg) of each plasmid was mixed together and used to transfect 70% confluent HEK-193 cells. After 12-18 hr, the medium was replaced and the cells were washed with PBS and harvested on day 3. The collected cells were subjected to 2-3 cycles of freeze/thaw, digested with benzonase (an endonuclease from *Serratia marcescens*) at 37°C for 15 mins and incubated with 0.5% sodium deoxycholate for a further 30 mins, before clarification by centrifugation at 200 g for 10 mins. The cleared lysate, sequentially filtered through a 5µm and 0.8µm

filters, was then loaded onto pre-equilibrated Heparin-Agarose resin (~200µl per 15 cm plate of HEK-293 cells) and, after repeated washing, the bound virus was eluted using PBS + 0.5M NaCl. The resultant viruses were concentrated, and buffer exchanged, using a low-protein binding 100kDa cut-off filter, aliquoted, snap-frozen and stored at -80 °C.

2.2.2.1.   Titration of produced AAVs – PAGE, RT-QPCR, Western blotting and FACS-based assays

The purity of these preparations was assessed on a Coomassie stained SDS-PAGE gel, and viral (protein) yield measured by comparing the surface proteins (VP1, 2 &3) to a bovine serum albumin (BSA) standard. Using the CMV Taqman probe and CMV_TFor & CMV_TRev primers, real-time quantitative PCR comparison with known quantities of the respective plasmids gave an accurate quantification of the number of genomic copies (GC) per preparation (Table 2 shows the sequence of primer and probes used). A dilution series of these viruses was then used to infect HEK-293 cells and the number of transducing units (TU) per preparation calculated by extrapolating the two highest dilutions where infected cells could be identified, by green fluorescence (for the hrGFP containing viruses) and by an antibody- based detection (for those expressing S25). By these methodologies, large quantities of highly pure AAV viral particles (VP) were successfully prepared; for example, AAV-hrGFP virus was >95% pure and showed a concentration of ~10^{11} VP/ml and ~ $1x10^9$ TU/ml (See fig. 14). The disparity between these values is due to the presence of some empty and damaged virions but is within permissible limits.

Furthermore, this prepared virus gave strong expression of hrGFP in widely different cells like bovine adrenal chromaffin cells (See fig. 14 and 15). Cell viability assays on a Beckman-Coulter FACS apparatus further demonstrated the innocuous nature of these viruses in HEK-293 cells (See fig. 15B). Using the CMV Taqman probe and CMV_TFor & CMV_TRev primers (Table 2), real-time quantitative PCR comparison with known quantities of the respective plasmids gave an accurate quantification of the number of genomic copies (GC) per preparation. A dilution series of these viruses was then used to infect HEK-293 cells and the number of transducing units (TU) per preparation calculated by extrapolating the two highest dilutions for which infected cells could be identified, using green fluorescence (for the hrGFP containing viruses) and by an antibody-based detection (for those expressing His_6-S25).
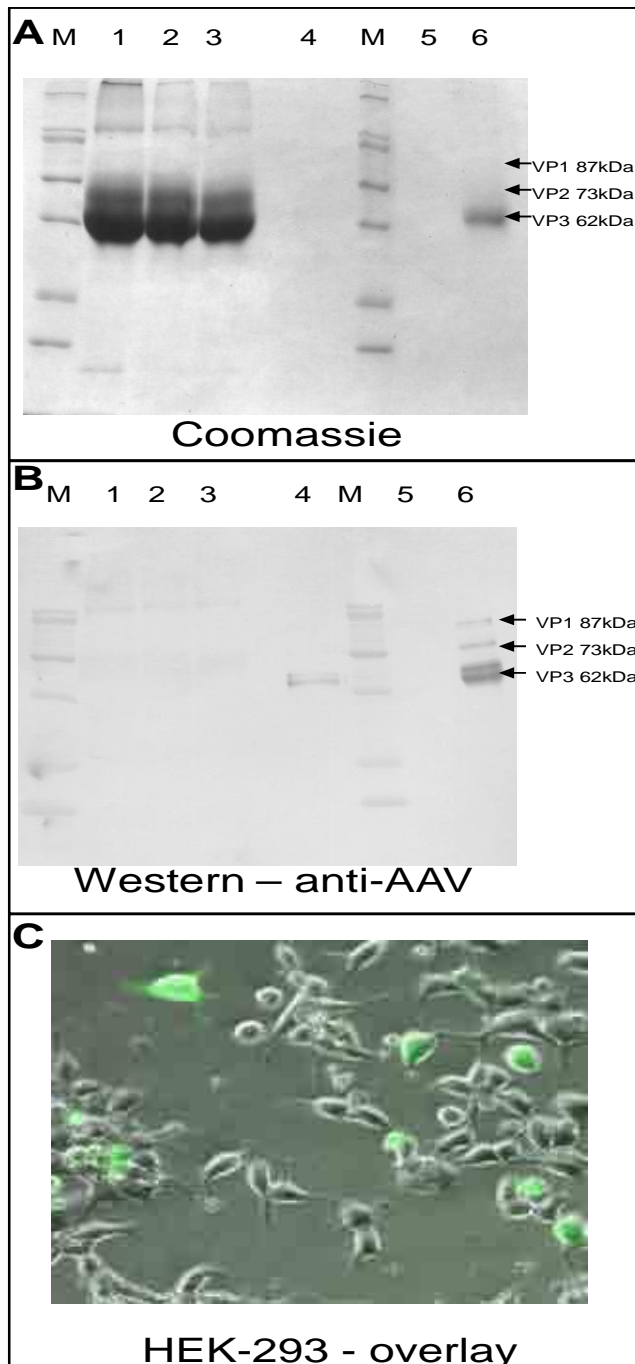
Fig. 14. Efficient production, purification and concentration of AAV-hrGFP virus:
A: Coomassie stained SDS-PAGE gel of aliquots taken at different points in the production process: M-prestained markers, 1-lysate, 2-deoxycholate extract, 3-Heparin agarose column flow-through, 4-eluate, 5- concentrator FT and 6-concentrated AAV-hrGFP. VP1, 2 and 3 are AAV surface proteins. **B:** Western blot of a duplicate of the gel in A, developed with an ECL reagent following detection with a rabbit anti-AAV and anti-rabbit-HRP. **C:** Overlay of a phase contrast and flourescent microscopic views of HEK-293 cells infected with AAV-hrGFP at an MOI of 1.

101

A

B

Bovine chromaffin

FACS analysis
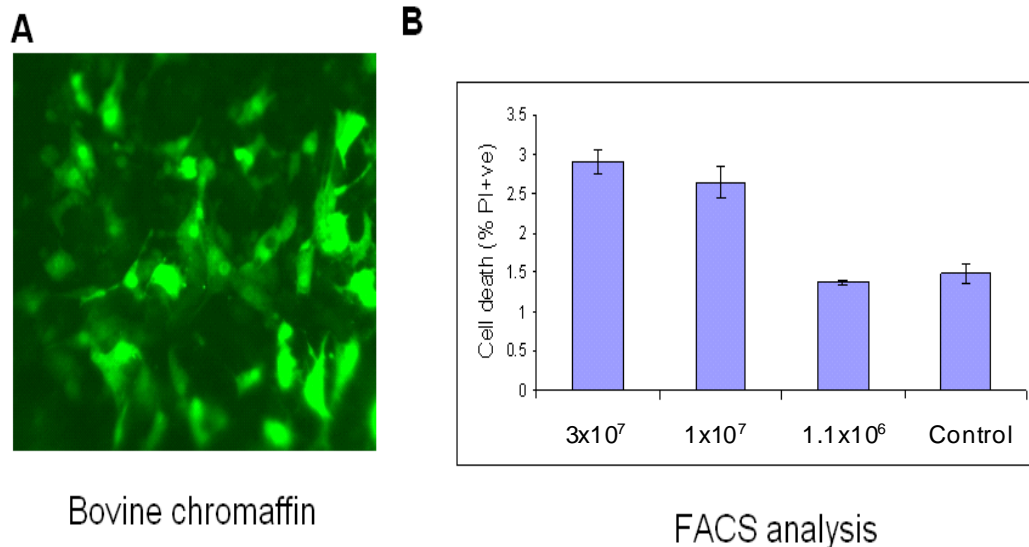
Fig. 15: The purified and concentrated AAVs show high infectivity without causing any deleterious effects. **A:** The produced viruses can efficiently infect bovine adrenal chromaffin cells and have only a minimal effect on HEK-293 cell viability. **B:** Cell death was determined by the ratio of propidium iodide (PI) stained to unstained cells on a Beckman-Coulter FACS apparatus, 5 days after treatment with various volumes of AAV-hrGFP, containing 1×10^9 TU/ml, or PBS. The percentage of PI positive cells was plotted as a ratio of the total cell number. An average of 4 runs, and standard deviation, is plotted in the graph
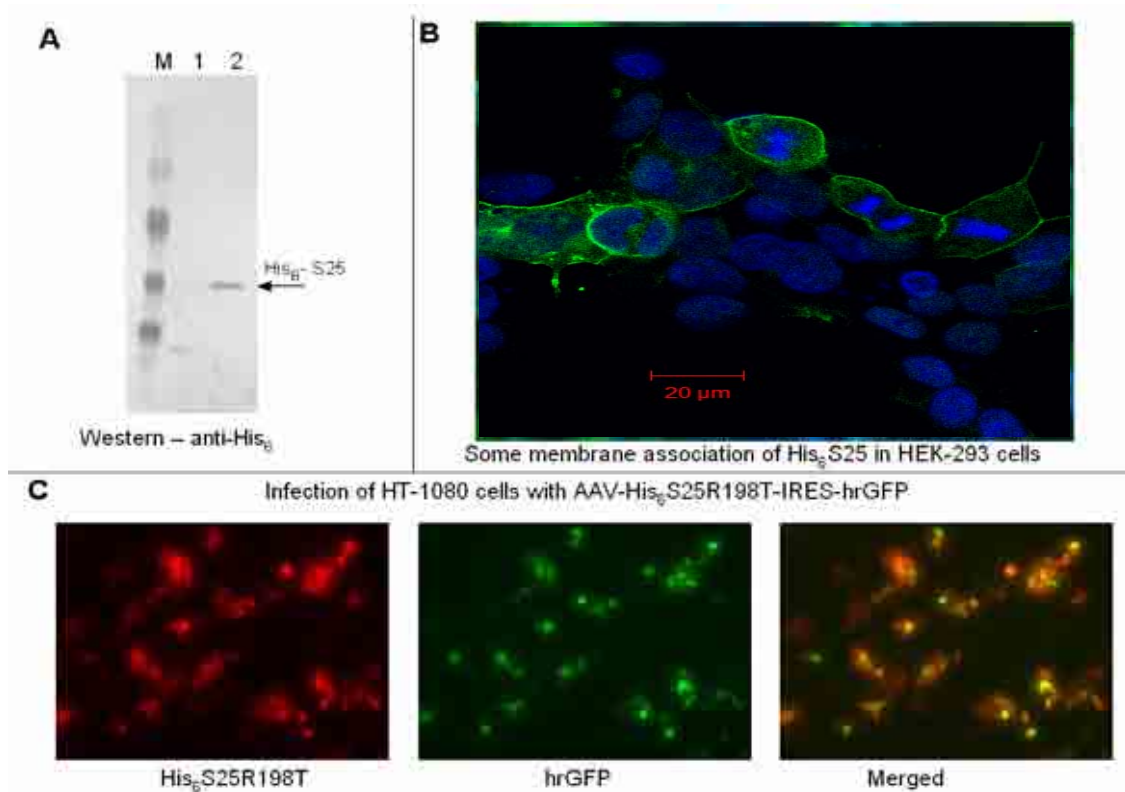
Fig. 16: The introduced His$_6$-tagged S25 is efficiently expressed and partially localized to the membrane. **A:** HEK-293 cells were infected with AAV-His$_6$-S25 virus for 5 days before lysis by freeze/thawing. Lysate was centrifuged at 18,000g for 1 hr; the supernatant (lane1) and pellet (lane 2) were separated and run on a 15% SDS-PAGE gel. After transfer, the Western blot was probed with mouse anti-His$_6$ antibody, followed by anti-mouse HRP conjugate and developed with an ECL-plus reagent. **B:** Representative picture showing some membrane-associated protein: HEK-293 cells infected with AAV-His$_6$-S25R198T were formalin fixed and methanol permeabalised before sequential application of mouse anti-His$_6$ and anti-mouse-Alexa 488 secondary antibodies. The photo was taken on an Olympus inverted fluorescent light microscope with a 40X objective. **C:** Co-expression of His$_6$-S25R198T with hrGFP: HEK-293 cells infected with AAV-His$_6$-S25R198T-IRES-hrGFP were treated as before except for the substitution of an anti-mouse-phycoerythrin secondary. Images corresponding to the His$_6$-S25R198T-red fluorescence (left) and hrGFP-green fluorescence (middle) were obtained and overlaid (right); yellow indicates cells expressing both these proteins.

103

2.2.2.2. Subcellular localisation of produced S25 by confocal microscopy

For AAV-His$_6$-S25 virus, sufficient expression and membrane association of the introduced protein was confirmed by Western blots on the membrane and cytosolic fractions, using a monoclonal anti-His$_6$ antibody followed by detection with an anti-mouse-HRP conjugate (See fig. 16). Briefly, the cells were lysed with 1% Triton X-100 in PBS, the cellular and membrane fractions separated, aliquots denatured in Laemmli gel loading buffer and run on 12% pre-cast PAGE gels from Invitrogen. The separated proteins were transferred onto PVDF membranes over-night at 4°C. The blots were blocked for 30 mins with 4% (w/v) milk-powder in TBS buffer, with 0.05% Tween-20 and probed with the required primary and secondary antibodies in the same buffer. The blots were washed well 3-4 times between the steps with TBS buffer + 0.05% Tween-20. Detection of species-specific secondary antibodies, covalently attached to horseradish peroxidase (HRP), required the addition of enhanced chemiluminescence reagents (ECL) for 5 mins and acquisition of phosphorescence images with a GeneSnap imager.

A large fraction of the expressed His$_6$-S25R198T protein was found associated with the plasmalemma, as revealed by immunohistochemistry on formalin-fixed and methanol-permeabalised cells using an anti-His$_6$ antibody detected by an Alexa-488 labeled anti-mouse antibody (Fig. 16). Co-expression of the hrGFP and His$_6$-S25R198T in cells infected with the AAV-His$_6$-S25R198T-IRES-hrGFP virus was confirmed by identification of hrGFP

fluorescence and immunodetection of a His$_6$ signal by a phycoerythrin labeled secondary (Fig. 16).

2.2.3. Determining the relative proteolytic activity of BoNT /A, /E and /C1 against mutant and wild-type S25

A highly sensitive assay using digitonin-permeabalised HEK-293 cells expressing wtSNAP-25 was used to determine the *in vitro* potency of the different toxins, their EC$_{50}$ for cleavage of membrane-associated post-translationally modified SNAP-25 and also to determine the cleavage-resistance of the different introduced mutations. Briefly, 5µg of plasmid DNA expressing wtSNAP-25, His$_6$SNAP-25RT and His$_6$SNAP-25-MTR was transfected using calcium phosphate into 80% confluent HEK-293 cells in a 10cm plate. The cells were washed the next day, treated with trypsin-EDTA to dissociate them from the plate surface and were seeded into 48-well plates. After another 24 h, the cells were treated with the toxin preparations in KGH permeabalisation buffer + 150µM digitonin (the different toxin preparations were supplemented with 50µM ZnSO$_4$ and reduced with 10mM DTT for 10 mins at 37°C before addition on to cells). After 30min incubation, the cells were collected and the toxin's activity stopped by addition of 1mM EDTA. They were freeze-thawed thrice and centrifuged at 18,000g for 30min at 4°C. The membrane enriched sediment was denatured in Laemmli gel loading buffer, run on 12% PAGE gels, transferred on to a PVDF membrane and probed with a rabbit anti-SNAP-25 antibody. The different bands were quantitated by the densitometry software, GeneSnap, and analysed (See fig. 17).

2.2.4. Culture of chromaffin cells, infection with recombinant AAVs, intoxication with BoNT/A and assay of catecholamine release

Chromaffin cells were isolated from bovine adrenal glands and maintained as described previously (Lawrence et al., 1996; O'Sullivan et al., 1999). Fresh Bovine adrenal glands were cleaned of surrounding fat and perfused with Locke's buffer with a syringe inserted into the portal vein. The gland was washed with this solution 4-5 times to ensure that all the blood was removed from the gland. Later it was perfused with the same solution containing 0.1% (w/v) pronase and incubated at 37ºC for 15 mins to digest the connective tissue between the adrenal medulla and cortex. The digested glands were sectioned and the medulla separated from the cortex using a sterile blade. The medulla was minced and incubated with sterile 0.1% collagenase in Locke's buffer at 37ºC for 30 mins with vigorous agitation. The dissociated chromaffin cells were filtered through two layers of muslin, centrifuged at 500g in a bench top centrifuge for 10 mins and resuspended in Locke's buffer. This process was repeated 2-3 times before a final centrifugation on a layer of Locke's buffer containing 4% (w/v) BSA at 300g for 10mins. The essentially RBC-free chromaffin cells were counted using a haemocytometer, resuspended in chromaffin growth medium and plated at a density 1 X 10^6 viable cells per well on 24-well tissue-culture plates. If needed the different AAVs were added to the media 24 h after plating the cells.

After a week of growth, the media was changed and the cells were incubated at 37ºC for 24 h in a low ionic strength medium (LISM) in the absence or presence of the BoNT toxins. Cells were re-equilibrated with the toxin-free

growth medium for 24 h before experiments were performed. They were exposed to 0.3 ml of 'basal medium' (Locke's buffer) at 25°C for 15 mins followed by a similar exposure to a 'stimulation medium' (2 mM Ba^{2+} in Locke's buffer). The non-released catecholamines were extracted through the addition of 0.3 ml of 'remaining medium' (1% Triton X-100 in Locke's buffer). The amount of catecholamines present in various samples was quantified using a fluorometric procedure (von Euler and Floding, 1959). Briefly, 2 ml of 1M CH_3COONa and 0.1 ml of 0.25% (w/v) $K_3Fe(CN)_6$ were added to the collected fraction, mixed and incubated for 5 mins, thereby converting adrenaline to adrenochrome. This unstable product was then converted to adrenolutin by the addition of 1 ml of 0.2% (w/v) ascorbic acid in 5M NaOH. Adrenolutin can be quantitated fluorometrically with a Perkin-Elmer spectrophotometer as it emits light between 510 - 530 nm when excited at 410 nm. The catecholamine content in each of the three fractions was determined and the % of Ba^{2+}-induced catecholamine release, with respect to the total content, to be calculated:

$$\frac{\{(\text{stimulated medium}) - (\text{basal medium})\}}{\{(\text{stimulated medium}) + (\text{basal medium}) + (\text{remaining medium})\}} \times 100$$

The amounts of release obtained after different viral and toxin treatments were then normalized to that in the presence of the toxin and represented as mean $^+/-$ SD of measurements from 4 different wells for each condition, from 2 or more sets of experiments. T-tests were used to determine the statistical

significance of all results.

2.2.5. Stereotaxic intra-spinal administration of AAVs for transfection of anterior horn neurons supplying the soleus muscle in rats

The precise location of the motor neurons innervating the soleus muscle was first determined by initial retrograde tracing of injected flourogold and from previously published literature (Greene, 1968; Nicolopoulos-Stournaras and Iles, 1983). Rats were anesthetized with medetomidine/fentanyl citrate (Medetomidine/Domitor from a stock solution of 1mg/mL – dose 0.4mg/kg subcutaneous; Fentanyl/Sublimaze from a stock solution of 0.05mg/mL – dose 0.45mg/kg IP) and injected with amoxicillin (Amoxycillin/Betamox from a stock solution of 150mg/mL – dose 140mg/kg subcutaneous). The surgical field was shaved, cleaned using 5% chlorhexidine gluconate (Hibitane) solution or Betadine surgical scrub. To prevent drying out of the eyes, Lacrilube was applied periodically.

The toe pinch and the tail base pinch reflexes were tested to confirm complete anethesisa, before the first incision was made over T10-L2 vertebras (up to an extra 1 mL of Fentanyl was injected intraperitoneally if the anethesia was found to be too shallow). The superficial fascia and the paravertebral muscles were separated to expose the vertebral bodies and spines before positioning in a stereotaxic frame (Stoelting); rat spinal adapters were used to firmly clamp two adjacent vertebras. The vertebral laminas over the T13 and L1 spinal levels were penetrated using a microdrill taking care not to damage the dura or the underlying spinal tissue. Using a 30G beveled needle attached to a

Hamilton microsyringe, known quantities of the virus were injected over 5 mins at the T13 level; the open bevel was positioned caudo-laterally to prevent any leakage into the posterior or contralateral horns. After a further 5 mins, the needle was slowly withdrawn and the procedure repeated at L1 and L2 levels; in most cases, twitching of the lower limb muscles confirmed the accurate placement of the needle. The paraspinal muscles were sutured back together with braided, absorbable vicryl sutures (4-0), followed by a similar approximation of the superficial fascia reinforced with a Prolene mesh (knitted, non-absorbable polypropylene) to strengthen the wound and prevent soft-tissue dehiscence. The skin was closed with a non-absorbable prolene (4-0) suture and atipamazole (Atipamazole/Antisedan from a stock solution of 5mg/mL – dose 1mg/kg subcutaneous) and nalbuphine (Nalbuphine/Nubain from a stock solution of 10mg/mL – dose 2mg/kg subcutaneous) administered to accelerate recovery from the anesthetic. Carprofen (Carprofen/Rimadyl from a stock solution of 50mg/mL – dose 2mg subcutaneous) and bupivacaine (Bupivacaine HCL from a stock solution of 0.25% w/v – dose 0.2mL at wound site) were injected for systemic and local pain relief. Rats were kept under observation till they had fully recovered from anaesthesia and only then were they returned to the animal facility.

Animals were carefully monitored post-operatively and adequate analgesia, antibiotics, food and hydration provided as needed. Depending on the individual animal, a saline injection to promote hydration was administered. A series of criteria was used to determine the post-operative condition of the animal, in conjunction with the experience of the regular animal handler. These

include observations of activity, appearance, food and water intake, excretions, breathing, vocalisation, weight and the condition of the surgical site. In general, pain is indicated by: "guarding" (protecting) the surgical site; vocalisation (squeaking) when the animal moves or if the surgical area is touched; limping, a "tucked up" abdomen, or other abnormal stances or posture; reclusive behaviour; lack of appetite; increased respiration rate or abnormal breathing patterns. In case of any undue distress, animals were euthanized by injection of Sodium Pentobarbitone (Dolethal from a stock solution of 20% w/v – dose 200mg/kg IP). All animals injected with viral vectors were kept in separate cages and treated as potential sources of biologically hazardous material.

2.2.6. *In situ* electrophysiological recording of the efficiency of neuromuscular transmission as a measure of synaptic exocytosis remaining after BoNT/A administration

Three weeks after the intra-spinal injection, these rats were sedated using medetomidine, the skin over the posterior part of the lower leg incised and ~1 mouse LD50 of BoNT/A in 10µL of normal saline (NS)/ BSA injected under visual guidance into the belly of the soleus muscle. The incision was then sutured, sedation reversed with atipamazole and the animal allowed to recover for 16-25 days. Later, they were again deeply anesthetized using medetomidine/fentanyl citrate and the Achilles tendon was exposed at the level of its insertion. The soleal contribution to this tendon was isolated and ligated to a sensitive force transducer (FORT10 – AD Instruments); the gastrocnemius and plantaris tendons were severed. The sciatic nerve was exposed at mid-

thigh level, separated from surrounding fascia and placed on a pair of silver electrodes. Two more electrodes were positioned on the belly of the exposed soleus muscle followed by stimulation at 1 Hz using 5V for 2 msec with a PowerLab 4/20T (AD Instruments). The tension in the muscle and the position of the electrodes were adjusted using a micrometer in order to obtain the maximal contraction. The nerve was then stimulated at 1Hz using 200 mV for 0.2 msec and the position of these electrodes adjusted to obtain the largest nerve-induced contraction. The ratio of the force obtained in response to a single supra-maximal stimulation of the nerve compared to that for a single supra-maximal stimulation of the muscle provided the efficiency of neuromuscular transmission (ENT). Stimulation of the nerve and muscle at 60 Hz provided the ENT at tetanic frequencies.

2.2.7. Immuno-histochemical detection of S25, His$_6$-S25, His$_6$-S25-R198T and GFP expression

The rats were euthanized at the end of each experiment with sodium pentobarbitone, perfused with 4% formalin, the spinal cord and relevant muscles excised and cryoprotected with graded solutions of up to 20% glycerol/2% DMSO in phosphate buffered saline (PBS). The tissues were then mounted using Tissue-Tek solution and 25 μm sections cut, thawed out just before use, washed twice with PBS, permeabalised with ice-cold methanol for 30 secs, washed again with PBS-T (PBS with 0.05% Tween-20) and blocked for up to 30 mins with filter-sterilized PBS-T with 1% BSA/2% goat serum. The

sections were then exposed to the primary antibody diluted into the same solution (1:50 for SMI-81, anti-NF200 and anti-His$_6$ antibodies; 1:100 for anti-hrGFP antibodies). After repeated washing at 37 °C, the samples were exposed to the relevant secondary antibodies (1:50 Alexa-488 or 1:100 A546/phycoerythrin labelled goat anti-mouse; 1:50 A564 conjugated goat anti-rabbit) with or without 1:500 fluorescently-tagged α-BuTx (with Alexa 488 or rhodamine). After further washing, the specimens were mounted under a coverslip with PBS/glycerol and visualized with an Olympus IX51 inverted fluorescent microscope or, when appropriate, a Zeiss confocal microscope (LSM510).

Protein expression in virally-infected mammalian cells lines or chromaffin cells was quantified in the membrane and cytosolic fractions of the lysed cells by separation on 12% pre-cast SDS PAGE gels and Western blotting. The blots were probed with different dilutions of the primary (1:5000 SMI-81, 1:1000 anti-His$_6$, or 1:2000 anti-hrGFP) and relevant secondary antibodies (1:4000 rabbit anti-mouse or 1:2000 goat anti-rabbit HRP-conjugated), developed with West-Dura reagents and chemiluminescence was captured using a cooled-CCD camera.

2.2.8. Determination of the distribution of ACh receptors at NMJs using fluorophore-conjugated α-BuTx

Random sections of soleus muscle from rats injected with BoNT/A alone, AAV-His$_6$-S25-R198T then BoNT/A and untreated controls were stained with a α-Butx-Alexa 488 conjugate, and images captured on an Olympus IX51

inverted fluorescent microscope with 10x objective and a fast digital camera (Evolution QEi monochrome, MediaCybernetics). A calibrated motorised stage and 'Stage-Pro' software allowed the serial acquisition and stacking of image-frames to obtain a picture of the whole muscle area. Scans of 20-40 sections of the muscle were acquired per treatment regime and analysed with 'Image-Pro Plus 5.1' software (MediaCybernetics). The automated 'count' function, after adjusting the ranges, permitted quantitation of the total endplate area, mean endplate area and size of the largest endplate in each section, along with the total muscle area. Data from more than 2000 endplates, as determined by the program, were quantified per treatment, normalized to the total muscle area, averaged over ~20 sections per treatment and compared to untreated and toxin-only treated muscles; t-test was used to determine statistical significance. Staining with anti-NF200 and fluorescently-tagged α-BuTx allowed monitoring of sprouting at NMJs protected by viral-mediated production of BoNT/A-resistant S25.
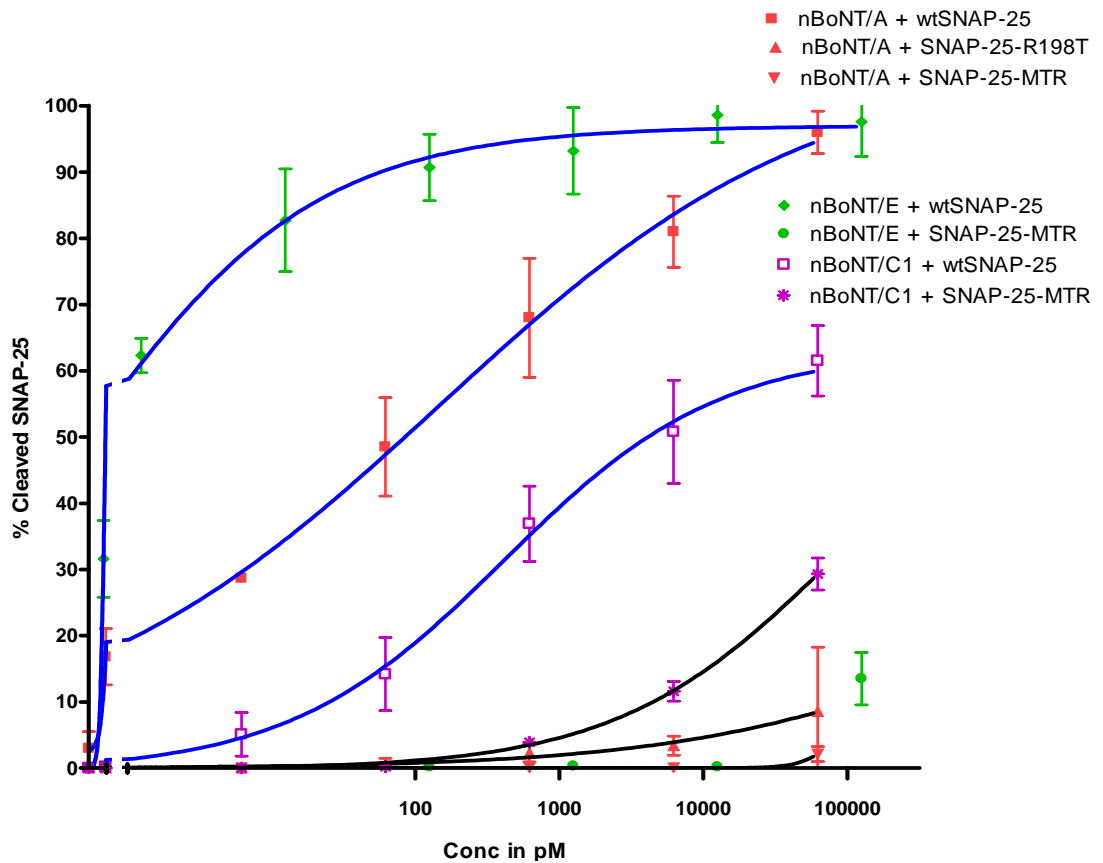
Fig. 17: Cleavage resistance of different SNAP-25 mutants to BoNT/A, /E and /C1: A sigmoidal dose response curve of SNAP-25 cleavage at different doses of BoNT/A, /E and /C1 is shown here. Blue lines represent cleavage of wtSNAP-25, while the black lines show cleavage of mutant SNAP-25. (Compared to wtSNAP-25, SNAP-25-R198T was more than 4 log orders resistant to BoNT/A mediated cleavage while SNAP-25-MTR was strongly resistant to all three serotypes – showing >5 log orders resistance to /A and /E and >2 log orders resistance to /C1).
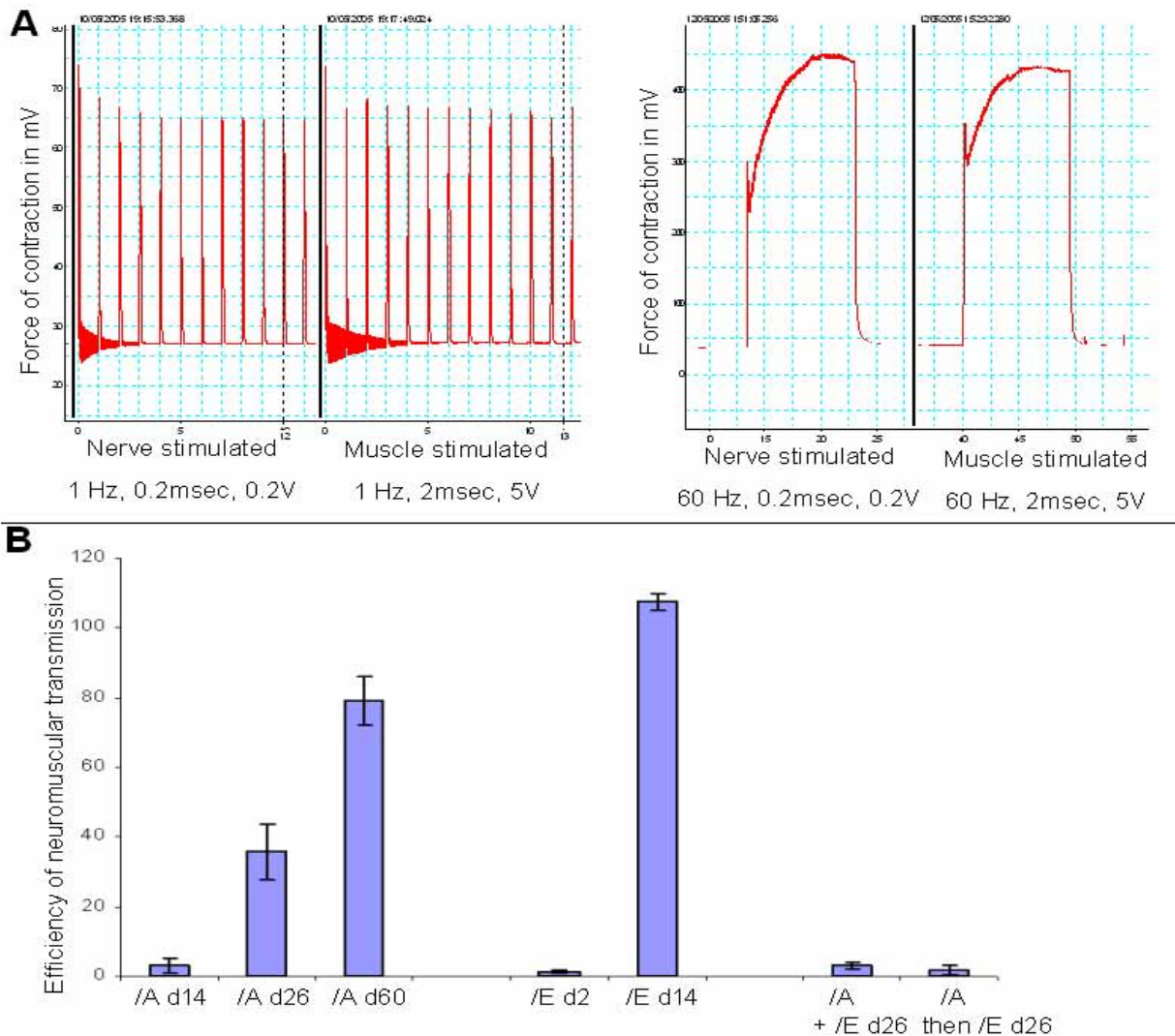
Fig. 18: Quantitation of ENT in the soleus muscle of live rats gives an accurate and reproducible measure of the blockade of ACh release induced by different BoNTs. **A:** The force generated by the soleus muscle after single supra-maximal stimulation of the sciatic nerve (0.2 msec, 200mV) is compared to that developed after direct stimulation of the muscle (2 msec, 5V) (Left). Similarly, peak force generated after nerve and muscle stimulation at tetanic frequencies is represented in the right panel. The ratio of the latter, when expressed as a %, defines the efficiency of neuromuscular transmission (ENT) – an accurate measure of peripheral neuromuscular transmission. In this untreated animal, the force developed by nerve and muscle stimulation are virtually identical – ENT is ≈100%. **B:** The neuroparalytic effects of BoNT/A in rat peripheral neuromuscular junctions lasts for a long time and is unaffected by concurrent or subsequent /E administration. BoNT/A (10 pg in 10 μL normal saline/BSA) or BoNT/E (1125 pg in 10 μl normal saline/BSA) was injected into the right gasto-soleus region of sedated rats on day 0 along with injections of the carrier into the contra-lateral region. ENT measurements were performed as described earlier on day 14, 26 and 60 for /A and on day 2 and 14 for /E injected animals. The /A then /E animals received BoNT/A as before and were injected with 1125 pg BoNT/E 2 days later. /A +/E animals received 10 pg BoNT/A + 112 5pg BoNT/E in 10 μL NS/BSA on day 0. ENT measurements on the latter two sets of animals were performed on day 26. Each bar represents the mean +/- SD of three measurements after stimulation at tetanic frequencies.

2.3. Results

Initial testing in HEK-293 and bovine chromaffin cells was performed to prove concept of botulism gene therapy. Later, the rat soleus muscle was chosen as an *in vivo* system to study the effects of viral vector-induced prophylaxis for subsequent blockade of Ach release by BoNT/A. The efficiency of neuromuscular transmission (ENT) – the ratio between the force of contraction elicited by nerve stimulation alone to that by direct muscle stimulation – provides an accurate and sensitive means to determine the progress of, and recovery from, toxin-induced neuromuscular paralysis. Direct spinal injection, which yields the best MOI for any virus was tested first, followed by peripheral intra-muscular injection. The results of these experiments, and others, are presented below.

2.3.1. Cleavage resistance of different SNAP-25 mutants to BoNT/A, /E and /C1

The induced mutations confer substantial resistance from cleavage by their respective BoNT toxins. Eukaryotically produced SNAP-25, which is post-translationally modified and membrane bound, is the natural substrate for the CNTs (O'Sullivan et al., 1999). While protease assays can be done with SNAP-25 fragments produced in *E.coli*, the availability of the natural substrate, produced in HEK-293, with its inherently higher BoNT susceptibility produces more physiologically relevant data. In addition, the relative absence of any natural SNAP-25 in these cells enables a clear determination of the different

116

toxin's enzymatic properties. While BoNTs cannot enter HEK-293 cells in sufficient quantity naturally, digitonin permeabalisation enables them to easily access their substrates.

SNAP-25-R198T is more than 4 log orders resistant to BoNT/A cleavage than the wtSNAP-25. SNAP-25-MTR is strongly resistant to all three serotypes – showing >5 log orders resistance to /A and /E and >2 log orders resistance to /C1 (See fig. 17). While only the R198T mutant was used in the following experiments, the proven ability of the MTR mutant, and the presence of similar flanking restriction sites, should enable an easy transfer to the latter, if multi-toxin-resistance becomes necessary.

## 2.3.2. Longevity of neuromuscular paralysis induced by BoNT/A and BoNT/E in rats models of botulism

Human cases of botulism, caused by BoNT/A, show a persistant neuromuscular paralysis that can last more than 6 months. While mouse models have been shown to suffer from exocytotic blockade for 4-6 weeks, the situation in rats was not yet fully clarified. There was also some controversy regarding the effect of BoNT/E administration with or after BoNT/A injection (See (Meunier et al., 2003) and (Adler et al., 2001)). For this reason a detailed dose-response study of the effects of BoNT/A, administered without/with/before BoNT/E was done. DAS provide an easy, non-invasive, repeatable, yet moderately inaccurate method of quantifying the function of the small muscles in rat hind limbs. When used in conjunction with an end-point ENT determination, a complete picture of the effects the different BoNTs, and the

117

utility of their treatments, can be obtained.

In rat models of botulism, BoNT/A shows a prolonged neuromuscular paralysis that persists for more than 60 days (See fig. 18 and 19). While there was some recovery by day 60, it did not reach the pre-injection levels. On the other hand, injection of BoNT/E alone caused a near total blockade of exocytosis 2 days after injection, with a complete recovery seen by day 14. Simultaneous or subsequent administration of BoNT/E did not cause any effect on the BoNT/A-mediated neuromuscular blockade.

Interestingly, the time-course of paralysis was strongly age-dependent (See fig. 19). Injection of weight-normalised doses of BoNT/A into younger animals resulted in a far shorter duration of exocytotic blockade at the NMJ. While not unexpected, this finding can still have exciting implications in the search for therapeutics against BoNT/A, as it is possible that a juvenile animal produces factors either enabling it to recuperate faster from the paralysis, by sprouting quicker or more profusely, or due to intra-cellular proteases or ubiquitinases that shorten the lifespan of the toxin's LC in the pre-synaptic terminals.
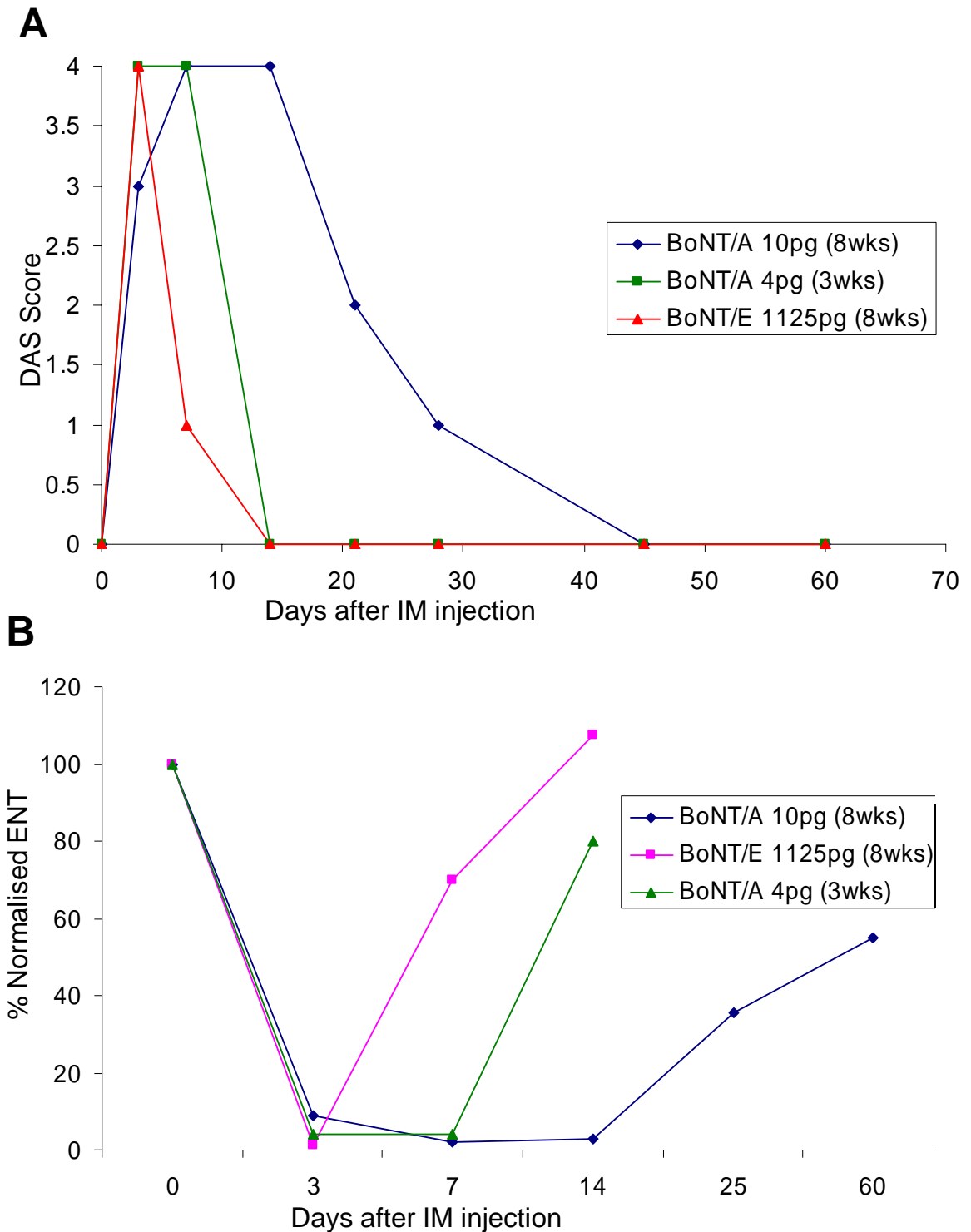
Fig. 19: Longevity of BoNT/A-mediated neuromuscular paralysis is age-dependent in rats: **A:** DAS scores after IM injection of BoNT/A or /E. 10pg of BoNT/A (~2.5 mLD$_{50}$) was injected into the soleus of 8-week old rats (~180-200gms, wistar female). Similarly, 5pg of BoNT/A (~1 mLD$_{50}$) was injected into 3-week old rats (~60-70gms, wistar female). The far shorter activity of BoNT/E (1125 pg) was also compared in this study. Younger rats show an accelerated recovery from BoNT/A as compared to older, adult, animals. **B:** ENT measurements confirm the shorter duration of action of BoNT/A in juvenile rats.

A hrGFP

B

(i)   (ii)   (iii)

α-hrGFP   α-His$_6$ α-S25

C

x = 10^7 GC/ml

Ba^{2+} evoked catecholamine release
(% change compared to 10 nM BoNT/A)

1x   2x   1x

3x   1x

4x   3x   2x   1x

-ve   WT SNAP-25   ←+Marker→

←—Control—→   ←—— Resistant ——→
                         SNAP-25
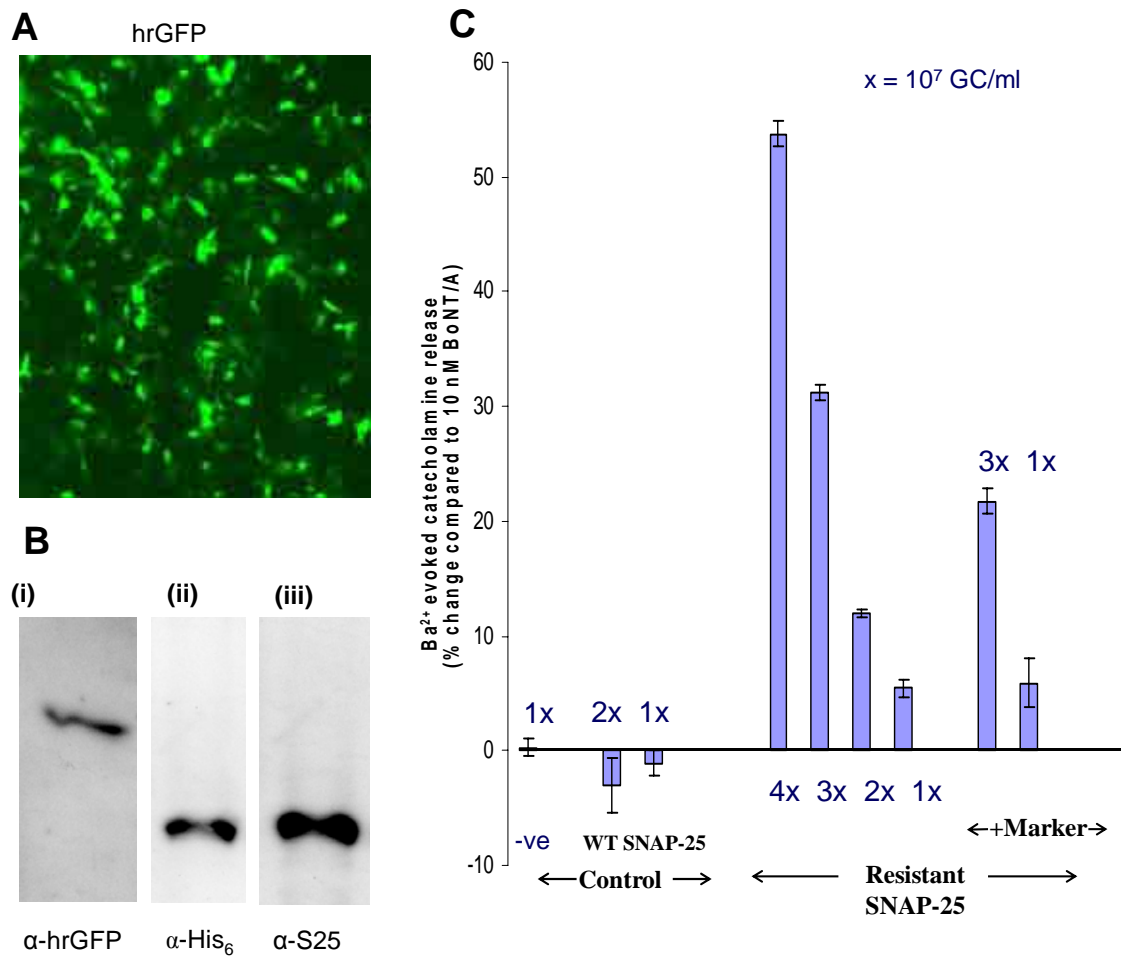
Fig. 20. AAV-mediated expression in chromaffin cells of cleavage-resistant S25, but not wild-type, antagonises inhibition of stimulated catecholamine release by BoNT/A. AAVs (10^7 GCs per well or multiples thereof) expressing either His$_6$-S25WT, His$_6$-S25R198T, His$_6$-S25R198T+ hrGFP or vehicle only were added to chromaffin cells and maintained for 7 days before further manipulations. Fluorescence microscopy demonstrated a high level of infection by AAVs, as reflected by expression of hrGFP (**A**); Western blotting confirmed co-expression of hrGFP and His$_6$-S25R198T (**B**). Infected and control cells were exposed to 10 nM BoNT/A for 24h before stimulating exocytosis with 2mM Ba^{2+} and quantifying evoked catecholamine release over 15 mins (see Methods). BoNT/A reduced the amount of evoked catecholamine release from non-infected cells by 70% compared to non-intoxicated controls [data not shown and (O'Sullivan et al., 1999)]. The average amounts of release from virus-treated cells are plotted (**C**) relative to those from cells exposed to vehicle alone (S.D.; n = 4). All the cells treated with clevage-resistant S25 containing virus showed a statistically significant increase in catecholamine release (* = P<0.01, as determined by a t-test) compared to untreated controls.

120
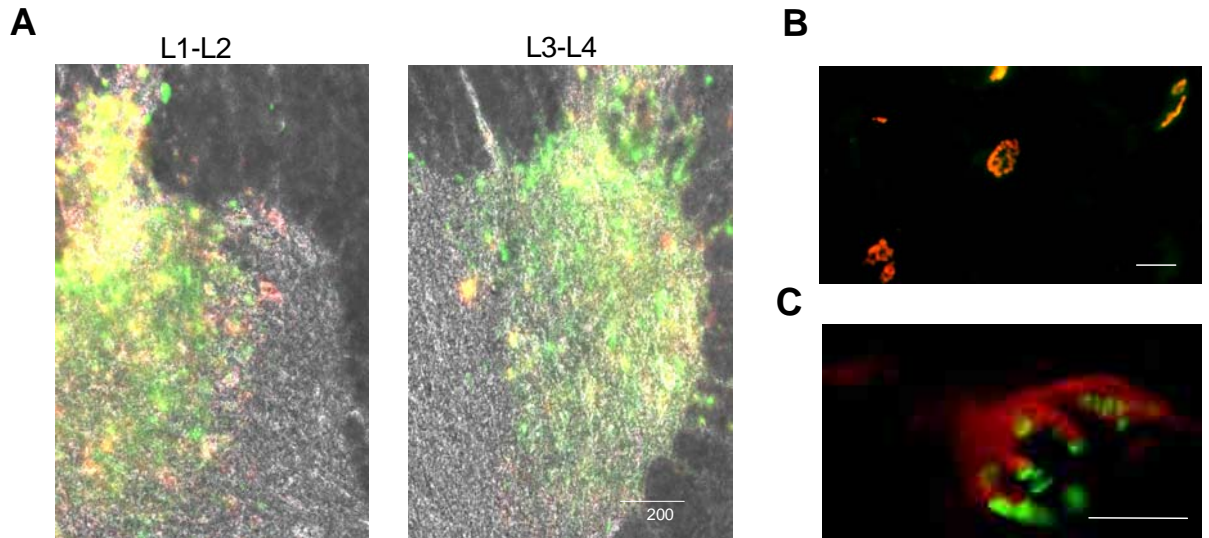
Fig. 21. Stereotaxic intra-spinal injection of therapeutic AAVs results in strong local expression and subsequent delivery of cleavage-resistant S25 and hrGFP proteins to the peripheral NMJs**.** **A**, Spinal cord sections from rats injected with AAVs expressing hrGFP and His_6-S25-R198T (5µL of 10^{11} GC/ml) were probed with an anti-His_6 antibody followed by a goat anti-mouse Alexa-568 conjugate. The green fluorescence of hrGFP and His_6-S25-R198T (red) co-localised in a circumscribed area in the right L1-L2 anterior horns. There is some vertical columnar diffusion of the injected virus, as revealed by similar fluorescence and co-localization at L3-L4. (scale bars = 200 µm). **B**, Delivery of hrGFP (green) to the presynaptic terminals is demonstrated by its co-localization with the post-synaptic ACh receptor, identified with a α-BuTx-rhodamine conjugate (red), in a soleal muscle section from a rat injected with AAV-hrGFP (scale bars = 20 µm). **C**, Soleal muscle sections from animals injected with AAV-His_6-S25-R198T probed with anti-His_6/goat anti-mouse-A568 antibodies to identify protected NMJs. The anatomical structure of the supplying nerve and its presynaptic terminal (red – binding to the His_6 tag) and the α-BuTx-Alexa488 bound post-synaptic ACh receptors (green) are clearly seen in this 63x fluorescent micrograph (scale bars = 20 µm).

2.3.3. Expression of BoNT-resistant S25 in mammalian cell lines using AAVs as gene transfer vectors

AAV helper-free vector system based on a non-pathogenic, non-immunogenic *Parvovirus* was used to construct recombinant type-2 AAVs incorporating the different genes. Initially, control viruses expressing the hrGFP marker protein were produced in HEK-293 cells triply-transfected with the different viral components. Heparin affinity chromatography (Zolotukhin et al., 1999) of the cell lysate yielded pure viruses with titers of 10^8-10^9 GC/μl, as seen on Coomassie-stained SDS-PAGE gels and corresponding Western blots; only bands corresponding to the viral surface protein were visualized (See fig. 13 and 14). Their titer and infectivity were determined in HEK-293 cells (See fig. 14 and 15). Later, wild-type or mutated S25, engineered to be non-susceptible to cleavage by BoNT/A due to a single residue being substituted at the scissile bond, were introduced into this vector, produced and purified as before; in some cases, the proteins were co-expressed with a hrGFP marker, using an IRES segment. These AAV constructs efficiently expressed His_6-S25 protein in mammalian cells; strong membrane association was confirmed by Western blots of the membrane and cytosolic fractions (See fig. 16). Confocal microscopy with an anti-S25 antibody revealed association of a large fraction of the expressed His_6-S25R198T protein with the plasmalemma (See fig. 16B). Co-expression of the hrGFP and His_6-S25R198T in cells infected with the AAV-His_6-S25R198T-IRES-hrGFP virus could be demonstrated by visualizing hrGFP fluorescence and immuno-detecting the His_6 signal, using a phycoerythrin

labeled secondary antibody (See fig. 16C). Success with viral-mediated expression of S25 in HEK-293 cells warranted functional testing in an *in vitro* chromaffin cell model.

2.3.4. Demonstration of dose-dependent protection of stimulated exocytosis from BoNT/A-induced blockade by prior expression in chromaffin cells of His$_6$-S25R198T but not wild-type S25

The protective ability of these viruses was assessed in chromaffin cultures exposed for 7 days to various concentrations of the recombinant viruses before challenge with 10 nM BoNT/A and measurement of catecholamine release. Expression of the introduced genes was established by fluorescence microscopic detection of viruses co-expressing hrGFP, or Western blotting of membrane fragments from lysed cells with antibodies specific for His$_6$, hrGFP or S25 (See fig. 20A and B). AAV-His$_6$-S25R198T viruses gave ~55% protection against BoNT/A-mediated blockade of exocytosis when applied at a MOI (multiplicity of infection) of 50 (highest concentration tested – which infected ~90% of the cells); this protective effect showed a clear dose-dependency (See fig. 20C). The AAV-His$_6$-S25R198T-IRES-hrGFP virus yielded a lower, yet significant, protection (~23%) while over-expression of wild-type S25 alone failed to show any effect (See fig. 20C). These strong prophylactic outcomes obtained, despite using large numbers (>10^6 cells per well) of post-mitotic neuroendocrine cells, justified progression from *in vitro* to *in vivo* testing of this gene therapy paradigm for botulism.
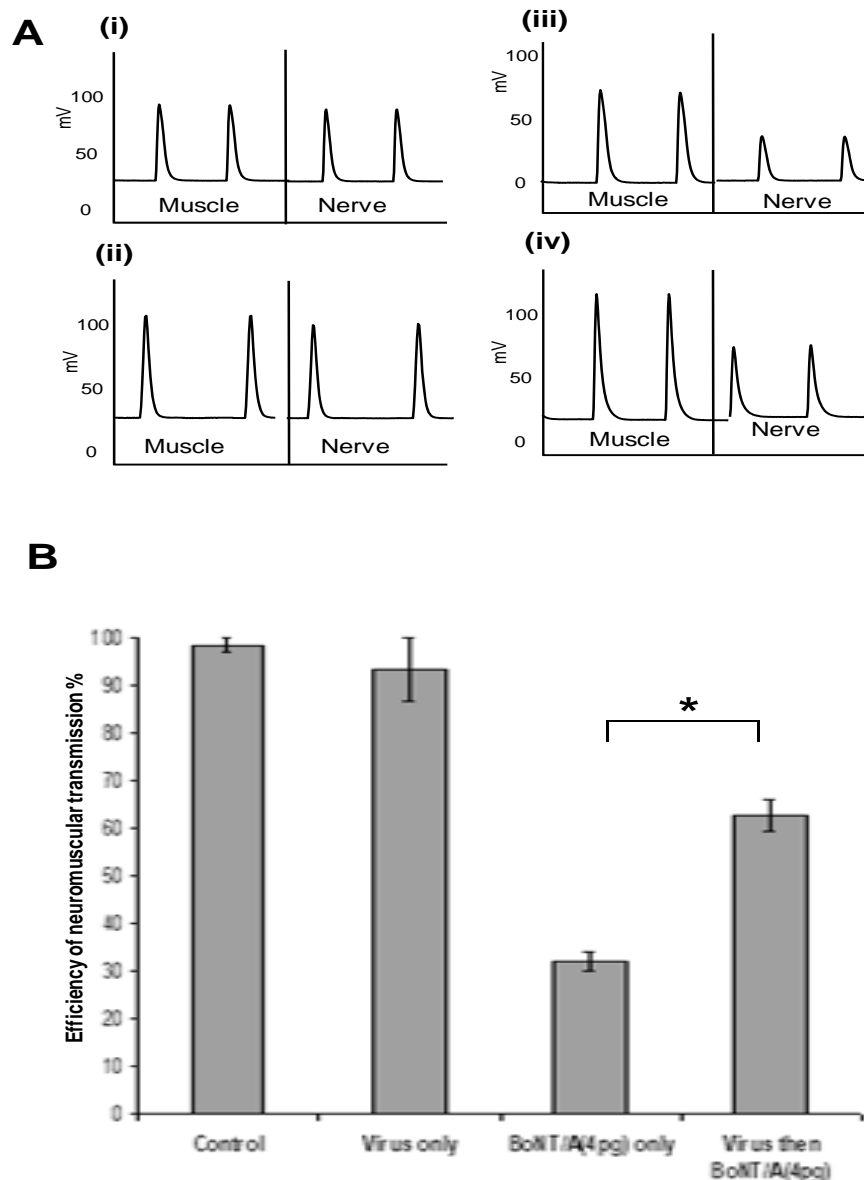
Fig. 22. Prophylactic treatment with AAV-His$_6$-S25R198T protects against neuromuscular paralysis induced by BoNT/A. **A,** The force of contraction elicited by nerve stimulation was compared to that by direct muscle stimulation in animals with and without protection against BoNT/A by prior spinal injection of AAVs expressing cleavage-resistant S25 in the right anterior T12, L1 and L3 spinal segments. Four groups of animals were used – (i), and (ii) & (iv) were injected with AAV-hrGFP and AAV-His$_6$-S25R198T respectively, with a control group (iii) injected with just the vehicle. Group iii and iv were injected with BoNT/A 21 days later. After a further 16 days, force generated by the soleus muscle after single supra-maximal stimulation of the sciatic nerve (0.2 msec, 200 mV) was compared to that after direct stimulation of the muscle (2 msec, 5V) (left). This ratio defines the efficiency of neuromuscular transmission (ENT) – an accurate measure of neuromuscular transmission. Representative contraction profiles for each treatment group, extracted from the recording program "Chart", are shown in **A**. The increased ratio between muscle and nerve stimulated contractions in virally pretreated (iv) compared to the un-protected (iii) animals demonstrates the prophylactic ability of the introduced cleavage-resistant S25. **B,** Summarized data showing the protective effect of viral pre-treatment on neuromuscular transmission from subsequent paralysis by BoNT/A; each bar represents the mean +/- S.D. of values from four animals (* = $p < 0.05$).

124

2.3.5. Efficient expression of cleavage-resistant S25 in peripheral nerve terminals of rats following intra-spinal administration of AAVs protects against the neuroparalytic effects of BoNT/A

Since animal models suffer from large inherent variability, an additional internal control was used i.e. ENT in the right muscle after BoNT treatment was compared to that for the vehicle-injected contra-lateral left soleus. Similarly, the BoNT-attenuating effect of viral pre-treatment of right soleal neurons could be accurately assessed by comparing ENT in this muscle with that in a similarly paralyzed but unprotected left muscle.

The stereotaxic co-ordinates to identify the relevant spinal segments, T12-L2, were determined; their right anterior horns were injected with AAVs expressing marker hrGFP and/or His$_6$-S25R198T. Localized co-expression of hrGFP and His$_6$-S25R198T in the right anterior horn, as determined by fluorescence/immuno- microscopy confirmed the accuracy of the micro-surgical procedure (See fig. 21); there was some expected vertical diffusion along the injected anterior motor column. After 6-7 weeks, the expressed proteins were also seen in the periphery at NMJs, identified by co-localization of α-Butx bound to ACh receptors (hrGFP & α-Butx in Figure 21B and His$_6$-S25R198T & α-Butx in Figure 21). Having confirmed the presence of cleavage-resistant S25 in pre-synaptic nerve terminals after AAV-mediated gene transfer, its functional effectiveness was established by a subsequent BoNT/A challenge. For such functional analysis, animals were injected thrice, into the right anterior T12, L1

125

and L3 spinal segments, with 5uL of various AAVs in order to maximize the chances of infecting a large portion of neurons supplying the right soleus. A precise bilateral injection of ~1 mouse LD_{50} of BoNT/A in NS/BSA was made 21 days later into the soleus using a small skin incision; after a further 16 days, ENT values were determined. Control animals injected with AAV-hrGFP or AAV-His_6-S25R198T alone displayed no significant variation in ENT between the left and right soleus [See fig. 22A (i) and (ii)]. The expected paralysis of nerve conduction in animals injected with BoNT/A alone was confirmed by the decreased signals compared with that for direct muscle stimulation. The maintenance of near-normal neurotransmission in unchallenged synaptic junctions over-expressing hrGFP or S25R198T demonstrates the non-deleterious nature of these introduced genes, purity of the preparations and the minimal trauma caused by the careful stereotaxic technique. Animals pre-injected with AAV-His_6 S25R198T showed a significantly greater retention of neuromuscular transmission [See fig. 22A (iv)] compared to the unprotected (contralateral) side after a BoNT/A challenge [See fig. 22A (iii)] ($p < 0.05$); summarized data from 4 animals for each group is depicted in Figure 22B. This attenuation of BoNT/A-induced neuroparalysis is the first ever demonstration of a non-immunological protective therapy in whole animals and establishes the functional effectiveness of the virally-delivered cleavage-resistant S25.
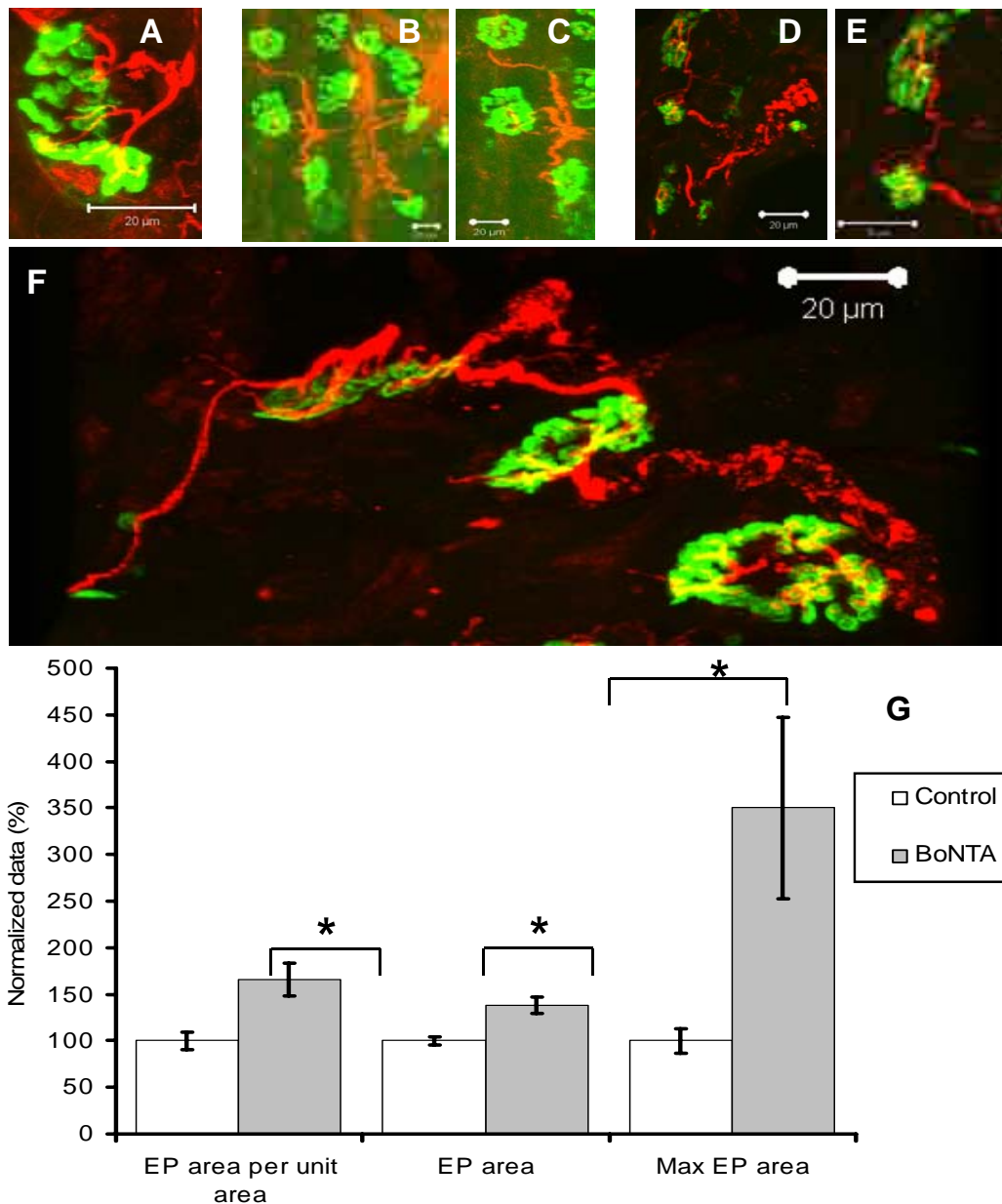
Fig. 23. Synaptic remodeling in adult soleus muscles exposed to BoNT/A. Confocal immuno-fluorescence pictures from control **(A)** and BoNT/A-treated muscles **(B-F)** show, respectively, NMJ (**A**), axonal sprouting (**B** and magnified in **C**), terminal sprouting (**D** and magnified in **E**) and mixed sprouting [**F,** axonal sprouting-arrow and terminal sprouting-arrowhead) (scale bars = 20 μm); α-NF200, in red with α-Butx-A488 in green]. An automated system was developed for the quantification of mean and maximum endplate (EP) sizes and total muscle area in randomly chosen 25 μm sections from control and BoNT/A-injected soleus muscles (see Methods). The fraction of the muscle area occupied by the EPs (EP area per unit area), the average EP area (the EP area) and the area of the largest EP (Max EP area) in each section of BoNT/A-treated muscles were expressed relative to the untreated muscles - average and S.E.M data from BoNTA-treated EPs (in grey) and control EP data (in white) are plotted (**G**). The results shows clear and significant (* = p ≤ 0.005 by unpaired t-test) differences in EP area per unit area, the EP area and max EP area per section.

127
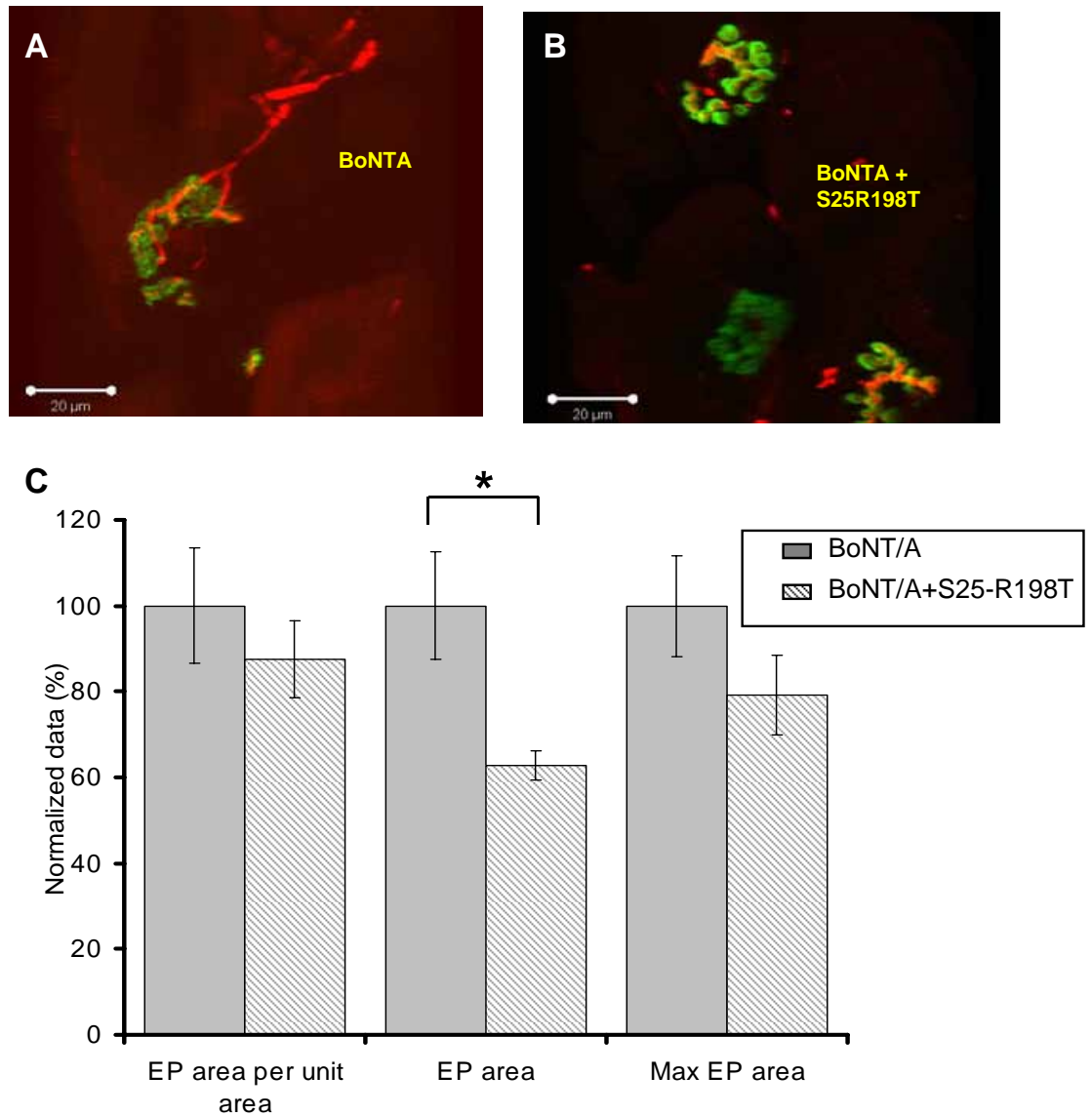
Fig. 24. Virally-expressed His$_6$-S25R198T attenuates BoNT/A-induced motor endplate remodeling *in vivo*. AAV-His$_6$-S25R198T was injected into the right anterior horn of rats and four weeks later ~2 x LD$_{50}$ BoNT/A was injected bilaterally into both soleus muscles (see Methods). After a further 25 days, both soleus muscles were removed, fixed and sectioned (25 μm thick) for immuno-histochemical staining. Representative confocal micrographs (detailed in Methods) show the pre-synaptic immunofluoresence signals observed with antibodies to NF-200 (red) and the distribution of post-synaptic nicotinic ACh receptors revealed with A488-conjugated α-Butx (green), in muscles from control (**A**) and virus-injected sides (**B**). Additionally, randomly chosen sections were stained with Alexa-488-conjugated α-Butx and subjected to automated endplate quantification (as described previously) (**C**). The average and SEM of EP area per unit area, the EP area and max EP area per section for virus pretreated muscles (hatched bars) are expressed as a % of those for muscles exposed to toxin alone (grey bars). The results shows a significant (* = p ≤ 0.005 by unpaired t-test) difference in the EP area in protected muscles.

2.3.6. BoNT/A-induced synapse remodelling is reduced by protection of neuromuscular transmission with a spinal injection of AAV-His$_6$-S25-R198T

Muscle paralysis induced by BoNT/A is known to cause motor axons to sprout and form new, functional synapses around the blocked parent terminals; in mice, the sprouts start to retract after 7 weeks, around the time when activity returns to the synapse (de Paiva et al., 1999). While it has been hypothesized that this sprouting is essential for the recovery of the intoxicated muscle (Juzans et al., 1996; de Paiva et al., 1999), its absolute contribution is unclear. For these reasons, it was decided to examine the amount of sprouting in 'protected (by AAV-His$_6$-S25-R198T) and challenged (by BoNT/A)' muscles compared to the situation in 'unprotected and challenged' or 'unprotected and unchallenged' muscles. The postsynaptic part of the NMJ was chosen for this quantification as it is known that any change there is tightly linked to alterations in presynaptic morphology and, as has been noted in published papers, changes in ACh receptor density and distribution are more sensitive to perturbations of synaptic transmission than modifications in the pre-synaptic compartment (Pestronk and Drachman, 1978b). The exquisitely specific binding and the strong fluorescence of bound α-Butx-A488 conjugate lends itself to automation (Powell et al., 1984; Askmark et al., 1991; Wang et al., 2005), whereas the heterogeneous presynaptic changes necessitate a more labour-intensive and subjective method of quantification. Using low magnification (to avoid artefacts from unfocused planes) and a software-controlled motorized stage, the amount of

sprouting evoked by BoNT/A and the effect of viral protection on this process could be determined.

The soleal muscles from BoNT/A-treated and control rats were dissected at various times after injection, sectioned and stained using α-Butx-A488 and an antibody against neurofilament 200 k isoform (α-NF) to visualize the post-synaptic and pre-synaptic parts of the NMJ, respectively. Comparison of muscle sections from control and these treated 16 or 25 days earlier with BoNT/A revealed a much greater number of sprouts in the latter (See fig. 23 A vs B-F). Additionally, in agreement with published results (Brown et al., 1980), it was observed that axonal and endplate sprouting frequently co-existed in the same muscle and, sometimes, in the same endplate (See fig. 23F). Exceptionally, some minimal endplate sprouting was also visualised in control muscles. When compared to untreated muscles, significant increases were found after BoNT/A treatment in the mean endplate area, the area of the largest endplates and, probably due to the muscle wasting that accompanies paralysis, an enlargement in the endplate space occupied per muscle section (See fig. 23G). After characterizing BoNTA-induced sprouting in the soleus muscle, the effect of protection on this process was determined. Immuno-staining of 16-day toxin-treated soleal sections with α-Butx-A488 and anti-αNF, to label endplates and axons respectively, showed less extensive sprouting at NMJs of rats that received BoNT/A-resistant S25 than those given toxin alone (See fig. 24A and B). Furthermore, examination of more than 30 random sections per treatment revealed that the average endplate area was significantly reduced in those endplates expressing S25 R198T compared to controls (treated with the toxin

alone). Lesser, but non-significant, reduction was seen in the maximum endplate and in the ratio of endplate to muscle areas (See fig. 24C).

2.3.7. Partial protection against BoNT/A-induced neuroparalysis in rats by neuronal expression of His$_6$-S25R198T after peripheral injection of its AAV construct

While intra-spinal AAV injection achieved efficient transduction and protection of motor neurons against BoNT/A with minimal effect on normal synaptic transmission, a peripherally-deliverable therapy is preferable as it can be injected into the affected muscles, thereby, decreasing the dose needed and reducing any potential risks. The control AAV-hrGFP virus, which was first tested due to the ease of identification of the expressed product, underwent retrograde transport to the spinal cord, as confirmed by expression of the marker protein in motor neurons of the anterior horn supplying the soleus muscle (See fig. 25A). Having confirmed the utility of such an approach, the ability of AAV-His$_6$-S25R198T to protect the motor neurons from BoNT/A-mediated paralysis was next evaluated. Injection of this therapeutic into the area encompassing the soleus muscle was followed a week later by toxin administration into the same muscle; the contra-lateral muscle was injected with the toxin alone. When tested 3 weeks after the viral injection, the protected NMJs in the best responding animals showed a 4-6 fold higher retention of synaptic transmission [18.5% v 3.2% for single stimulation [See fig. 25C (i)] and 62.5% v 15.3% for tetanic stimulation [See fig. 25C (ii)]. The combined results,

from 6 animals for each treatment, showed that the side injected with the virus gave a >2.5-fold increased retention of muscle strength in response to tetanic stimulation (27.5% vs 10.5%) (See fig. 25B). These initial investigations provide an encouraging demonstration of the potential of minimally-invasive paths to a gene therapy for botulism.

A (i)

Virus + BoNT/A BoNT/A only

(ii) Virus + BoNT/A BoNT/A only

Force of contraction in mV

Nerve Muscle

1 Hz

Force of contraction in mV

Nerve Muscle

60 Hz

B

Efficiency of neuromuscular transmission

Virus + BoNT/A BoNT/A

Treatment

C

Spinal cord (hrGFP)
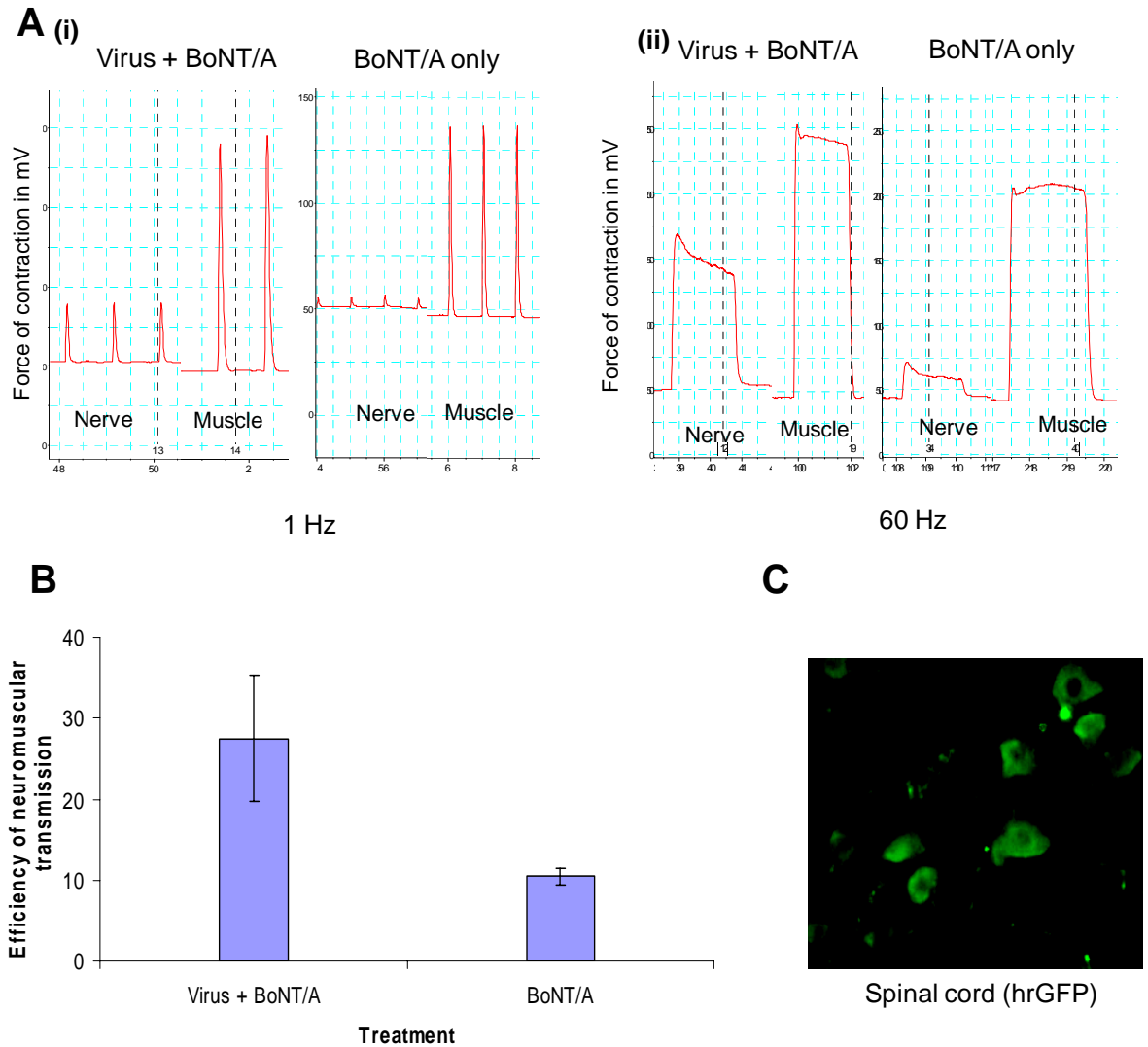
Fig. 25. Peripheral administration of therapeutic AAVs results in their retrograde transport and partial protection against subsequently administered BoNT/A. **A,** Florescence microscopic detection of hrGFP in large spinal motor neurons in the right lumbar spinal cord after peripheral administration of AAV-hrGFP. **B,** Rats were injected with 3x50µl of 10^{11} GCs/ml of AAV-His$_6$-S25R198T in PBS into the right soleus muscle; after 7 days, ~2 x LD_{50} of BoNT/A was injected bilaterally. Summarized data from ENT measurements 15 days later shows partial, albeit non-significant, protection induced by peripheral AAV pre-administration (**B**). Each bar = mean +/- SEM of the ENTs gathered from 6 rats. **C,** Single stimulus in (i) and tetanic stimulation in (ii) from best responding rats show the improvement due to viral pre-injection.

133

2.4. Discussion

To overcome the prolonged convalescence associated with human botulism caused by BoNT/A, a clinically-effective therapy needs to act at multiple stages by preventing the toxin's binding or uptake, inhibiting its breakdown of S25 and/or hastening recovery by replenishing truncated S25 with a functional, BoNT-resistant form (O'Sullivan et al., 1999). While progress towards the first two goals can, and is, being achieved by pharmacological means using antibodies and peptide or chemical inhibitors of the toxin's protease, a novel gene therapy approach is necessary to attain the final stages, especially in light of the extraordinary persistence of /A protease at nerve terminals (Adler et al., 1998; Keller et al., 1999; Foran et al., 2003; Meunier et al., 2003). The applicability of gene therapy was initially revealed by experiments demonstrating the attenuation of this toxin's inhibition of secretion from chromaffin cells following over-expression of a cleavage-resistant form of S25, which has a point mutation at the scissile bond (arginine at 198 position to threonine) that does not affect its participation in exocytosis (O'Sullivan et al., 1999). As the classical gene transfection used in that earlier study gave very low efficiency (<0.25%), much more effective gene delivery is a prerequisite for *in vivo* therapeutic purposes. To this end, the gene for S25-R198T was transferred into an AAV vector yielding a highly efficient, non-pathogenic means for transferring genes into non-dividing neurons.

2.4.1. AAV vectors are highly efficient neuronal gene delivery vehicles

when directly injected into spinal cord

Initial experiments confirmed that over-expression of a poly-His tagged version of cleavage-resistant S25 in eukaryotic cells does not overwhelm the intrinsic post-translation modification processes, especially palmitoylation, as revealed by the membrane association observed for this protein. This is important in light of evidence for the failure of free cytoplasmic S25 to take part in productive exocytosis (Washbourne et al., 2001) and due to the necessity for toxin-resistant S25 to antagonize disabled S25 at the membrane (O'Sullivan et al., 1999). The administered viruses infected 90% of ~10^6 cells and produced enough BoNT/A-resistant S25 to overcome the inhibitory effects of the toxin. Another outcome is the discovery that AAV-2 vectors can efficiently infect adrenal tissue, adding to the list of neuronal and neuro-endocrine types that can be targeted by this versatile virus (Burger et al., 2005).

While the results obtained *in vitro* validated the rationale behind the strategy, it was necessary to establish its applicability to the much more complex *in vivo* system. Paralysis and recovery from BoNT/A treatment can be accurately followed by measuring the force of contraction evoked by stimulation of the sciatic nerve in the lower limb muscles of rat (Adler et al., 2001); expressing this as a ratio to the force elicited by direct muscle stimulation reduces variations between animals. The well documented synaptic remodeling of rat soleal NMJs following neuroparalysis by BoNT/A (Pestronk and Drachman, 1978a; Brown et al., 1980; Son and Thompson, 1995) was another reason for choosing this muscle. Direct injection into the spinal anterior horn was prioritized for the initial mode of delivery as it results in a more intense

infection of motor neurons and, consequently, recombinant protein production than intra-thecal administration (Mannes et al., 1998). The controversy in the literature about the exact coordinates of the lumbar spinal levels supplying the lower limb between (Greene, 1968) and (Nicolopoulos-Stournaras and Iles, 1983) necessitated retrograde tracing using fluorogold injected into the soleus; the results obtained, T13-L2, agree with the latter. Stereotaxic intra-spinal injection of cleavage-resistant S25-expressing AAVs resulted in the localized expression of this protein in the lumbar anterior horns and, subsequently, their peripheral transport to the NMJs supplied by these motor neurons (Fig. 21). There was no evidence of any adverse effect on the synapse at the microscopic or functional levels; binding of fluorescently-labeled α-Butx showed normal distribution of post-synaptic ACh receptors; accordingly, only a small, non-significant, difference could be detected in ENT values between muscles innervated by virally-infected lumbar motor neurons and vehicle-injected control neurons. While spinal motor neurons were found to be relatively refractory to uptake of this capsid type-2 pseudotyped AAVs compared to other central neurons [agreeing with previous reports (Burger et al., 2004)], this was overcome by using larger volumes and multiple injections of high titers.

2.4.2. Delivery of cleavage resistant S25 to the exocytotic terminals ameliorates the transmission blockade induced by a later toxin challenge

Significantly, the expressed and peripherally-localized transgenic protein successfully substituted for native cleavage-susceptible S25, as clearly

demonstrated by enhanced retention of nerve-stimulated muscle contractility in pre-protected animals challenged with BoNT/A 16 days later (Fig. 22). This was detected using two different modes of stimulation – discrete single supra-maximal stimuli or trains of tetanic pulses – with the recorded protection being more marked when measured using the latter protocol. Such protection against a later BoNT/A injection was only observed after pre-injecting AAVs expressing His_6-S25R198T whereas administering AAVs that produce hrGFP or wild-type His_6-S25 failed to show any significant difference from vehicle-only controls. This is the first report on successful antagonism of BoNT/A action in live animals using viral vector-mediated gene delivery. The protection seen demonstrates that the produced protein can not only overcome the persistent protease activity of the toxin at motor neuron terminals (Adler et al., 1998; Keller et al., 1999; Foran et al., 2003; Meunier et al., 2003) but, also, any probable inhibition from the truncated native S25 (Dolly and Aoki, 2006). A combination of such gene delivery with the recently-described inhibitors (Schmidt et al., 1998; Schmidt and Stafford, 2005; Park et al., 2006), should yield supplementary benefits in providing immediate and prolonged therapy.

2.4.3. The retrograde trafficking ability of AAVs in rats – necessity to develop efficient targeting agents

Published data suggested that AAVs undergo successful retrograde transport from mouse NMJs and can efficiently infect anterior horn motor neurons supplying the targeted muscles, with efficiencies ~1 in 1000 virions

reaching the spinal cell body (Kaspar et al., 2003). While injection of >5x10^{11} AAVs into soleal muscle proved necessary to successfully detect infected motor neurons, this mode of administration offers advantages of minimal trauma and faster recovery from the operating procedure; most notably, in terms of possible clinical application, it allows easier access to important respiratory muscles (intercostal and diaphragmatic muscle). The functional value of this peripheral mode of application is reflected by the promising protection obtained, though the intrinsic variability in the responses of whole animals prevented a more convincing outcome.

The large difference in efficacy between published studies in mice and this study in adult rats poses fundamental questions about the potential of peripheral delivery for motor neuron gene therapy. An average mouse weighs 20g, compared to 200-400g for an average rat, and has a sciatic nerve that is less than 2cms in length, compared to more than 8 cms for an average rat (>100cms in an average human). Any delivered AAV has to negotiate the whole length of this nerve in order to reach the spinal motor neuron supplying the injected muscle. If an increase of 6cms strongly reduces the retrograde transport of AAVs in rats, the possibility of any virus reaching the MN in humans seems increasingly miniscule. Also, the greater muscle mass in larger animals will probably reduce the amount of virus reaching the NMJ, further complicating matters. One way of increasing retrograde transport would be to increase the number of AAVs delivered to every NMJ, thus increasing chances that a few will successfully navigate up the length of the sciatic nerve (or phrenic nerve and intercostals nerves, if the respiratory muscles are to be targeted). Thus

targeting with a NMJ specific molecule will be an essential step in graduating gene therapy from the laboratory to the clinic. Initial attempts at exploiting the known cholinergic specificity of CNTs to target viral vectors are described in Section 3.

2.4.4. Sprouting induced by BoNT/A is a result of exocytotic blockade and is reduced by the alleviation of such paralysis

It is believed that synaptic remodeling after BoNT/A-induced paralysis plays an important role in the early phases of recovery (Juzans et al., 1996; de Paiva et al., 1999; Meunier et al., 2003). The quantity of sprouts is thought to depend strongly on the amount of toxin introduced [for a more detailed discussion see (Connold and Vrbova, 1991; Tam and Gordon, 2003)], the kind of muscle [fast muscles have lower amounts of mostly axonal sprouting, compared to slow muscles which show a higher percentage of terminal sprouts (Pestronk and Drachman, 1978b; Brown et al., 1980) and the duration of paralysis (long-acting serotypes like /A induce a more extensive pattern of sprouting than short-acting /F; the extremely short duration of paralysis induced by /E results in no observable sprouts (Meunier et al., 2003)). Further complicating this picture is the effect of factors released from perisynaptic Schwann cells and muscle (Gomez et al., 1982; Son and Thompson, 1995; De Winter et al., 2006; Wright and Son, 2007). The data obtained from the present study points to a reduction in synaptic remodeling when the extent of paralysis is limited by over-expression of cleavage-resistant S25 in presynaptic nerve endings, substantiating the hypothesis that the extent of neurotransmission

blockade, along with the duration, are strong determinants of the amount of remodeling. The changes in sprouting seen upon treatment with the same dose of /A toxin in the presence or absence of viral protection seems to confirm that the differential effects on sprouting seen previously with the different toxin serotypes are a property of the duration of paralysis and not of the substrate cleaved or properties of their proteases. While these results do not reduce the importance of the contributions made by other factors towards initiating sprouting at a NMJ, it does hint that these are ultimately dependent on, and controlled by, the evoked exocytosis from the motor nerve terminals.

This study reports the attainment of an important milestone in the goal of a peripherally-deliverable gene therapy that can be administered after exposure to long-acting BoNT serotypes, raising the exciting prospect of a powerful means of successfully managing the late stages of botulism which presently involve a prolonged, resource-intensive recovery phase. The proof of principle obtained provided an encouraging foundation upon which to build more versatile vectors based on LVs that could allow the simultaneous transfection of neurons with multiple-toxin resistant S25, VAMP-2 and syntaxin for combating several toxin serotypes and even novel chimera. Furthermore, this model circumvents problems associated with using conventional murine models of human motor neuron diseases. The ability to control the extent/severity of 'disease' (i.e. neuroparalysis) when combined with the availability of a sensitive assay for measuring peripheral neurotransmission and the knowledge of the gene required to protect against the toxin's effects, allows prediction of the response to successful delivery. The elimination of these multiple variables

should enable a more focused investigation of the different changes needed to

obtain a peripherally-deliverable viral vector targeted to motor neurons.

3. Targeting viral vectors to cholinergic nerve terminals

3.1.1. Introduction – rationale behind the utilisation of the cholinergic targeting property of Clostridial neurotoxins to target therapeutic viral vectors to NMJs

There are two major aspects to peripherally delivered gene therapy for motor neurons – the first is to get the virus into the pre-synaptic terminal and second is getting internalised virus retrogradely back up the axon to the motor neuron nucleus. Indeed, every virus that's used for gene therapy can, and does both, of these things to some extent. But the specialised anatomical aspect of the NMJ-axon-spinal motor neuron complicates matters considerably. Therefore, peripherally delivered gene therapy for spinal motor neurons is relatively inefficient – the best case scenario in mice needs a >1000 fold excess of viruses for efficient transduction compared to direct delivery (Kaspar et al., 2003). Indeed, the present study in rats showed it is more than three log orders less efficient than in mice. Therefore there is an urgent need to funnel the delivered viruses towards NMJs thereby, increasing the delivery of viruses that can undergo retrograde transport and thus successfully infect the supplying motor neurons. This also decreases the number of viruses infecting muscle and connective tissue, reducing substantially the hazard of insertional mutagenesis and oncogenesis and also any transgene induced toxic effects. Another

advantage is the reduced proliferation of the introduced viruses into the blood and lymphatic systems, thereby avoiding sensitizing the immune system for viral components.

There are many potential ways of achieving these goals. The easiest is to use viruses that are naturally motor neuron specific and modify them to eliminate their pathogenicity (Keir et al., 1995). But such a procedure is laborious and discards the huge amount of work that has already gone into making safe and efficient general viral vectors. Another potential method is pseudo-typing an existing virus with the components of a motor neuron specific virus – e.g. lentivirus with a rabies virus glycoprotein (Mazarakis et al., 2001). Pseudo-typing is a well-established strategy to modfy viral, expecially lentiviral, specificity (Cronin et al., 2005). Indeed the current generation of lentiviruses use the envelope protein from the Vesicular stomatitis virus (VSV-G) (Zufferey et al., 1998). But, rabies virus glycoprotein pseudo-typing for NMJ targeting suffers from some disadvantages – this can only be used in lipid-enveloped viruses, like retrovirally-derived vectors, and while it does induce retrograde transport once inside the nerve terminal, it does not seem to substantially increase the chances of the virus entering such a terminal. This method of targeting also complicates assignment of a valid bio-safety profile to these viruses, containing as they do components of two different, and potentially dangerous, viruses. Another alternative is attaching immune, or immune-derived, molecules specific for NMJ surface constituents to the therapeutic viruses (Hedley et al., 2006). The advantage with this method is that it can be modified relatively easily, with suitable adapters, for use with enveloped or non-enveloped viruses. While this

method does increase the chances of the virus encountering and sticking to a cholinergic terminal, it does not increase the probability of viral endocytosis or of retrograde transport.

The natural cholinergic specificity of CNTs is an attractive option to achieve vector concentration on nerve-terminals. The bi-partite mechanism for cholinergic binding and internalisation inherent in all CNTs results in their exquisite specificity (See section 2.1). Exploitation of this specificity to deliver cargo is an attractive means of achieving motor nerve targeting. The ready availability of protease-inactive BoNT/E (BoTIM) led to its choice as the first candidate NMJ targeting molecule. An early decision was made to construct flexible NMJ-targeting molecules that can, with very little effort, be used to target various cargo, small molecules, liposomes or viral vectors, to NMJs. For this reason, BoTIM was conjugated at the genetic level to core-streptavidin (CS). This hybrid molecule should bind any biotinylated cargo while retaining the cholinergic specificity of BoTIM, thereby successfully delivering the bound cargo to NMJs. Some of the preliminary proof of principle studies in this regard are present in the following sections.

3.1.2. Core-Streptavidin

The high affinity of avidin, derived from egg-white, and streptavidin, produced by *Streptomyces avidinii*, for biotin has long been exploited in histological and biochemical applications (Bayer and Wilchek, 1990). Native streptavidin is a nonglycosylated, 52Kda tetramer with a near-neutral isoelectric point, that binds 4 moles of biotin per mole of protein with high selectivity and

affinity ($Kd\sim10^{-15}M$) (Bayer and Wilchek, 1980). The minimal, biotin binding part of a streptavidin molecule is called the core-streptavidin. The latter was chosen over the former, as it is far smaller, ~13Kda, and therefore easier to clone into the BoTIM gene without greatly perturbing its cholinergic binding abilities.

There are some potential problems with the use of CS. These molecules retain a strong tendency to tetramerize, and reconstitute the parent streptavidin, which could cause problems later with, potentially insoluble, aggregates of CS-BoTIM. In addition, the position of the CS in BoTIM, N- or C-terminal, could destabilise either the CS or the BoTIM leading on to a loss of biotin-binding or cholinergic-binding abilities. Also, because a complete biotin binding site in each CS subunit requires the contribution of tryptophan 120 from a neighboring subunit, a forcible monomerization, due to the attachment of a large BoTIM molecule, can reduce affinity towards biotin (Qureshi et al., 2001; Wu and Wong, 2005). But the high starting affinity results in a lot of leeway in biotin-binding affinity and indeed, a reduced affinity might be useful in allowing a targeted cargo to escape from the targeting molecule. While some monomeric, minimal streptavidins are now available (Qureshi and Wong, 2002), their performance in large chimeric hybrids are, as yet, unknown.
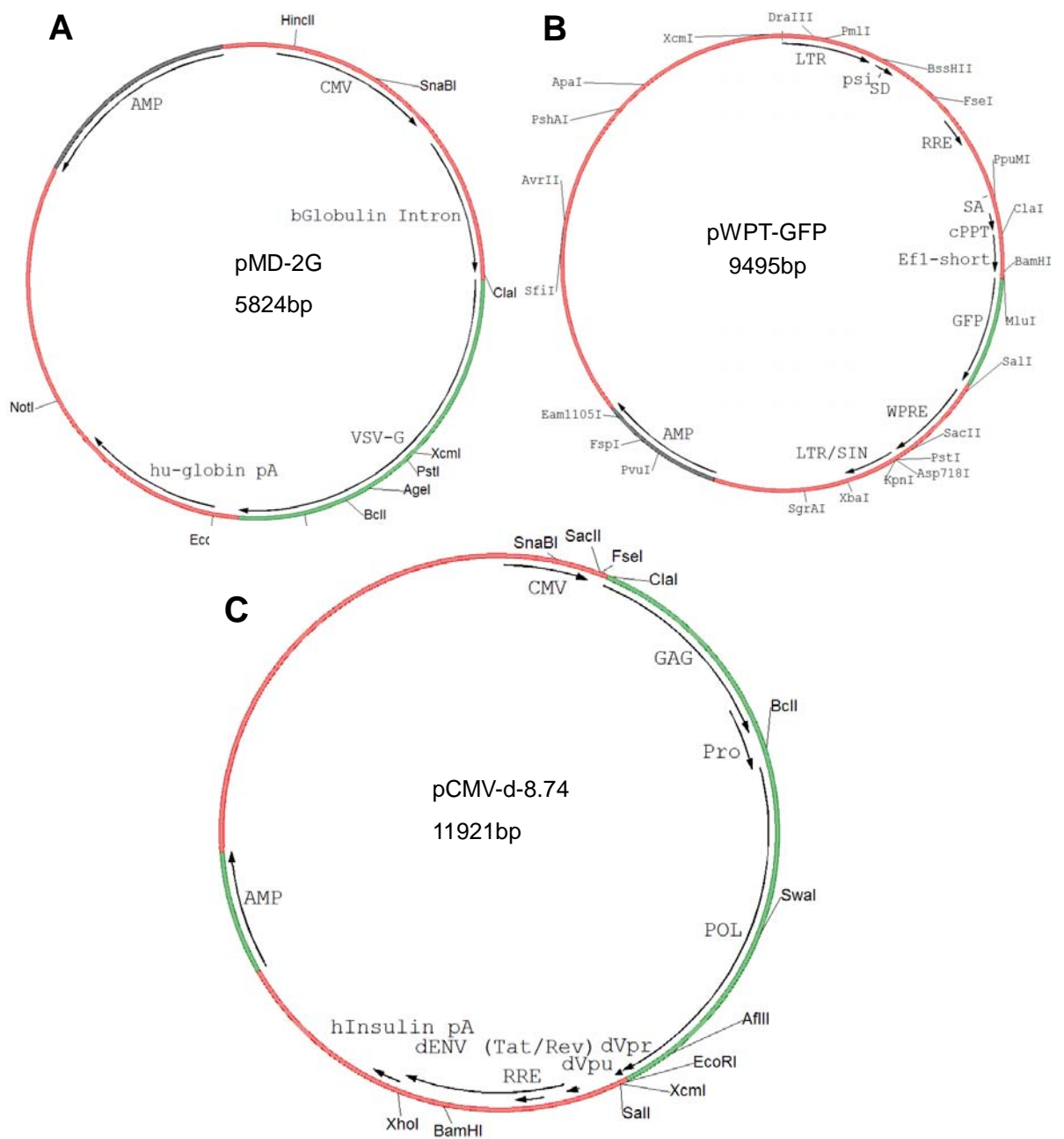
Fig. 26: Constituents of the LV production system: **A:** The VSV-G containing plasmid – pMD-2G: An annotated plasmid map, generated using Gene Construction Kit (GCK 2.5) showing the important constituents and unique restriction site. AMP – beta-lactamase gene; CMV – cytomegalovirus promoter; hu-globin pA – human globin poly-adenylation site. **B:** The transfer construct, pWPT-GFP, containing the essential cis-acting sequences. LTR – Long terminal repeats; SA/SD – splice acceptor and splice donor; RRE – reve responsive element; cPPT – central poly-purine tract; EF1 – elongation factor 1 promoter; SIN – self-inactivating. **C:** The trans-acting construct, pCMV-d-8.74. GAG – group specific antigen; Pro – protease; POL – polymerase; dVpu. dVpr and dENV – deleted viral protein U, viral protein R and envelope proteins; hInsulin pA – human insulin polyadenylation sequence. For more details about all these different proteins and sequences, please see section 3.1.3.
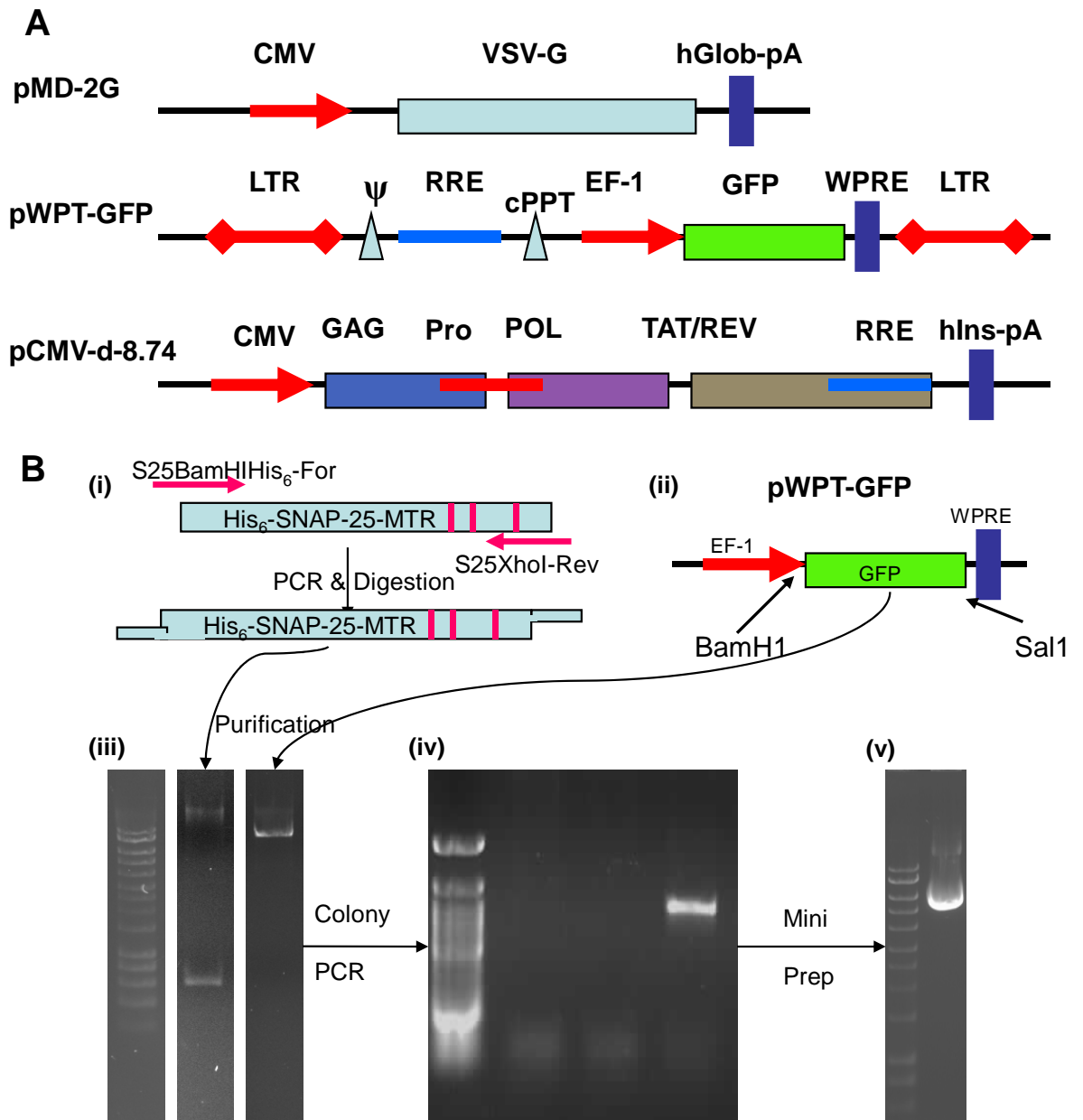
Fig. 27: Creating LVs expressing wt and mutant SNAP-25: **A:** A pictorial representation of different plasmids, showing the relative positions of the important constituents and the cloning site for any introduced transgene (See Fig. 26 and section 3.1.3 for more details). **B:** Cloning His$_6$-tagged multi-toxin resistant SNAP-25 into the cis-transfer construct, pWPT-GFP, by replacing the original GFP gene. PCR, with BamHI and XhoI containing primers, followed by restriction digestion with the relevant enzymes yielded His$_6$-SNAP-25-MTR [(i) and (iii)]. This was then cloned into a pWPT plasmid [(ii) and (iii)], digested with BamHI and SalI, and transformed into Dh5α chemically competent *E.coli.* Colony PCR with bglob-For and WPRE-Rev primers enabled the selection of only those clones containing the right insert (iv). These were then expanded into giga-preps and purified to yield highly pure plasmids, suitable for transfection of HEK-293 cells in culture (v).

3.1.3. Lentiviral vectors (LV)

The LV system is a replication-deficient, hybrid viral vector system made from the core proteins and enzymes of human immunodeficiency virus type I (HIV-1) and the envelope of a vesicular stomatitis virus glycoprotein (VSV-G) (reviewed in (Zufferey et al., 1998; Rohll et al., 2002)). These gene transfer vectors can mediate efficient integration of the transgene into the host genome, do not express any viral genes, are not affected by pre-existing immunity in the recipient and demonstrate the ability to infect non-dividing cells. Their biosafety profile has been improved by the separation of cis-acting sequences required for the transfer of the transgene to target cells, from the trans-acting sequences encoding the essential viral proteins, thus rendering them replication-deficient. Furthermore, the complete deletion of the native lentiviral envelope proteins and their replacement by a heterologous, VSV-G, envelope protein (pseudotyping), increases their infectivity towards a wide spectrum non-immune target cells and increases their safety, by reducing the chances of recombination with any native HIV viruses. While other retroviruses, like the feline, simian, bovine or equine immunodeficiency viruses, have been modified to suit gene delivery, the HIV based one is the most widely used and studied (reviewed by (Delenda, 2004)). The most widely used Lentiviral system utilises the simultaneous transfection of HEK-293 cells by three different plasmids to produce lentiviral particles (See Fig. 26). The essential cis-acting elements are found in the pWPT or pWPI plasmids, with the latter containing an IRES sequence for the co-expression of GFP with the gene of interest. It contains the two long terminal repeats (LTR),

encapsidation signal (psi), major splice donor (SD), rev responsive element (RRE), major splice acceptor (SA) and a central polypurine tract (cPPT). LVs have a large packaging capacity of approximately 8kb (see Fig. 26-27). The gene of interest in this plasmid is driven by a very efficient eukayotic promoter (elongation factor 1a or its minimal domain - EF-1a or short EF-1) and is flanked at its C-terminal by a woodchuck post-translational regulatory element (WPRE), which promotes the efficiency of polyadenylation of the nascent transcript and increases its total amount in the cells. These constructs are self-inactivating, with a major deletion in the U3 region of the LTR, containing the viral enhancer and promoter sequences. When infected into target cells, they duplicate this deletion, resulting in the transcriptional inactivation of the LTR. Such a self-inactivating vector diminishes the risk of oncogene activation, by promoter insertion and further reduces the chances of vector mobilization and recombination with wild-type virus. Also, self-inactivation of the LTRs eliminates the possibility of their interference in transgene expression, enabling the insertion of desirable promoters for tissue specific or regulatable activity.

The second plasmid is pCMV-d8.74 containing the GAG, pro, POL and Tat/Rev coding sequences. The complete deletion of the ENV sequence, coding for the surface glycoprotein, and Vif/Vpu/Nef/Vpr sequences, coding for additional non-essential deleterious proteins, further reduces the viral pathogenicity. The Tat protein acts as a transcriptional activator and Rev is required for expression of unspliced, packageable transcripts from the transfer vector construct. The GAG gene, which is codon optimized for optimum efficiency, provides the viral matrix proteins, RNA genome binding proteins and

149

the major proteins comprising the nucleoprotein core particle. The codon optimised POL gene encodes the reverse transcriptase, integrase and RNase H activity. Addition of the third plasmid, pMD2G, coding for an envelope G-glycoprotein from vesicular stomatitis virus increases the vectors' tropism (but could be limiting intracellular transport to relatively short distances). The use of this heterologous envelope protein strongly limits the theoretical possibility that multiple recombination events can join the viral cis-acting sequences in the transfer vector to trans-acting viral genes in packaging constructs to generate replication competent recombinants (RCR). While further gains in biosafety can be achieved by removing the Tat gene and separating the Rev gene into a separate plasmid, the compromised expression resulting from this is not considered a viable payoff for the concomitant increase in safety.

The LV system has a higher gene delivery capacity than AAV; with a capacity of ~8kb, it can accommodate most genes and tissue specific promoters. An additional advantage is the relative ease of swapping out the VSV-G surface glycoprotein for another - e.g., rabies virus (for retrograde transport (Mazarakis et al., 2001; Wong et al., 2004)), Ross River (more efficient on glial cells than neurons (Kang et al., 2002)), lymphocytic choriomeningitis virus (preferentially transduce murine neural stem cells and human glioma cell lines (Steffens et al., 2004; Stein et al., 2005)). One can also modulate its activity by attachment of molecules providing specificity for certain cell types, e.g., by IgG fragments or by clostridial toxins. However, since LVs are derived from pathogenic viruses, i.e, HIV-1, it is crucial that sufficient precautions be maintained to ensure adequate biosafety both during production

and administration; the AAV virus, a naturally non-pathogenic strain does not suffer from this drawback. The un-modified viruses also differ in their propensity to infect neurons over glia, with the ratio changing depending on the site of administration. But in general, transduction of most neurons has been demonstrated *in vivo* in rodent and primate models, using both the systems (Galimi and Verma, 2002; Azzouz et al., 2004). Neuronal gene transfer could be compromised by innate or induced immunity against viral proteins or the transgene products. This is more problematic for the AAV system, as AAVs can exist as a widespread and quiescent infection in certain populations (Peden et al., 2004). Innate immune responses are not problematic for LVs as only minimal and asymptomatic inflammation has been observed in animal models after their administration (Kordower et al., 2000). The problem of transgene induced immunity, while theoretically present, can be resolved by the judicious choice of proper proteins from the same, or highly homologous, species. A greater problem is that of transgene induced toxicity – the large gene capacity of the LV system, with their predictable copy numbers and low silencing effects, allows the introduction of regulated gene expression derived from bacterial operons such as the Tet repressor or engineered eukaryotic transcription factors (Vigna and Naldini, 2000; Pluta et al., 2005).

Gene delivery for neurological disorders often requires intricate and highly invasive surgery; therefore, long-term, stable expression at therapeutic levels is essential. Expression of transgenes after *in vivo* LV administration lasts for up to 16 months and these animals usually maintain expression without silencing after the first month (Kordower et al., 2000; Bienemann et al., 2003).

The biology of LV infection strongly indicates that there would be a reduction in transgene expression over time – initially there is a high level of mRNA production from all the LVs that manage to enter the nucleus, but later, only the integrated forms (in permissive environments) are capable of producing transgene mRNA while the untegrated ones are culled through natural cellular processes. The level, timescale and duration of this slump are not fully studied.

3.2. Experimental strategies employed

Many of the tools and techniques below are described in greater detail in section 2.2. The constituents of all the buffers and solutions can be found in Appendix 1. Animal surgery protocols are described in sections 2.2.1 and 2.2.5.

3.2.1. Development of LVs carrying marker EGFP and/or S25 mutants resistant to /A or /A, /E and /C1

SNAP-25 mutants described in section 2.2 were cloned into the pWPT-GFP plasmid, after the excision of GFP (See Fig. 27). In addition, SNAP-25-197 and SNAP-25-180, mimicing the residual cleavage products after BoNT/A and /E proteolysis) were cloned into pWPT-GFP. These purified plasmids, in addition to control plasmid pWPT-GFP and pWPT-SNAP-25 wt, were triple transfected into HEK-293 cells (20µg per 10cm plate) along with pMD2G (5µg per 10cm plate) and pCMV-d-8.74 (10µg per 10cm plate). After 12-24 h, the cells were washed 2-3 times and the media replaced. The LVs, secreted into the cellular supernatant, were concentrated using protocols modified from (Zufferey et al., 1998). The supernatant was harvested 24 h after media

change, spun down at ~500-1000G and filtered through a 45µm filter, before storage at 4ºC. Another batch of the supernatant was harvested after a further 24 h and treated as before. The two supernatant were mixed together, layered on 20% sucrose in PBS solution and centrifuged at 45,000 G for 2 h. The visible pellet was resupended in more PBS, pooled and centrifuged once again at 45,000G. The final pellet was resuspended in either PBS/5% BSA or DMEM medium, aliquoted and frozen at -80ºC.

3.2.1.1.   Titration of produced LVs by p24 ELISA

LVs were titered using a modified HIV-1-p24 ELISA kit obtained from Aalto Bio-reagents Ltd. This is a twin-site sandwich ELISA based on the capture of p24 antigen, from a detergent lysate of virions, onto a polyclonal antibody adsorbed onto a solid phase. The bound p24 is then detected with an alkaline phosphatase-conjugated anti-p24 monoclonal antibody and read using the luminescent detection system (Moore et al., 1990). Briefly, a sheep polyclonal anti-HIV-1-p24-gag antibody, diluted 1:400 into 100mM $NaHCO_3$ pH 8.5 buffer, is coated onto ELISA plates. After an overnight incubation, the plates are washed and blocked with 2% milk in TBS and stored at -20ºC till use. In the mean time, viral samples are inactivated by adding Empigen zwitterionic detergent to a final concentration of 1%. These inactivated viruses were then added to washed plates prepared as described previously and incubated for 3 h at room temperature. A standard curve, prepared from dilutions of HIV-1-p24 protein obtained from Aalto, is run in parallel with every ELISA reaction. After washing the plates, a 1:7500 dilution of the secondary antibody, anti-HIV-1-p24

mouse monoclonal alkaline phophatase conjugate, is added for a futher 1hr. The plates are washed again with PBS/0.1% Tween-20, tapped dry and developed with a Tropix system. The Tropix-ELISA cheimiluminescent detection system from Applied Biosytems uses CSPD 1, 2-dioxetane substrate to enable the rapid, sensitive and linear detection of alkaline phosphatase in ELISAs. The plates are rinsed with a 1x solution of the Tropix wash buffer, before addition of a CSPD substrate. The luminescence emitted from each well is calculated using a luminescene plate reader. Plotting the standard curve and extrapolating the values of the unknown samples onto the curve yields the p24 concentrations of the viral preparation (See Fig. 28). In addition, estimation of the total protein content, with a BCA assay, and viral infectivity, by a series of limiting dilutions on camptothecin treated HEK-293 cells, yields additional data about the titer, purity and infectivity of the viral preparation (See Fig. 28. The viral particle titers are obtained by multiplying the p24 values in ng/ml by a factor of 10^7).

3.2.1.2.   Biotinylation of purified LVs

Biotinylation of the surface proteins in LVs is a relatively simple chemical procedure that can enable the later addition of different targeting moieties, via CS, to its surface. The EZ-Link Sulfo-NHS-SS-Biotin reagent (sulfosuccinimidyl-2-[biotinamido]ethyl-1,3-dithiopropionate) from Pierce, a thiol-cleavable amine-reactive biotinylation reagent, enables the attachment of a biotin that is separated by an extended spacer arm from the LV surface, thus reducing any steric hindrances (Altin and Pagler, 1995). This water-soluble, and lipid-insoluble, reagent only biotinylates the surface proteins, thereby preventing any

potential interference in the activity of the important packaged enzymes in the viral core. The N-hydroxysulfosuccinimide (NHS) ester group on this reagent reacts with the ε-amine of lysine residues to produce at neutral to basic pH values. Release of N-hydroxysulfosuccinimide and hydrolysis of the NHS-ester completes the reaction. A 5-20 fold-molar excess of the reagent was used in order to adequately biotinylate the surface VSV-G. The exact molar excess of this reagent needed is difficult to calculate and varies from viral prep to prep; if the prep is relatively clean with few contaminating proteins or cellular debris, a 1-5 fold excess is chosen in order to prevent over-biotinylation. On the other hand impure preps, with other competing proteins for the NHS group, need the higher figure. In any case, the reagent was freshly constituted in PBS before addition to the viral prep for 15-30 mins at RT. The reaction was then stopped by the addition of an excess of TBS or serum containing culture media. The viruses were spun down over a sucrose cushion as before to yield pure LVs, uncontaminated with any Ez-link reagent. In very case, multiple molar excesses of the reagent were used and LV viability tested for each batch to determine if the reaction had severely compromised LV infectivity or titer. A small aliquot of the final, purified LV was tested with a HABA-avidin kit (Sigma) to determine the number of biotin molecules per LV (Green, 1965).

A

p24 standard curve
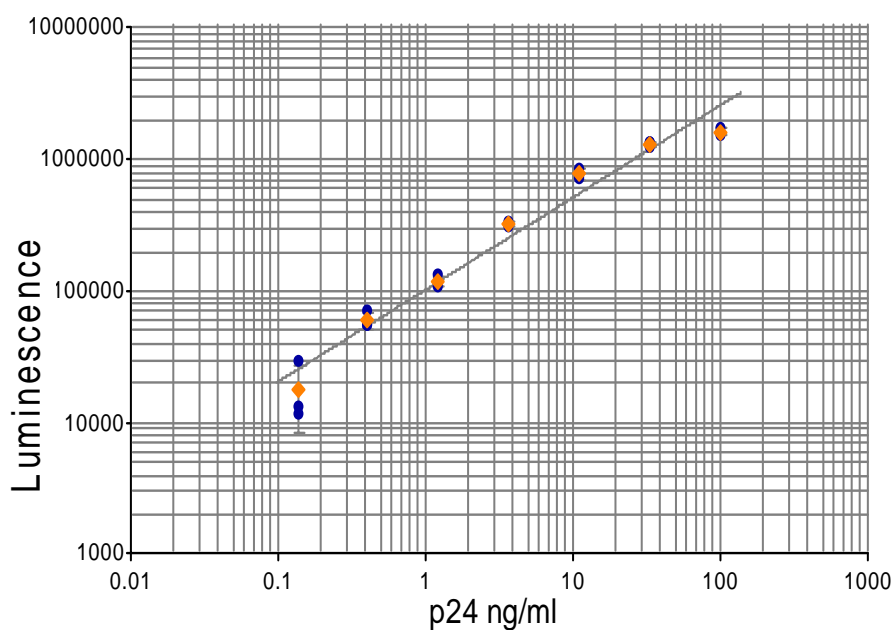
Curve Formula	A	B	R	R²
Log(Y) = A*Log(X)+B	0.701	5.01	0.985	**0.97**

B

Name	Amount of p24		No. of Lentiviral particles		No. of Infectious Units	
Lenti-hisS25 Unconcentrated	100	ng/ml	1.00×10^9	LVs/ml	1.00×10^7	IUs/ml
Lenti-hisS25 Concentrated	2550	ng/ml	2.55×10^{10}	LVs/ml	2.55×10^8	IUs/ml
Lenti-hisRT Unconcentrated	90	ng/ml	9.00×10^8	LVs/ml	9.00×10^6	IUs/ml
Lenti-hisRT Concentrated	2700	ng/ml	2.70×10^{10}	LVs/ml	2.70×10^8	IUs/ml
Lenti-hisMTR Unconcentrated	70	ng/ml	7.00×10^8	LVs/ml	7.00×10^6	IUs/ml
Lenti-hisMTR Concentrated	1800	ng/ml	1.80×10^{10}	LVs/ml	1.80×10^8	IUs/ml
Lenti-GFP H1 Concentrated	24693	ng/ml	2.47×10^{11}	LVs/ml	2.47×10^9	IUs/ml
Lenti-GFP H2 Concentrated	31633	ng/ml	3.16×10^{11}	LVs/ml	3.16×10^9	IUs/ml
Lenti-hisS25180 Concentrated	1647	ng/ml	1.65×10^{10}	LVs/ml	1.65×10^8	IUs/ml
Lenti-hisS25197 Concentrated	1844	ng/ml	1.84×10^{10}	LVs/ml	1.84×10^8	IUs/ml

Fig. 28: p24 ELISA to determine LV titers: **A:** p24 standard curve plotted against the luminescence detected. On the X-axis is the concentration of p24 in ng/ml and on the Y-axis is arbitrary luminesnce units acquired. **B:** Concentration of some important LV preparations used for later experiments. (IU – infectious units; LV – lentiviral particles).

3.2.2. Isolation of cerebellar granule neurons (CGNs) from neonatal rat cerebellum

Cerebellar granule neurons are the most abundant type of homogenous neurons in mammalian CNS. First described by Ramón y Cajal, these small neurons are found in the granular layer of the cerebellum. They receive afferents from mossy fibers while sending out glutaminergic efferent axons which are in turn organised into a parallel network synapsing with Purkinje cells. These cells, an ideal neuronal model system, were cultured as per protocols derived from (Foran et al., 2003).

Briefly, coverslips were inserted into the necessary number of wells and coated overnight with poly-L-lysine (0.25 mg/ml in dH_2O). After removal of the poly-l-lysine, the wells were rinsed briefly with dH_2O and dried in CO_2 incubator. Rat pups, 6 – 10 days old, were killed with sodium pentobarbital and the cerebelli dissected out into cold basal media eagle (BME). The isolated cerebelli were finely minced and resuspended into fresh BME. They were then spun down at 150-200G for 5 mins at 4ºC, resuspended in PBS and dispersed into a 1:1 trypsin-EDTA (Invitrogen – 1x) and PBS mixture. The cells were triturated with a 5ml pipette and incubated at 37ºC for 20 mins with frequent agitation. Benzonase was added to dissociate any clumps and obtain a clear suspension. The cells were spun at 200G for 5 mins, resuspended in 15ml partial cerebellar growth medium (PCGM) and filtered through a 100µm filter. The single cell suspension of predominantly cerebellar granule neurons, free of contaminating RBCs, was plated at a density of 1.5×10^6 /well for a 24-well

plate and grown at 37⁰C in a CO2 incubator. The PCGM was replaced with a complete cerebellar growth media (CCGM), containing the mitotic inhibitor AraC, after 24-48 h in order to prevent the overgrowth of micro and macro glial cells. After a further 5-6 days in CCGM, the cells exhibit profuse axo-dendritic proliferation, express synaptic proteins abundantly and secrete glutamate in response to an action potential. Cells could be kept alive easily for 10-12 days, and if needed longer, by replacing half of the existing media every 7-10 days.

3.2.2.1.   Radioisotopic measurement of K^+-evoked, and Ca^{2+}-stimulated, ^{14}C-glutamate release from CGNs

To measure the functional exocytosis present in these neurons, a radioisotopic measurement of K^+-evoked, and Ca^{2+}-stimulated, ^{14}C-glutamate release from CGNs was used. A representation of the processes involved in a typical glutamatergic synapse is shown in Fig. 29. Cells, cultured for more than 5 days, were exposed to 0.25 µCi/ml of C^{14}-L-Glutamine in 0.5ml of warmed-oxygenated Hepes basal buffer (HBB). After 60mins incubation at 37⁰C, the supernatant was removed and the cells were washed thrice with HBB. The basal, unstimulated, glutamate release was measured by the addition of 0.5ml of HBB for 5mins at 37⁰C. A high K^+-containing Hepes stimulation buffer (HSB) was added for a similar period to elicit K^+-evoked, and Ca^{2+}-stimulated exocytosis. Finally, addition of HBB with 1% triton enabled the extraction any remaining glutamate. The fractions were centrifuged at 14,000G for 15mins at 4⁰C and 200µL of supernatant from each was added to 2ml of EcoScint-H scintillation fluid, mixed and counted using a Beckmann-Coulter counter.
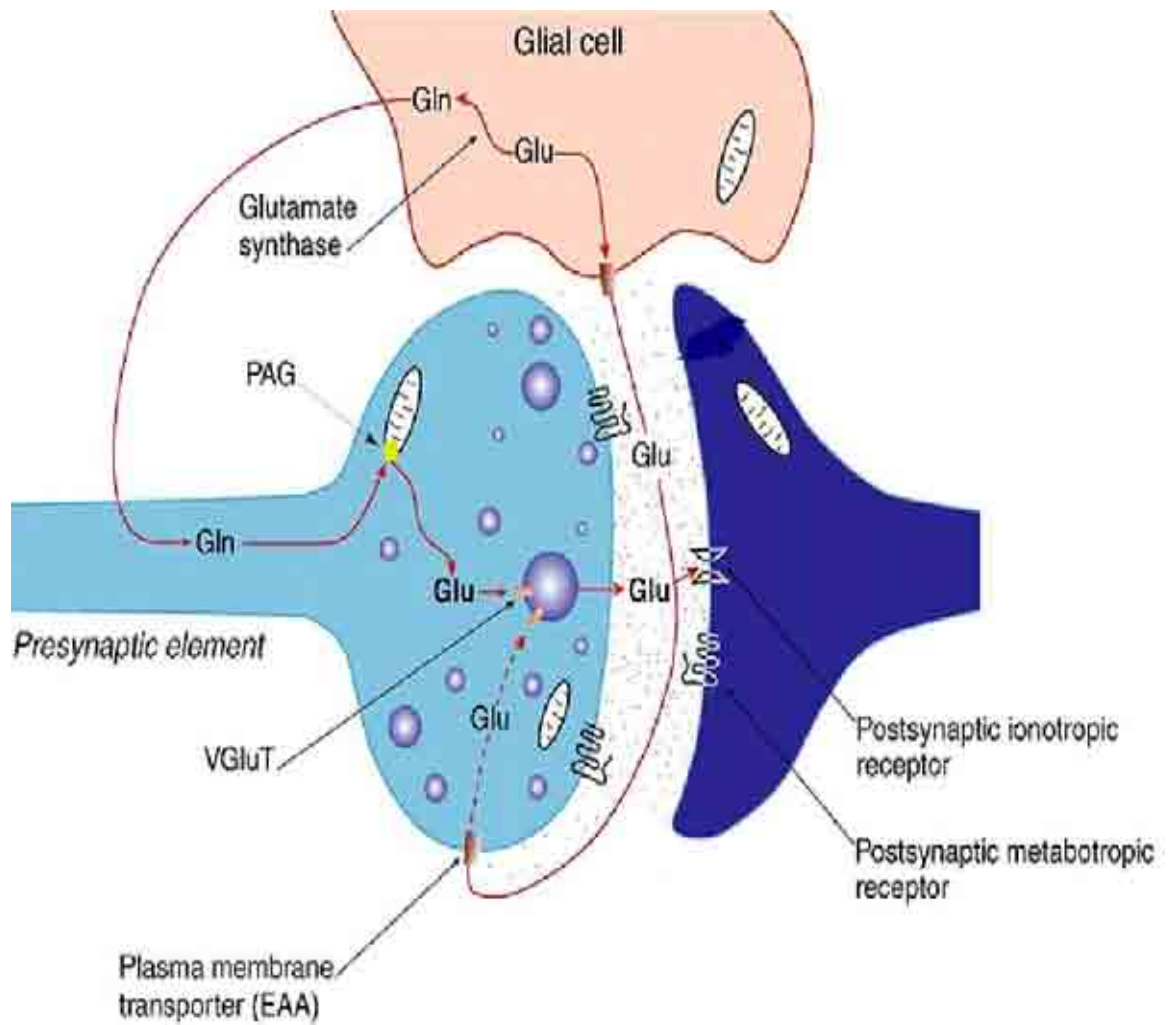
Fig. 29: A typical glutamatergic synapse: Free cytoplasmic glutamate, synthesized metabolically or from breakdown of glutamine, is actively transported into synaptic vesicles by VGluT. Upon release, glutamate binds to the post synaptic ionotropic or metabotropic receptors (labelled) or to pre-synaptic autoreceptors. Any free glutamate is rapidly taken up by glial cells or by transporters in the pre-synaptic membrane. Glial glutamate is converted to glutamine by glutamate synthase enzyme and transported back into the pre-synaptic neuron, thus completing the cycle. (Glu – glutamate; Gln – glutamine; PAG – phosphate activated glutaminase; EAA – excitatory amino acid transporter; VGluT – vesicular glutamate transporter). Adopted from (Squire et al., 2003)

159

3.2.3. *In vitro* and *in vivo* assays of LV function

As CGNs were found to be relatively refractory to AAV or LV infection after more than 48 h in culture, only protection studies can be done with these cells. LVs were added to cultures 2-4 h after plating and were washed out 48 h later. BoNT/A were added 7 or 11 days after plating and removed before continuation with the release assay. Some of the cells were not treated with the toxin and were instead used for immunohistochemical localisation of expressed SNAP-25 variants (Fig. 30 A-D). The basal release was subtracted from the evoked C^{14}-glutamate release and expressed as a fraction of the total content of neuronal glutamate (basal + stimulated + total). In order to quantify the absolute effect of viral-mediated SNAP-25 variant expression, the evoked component from toxin-and-LV treated cells was normalised to that from LV-only treated ones and plotted as a graph (Fig. 30 E).

The effect of SNAP-25-197 and SNAP-25-180 on stimulated exocytosis was quantified in cells that were exposed to the relevant LVs for 8 or 12 days. LVs expressing wtSNAP-25 were used as a control (Fig. 31). In addition, the effect of increasing MOI on the final protein expression was quantified by western blots of lysed cells probed with anti-His and anti-SNAP-25 antibodies (Fig. 31).

The *in vivo* effects of direct LV-His$_6$-SNAP-25 injection into the spinal cord anterior horn was tested as before in 8-week old Wistar rats. Animals were euthanized 8, 15 or 21 days after injection, the spinal cords cryo-preserved, sectioned, immuno-probed and examined under a fluorescent microscope (the

best expression level, seen 8 days after injection, is shown in Fig. 32).

3.2.4. Development of core-streptavidin tagged protease-inactive and active BoNT/E targeting chimeras

BoNT/E with a E12Q mutation in its HEXXH-E protease domain has been shown to be inactive (Agarwal et al., 2004). This molecule, henceforth termed BoTIM (Botulinum toxin inactive mutant) has been proposed as a putative targeting agent to deliver cargo to motor neuron terminals. A version of this molecule available in our laboratory, with an N-term His_6 tag and a C-term Strep tag, was used to generate core-streptavidin tagged protease-inactive BoNT/E targeting chimeras (See Fig. 33 for a schematic of the cloning process). This molecule also had PreScission protease recognition sites between the LC and HC and between the tags and BoTIM (the enzyme is a genetically engineered human rhinovirus 3C protease and was acquired from GE healthcare. It recognises the amino acid sequence LFQ/GP (Cordingley et al., 1990)).

Briefly, the two existing tags were removed and replaced by a single His_6 tag at the C-terminal. In addition, convenient restriction sites, BamHI before the LC at the N-terminal and XhoI before the His_6 tag at the C-term just, were introduced. The created molecule, BoTIM-His_6, was used for subsequent cloning procedures. A codon-optimised synthetic CS with long, flexible glycine-serine linker and suitable restriction sites at both ends was designed (pI of 6.7 and M_r of 17.4kDa – the sequence was based on that used in (Schmiedl et al., 2000) and (Sano et al., 1995)). This was synthesized at Eurofins Medigenomix

and cloned into BoTIM as shown in Fig. 33. The orientation of the inserts in the new plasmids created, pQE-CS-BoTIM-His$_6$ and pQE-BoTIM-CS-His$_6$, was checked by sequencing. The sequence confirmed plasmids were transformed into chemically competent M16(pREP4) E.coli strains. These transformed bacteria were grown in 2TY media (Sigma) overnight and 1 ml of this dense culture seeded into 120ml of fresh 2TY in a 2L baffle flask. They were allowed to grow at 37 °C for 3 h before induction with 100µM IPTG. After the addition of IPTG, the temperature was turned down to 21 °C and the culture grown overnight with vigorous shaking. The bacteria were then harvested by centrifugation at 6000G, resuspended in a Tris-NaCl buffer containing 1xProtease inhibitor cocktail type 3 (Calbiochem). The cells were lysed using lysozyme and several freeze/thaw cycles and the insoluble material was removed by centrifugation. The different BoTIMs, and CS-His$_6$, were trapped by immobilized metal affinity chromatography (IMAC) on TALON resin, eluted with 500mM imidazole, and fractions rich in the eluted proteins were pooled into HEPES-NaCl buffer (pH 8.1) using a Zeba-Spin desalt column (Pierce) (See Figs. 34 and 35). These were then aliquoted and stored at –80 °C. Some of SC BoTIM molecules were proteolytically nicked by PreScission protease (20units/mg of BoTIM) for 1 h at 25 °C to create a di-chain version free of the His$_6$ tag (See Fig. 36). All long term storage was in HEPES-NaCl buffer (pH 7.4). The expression, purity and nicking of these proteins was monitored on Coomassie-stained SDS-PAGE gels and by Western blotting with primary antibodies followed by horseradish peroxidase-conjugated anti-species secondary antibodies and visualized using an ECL protocol (See Fig. 34, 35 and

162

36 for more details). The protein concentrations were determined using the Bradford assay and purity assessed based on Coomassie-stained SDS-PAGE gels.

After the confirmation of the producibility of CS-tagged BoTIMs, versions with an active LC were created by PCR cloning techniques. These were expressed and purified as described for their inactive relatives.

3.2.5. Testing the targeting abilities of different CS-tagged BoTIMs

The protease-active CS-tagged BoNT/Es are a valuable proxy to measure the targeting of CS-tagged BoTIMs (since they differ in only one single amino acid from the latter). They were applied at different concentration to 8 day old CGNs in culture for 1hr at 37C, washed out and the cells were lysed and blotted the next day. ECL estimation of the amount of SNAP-25 cleavage at different concentrations provided an accurate and quantitative assessment of the perturbation, if any, caused by the attached CS-tag to the various processes that underlie toxin-mediated SNARE cleavage – binding, internalisation, extravasation from the lysosome, target finding and finally cleavage. Nicked and un-nicked versions of the tagged BoNT/Es, along with LC_E and BoNT/E DC provided valuable controls to fully asses this process (See Fig. 37). In addition, the lethal dose of the toxin in mice was determined by the intra-peritoneal injection of various concentrations, followed by monitoring for 5 days (See section 2.2.1 more more details). The amount of toxin that killed 50% of mice within 4 days was taken as one minimal lethal dose – for some SC versions the maximum dose injected, which did not kill the animal, is represented in Fig. 37.

Another important test was measuring the ability of CS-tagged BoTIMs to antagonise the activity of BoNT/E in CGN cultures. Various concentrations of the BoTIMs were added to CGN cultures 1hr before the addition of 500pM BoNT/E. They were allowed to act for a further hour, before replacement of the media with fresh CCGM. After an overnight incubation, the cells were tested for glutamate release and SNAP-25 cleavage (See Fig. 38).

3.2.5.1. Immuno-histochemical determination of binding of CS-tagged BoTIMs to CGNs

The tagged BoTIMs were applied at various concentrations to 4 day old CGNs in culture. They were allowed to bind overnight and the cells were repeatedly washed using PBS the next day to get rid of any unbound proteins. They were then fixed with ice-cold 4% paraformaldehyde in PBS, permeabalised with methanol and PBS/0.1%Tween and probed with a rabbit anti-streptavidin antibody. Probing with a goat anti-rabbit-A546 fluorescent conjugate releaved the binding pattern of CS-BoTIM and BoTIM-CS (See Fig. 39). To elicit the microscopic details of this binding, some of the slides were counter-stained with a mouse anti-SNAP-25 antibody and a goat anti-mouse-A488 fluorescent conjugate (See Fig. 40).

3.2.6. Testing the ability of CS-tagged BoTIMs to bind various biotinylated cargo

Biotinylated horse radish peroxidase (biot-HRP – Sigma) was extensively used to not just quantify the binding of the CS-tagged proteins, but also as a

screening tool to identify high-producing colonies during the cloning process (See Fig. 41). In brief, a 1:1500 dilution of biot-HRP (5mg/ml - Pierce) was diluted into PBS/5% BSA and used to probe aliquots of the different stages of the BoTIM purification process blotted onto nitrocellulose. After repeated washing, a commercial ECL kit (Millipore) was used to identify and quantitate the amount of bound biot-HRP. A similar procedure was used to elucidate the effect of pH, buffer constituents and detergents on the affinity of the CS tag to biot-HRP (See Fig. 41).

3.2.7. Chromatographic analysis of CS-tagged BoTIMs

A 50cm chromatographic column filled with Superose 6 resin (GE Healthcare – useful fractionation range of 5kDa-5000kDa, particle size of 13µm and flow rate of 0.1-0.5ml/min) was used to measure the molecular weights of the different CS-tagged BoTIMs in PBS. Initially, the characteristics of the column were determined by running different protein and non-protein standards (GE Healthcare; See Fig. 42). The protein concentration in the different fractions was analysed by Bradfords assay and the peak elution volume for each standard calculated. A standard curve was generated, showing the relationship between the K_{av} and M_r, and used to calculate the molecular weights of the CS, BoTIM and CS-BoTIM (See Fig. 43).

3.2.8. Assessment of the ability of CS-tagged BoTIMs to bind larger cargo – biotinylated microspheres and LVs

Two, prototype, large cargos were chosen – biotinylated fluorescent

microspheres – bFM (FluoSpheres from Invitrogen - biotin-labeled microspheres, 0.2μm in diameter, containing yellow-green fluorescent cargo with 505nm excitation and 515nm emission, comprising a suspension of 1% solids) and biotinylated LVs described previously. Chromatographic analysis of the binding of CS-BoTIM to bFM was performed, as before, on a superose 6 column. In addition to protein content estimation of the different fractions, the fluorescent content was estimated on a plate reader and plotted (See Fig. 44).

Biotinylated LVs, with ~2000 biotins per LV, were the second large cargo tested. CS-BoTIM, un-nicked and still containing the His-tag, was passed through a column containing 50ul of TALON resin. Once the resin was saturably bound with CS-BoTIM, a solution of biot-LVs was passed through the column. After repeated washing, PBS/1mM EDTA was used to dislodge the bound CS-BoTIM and a western blot of this probed with antibodies against streptavidin and p24, identifying the fractions containing CS-BoTIM and biot-LV respectively (See Fig. 44). A parallel and related experiment was to test the effect of bound cargo on CS-tagged BoNT/E's exocytotic blockade activity. CGNs were treated overnight to a mixture of the CS-tagged BoNT/Es bound to different cargo – from the biotin (0.4kDa), biot-HRP (60kDa) and bFM (>5000kDa). The cells were then washed repeatedly, lysed and contents run on a western blot. The amount of SNAP-25 cleavage was quatified for each mixture and plotted (See Fig. 45).

3.2.9. Effect of bound CS-BoTIM on biot-LV infectivity

HEK-293 and CGNs in culture were treated with a mix of biot-LVs and CS-BoTIM (or BoTIM-CS). Untargeted biot-LV and non-biotinylated LVs were used as controls. The mixture was washed off after an overnight incubation and the cell were allowed to grow for 48 h (HEK-293) – 96 h (CGN) before imaging the expressed GFP fluorescence. A fluorescence plater reader was also used to obtain quantitative data, by measuring, and summating, fluorescence readings from 25 different points in each of the wells (See Fig. 46 and 47).
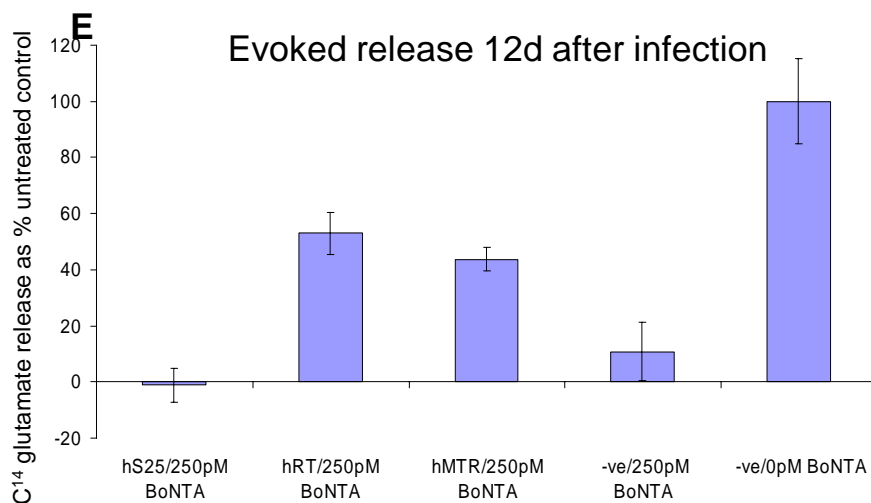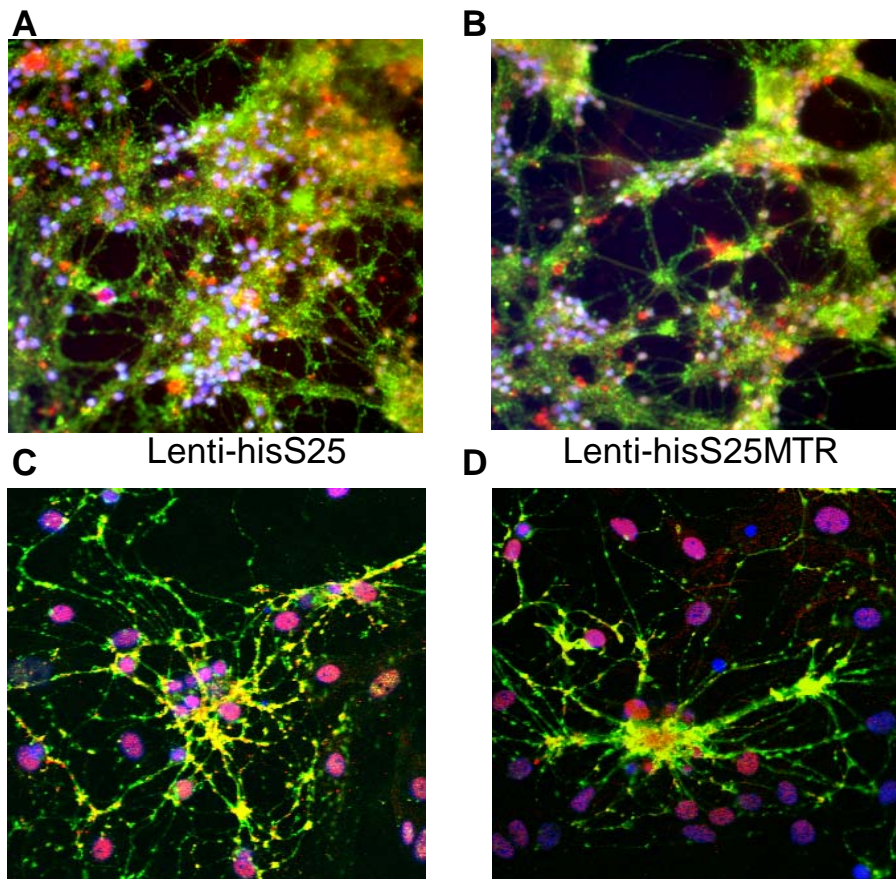
Fig. 30: Evaluation of LV-mediated wt, RT and MTR SNAP-25 expression in CGNs: Immunohistochemical detection of expressed SNAP-25 variants in 5 day old CGN cultures probed with a anti-His$_6$ antibody (in red), anti-VAMP antibody (in green) and the nuclear stain DAPI (in blue). The extensive colocalisation of His$_6$-SNAP-25 (**A:** 10x and **C:** 40x) and His$_6$-SNAP-25-MTR (**B:** 10x and **D:** 40x) with VAMP is clearly seen. **E:** Functional evaluation of expressed cleavage-resitant SNAP-25 mutants in CGNs challenged with 250pM of BoNT/A. The purely evoked component of the K$^+$-evoked Ca^{2+}-mediated C^{14}-glutamate exocytosis in CGNs treated with LV+toxin was normalised to that from toxin-free controls, treated with just the virus, and plotted on a graph. (Three replicates each were calculated for each viral and toxin dose. 10^7 IUs of LV was added to the wells)
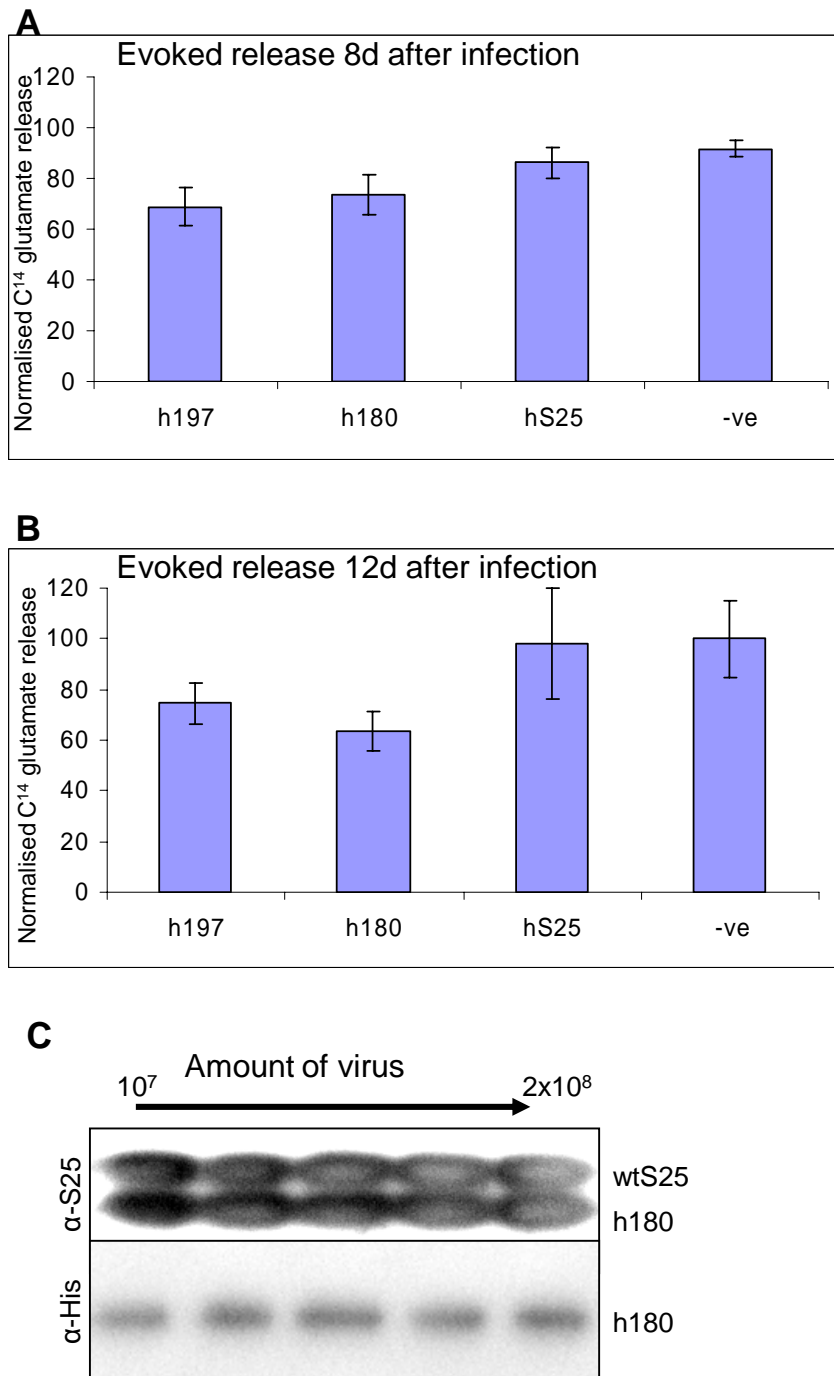
Fig. 31: Effect of His₆-SNAP-25-197 and -180 expression on K⁺-evoked Ca²⁺ mediated exocytosis in CGNs: **A and B:** Normalised evoked release 8 or 12 days after infection with the relevant LVs shows a slight, non-significant, decrease in the evoked component of release in cells expressing the 197 or 180 isoforms. In contrast, cells expressing the full-length, wild-type SNAP-25 show no difference in exocytotic release compared to untreated cells. **C:** The introduced SNAP-25 variant does not overwhelm the native SNAP-25. A significant quantity of wt-SNAP-25 persists in CGNs. Even infection with a high dose dose not lead to a significantly higher protein expression level – a plateau effect that may be mediated at the level of viral infectivity, integration or mRNA expression.

Thoracic

A

B

Lumbar

Center   Anterior

SC - Anti-His – 10x composite

SC - Anti-His – 20x
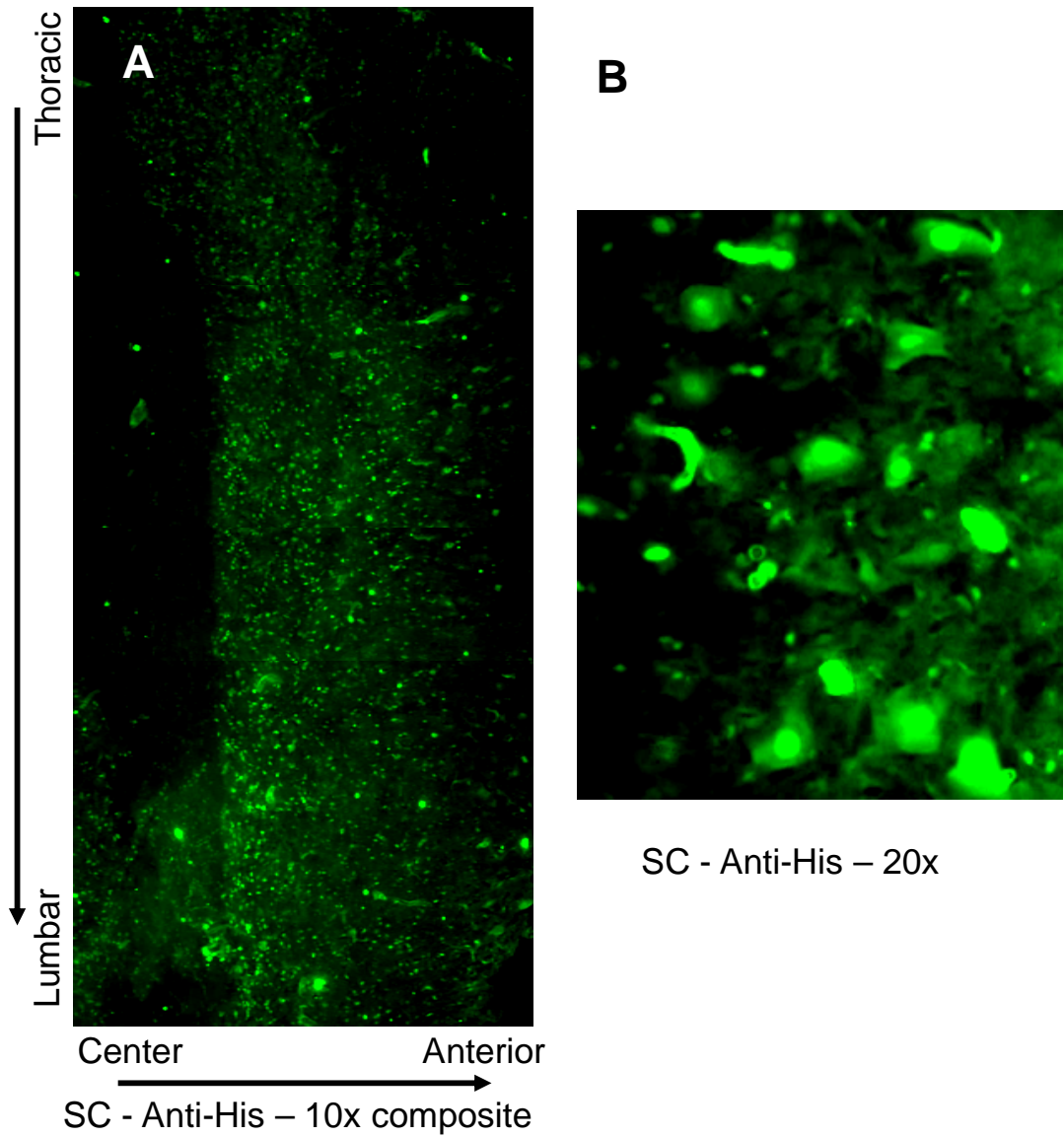
Fig. 32: Spinally-**i**njected LVs efficiently infect and rapidly produce the introduced transgene in spinal neurons. **A:** Assembled low magnification images show the spread of injected LVs and the relatively wide area of transgene expression. **B:** A higher magnification enables the identification of the characteristically large anterior horn motor neurons among the infected cells.

3.3. Results

3.3.1. LVs are an efficient tool to deliver genes into neurons – *in vivo* and in culture

A second generation lentiviral-vector system, obtained from Prof. Trono, was used to create LVs expressing GFP, wtSNAP-25, SNAP-25-RT, SNAP-25-MTR, SNAP-25-197 and SNAP-25-180 (See Fig. 26-28). GFP containing viruses were produced to control for the effects of viral infection, if any, on cell viability and exocytotic processes. Similarly, wtSNAP-25 is a valuable control to elicit the effects of SNAP-25 over-production, if any, on the efficiency of synaptic exocytosis. The BoNT/A resistant SNAP-25-RT and the /A, /E and /C1 resistant SNAP-25-MTR are the therapeutic genes that has been proven to introduce resistance to the exocytotic blockade by the respective serotypes. The process of creation of these two has been shown in Fig. 27. A commericially available p24 ELISA kit, based on a sandwich ELISA utilising a sheep anti-p24 capturing antibody and a alkaline phosphotase tagged mouse monoclonal anti-p24 secondary was used to detect the titers of the produced lentiviruses. Standard curves were generated using known quantities of a recombinant p24 protein and the estimated yields extrapolated, using published figures, to obtain the viral particle and infectious unit yields (See Fig. 28). High titers were obtainable with LVs expressing GFP; the introduction of SNAP-25 into the system resulted in a lower, yet sufficient for most *in vitro* and *in vivo*

procedures, titer. These viruses were further tested by application of serial dilutions onto HEK-293 cells, treated with camptothecin to limit overgrowth, followed by visual/immunohistochemical examination of expressed transgene products.

The functionality of the RT and MTR SNAP-25 carrying viruses was tested in CGNs. Application of 10-20 MOIs of the virus onto CGNs resulted in strong production of the SNAP-25 variants that could be identified immunohistochemically and functionally (See Fig. 30 and 31). GFP and mutant SNAP-25 products produced by LV based gene-delivery were identifiable after 2-3 days and showed a strong expression 5 days after infection. Examination of radio-labelled glutamate release enabled a quantitative, and sensitive, observation of the effect of the mutant SNAP-25s on BoNT/A mediated exocytotic blockade (see Fig. 30). There was a strong protective effect, with the amount of exocytosis increasing to ~60% and ~40% of the normal controls; in contrast, CGNs treated with wtSNAP-25 showed no perceivable improvement. CGNs were found to be relatively refractory to AAV or LV infection after more than 48 h in culture; while this restricts the experiments that can be performed with these cells to protection studies only, they still offer a valuable model system to study the perturbation of exocytosis by CNTs.

In a parallel experiment, the total amount of recombinant protein produced as a percentage of the total natural protein was examined using LVs expressing the truncated SNAP-25 isoforms. These, due to the difference in molecular weights, can be easily differentiated from the native SNAP-25, yet probed with the same antibody. The results obtained show that the introduced

protein is produced at levels that rival the natural protein (See Fig 31 C). But beyond a certain level, increasing the MOI does not lead to an increase in the produced protein. In addition, the effects of these truncated mutants on normal exocytosis in CGNs was tested - the application of SNAP-25-197 and -180, resulted in a reduction, albeit non-significant, in exocytotic activity of CGNs when measured after 8 or 12 days (See Fig. 31 A and B).

The *in vivo* activity of these viruses was tested by direct injection into rat spinal cord anterior horns. When the cords were dissected after 8 days and observed, the viruses were found to be very active *in vivo* and had transduced a large area of the spinal cord. Viral-mediated SNAP-25 and GFP expression kicked in by day 8 and seemed to strongly infect, the anatomically identifiable, motor neurons (See Fig 32). Interestingly, the viruses had also diffused vertically along the spinal cord and had infected muti-verterbral levels spanning anterior horns.
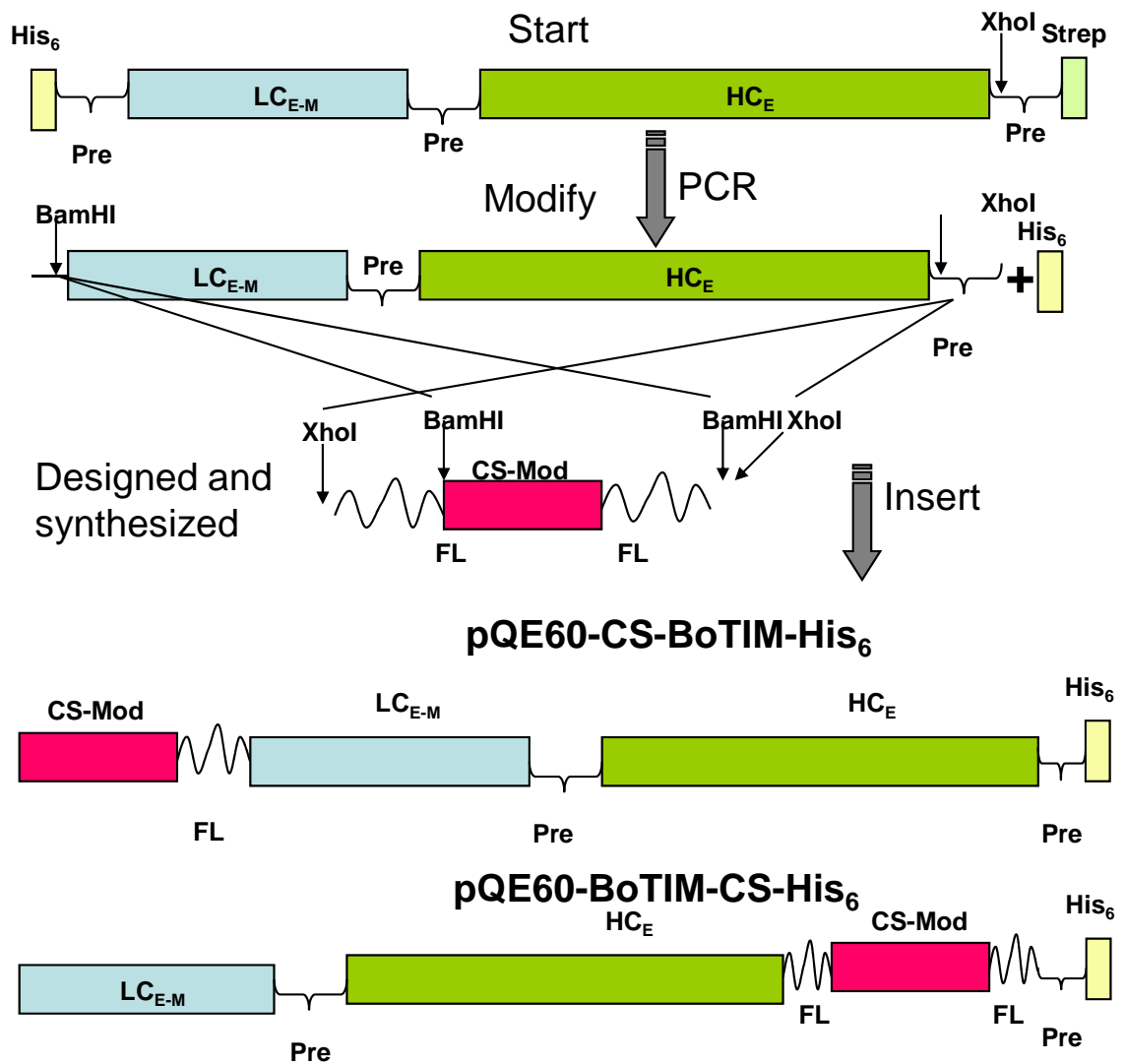
Fig. 33: Schematic of the creation of CS-BoTIM and BoTIM-CS. PCR based modification of a N-term His$_6$ and C-term Strep tagged BoTIM yielded the single C-term His$_6$ tagged BoTIM-E-His$_6$. Insertion of the designed and synthesized CS in the N- and C-terminals of this molecule yielded CS-BoTIM-His$_6$ and BoTIM-CS-His$_6$ respectively. Long, flexible gycine-serine linkers were introduced at the junctions between CS and BoTIM and between CS and His$_6$. (Pre – PreScission site; LC$_{E-M}$ – light chain of BoNT/E with E212Q mutation; HC$_E$ – heavy chain of BoNT/E; FL – flexible linker; CS-mod – designed core streptavidin)

A

Expression and purification of CS-His$_6$

L FT W E1 E2 E3 E4 M   L FT W E1 E2 E3 E4 M

Coomassie   Anti-His

B

Expression and purification of BoTIM-His$_6$

M L FT W E1 E2 E3 E4   M L FT W E1 E2 E3 E4
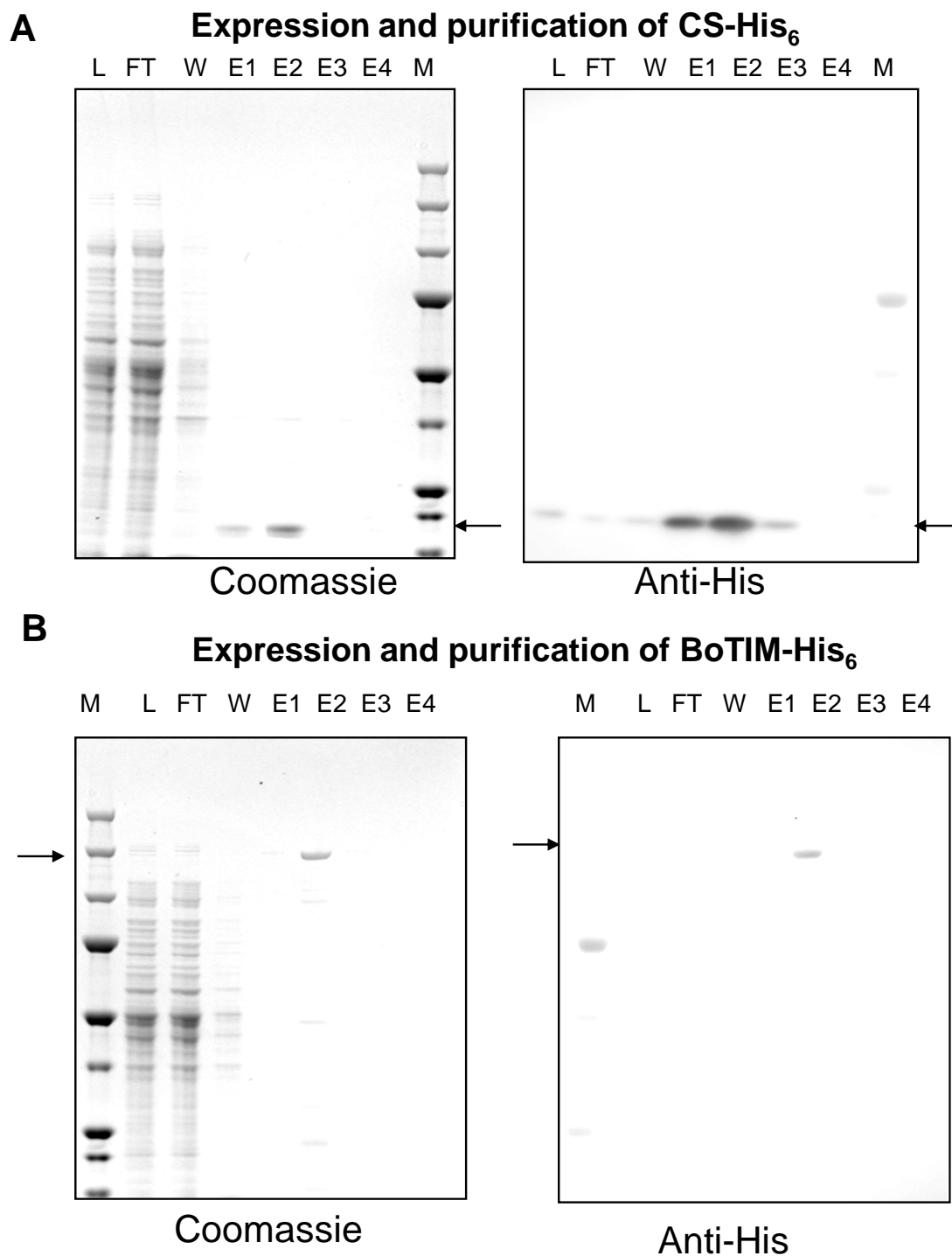
Coomassie   Anti-His

Fig. 34: Expression and purification of CS-His$_6$ and SC BoTIM-His$_6$. **A:** Coomassie stained SDS-PAGE gels (left) and corresponding Western blot (right) with an anti-His antibody of aliquots from the different stages of purification of CS-His$_6$. The arrow points to the sharp single band visible below 15kDa in both the panels. **B:** Coomassie stained SDS-PAGE gels (left) and corresponding Western blot (right) with an anti-His antibody of aliquots from the different stages of purification of BoTIM-His$_6$. The arrow points to the sharp single band visible at 150kDa in both the panels. (L – lysate; FT – flow-through from the TALON resin column; E1-4 – elute fractions; M – pre-stained protein molecular weith marker from Pierce)

175

A

Expression and purification of CS-BoTIM-His$_6$

L   FT   W   E1   E2   E3   M   L   FT W E1 E2 E3 M

Coomassie   Anti-His

B

Expression and purification of BoTIM-CS-His$_6$

L   P   FT   W   E1   E2   E3   E4   M   M   L   P FT W E1 E2 E4
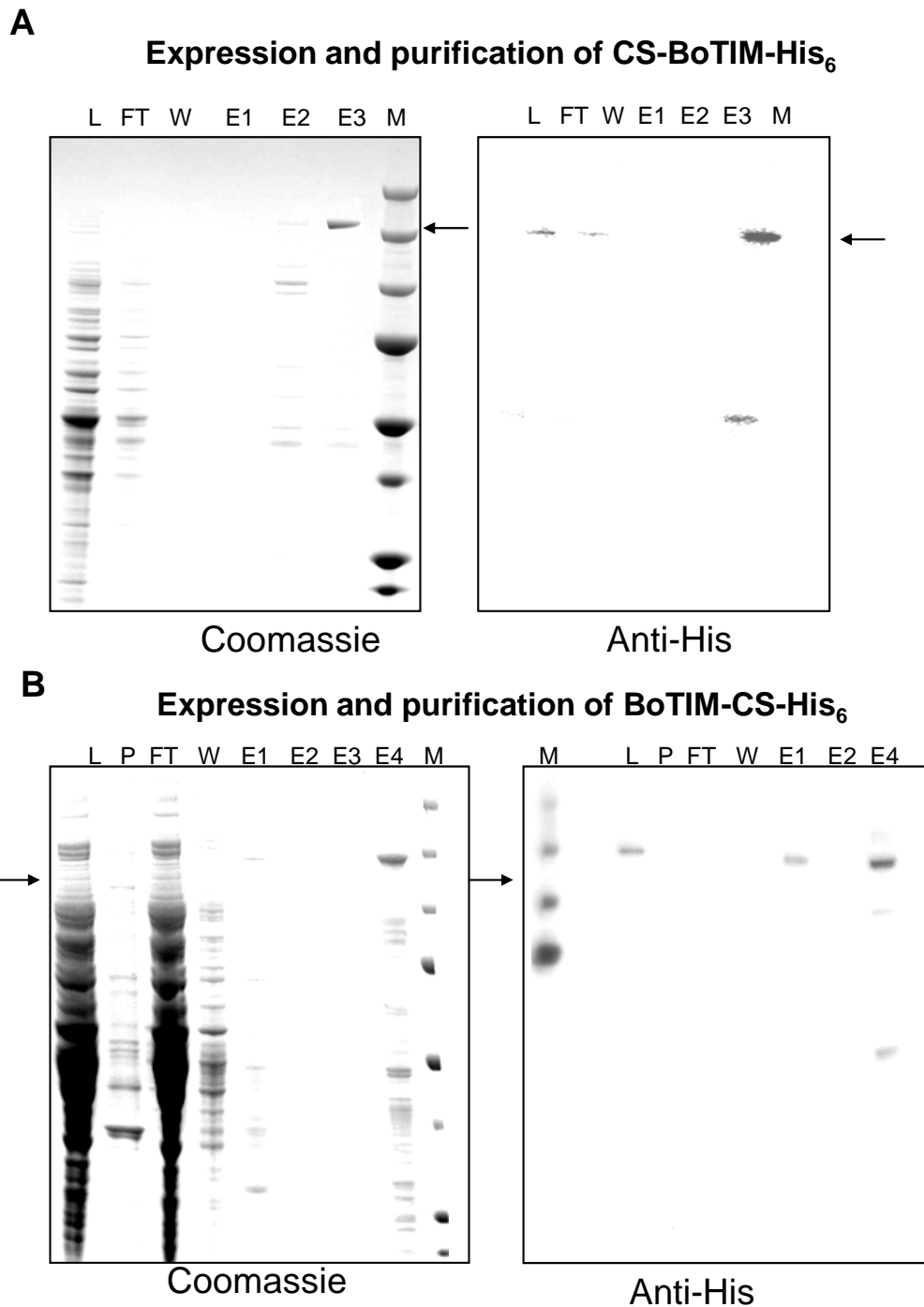
Coomassie   Anti-His

Fig. 35: Expression and purification of SC CS-BoTIMHis$_6$ and SC BoTIM-CS-His$_6$. **A:** Coomassie stained SDS-PAGE gels (left) and corresponding Western blot (right) with an anti-His antibody of aliquots from the different stages of purification of CS-BoTIM-His$_6$. The arrow points to the largest and most abundant band visible higher than 150kDa in both the panels. **B:** Coomassie stained SDS-PAGE gels (left) and corresponding Western blot (right) with an anti-His antibody of aliquots from the different stages of purification of BoTIM-CS-His$_6$. The arrow points to the largest and most abundant band visible higher than 150kDa in both the panels. (L – lysate; P – resuspended cellular pellet; FT – flow-through from the TALON resin column; E1-4 – elute fractions; M – pre-stained protein molecular weith marker from Pierce)

176

A Preparation of His-Tag free di-chain CS-BoNT/E-His₆
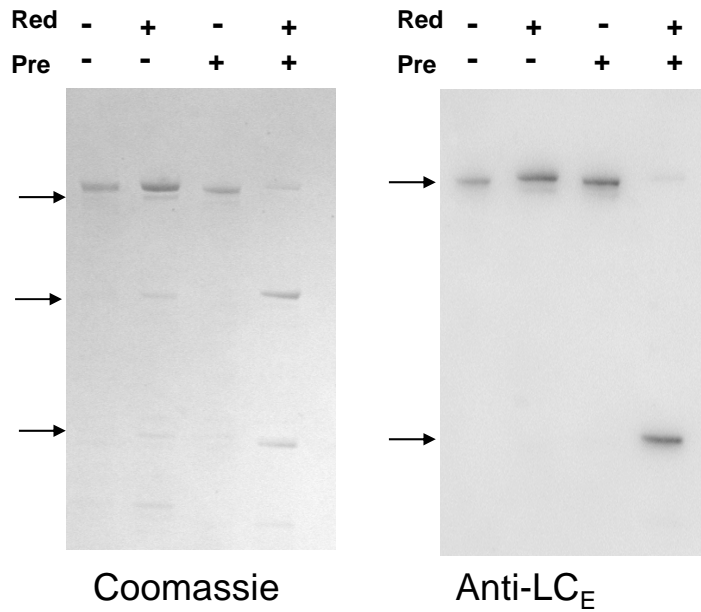
Coomassie

Anti-LC_E

B   Preparation of His-Tag free di-chain CS-BoTIM-His₆

Anti-LC_E

Anti-His
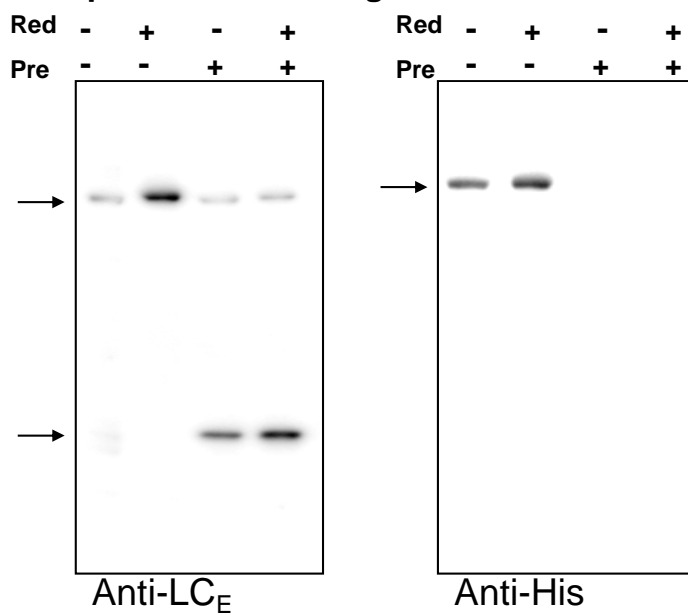
**Fig. 36:** Nicking of CS-BoTIM-His$_6$ and CS-BoNT-E-His$_6$ to generate His-tag free dichains. **A:** Coomassie stained SDS-PAGE gels (left) and corresponding anti-LCE Western blot (right) of aliquots, PreScission nicked and un-nicked and reduced and unreduced, of CS-BoNT-E-His$_6$. The arrows on the left panel point to the SC, HC and LC respectively, while the arrows on the right panel point to the SC and LC. The HC and LC are seen clearly in the reduced and nicked fractions. **B:** Western blots of PreScission nicked and un-nicked, and reduced and unreduced, CS-BoTIM-His$_6$ aliquots probed with anti-LCE (left) and anti-His (right) antibodies. The arrows on the left panel point to the SC and LC forms, while the one on the right points to the SC form. The arrow in the right panel points to the SC form. The absence of free LC in the un-nicked fractions and absence of His-tag in the nicked fractions confirm the totality of nicking (PreScission scission was carried out using 10units/µg protein with 1mM DTT; Red: reduced with 50mM DTT)

3.3.2. CS-tagged BoTIMs retain the properties of both their parent molecules

Having proved the ability of LVs to infect the target cell types, the next step was to produce the prototype targeting agent. BoTIM, the inactive version of BoNT/E, was conjugated at the genomic level to a small CS tag. Initially, the synthetic CS-His$_6$ gene was introduced into the pQE-60 plasmid and its expression and biotin binding abilities were tested. This minimal-biotin binding fragment expressed well and bound free biotin and biotin-HRP well (See Fig 34 and 41). Crucially, neither the His tag nor the included long, flexible glycine-serine linker seemed to interfere with the properties of this protein. Later, this was cloned into different parts of, the already developed, BoTIM. Attempts were made to develop four different versions, with the CS tag at the N-terminus, C-terminus, between the HC and LC and with a tandem linked version with two CS molecules at the C-terminus (see Fig 33). Of these, only the first two expressed well enough and showed minimal degradation; production procedures were then optimised to obtain relatively pure protein (See Fig 33-36). Utilisation of small culture volumes, reduction of production temperature to 20ºC and rapid shaking enabled production of quantities sufficient for in vitro and in vivo use (see Fig 35). After IMAC purification, these single-chain molecules were then treated with PreScission to convert them into di-chain version, thereby also removing the His$_6$ tag (see Fig 36). In order to test the effects of the attached CS, active versions of these BoTIMs were then prepared – a useful and sensitive proxy to track the properties of the inactive-mutant. PCR-based mutagenesis using primers to restore the essential glutamic acid, at

position 212 within the Zn2+-dependent protease active site of the LC yielded active versions of CS-tagged BoTIMs. These were then produced, purified and nicked as before to yield CS-BoNT/E (see Fig 36a) and BoNT/E-CS. In total, 13 different proteins were produced and tested – CS-His$_6$, BoTIM-His$_6$ SC, BoTIM DC, CS-BoTIM-His$_6$ SC, CS-BoTIM DC, BoTIM-CS-His$_6$ SC, BoTIM-CS DC, BoNT/E-His$_6$ SC, BoNT/E DC, CS-BoNT/E-His$_6$ SC, CS-BoNT/E DC, BoNT/E-CS-His$_6$ SC and BoNT/E-CS DC.

An initial and essential test was to determine if the addition of the CS-tag has destabilised the natural neuronal and cholinergic specificity of BoTIM. Two different approaches were undertaken for this purpose – the first was to use the active LC in CS-tagged BoNT/E as a reporter (differing in only one single amino acid from the corresponding BoTIMs) and the second was to test the binding of CS-tagged BoTIMs themselves. The former yields highly relevant and quantitative data, while the latter yields a corroborative and qualitative confirmation. CGNs were used as neuronal model systems for the former test and the CS-tag seemed to be pretty innocuous and the CS-tagged active BoNT/E showed properties similar to their unmodified counterpart (See Fig. 37). While the CS-tagged di-chains plateau early compared to the non-tagged BoNT/E, it still was found to be many order of magnitude more active than just the LC on its own or the un-nicked single chains.

Fig. 37: CS-tagged BoNT/E variants show similar activity to their un-modified counterparts in neuronal/cholinergic model systems: **A:** SNAP-25 cleavage in CGNs exposed to various concentration of the BoNT/E and its CS-tagged variants. The clear demonstration of targeting, binding, internalisation and pathfinding properties of the DC forms shows that the presence of the tag has only a small effect on the toxin's natural properties. While the SNAP-25 cleavage does plateau earlier compared to the un-modified toxin, the comparitively low cleavage seen with just the LC, or with the SCs, clarifies that the tagged toxins still demonstrate an active, specific and efficient neuronal targeting property. **B:** Summarised data of the EC_{50}, EC_{25} and mLD_{50} values of the different toxins. Due to the very low activity of the SCs and the LC, not all data could be obtainable.

	--	CS-BoTIM 10nM	CS-BoTIM 100nM	BoTIM-CS 10nM	BoTIM-CS 100nM	BoTIM/E 10nM	BoTIM/E 100nM
☐ % Release	38.5	34.3	54.2	45.1	47.7	39.3	47.1
☐ % Cleavage	39.2	34.7	30.0	32.4	31.4	31.8	28.5
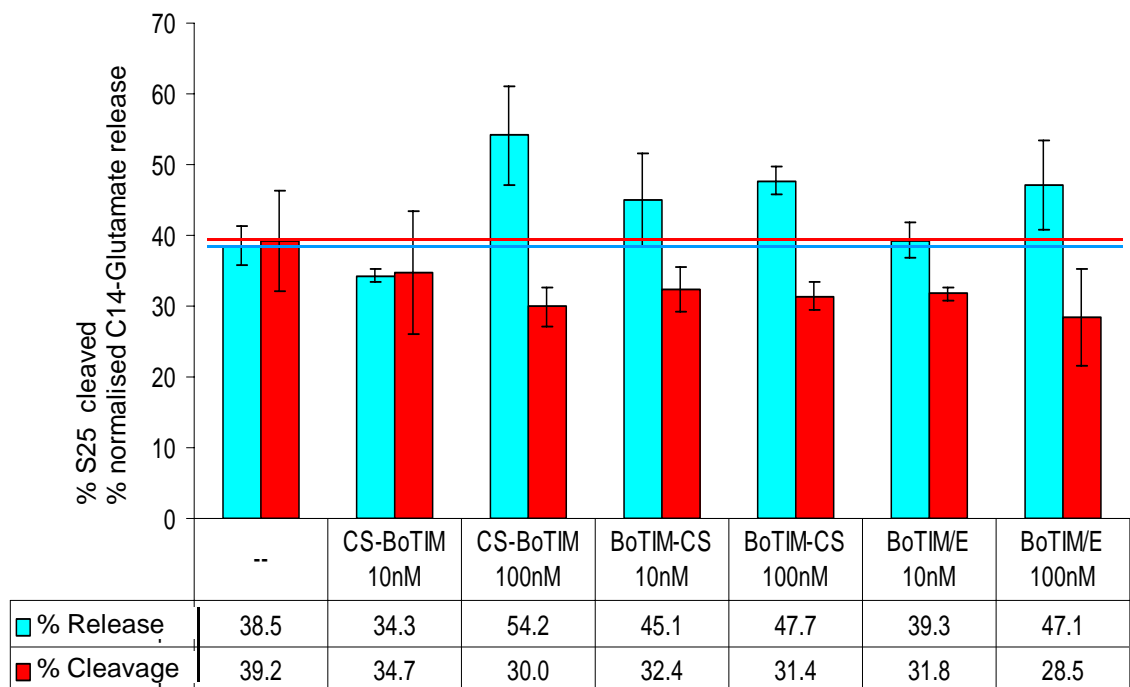
Fig. 38: The various CS-tagged BoTIMs show only a small competitive antagonism of the un-modified toxin's activity in CGNs. 500pM of BoNT/E applied to CGNs in combination with various concentrations of CS-tagged BoTIMs and BoTIM. The amount SNAP-25 cleavage and the amount of evoked C14-Glutamate release was quantitated, normalised and plotted here. While there is some inhibition of cleavage, which corresponds to an increase in glutamate relase, there does not seem to be a significant effect with any of the concentrations tested. (Four replicates were performed per dose and the SD are shown).

181

One test to determine if the addition of the CS-tag has destabilised BoTIMs properties is to attempt a competitive antagonism of BoNT/E action by molar excesses of CS-BoTIM and BoTIM-CS. In this test however, these inactive molecules were not able to significantly antagonise the activity of native BoNT/E (See Fig. 38). But when BoTIM on its own was tested, it also showed a similar lack of significant competitive antagonism. One of the reasons for this could be the previously described dual-receptor dual-affinity mode of uptake in neurons. The presence of such a large number of binding sites, actively undergoing recycling, could be the cause of this absence of competitive antagonism.

When tested on its own, CS-tagged BoTIM bound strongly and specifically to neurons in culture – a property similar to BoTIM, and BoNT/E, and missing in CS. This binding was even identifiable at very low protein concentrations, reflecting the specificity of BoTIMs natural neuronal targeting, and the sensitivity of the detection method employed (See Fig 39). The availability of a highly sensitive anti-streptavidin antibody significantly aided in this analysis. Investigation of the microscopic details of this binding in CGNs, with co-staining by a SNAP-25 antibody, revealed that the tagged BoTIMs bounds predomionantly to the neuronal cell bodies, with a large component bound to the axo-dendritic proceses (See Fig. 40). This is significant as the native BoNT/E binds and internalises at the active-zones in the axonal processes of neurons.

The addition of immunohistochemical data to that obtained by the use of CS-BoNT/E and BoNT/E-CS conclusively proves that most of the properties of

BoTIM have been retained by its derivatives.

A 100nM CS

B Anti-Strep antibody

C 50nM CS-BoTIM DC

D 50nM BoTIM-CS DC

E 50nM CS-BoTIM SC

F 50nM BoTIM-CS SC
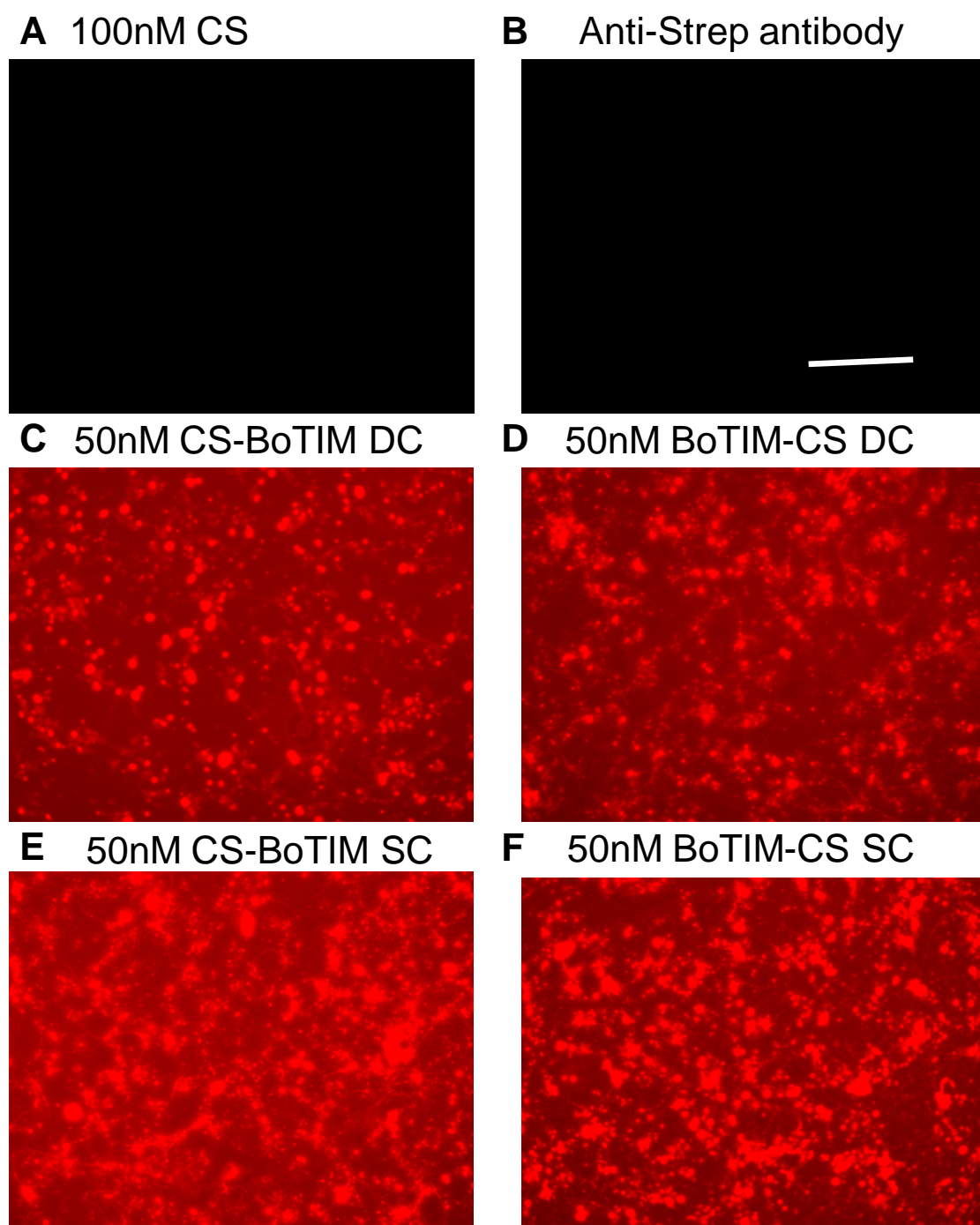
Fig. 39: CS-tagged BoTIMs strongly and specifically bind to CGNs: A 12hr incubation of various concentrations of CS (**A**), CS-BoTIM DC (**C**), CS-BoTIM SC (**E**), BoTIM-CS DC (**D**) and BoTIM-CS SC (**F**) with 4 day old CGNs in culture was probed with an anti-Streptavidin primary and revealed with an anti-Rabbit-A546 secondary (red). The abundant signals found in cells treated with the CS-tagged BoTIMs and their absence in cells treated with just CS on its own demonstrates the strength and specificity of binding. Untreated cells were probed with just the antibodies as a negative control (**B**). (Scale bar 100 µm)
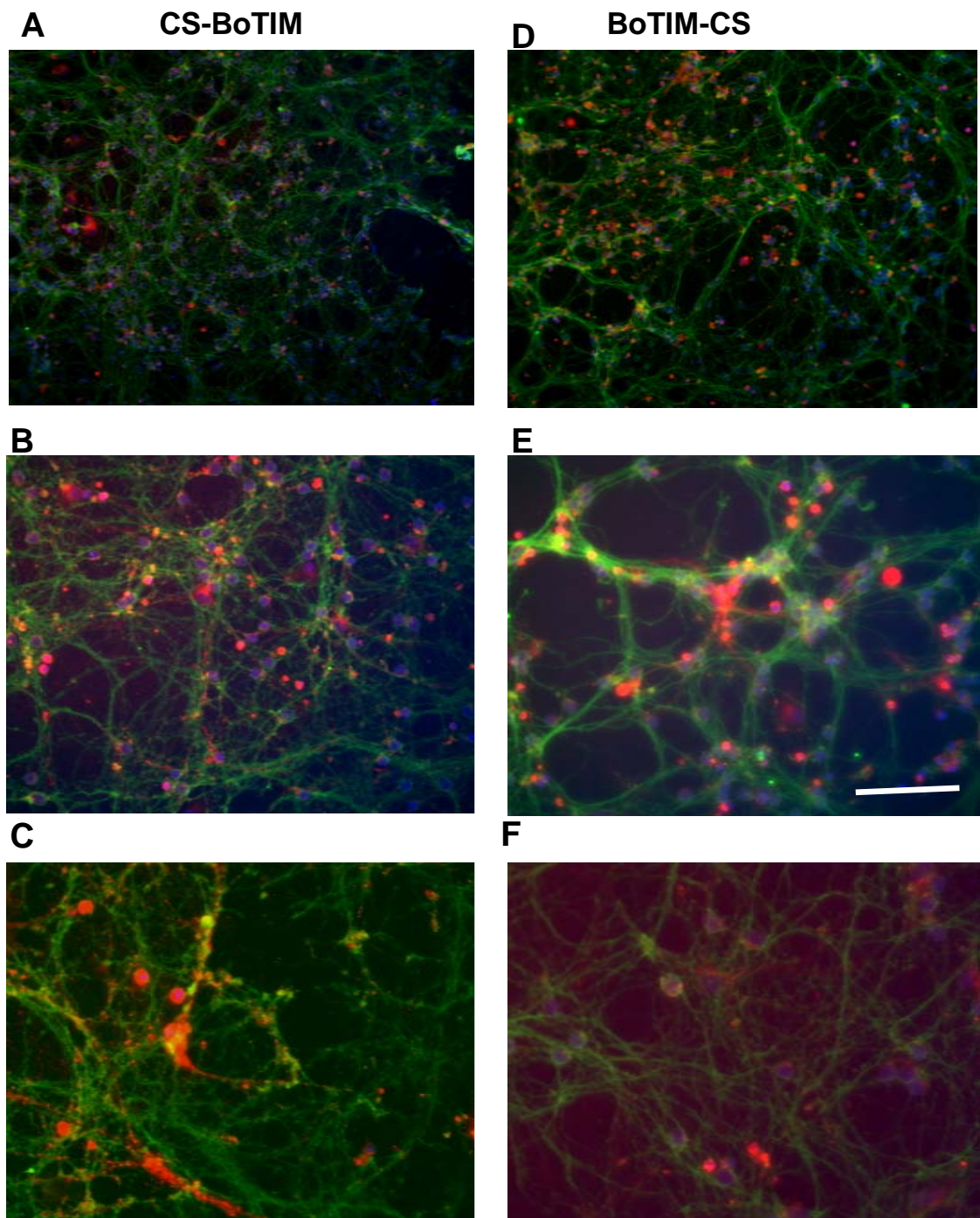
Fig. 40: The CGN binding of the CS-tagged BoTIMs is detectable even at single-digit nM concentrations. CGNs were treated, as before, with CS-BoTIM DC (4nM – **A & B** and 2nM - **C**) and BoTIM-CS DC (2nM – **D & E** and 1nM - **F**). Probing with rabbit anti-streptavidin and mouse anti-SNAP-25 antibodies followed by a goat anti-rabbit-A546 (red) and goat anti-mouse-A488 (green) antibodies revealed the microscopic details of binding. The cells were then counterstained with DAPI and the images overlaid. Representative fluorescent micrographs at 20x (A & D), 40x (B & E) and 60x (C & F) magnification are shown here. (Scale bar 20µm)

A detailed gel-filtration analysis of the effects of the CS-tag on BoTIM was undertaken to determine the conditions of efficient biotin, and biotinylated cargo, binding and to examine if there was any polymerisation of the molecules in solution. The efficacy of biotin-binding was not compromised, with biotin-HRP being bound strongly to CS and CS-tagged BoTIMs in solution (See Fig. 41). Most physiological buffers, at physiological pH, were found to be acceptable for such binding; one interesting finding was that the presence of even small quantities of detergent in the buffer could destabilise and inhibit biotin binding. These results prove that the presence of BoTIM does not subvert the properties of CS.

In order to determine the degree, or presence of polymerisation of the molecules in solution, a detailed gel-filtration analysis was undertaken. This is important for later experiments *in vivo*, as large multi-molecular aggregates could be inactive *in vivo* despite being active *in vitro*. The characteristics of the home-made column were determined using a variety of protein molecular weight standards and phenol red/blue dextran (see Fig. 42). The elution peaks of CS, 37.8 – 39.6ml, corresponds to a tetramer of ~50-60kDa compared to its native molecular weight of 13.4 kDa. BoTIM elutes from the column between 35.5-36.5ml corresponding to a Mr of ~130-170kDa, while the elution peaks of CS-BoTIM, at 27, 29, 32 and 33 ml, corresponds to a complex multimer ranging from >660 to 150kDa (see Fig. 43). Thus there is some degree of polymerisation of CS-BoTIM – a strong contributor for this effect could be the propensity of CS on its own to form tetrameric aggregates.
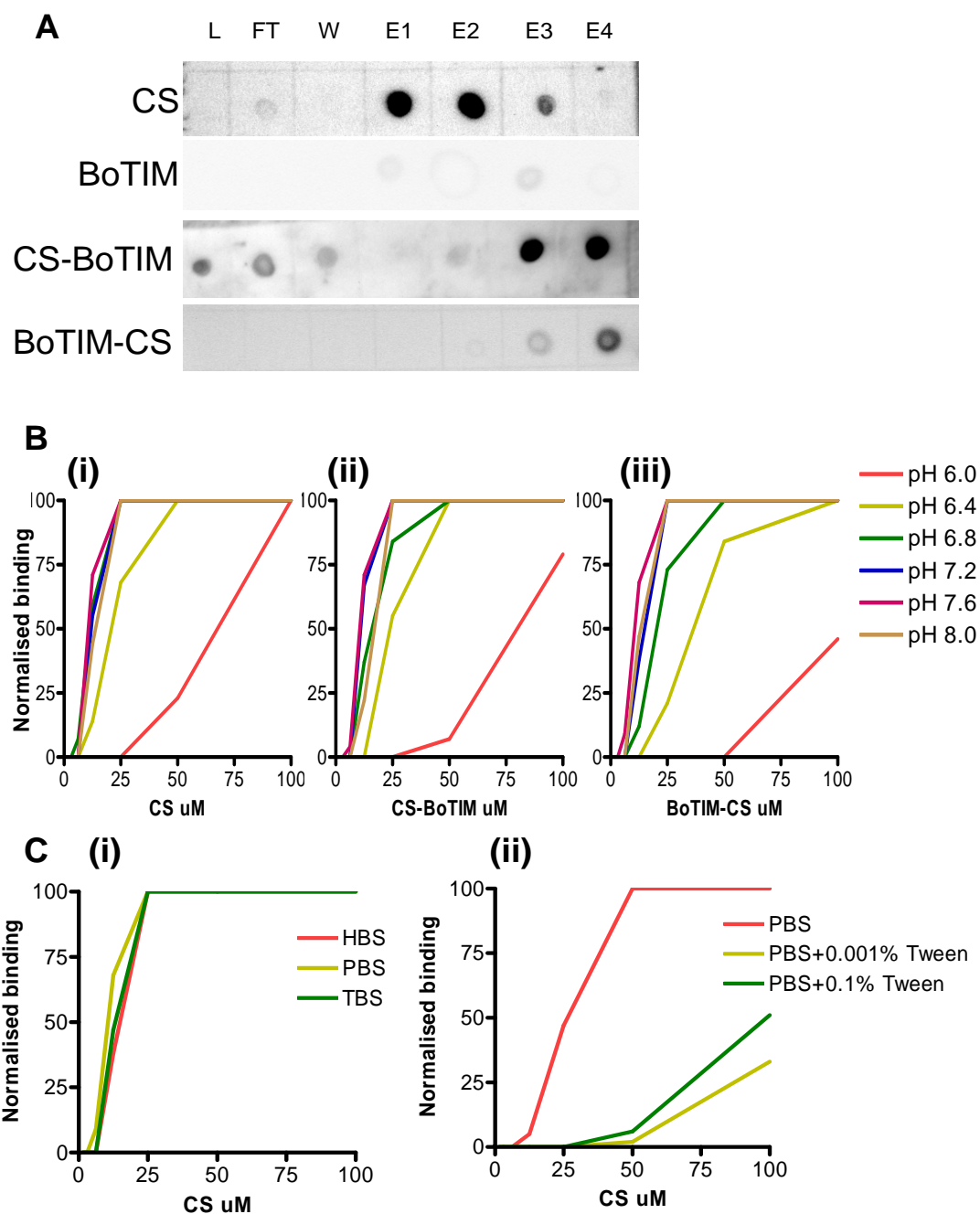
Fig. 41: CS and CS-tagged BoTIMs efficiently bind to biot-HRP. **A:** Aliquots from the IMAC purification process were blotted onto a nitrocellulose membrane and probed with biot-HRP. The blots show the strong and efficient binding of CS, and CS-tagged BoTIMs, to biot-HRP and the efficient concentration afforded by IMAC purification. (L – lysate; FT – flow-through from the TALON resin column; E1-4 – elute fractions; M – pre-stained protein molecular weith marker from Pierce). **B:** CS, and CS-tagged BoTIMs, are capable of binding biot-HRP at physiological pH. Various concentrations of CS and CS-tagged BoTIMs were blotted onto nitrocellulose membranes, blocked with PBS/5% BSA and probed with a 1:1500 dilution of biot-HRP in PBS buffers of pH 6.0 to 8.0. After development with an ECL reagent, the luminescence values were calculated with GeneSnap software, normalised to the maximum for each protein and plotted. **C:** The effect of different buffers and dertergents on the binding of biot-HRP to CS was determined. While binding is efficient in the physiological buffers tested, PBS, HBS and TBS (pH 7.2), the presence of even small quantities of a mild detergent (Tween 20) is enough to strongly inhibit such binding.

186

A: Elution profiles legend: Blue Dextran, Ferritin, Aldolase, Ovalbumin, Aprotinin, Phenol red
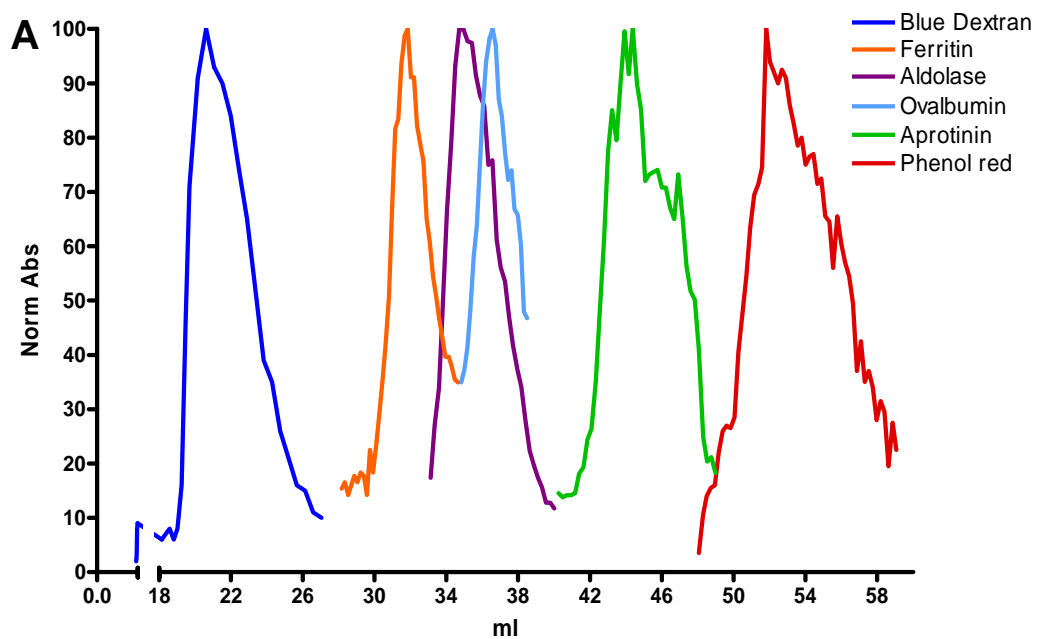
B:

Protein	M_r in kDa	V_e in ml	K_{av}
Aprotinin	6500	44.3	0.92
Ribonuclease A	13700	40.8	0.78
Lysozyme	14300	40.2	0.76
Ovalbumin	43000	37.5	0.66
Aldolase	158000	35.3	0.58
Ferritin	440000	31.8	0.44
Thyroglobulin	669000	29.6	0.36
Streptavidin	60000	36	0.60

C:

$$K_{av}= V_e-V_o/V_t-V_o$$

Length	l	49	cm
Diameter	d	1.1	cm
Geometric column Volume	V_t	46.6	ml
Void volume	V_o	20	ml
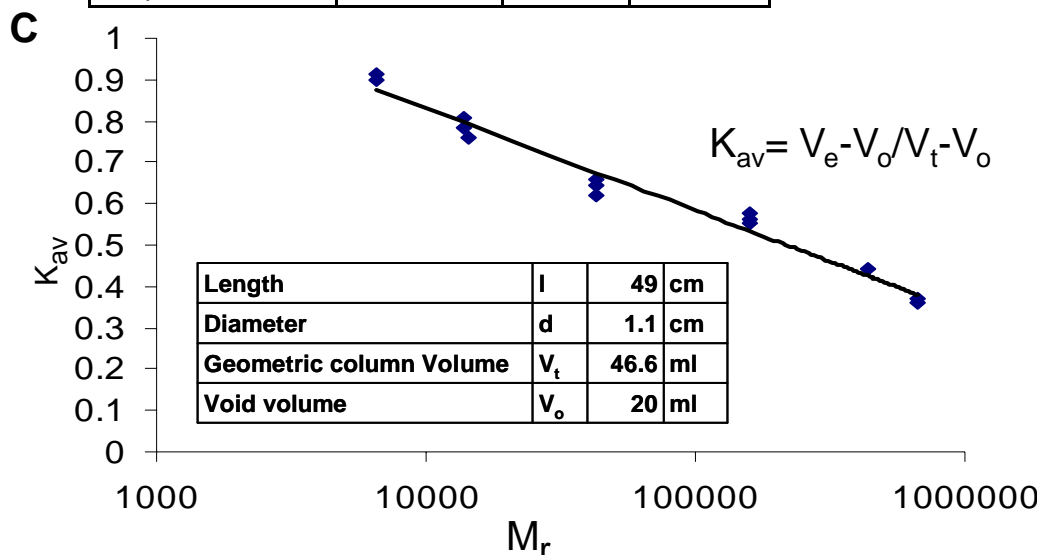
Fig. 42: Characterisation of the properties of a Superose 6 column: **A:** Elution profiles of proteins of different M_r superimposed on that of Blue dextran and phenol red. **B and C:** The relationship between protein M_r, V_e and, the calculated, K_{av}. A table with the individual values and a semi-log graph of the same is represented here.
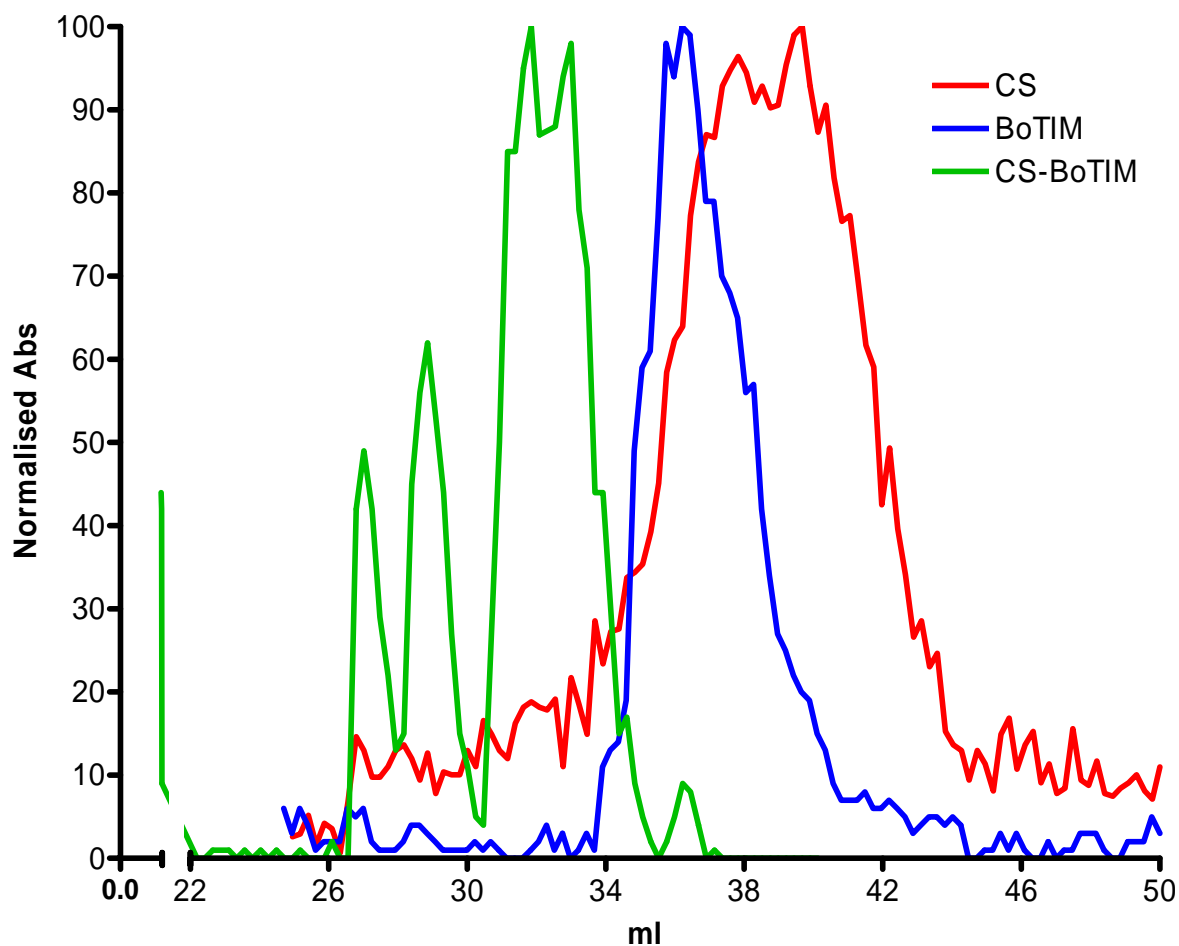
Fig. 43: Chromatographic determination of the molecular weights and conformation of CS, BoTIM and CS-BoTIM in solution. The elution peaks of CS, 37.8 – 39.6ml, corresponds to a tetramer of ~50-60kDa. BoTIM elutes from the column between 35.5-36.5ml corresponding to a Mr of ~130-170kDa, while the elution peaks of CS-BoTIM, at 27, 29, 32 and 33 ml, corresponds to a complex multimer ranging from >660 to 150kDa.

Another query that needs to be clarified if the relative efficiency of binding to larger biotinylated cargo is different that from smaller ones – an aspect that is important in determining if there is an in-built limit to CS-tagged BoTIM's targeting capacity. The prototype cargo chosen was commercially available biotinylated fluoromicrospheres. This large, multi-molecular, cargo was efficiently bound and, most importantly, not dislodged by repeated washing with physiological buffers (see Fig. 44A). In addition, the actual cargo that will be used, biotinylated LVs was also tested – due to the hazards involved in using large amounts of LVs on the bench, a modification of the gel-filtration experiment was used. Un-nicked CS-BoTIM was bound to an IMAC column and biotinylated LVs were passed through this. As expected, these LVs bound strongly to the immobilised CS-BoTIM and could be eluted using EDTA (see Fig. 44B).

Another test to measure the effect of bound cargo on the native targeting ability of BoNT, was to measure SNAP-25 cleavage in CGNs after attaching various biotinylated molecules, of increasing sizes, to CS-BoNT/E and BoNT/E-CS. There was a small effect on LC entry, and thus SNAP-25 proteolysis, which seemed to be directly proportional to the size of the attached cargo – interestingly, activity was retained even in molecules handicapped with bFM (see Fig. 45). The position of CS on BoTIM did not strongly affect the amount of SNAP-25 proteolysis, probably due to the fact that most of the cargo is detached in the acidic lysosomal environment.
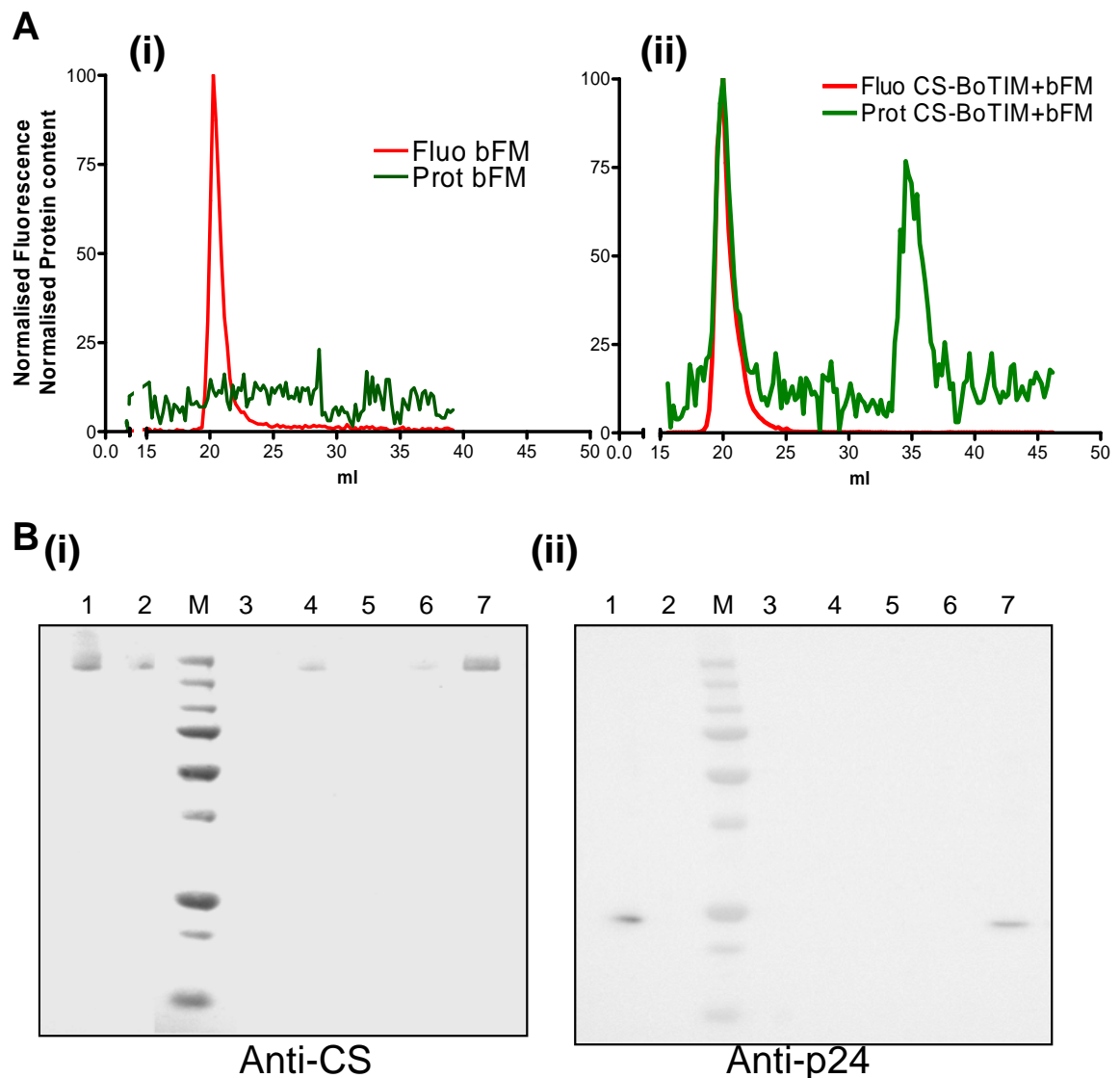
Fig. 44: CS-BoTIM binds efficiently to large biotinylated cargo. **A:** The elution profiles of biotinylated fluoromicrospheres (bFM) – bound to CS-BoTIM (ii) or free (i). Panel (ii) shows the strong and specific association between the biotin on bFM and CS on CS-BoTIM. (The normalised fluorescence readings are plotted in red and protein concentrations, measure by a Bradford's assay, are shown in green. **B:** CS-BoTIM can bind specifically to Biotinylated decorated. A crude mixture of an excess of CS-BoTIM (30ug) and biotinylated lentiviruses (~$2x10^{11}$ VPs) was loaded onto a mini-clumn containing 20µl TALON resin (1). Samples from the flow-through (2), wash with 1 ml PBS pH7 (3), FT after adding more CS-BoTIM (30ug) (4) wash with 1 ml PBS pH7 (5), first elute (10mM EDTA) (6) and 2nd elute (50mM EDTA) (7) were then run on an SDS-PAGE gel and blotted with an anti-streptavidin and anti-p24 antibodies. The presence of viral and protein bands in the 2nd elute clearly shows the specific binding of CS-BoTIM to biot-LVs.[Biot-LV concentrations: starting p24 ELISA – $2x10^{11}$; 2nd Elute p24 ELISA - ~10^{11})].
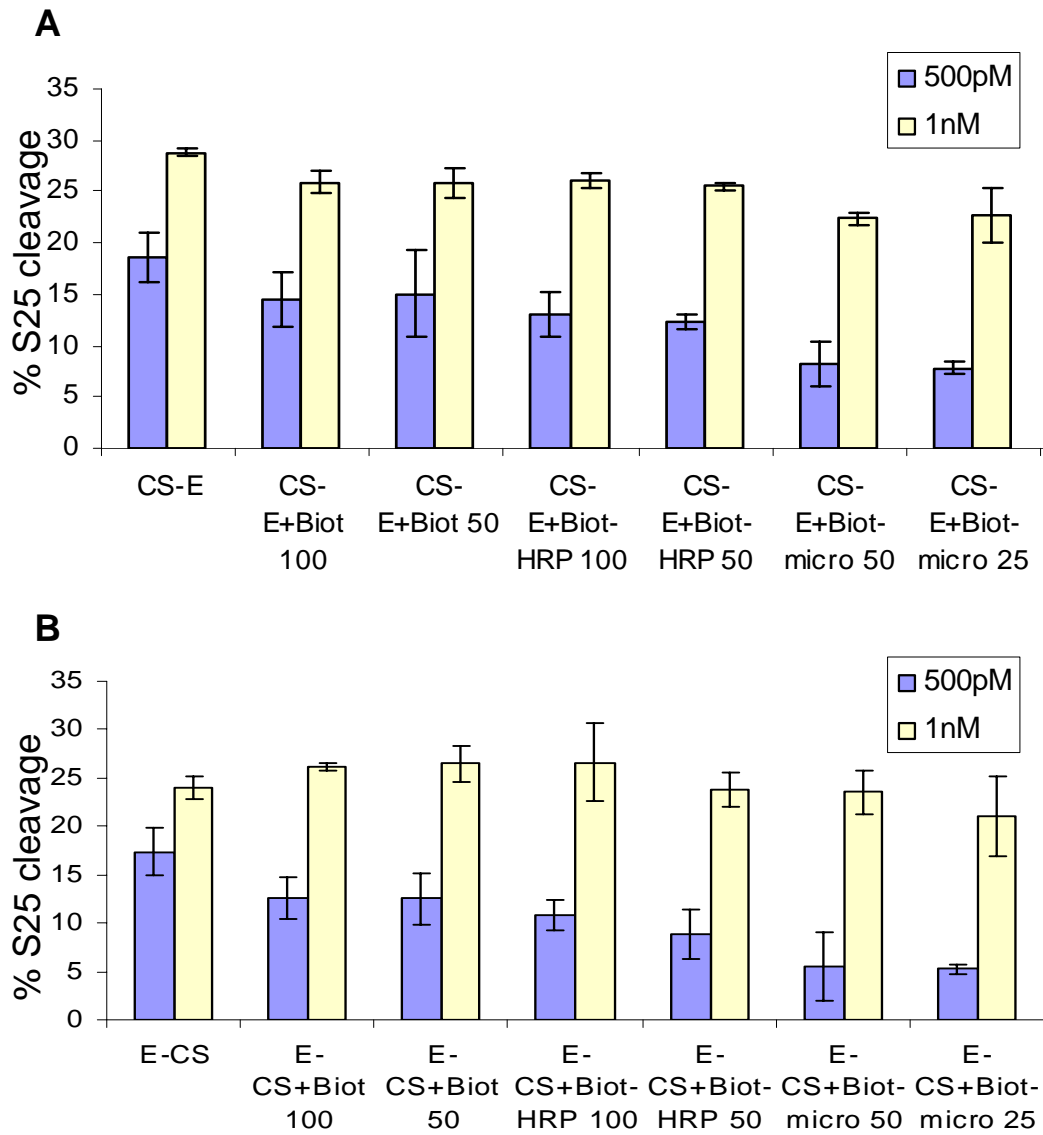
Fig. 45: The effect of bound cargo on the cleavage of SNAP-25 in CGNs by CS-tagged BoNT/Es. **A:** The effect of saturably bound biotin (biot – 50 and 100μM), biot-HRP (50 and 100μM) and biotinylated microspheres (biot-micro – 50 and 100μM equivalent) on the cleavage of SNAP-25 in CGNs by N-terminally CS-tagged BoNT/E (CS-E). **B:** The effect of previously described cargo binding on the cleavage of SNAP-25 in CGNs by C-terminally CS-tagged BoNT/E (E-CS).

Preliminary tests were then done on targeting LVs – the prototype large cargo chosen. HEK-293 cells were the chosen non-neuronal cells and CGNs were the chosen neurons. While a more rigorous test would have been that using muscle cells and cholinergic spinal motor neurons in the same dish, there were difficulties in creating such a co-culture system. Attachment of CS-BoTIM and BoTIM-CS to the surface of biot-LVs strongly reduced its promiscuity to non-neuronal cells (see Fig 46), while having a minimal effect of the viruses natural neuronal affinity (see Fig.47). The effect of targeting on viral infectivity to HEK-293s was very evident, at least at higher concentrations of the targeting molecule, while there was no obvious improvement in their neuronal infectivity. While the reasons for this are yet to be determined, it must be noted that LVs strongly and readily infect neurons in culture and increasing this pronounced, pre-existing, neuronal affinity might not be easily achieved. The achieved decrease in non-neuronal promiscuity does realize the same result as increasing neuronal infectivity and is an integral part of the goal of cholinergic targeting.

A

(i)

(ii)

LentiGFP – Untargeted

Biot-LentiGFP – Untargeted

B

(i)

(ii)

Biot-LentiGFP + CS-BoTIM

Biot-LentiGFP + BoTIM-CS
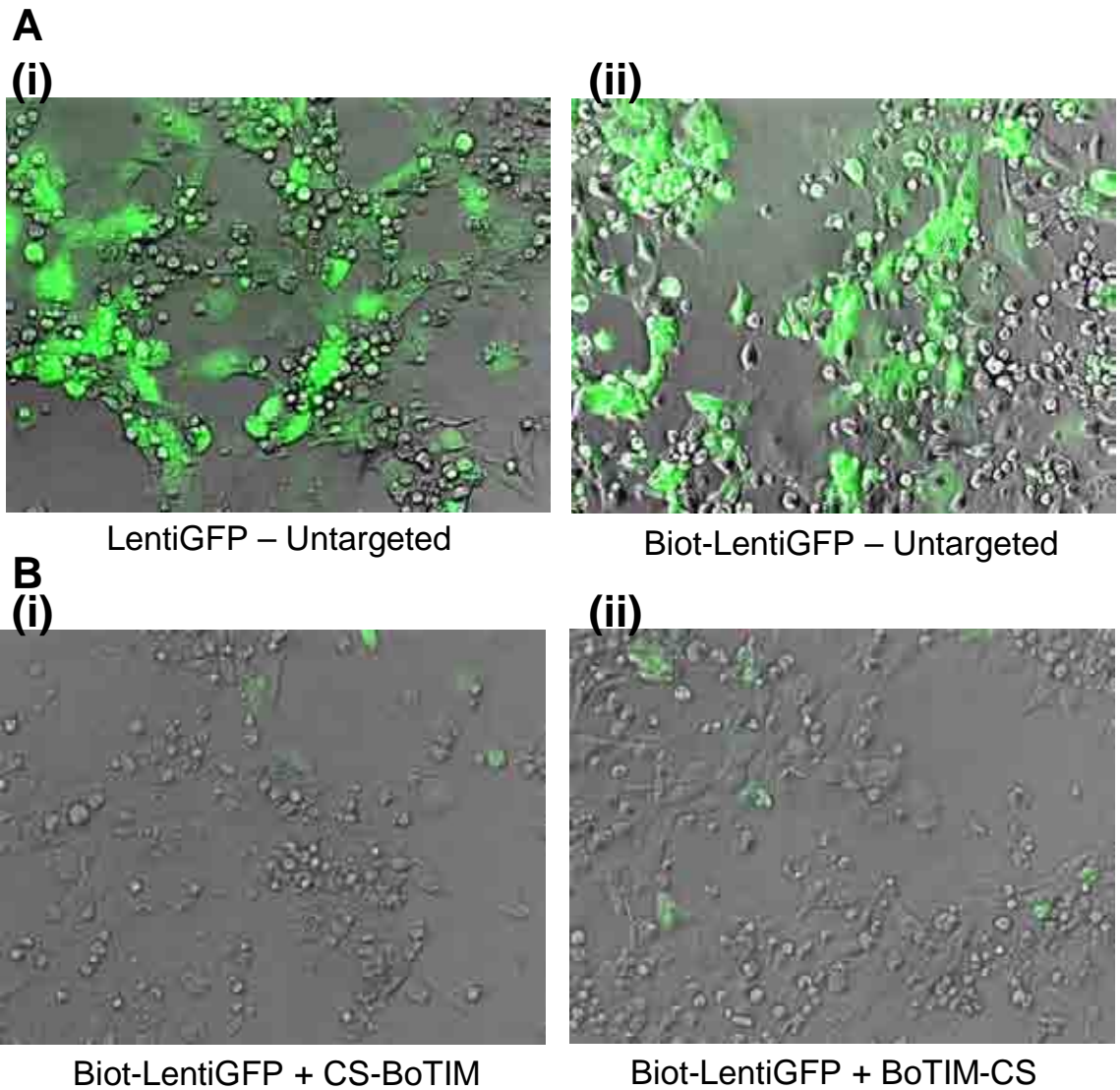
Fig. 46: Partial ablation of the promiscuous infectivity of LVs by attachment of CS-tagged BoTIMs: HEK293 cells used as a prototype non-neuronal cells. GFP expression after infection with un-targeted LVs [**A(i)** shows unmodified and **A(ii)** biotinylated] is compared to that after targeting with bound CS-BoTIM [**B(i)**] and BoTIM-CS [**B(ii)**]. Pre-incubation with a 10-fold molar excess of CS-BoTIM and BoTIM-CS reduces the number of cells expressing GFP after 48 h.
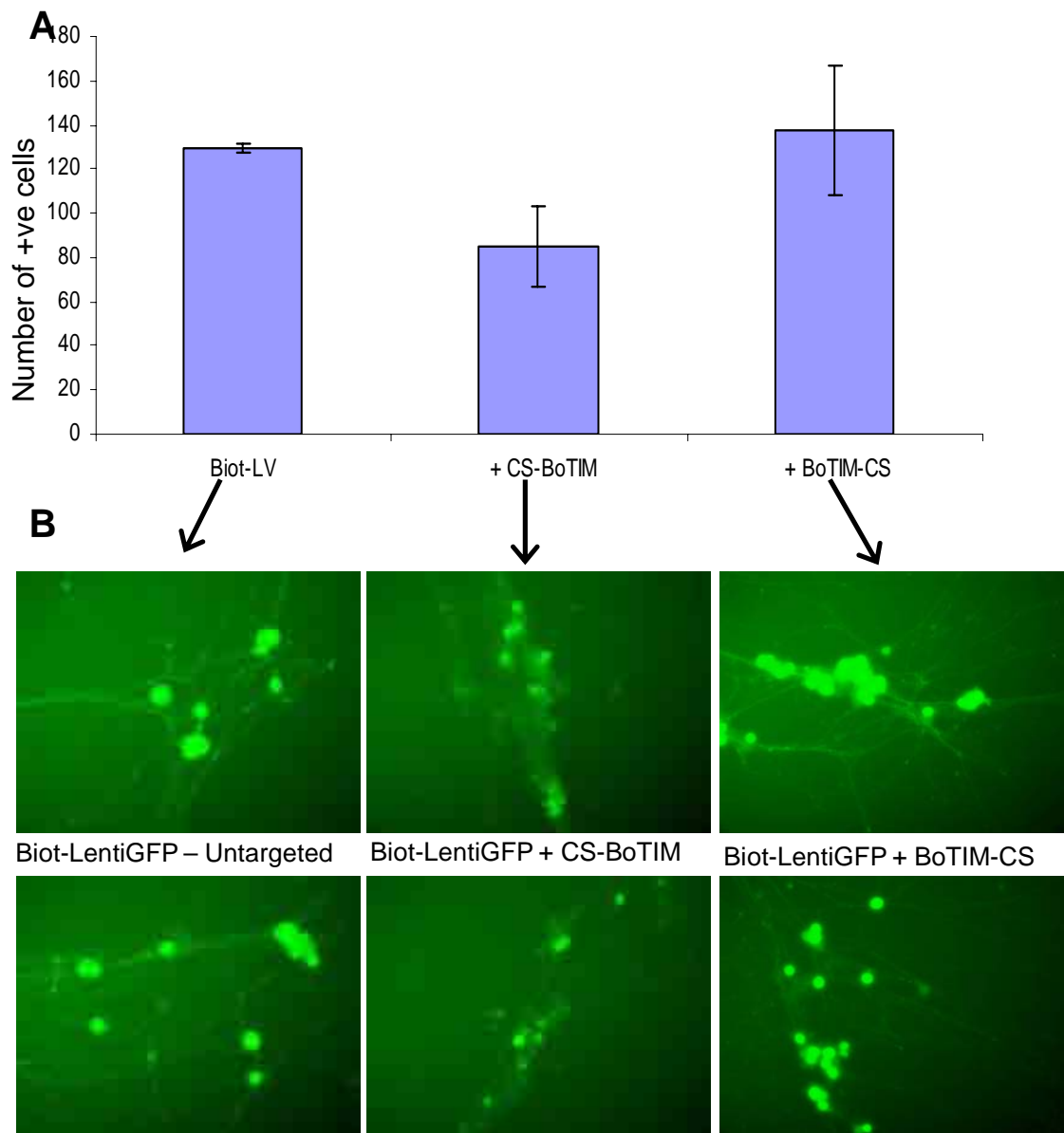
Fig. 47: LV infectivity towards neurons is not affected by attachment of CS-tagged BoTIM. The cell counts after treatment with biot-LV (targeted or untargeted – as described previously) are shown in **A**, while representative photomicrographs are shown in **B**. The cumultive counts from 4 different wells, obtained with a scanning plate readers are plotted along with their SDs.

3.4. Discussion

The extra-ordinary specificity of CNTs to NMJs creates formidable problems that need to be overcome if a successful therapy against botulism is to be devised. On the other hand, if this very same specificity can be exploited to deliver therapeutic molecules to NMJs, and their supplying motor neurons, novel, highly effective, peripherally deliverable and minimally-invasive treatments can be developed.

The deliverable therapeutic could be a small peptide molecule, a medium-sized protein/antibody, a virus or even a liposome. Having targeting molecules that are flexible enough to target all, or atleast many, of these varied therapeutics, would substantially advance and expand, the currently limited, area of spinal cord treatments. Attachment of biotin, a small 0.4kDa molecule should not strongly affect the therapeutic potential of the delivered cargo – indeed this biotin could have a long, cleavable linker, between itself and the attached cargo, further minimising deleterious effects. Attaching such a modified cargo via a streptavidin linker to the CNT based targeting molecule will bring to fruition the proposed versatile targeting strategy. Thus the currently study uusing a CS-tagged BoTIM based targeting molecule delivering a biotinylated LV to neuronal/cholibergic terminals, while limiting its promiscuous infectivity to non-neuronal cells, was formulated.

Of course, during these involved processes, a large number of things could go wrong – the cargo could be inactivated by biotinylation, the targeting properties of BoTIM could be destroyed by the attachment of CS or the biotin

binding property of CS destabilised by the attachment of BoTIM. In addition, the final, assembled, multi-molecular conglomerate might not work as proposed, despite the individual components being perfectly functional. This study was primarily aimed at solving the first three set of problems and in only obtaining some proof-of-principle for the final, and ultimate, goal.

A LV system was chosen for this part of the project, in preference to an AAV, as is has a larger cloning capacity, easier production of high titers and since the functional protein core is separate from the protein-studded lipid envelope. The large amount of work done in re-targeting LVs, albeit by pseudo-typing rather than targeting, was another reason for its choice. The obtained LVs performed as described by others and was able to replicate important results obtained with AAVs – protection from a later application of BoNT/A in CGNs. In addition, the devised biotinylation protocols worked efficiently while not perturbing the LV's infectivity or titer.

The CS-tagging of BoTIMs was another success, with a total of 13 different molecules generated. The molecules not only bound small biotinylated proteins like biot-HRP, but also larger cargo like Biotinylated LVs and microspheres. One, expected, result from the chromatographic analysis of CS-BoTIM was the finding that it exists as a di-tri-tetrameric mixture in physiological buffers. But this seemed to not have any strong, or identifiable, effects in the *in vitro* tests conducted. A crucial finding was the retention of exocytotic blockade activity by CS-tagged BoNT/Es – validating all the processes that lie behind this blocklade i.e., specific binding, internalisation, extra-vasation into the cytoplasm, path-finding to membrane bound SNAP-25 and its disablement by cleavage of a

27 AA fragment. The difference of only one single a between the active and the inactive versions, connotes that all the CS-tagged BoTIMs also undergo the same steps and therefore are valid as targeting agents.

The final series of tests was the attempted targeting of biot-LVs – this can be achieved by either increasing their affinity to neurons or by decreasing their affinity to non-neuronal cells. An ideal targeting molecule should accomplish both the aspects. But since the LVs seem to naturally prefer neurons, it was always doubtful if any significant increase in neuronal infectivity could be conferred by targeting, or indeed if this could be identified by the end-point assays available. The results obtained demonstrate a clear reduction in viral infection of HEK-293 cells, with no identifiable effects on their infectivity towards CGNs in culture.

Targeting peripherally delivered viruses into spinal motor neurons is an exceptionally difficult proposition (for reasons discussed in the introduction). The targeting molecule has to overcome the virus's natural properties till it reaches the motor neuron nucleus and then has to immediately give way for the viral properties to come to the fore, to enable successful infection. This inherent conflict might be difficult to resolve using the currently available tools and techniques. However, the procedures developed during this study demonstrate that some aspects of this strategy can be successfully attained, at least in *in vitro* model systems. Futher refinements of this protocol, with different targeting molecules and/or viruses, might soon enable the acquisition of a complete, clinically-applicable, therapy.

4. General Discussion and future prospects

Counter-measures for botulism must contend with several difficulties posed by the toxins' intracellular action, the persistence of the protease activity of some serotypes (e.g. /A, /C1) for months inside neurons and the extended time required to restore normal neuromuscular transmission (including replacement of the truncated SNARE and completion of the endplate remodeling that follows paralysis by most serotypes). To cope with these challenges, a multi-pronged strategy utilising conjunctive therapies must be used – an immediate active/passive immunisation based mopping up of the toxin from systemic circulation, direct interventions at the NMJ including delivery of protease inhibitors to limit the exocytotic blockade and, finally, delivery of resistant SNARE genes to obtain sustained rescue from neuro-paralysis. The exquisite specificity and extreme activity of the BoNTs will probably necessitate that all these three modes be developed in order to obtain a clinically relevant treatment for botulism.

The present study, which investigates the most optimal way of delivering resistant SNAP-25 genes to motor neurons, is an attempt to accomplish the final facet in this holistic BoNT therapy strategy. The use of viral vectors to deliver and expressed resistant SNAREs has many advantages – once infected, there is long-term expression, sustained production and delivery to presynaptic terminals. The multiple serotypes of BoNTs found in nature, each highly potent, complicates any potential therapy – especially considering that

the main application would be to counter malicious and deliberate dispersal of such toxins. But, when used in conjunction with neutralizing antibodies that sequester BoNTs in the extracellular environment preventing further uptake and inhibitors delivered to cholinergic terminals that counteract the internalized toxin, viral vector based delivery of multi-toxin resistant SNAREs, and even multiple SNAREs, could result yield such a versatile treatment. The biggest problem with viral vector mediated delivery is the amount of time taken by the virus to infect the neurons, integrate into the chromosome and to start producing the resistant SNAREs. Indeed in rats and mice, the true value of such therapy cannot be measured as the toxin's natural half-life only slightly overlaps with the viral-vector's optimal expression time period. It is for these reasons that protection based assays were chosen to prove the efficacy and utility of gene delivery as a mode of treatment. Indeed, it is possible that the real value to gene delivery can only be gauged in larger animals, with their longer paralytic time periods. But the effect of size on the efficiency of viral delivery and infection is a factor that could confound such effectiveness. Another potential roadblock is the known side-effect of insertional mutagenesis seen in many gene therapy trials. Therefore, limiting viral entry to only those neurons that are affected will prove to be a critical aspect of a successful therapy. This will necessitate the development of a virus specific for motor neurons.

Direct spinal delivery is currently the most effective mode of ensuring viral infection of anterior horn motor neurons. But this is a highly invasive and time consuming procedure that might not find much use outside a lab environment. Peripheral delivery, by intravenous/intramuscular injection, will be

far easier and, therefore, more clinically applicable – especially in treatments of mass epidemics of botulism. But since the viruses, AAV and LV, will infect all cells, the previously described insertional mutagenesis will be a bigger problem for peripheral delivery. In addition, not enough virus will enter the nerve terminals and therefore not provide adequate resistant SNARE proteins to enable measurable rescue. Targeting viruses to the pre-synaptic cholinergic terminals will materially advance prospects of peripherally delivered gene therapies for botulism. In addition, such a method, will have great potential in the treatment of other biological threats that often affect peripheral nerve endings.

The specificity of CNTs, especially BoNTs, for nerve terminals, which till now has been the prime stumbling block, has been harnessed here to therapeutic effect. The proof of principle already obtained for the prophylaxis of BoNT/A-induced neuromuscular paralysis in rodents by Adeno-associated viral (AAV) delivery of a gene encoding SNAP-25 mutant resistant to BoNT/A (Raghunath et al. 2007) when combined with the work that has been started on targeting viruses has the potential to yield such a therapy. The ultimate goal is a therapy that utilises the properties of LVs and BoNTs to create a hybrid virus and also contains larger gene inserts necessary for achieving rescue from all relevant BoNT serotypes, incorporates a cholinergic promoter to give absolute specificity and uses regulatory elements for controlling expression.

The next phase leverages the novel tools and techniques developed in this project to further modify the existing and proven delivery vehicles and

assess the effects of such changes on their targeting efficiency. Building on the initial success with AAV-mediated expression of cleavage-resistant SNAP-25, the newly-developed second-generation LV gene delivery system adopted has proven more flexible – with its larger insert capacity, facility for bi-cistronic production of two genes from the same virus, potential for inserting specific and regulatable promoters and ease of modifying viral specificity by introducing/modifying/pseudotyping the surface glycoproteins. Three sequential experimental strands will be investigated to promote LV mediated gene delivery after peripheral injection. Firstly, the ability of these LVs to seek and preferentially bind to nerve terminals will be enhanced by the addition of cholinergic targeting molecules, thereby, increasing motor neuron expression of introduced genes whilst decreasing the deleterious effects of non-neuronal viral integration. The second strand will be the incorporation of promoters that, in case the LVs enter non-neuronal cells, limit gene expression; another track in this endeavour will be the incorporation of regulatable promoters that can be switched off once the toxin's effects have been effectively countered. Finally, in order to leverage the maximum scope for treating different outbreaks of botulism or exposure to the commonly encountered toxins, LVs will be modified to co-express in neurons multi-toxin resistant (MTR) SNAP-25 and VAMP2 – two major BoNT targets. Current investigations of LV have shown that, even unmodified, they preferentially infect neurons and the introduced genes are transcribed at a highly accelerated pace. Additionally, their surface glycoproteins have been successfully biotinylated, with long, reducible, linkers between biotin and the viral surface; such biotinylated LVs retain infectivity.

MTR SNAP-25, proven to be resistant to cleavage by BoNT/A, /E and /C1, has already been successfully incorporated; LV-induced expression of this protein in cultured neurons has been shown to confer protection of glutamate exocytosis against a subsequent challenge by BoNT/A or /E.

The previously developed, CS-tagged, toxin- and immune-based targeting molecules will be attached to these viruses and their infectivity plus specificity tested in pure neuronal and mixed neuron/glia/muscle cultures. The neuronal specificity imparted by the targeting agents will be estimated by immuno-fluorescent tracking of trans-gene expression. In addition, the availability of fluorescent Taqman-based real-time quantitative PCR assays will allow a rapid measurement of the number of viral particles entering the target neurons. Compartmentalised cultures of neurons will be used to track the retrograde transport of applied targeted-LVs after application to the terminals. While targeting should enhance motor neuron infection, there will still be some LVs that promiscuously bind to non-neuronal cells (which grossly outnumber the motor terminals). Eliminating their expression of the introduced cleavage-resistant SNAREs should allow the injection of even higher LV doses, thereby, increasing chances of motor neuron infection. The best optimised promoter is the choline acetyl-transferase promoter (CHAT – 2-4kb), which is only active in cholinergic neurons (though, the smaller and proven human synapsin promoter will also be tried) – it will be used to replace the native elongation factor-1 promoter. RT-QPCR after LV application to cerebellar granule neurons, motor neurons and myoblasts in culture (or mouse cholinergic neuronal SN6 line, mouse non-cholinergic neuronal LAN5 line and rat fibroblast FR3T3 line) will

facilitate the assessment of introduced cholinergic specificity.

An alternative/additional sophistication is the use of regulatable promoters. While multiple choices exist (eg. Ecdysone, RU486 and rapamycin based regulation), the tetracycline-induced regulatable system (TiRS) offers advantages of rapid induction and minimal promoter leakage, with up to a 1,000-fold dose-dependent induction of gene expression from the basal state. The TiRS system uses a rtTA (reverse tetracycline-controlled transactivator attached to 3 repeats of a minimal VP16 transcription activation domain) and a TRE (tet-responsive element containing the modified tet-operator in conjunction with a minimal CMV promoter driving cleavage-resistant SNARE expression). Only upon binding to the tetracycline derivative, doxycycline, is the TRE activated and cleavage-resistant SNAREs produced. While the TiRS system originally required two different viruses to provide rtTA and TRE systems, use of LV and WPRE (Woodchuck hepatitis virus post-translational regulatory element) permits their incorporation into a single viral molecule. Once again, the use of RT-QPCR will facilitate the measurement of gene induction upon introduction of doxycycline; use of a human synapsin promoter to drive rtTA expression would add neuron-specificity to this TiRS based regulatable promoter.

The existence of several toxin serotypes with different SNARE substrates/cleavage sites and the potential to create chimeric toxins demand the introduction MTR SNAREs into susceptible neurons. An important demonstration of the practicability of such an advance is the proven ability of

MTR SNAP-25(mutated at D179K, M182T and R197T) to resist cleavage by BoNT/A, /E and /C1 in protease assays in vitro and by BoNT/A and /E in neuronal cultures. To complement this, MTR forms of VAMP2 will be created – with mutations at Q76V conferring resistance to BoNT/B (and TeNT) and K59A to /F (and possibly /D). This MTR-VAMP2 will be tested in vitro and in vivo before incorporation into the LV system. Its capacity to participate in productive synaptic exocytosis and to resist BoNTs will be determined in neurons infected with the virus, and treated with or without BoNTs. If successful, MTR-VAMP2 will be integrated into the existing LV-MTR-SNAP25 viral system. Co-expression of MTR-SNAP-25 and MTR-VAMP2 from the same promoter (neuron-specific and/or regulatable) can be ensured by addition of an IRES sequence (internal ribosome entry site) before the second gene. The bi-cistronic MTR-SNARE expressing LVs will be tested, as before, in neuronal model systems.

While not all of the modifications will succeed, the multi-pronged approach described should lead to improvements that could later be adapted in clinically-applicable pre- or post-exposure therapies for botulism.

Bibliography

Adler M, Nicholson JD, Cornille F, Hackley BE, Jr. (1998) Efficacy of a novel metalloprotease inhibitor on botulinum neurotoxin B activity. FEBS Lett 429:234-238.

Adler M, Keller JE, Sheridan RE, Deshpande SS (2001) Persistence of botulinum neurotoxin A demonstrated by sequential administration of serotypes A and E in rat EDL muscle. Toxicon 39:233-243.

Advani RJ, Bae HR, Bock JB, Chao DS, Doung YC, Prekeris R, Yoo JS, Scheller RH (1998) Seven novel mammalian SNARE proteins localize to distinct membrane compartments. Journal of Biological Chemistry 273:10317-10324.

Agarwal R, Eswaramoorthy S, Kumaran D, Binz T, Swaminathan S (2004) Structural analysis of botulinum neurotoxin type E catalytic domain and its mutant Glu212-->Gln reveals the pivotal role of the Glu212 carboxylate in the catalytic pathway. Biochemistry 43:6637-6644.

Aguado F, Majo G, Ruiz-Montasell B, Llorens J, Marsal J, Blasi J (1999) Syntaxin 1A and 1B display distinct distribution patterns in the rat peripheral nervous system. Neuroscience 88:437-446.

Ahnert-Hilger G, Bader M-F, Bhakdi S, Gratzl M (1989) Introduction of macromolecules into bovine adrenal medullary chromaffin cells and rat pheochromocytoma cells (PC-12) by permeabilization with streptolysin-O: inhibitory effect of tetanus toxin on catecholamine secretion. Journal of Neurochemistry 52:1751-1758.

Altin JG, Pagler EB (1995) A one-step procedure for biotinylation and chemical cross-linking of lymphocyte surface and intracellular membrane-associated molecules. Anal Biochem 224:382-389.

An SJ, Almers W (2004) Tracking SNARE complex formation in live endocrine cells. Science 306:1042-1046.

Aoki KR (2004) Botulinum toxin: a successful therapeutic protein. Curr Med Chem 11:3085-3092.

Arnon SS, Schechter R, Maslanka SE, Jewell NP, Hatheway CL (2006) Human botulism immune globulin for the treatment of infant botulism. N Engl J Med 354:462-471.

Arnon SS, Schechter R, Inglesby TV, Henderson DA, Bartlett JG, Ascher MS, Eitzen E, Fine AD, Hauer J, Layton M, Lillibridge S, Osterholm MT, O'Toole T, Parker G, Perl TM, Russell PK, Swerdlow DL, Tonat K, for the Working Group on Civilian B (2001) Botulinum Toxin as a Biological Weapon: Medical and Public Health Management. JAMA 285:1059-1070.

Askmark H, Backman E, Gillberg PG, Henriksson KG (1991) Quantification of extrajunctional acetylcholine receptors in human muscle biopsies. Acta Neurol Scand 83:259-261.

Azzouz M, Kingsman SM, Mazarakis ND (2004) Lentiviral vectors for treating and modeling human CNS disorders. J Gene Med 6:951-962.

Bade S, Rummel A, Reisinger C, Karnath T, Ahnert-Hilger G, Bigalke H, Binz T

(2004) Botulinum neurotoxin type D enables cytosolic delivery of enzymatically active cargo proteins to neurones via unfolded translocation intermediates. J Neurochem 91:1461-1472.

Bajjalieh SM, Frantz GD, Weimann JM, McConnell SK, Scheller RH (1994) Differential expression of synaptic vesicle protein 2 (SV2) isoforms. J Neurosci 14:5223-5235.

Bark IC (1993) Structure of the chicken gene for SNAP-25 reveals duplicated exons encoding distinct isoforms of the protein. Journal of Molecular Biology 233:67-76.

Bark IC, Hahn KM, Ryabinin AE, Wilson MC (1995) Differential expression of SNAP-25 protein isoforms during divergent vesicle fusion events of neural development. Proceedings of the National Academy of Sciences of the United States of America 92:1510-1514.

Bayer EA, Wilchek M (1980) The use of the avidin-biotin complex as a tool in molecular biology. Methods Biochem Anal 26:1-45.

Bayer EA, Wilchek M (1990) Biotin-binding proteins: overview and prospects. Methods Enzymol 184:49-51.

Berns KI, Linden RM (1995) The cryptic life style of adeno-associated virus. Bioessays 17:237-245.

Bevan S, Steinbach JH (1977) The distribution of alpha-bungarotoxin binding sites of mammalian skeletal muscle developing in vivo. J Physiol 267:195-213.

Bienemann AS, Martin-Rendon E, Cosgrave AS, Glover CP, Wong LF, Kingsman SM, Mitrophanous KA, Mazarakis ND, Uney JB (2003) Long-term replacement of a mutated nonfunctional CNS gene: reversal of hypothalamic diabetes insipidus using an EIAV-based lentiviral vector expressing arginine vasopressin. Mol Ther 7:588-596.

Bigalke H, Dreyer F, Bergey G (1985) Botulinum A neurotoxin inhibits non-cholinergic synaptic transmission in mouse spinal cord neurons in culture. Brain Research 360:318-324.

Black JD, Dolly JO (1986a) Interaction of 125I-labeled botulinum neurotoxins with nerve terminals. I. Ultrastructural autoradiographic localization and quantitation of distinct membrane acceptors for types A and B on motor nerves. J Cell Biol 103:521-534.

Black JD, Dolly JO (1986b) Interaction of 125I-labeled botulinum neurotoxins with nerve terminals. II. Autoradiographic evidence for its uptake into motor nerves by acceptor-mediated endocytosis. J Cell Biol 103:535-544.

Black JD, Dolly JO (1987) Selective location of acceptors for botulinum neurotoxin A on central and peripheral nerves. Neuroscience 23:767-779.

Black RE, Gunn RA (1980) Hypersensitivity reactions associated with botulinal antitoxin. Am J Med 69:567-570.

Blasi J, Chapman ER, Yamasaki S, Binz T, Niemann H, Jahn R (1993a) Botulinum neurotoxin C1 blocks neurotransmitter release by means of cleaving HPC-1/syntaxin. Embo J 12:4821-4828.

Blasi J, Egea G, Castiella MJ, Arribas M, Solsona C, Richardson PJ, Marsal J (1992) Binding of botulinum neurotoxin to pure cholinergic nerve

terminals isolated from the electric organ of Torpedo. J Neural Transm Gen Sect 90:87-102.

Blasi J, Chapman ER, Link E, Binz T, Yamasaki S, De Camilli P, Südhof TC, Niemann H, Jahn R (1993b) Botulinum neurotoxin A selectively cleaves the synaptic protein SNAP-25. Nature 365:160-163.

Bohnert S, Schiavo G (2005) Tetanus toxin is transported in a novel neuronal compartment characterized by a specialized pH regulation. J Biol Chem 280:42336-42344.

Bonner PH, Friedli AF, Baker RS (1994) Botulinum A toxin stimulates neurite branching in nerve-muscle co-cultures. Developmental Brain Research 79:39-46.

Boquet P, Duflot E (1982) Tetanus toxin fragment forms channels in lipid vesicles at low pH. Proceedings of the National Academy of Sciences of the United States of America 79:7614-7618.

Breidenbach MA, Brunger AT (2004) Substrate recognition strategy for botulinum neurotoxin serotype A. Nature 432:925-929.

Breidenbach MA, Brunger AT (2005) New insights into clostridial neurotoxin-SNARE interactions. Trends Mol Med 11:377-381.

Brennwald P, Kearns B, Champion K, Keranen S, Bankaitis V, Novick P (1994) Sec9 is a SNAP-25-like component of a yeast SNARE complex that may be the effector of Sec4 function in exocytosis. Cell 79:245-258.

Brin MF (1997) Botulinum toxin: chemistry, pharmacology, toxicity, and immunology. Muscle Nerve Suppl 6:S146-168.

Brown MC, Holland RL, Ironton R (1980) Nodal and terminal sprouting from motor nerves in fast and slow muscles of the mouse. J Physiol 306:493-510.

Bruijn LI, Miller TM, Cleveland DW (2004) Unraveling the mechanisms involved in motor neuron degeneration in ALS. Annu Rev Neurosci 27:723-749.

Brunger AT (2005) Structure and function of SNARE and SNARE-interacting proteins. Q Rev Biophys 38:1-47.

Brunger AT, Breidenbach MA, Jin R, Fischer A, Santos JS, Montal M (2007) Botulinum neurotoxin heavy chain belt as an intramolecular chaperone for the light chain. PLoS Pathog 3:1191-1194.

Bullens RW, O'Hanlon GM, Wagner E, Molenaar PC, Furukawa K, Furukawa K, Plomp JJ, Willison HJ (2002) Complex gangliosides at the neuromuscular junction are membrane receptors for autoantibodies and botulinum neurotoxin but redundant for normal synaptic function. J Neurosci 22:6876-6884.

Bullens RW, O'Hanlon GM, Wagner E, Molenaar PC, Furukawa K, Furukawa K, Plomp JJ, Willison HJ (2003) Roles of complex gangliosides at the neuromuscular junction. Ann N Y Acad Sci 998:401-403.

Buning H, Perabo L, Coutelle O, Quadt-Humme S, Hallek M (2008) Recent developments in adeno-associated virus vector technology. J Gene Med 10:717-733.

Burger C, Nash K, Mandel RJ (2005) Recombinant adeno-associated viral vectors in the nervous system. Hum Gene Ther 16:781-791.

Burger C, Gorbatyuk OS, Velardo MJ, Peden CS, Williams P, Zolotukhin S, Reier PJ, Mandel RJ, Muzyczka N (2004) Recombinant AAV viral vectors

207

pseudotyped with viral capsids from serotypes 1, 2, and 5 display differential efficiency and cell tropism after delivery to different regions of the central nervous system. Mol Ther 10:302-317.

Burke RE, Fedina L, Lundberg A (1971) Spacial synaptic distribution of recurrent and group Ia inhibitory systems in cat motoneurons. Journal of Physiology 214:305-326.

Burri L, Varlamov O, Doege CA, Hofmann K, Beilharz T, Rothman JE, Sollner TH, Lithgow T (2003) A SNARE required for retrograde transport to the endoplasmic reticulum. Proc Natl Acad Sci U S A 100:9873-9877.

Caroni P (1997) Intrinsic neuronal determinants that promote axonal sprouting and elongation. Bioessays 19:767-775.

Caroni P, Grandes P (1990) Nerve sprouting in innervated adult skeletal muscle induced by exposure to elevated levels of insulin-like growth factors. J Cell Biol 110:1307-1317.

Caroni P, Schneider C, Kiefer MC, Zapf J (1994) Role of muscle insulin-like growth factors in nerve sprouting: suppression of terminal sprouting in paralyzed muscle by IGF-binding protein 4. J Cell Biol 125:893-902.

Catterall WA (1999) Interactions of presynaptic Ca^{2+} channels and SNARE proteins in neurotransmitter release. Annals of the New York Academy of Sciences 868:144-159.

CDC (1998) Botulism in the United States, 1899-1996. In: (Handbook for Epidemiologists C, and Laboratory Workers, Atlanta, GA, ed): Center for disease control and prevention.

Ceccarelli B, Hurlbut WP, Mauro A (1973) Turnover of transmitter and synaptic vesicles at the frog neuromuscular junction. J Cell Biol 57:499-524.

Chen R, Cohen LG, Hallett M (2002) Nervous system reorganization following injury. Neuroscience 111:761-773.

Chen YA, Scheller RH (2001) SNARE-mediated membrane fusion. Nat Rev Mol Cell Biol 2:98-106.

Cherington M (1998) Clinical spectrum of botulism. Muscle Nerve 21:701-710.

Cherington M (2004) Botulism: update and review. Semin Neurol 24:155-163.

Chernomordik LV, Kozlov MM (2003) Protein-lipid interplay in fusion and fission of biological membranes. Annu Rev Biochem 72:175-207.

Choi VW, McCarty DM, Samulski RJ (2005) AAV hybrid serotypes: improved vectors for gene delivery. Curr Gene Ther 5:299-310.

Connold AL, Vrbova G (1991) Temporary loss of activity prevents the increase of motor unit size in partially denervated rat soleus muscles. J Physiol 434:107-119.

Cordingley MG, Callahan PL, Sardana VV, Garsky VM, Colonno RJ (1990) Substrate requirements of human rhinovirus 3C protease for peptide cleavage in vitro. J Biol Chem 265:9062-9065.

Cornille F, De Loye F, Fournie-Zaluski MC, Roques BP, Poulain B (1995) Inhibition of neurotransmitter release by synthetic proline-rich peptides shows that the N-terminal domain of vesicle-associated membrane protein/synaptobrevin is critical for neuro-exocytosis. Journal of Biological Chemistry 270:16826-16832.

Cronin J, Zhang XY, Reiser J (2005) Altering the tropism of lentiviral vectors through pseudotyping. Curr Gene Ther 5:387-398.

Daniels-Holgate PU, Dolly JO (1996) Productive and non-productive binding of botulinum neurotoxin A to motor nerve endings are distinguished by its heavy chain. J Neurosci Res 44:263-271.

Davidson BL, Breakefield XO (2003) Viral vectors for gene delivery to the nervous system. Nat Rev Neurosci 4:353-364.

de Paiva A, Dolly JO (1990) Light chain of botulinum neurotoxin is active in mammalian motor nerve terminals when delivered via liposomes. FEBS Letters 277:171-174.

de Paiva A, Meunier FA, Molgo J, Aoki KR, Dolly JO (1999) Functional repair of motor endplates after botulinum neurotoxin type A poisoning: biphasic switch of synaptic activity between nerve sprouts and their parent terminals. Proc Natl Acad Sci U S A 96:3200-3205.

de Paiva A, Ashton AC, Foran P, Schiavo G, Montecucco C, Dolly JO (1993) Botulinum A like type B and tetanus toxins fulfils criteria for being a zinc-dependent protease. J Neurochem 61:2338-2341.

De Winter F, Vo T, Stam FJ, Wisman LA, Bar PR, Niclou SP, van Muiswinkel FL, Verhaagen J (2006) The expression of the chemorepellent Semaphorin 3A is selectively induced in terminal Schwann cells of a subset of neuromuscular synapses that display limited anatomical plasticity and enhanced vulnerability in motor neuron disease. Mol Cell Neurosci 32:102-117.

Deinhardt K, Berninghausen O, Willison HJ, Hopkins CR, Schiavo G (2006) Tetanus toxin is internalized by a sequential clathrin-dependent mechanism initiated within lipid microdomains and independent of epsin1. J Cell Biol 174:459-471.

Delenda C (2004) Lentiviral vectors: optimization of packaging, transduction and gene expression. J Gene Med 6 Suppl 1:S125-138.

Dolly JO et al., (2009) Mutiple steps in the blockade of exocytosis by Botulinum neurotoxins. In : Botulinum toxin: Therapeutic clinical practice and Science

Dolly JO, Aoki KR (2006) The structure and mode of action of different botulinum toxins. Eur J Neurol 13 Suppl 4:1-9.

Dolly JO, Black J, Williams RS, Melling J (1984a) Acceptors for botulinum neurotoxin reside on motor nerve terminals and mediate its internalization. Nature 307:457-460.

Dolly JO, de Paiva A, Poulain B, Foran P, Ashton A, Tauc L (1992) Insights into the neuronal binding, uptake and intracellular activity of botulinum neurotoxins. In: Proceedings of the 5th European Workshop on Bacterial Protein Toxins (Witholt, ed), pp 31-45. Stuttgart: Gustav Fischer.

Dolly JO, de Paiva A, Foran P, Lawrence G, Daniels-Holgate P, Ashton AC (1994) Probing the process of transmitter release with botulinum and tetanus neurotoxins. Sem Neurosci 6:149-158.

Dolly JO, Halliwell JV, Black JD, Williams RS, Pelchen-Matthews A, Breeze AL, Mehraban F, Othman IB, Black AR (1984b) Botulinum neurotoxin and dendrotoxin as probes for studies on transmitter release. J Physiol (Paris) 79:280-303.

Dolly O (2003) Synaptic transmission: inhibition of neurotransmitter release by botulinum toxins. Headache 43 Suppl 1:S16-24.

Dong M, Richards DA, Goodnough MC, Tepp WH, Johnson EA, Chapman ER (2003) Synaptotagmins I and II mediate entry of botulinum neurotoxin B into cells. J Cell Biol 162:1293-1303.

Dong M, Yeh F, Tepp WH, Dean C, Johnson EA, Janz R, Chapman ER (2006) SV2 is the protein receptor for botulinum neurotoxin A. Science 312:592-596.

Duchen LW, Strich SJ (1968) The effects of botulinum toxin on the pattern of innervation of skeletal muscle in the mouse. Q J Exp Physiol Cogn Med Sci 53:84-89.

Dulubova I, Khvotchev M, Liu S, Huryeva I, Sudhof TC, Rizo J (2007) Munc18-1 binds directly to the neuronal SNARE complex. Proc Natl Acad Sci U S A 104:2697-2702.

Dulubova I, Sugita S, Hill S, Hosaka M, Fernandez I, Sudhof TC, Rizo J (1999) A conformational switch in syntaxin during exocytosis: role of munc18. Embo J 18:4372-4382.

Erbguth FJ (2007) From poison to remedy: the chequered history of botulinum toxin. J Neural Transm.

Fasshauer D, Sutton RB, Brunger AT, Jahn R (1998) Conserved structural features of the synaptic fusion complex: SNARE proteins reclassified as Q- and R-SNAREs. Proceedings of the National Academy of Sciences of the United States of America 95:15781-15786.

Fernandez-Salas E, Ho H, Garay P, Steward LE, Aoki KR (2004a) Is the light chain subcellular localization an important factor in botulinum toxin duration of action? Mov Disord 19 Suppl 8:S23-34.

Fernandez-Salas E, Steward LE, Ho H, Garay PE, Sun SW, Gilmore MA, Ordas JV, Wang J, Francis J, Aoki KR (2004b) Plasma membrane localization signals in the light chain of botulinum neurotoxin. Proc Natl Acad Sci U S A 101:3208-3213.

Fiebig KM, Rice LM, Pollock E, Brunger AT (1999) Folding intermediates of SNARE complex assembly. Nature Structural Biology 6:117-123.

Fischer A, Montal M (2007a) Single molecule detection of intermediates during botulinum neurotoxin translocation across membranes. Proc Natl Acad Sci U S A 104:10447-10452.

Fischer A, Montal M (2007b) Crucial Role of the Disulfide Bridge between Botulinum Neurotoxin Light and Heavy Chains in Protease Translocation across Membranes. J Biol Chem 282:29604-29611.

Fischer A, Garcia-Rodriguez C, Geren I, Lou J, Marks JD, Nakagawa T, Montal M (2008) Molecular architecture of botulinum neurotoxin E revealed by single particle electron microscopy. J Biol Chem 283:3997-4003.

Fischer von Mollard G, Sudhof TC, Jahn R (1991) A small GTP-binding protein dissociates from synaptic vesicles during exocytosis. Nature 349:79-81.

Fisher A, Montal M (2006) Characterization of Clostridial botulinum neurotoxin channels in neuroblastoma cells. Neurotox Res 9:93-100.

Foran P, Shone CC, Dolly JO (1994) Differences in the protease activities of tetanus and botulinum B toxins revealed by the cleavage of vesicle-associated membrane protein and various sized fragments. Biochemistry 33:15365-15374.

Foran P, Lawrence G, Dolly JO (1995) Blockade by botulinum neurotoxin B of

catecholamine release from adrenochromaffin cells correlates with its cleavage of synaptobrevin and a homologue present on the granules. Biochemistry 34:5494-5503.

Foran P, Lawrence GW, Shone CC, Foster KA, Dolly JO (1996) Botulinum Neurotoxin C1 Cleaves Both Syntaxin and SNAP-25 In Intact and Permeabilized Chromaffin Cells - Correlation With Its Blockade of Catecholamine Release. Biochemistry 35:2630-2636.

Foran PG, Mohammed N, Lisk GO, Nagwaney S, Lawrence GW, Johnson E, Smith L, Aoki KR, Dolly JO (2003) Evaluation of the therapeutic usefulness of botulinum neurotoxin B, C1, E, and F compared with the long lasting type A. Basis for distinct durations of inhibition of exocytosis in central neurons. J Biol Chem 278:1363-1371.

Forster F, Medalia O, Zauberman N, Baumeister W, Fass D (2005) Retrovirus envelope protein complex structure in situ studied by cryo-electron tomography. Proc Natl Acad Sci U S A 102:4729-4734.

Froehner SC (1991) The submembrane machinery for nicotinic acetylcholine receptor clustering. J Cell Biol 114:1-7.

Galazka A, Gasse F (1995) The present status of tetanus and tetanus vaccination. Curr Top Microbiol Immunol 195:31-53.

Galimi F, Verma IM (2002) Opportunities for the use of lentiviral vectors in human gene therapy. Curr Top Microbiol Immunol 261:245-254.

Ganong (2003) Review of Medical Physiology, 21st Edition.

Geppert M, Goda Y, Hammer RE, Li C, Rosahl TW, Stevens CF, Sudhof TC (1994) Synaptotagmin I: a major Ca2+ sensor for transmitter release at a central synapse. Cell 79:717-727.

Gomez S, Duchen LW, Hornsey S (1982) Effects of x-irradiation on axonal sprouting induced by botulinum toxin. Neuroscience 7:1023-1036.

Gonzalo S, Linder ME (1998) SNAP-25 palmitoylation and plasma membrane targeting require a functional secretory pathway. Molecular Biology of the Cell 9:585-597.

Gonzalo S, Greentree WK, Linder ME (1999) SNAP-25 is targeted to the plasma membrane through a novel membrane-binding domain. Journal of Biological Chemistry 274:21313-21318.

Granseth B, Odermatt B, Royle SJ, Lagnado L (2006) Clathrin-mediated endocytosis is the dominant mechanism of vesicle retrieval at hippocampal synapses. Neuron 51:773-786.

Green NM (1965) A Spectrophotometric Assay for Avidin and Biotin Based on Binding of Dyes by Avidin. Biochem J 94:23C-24C.

Greene EC (1968) The Anatomy of the Rat: Hafner Publishing Company, New York and London.

Habermann E, Erdmann G (1978) Pharmacokinetic and histo-autoradiographic evidence for the intra-axonal movement of toxin in the pathogenesis of tetanus. Toxicon 16:611-623.

Habermann E, Dreyer F, Bigalke H (1980) Tetanus toxin blocks the neuromuscular transmission *in vitro* like botulinum A toxin. Naunyn-Schmiedeberg's Archives of Pharmacology 311:33-40.

Hanson MA, Stevens RC (2000) Cocrystal structure of synaptobrevin-II bound to botulinum neurotoxin type B at 2.0 A resolution. Nat Struct Biol 7:687-

692.

Hanson PI, Jahn R (1997) Mechanistic analysis of SNARE complex disassembly by NSF. Molecular Biology of the Cell 8:1729.

Harlow ML, Ress D, Stoschek A, Marshall RM, McMahan UJ (2001) The architecture of active zone material at the frog's neuromuscular junction. Nature 409:479-484.

Hayashi T, McMahon H, Yamasaki S, Binz T, Hata Y, Südhof TC, Niemann H (1994) Synaptic vesicle membrane fusion complex: Action of clostridial neurotoxins on assembly. EMBO Journal 13:5051-5061.

Hedley SJ, Auf der Maur A, Hohn S, Escher D, Barberis A, Glasgow JN, Douglas JT, Korokhov N, Curiel DT (2006) An adenovirus vector with a chimeric fiber incorporating stabilized single chain antibody achieves targeted gene delivery. Gene Ther 13:88-94.

Hess DT, Slater TM, Wilson MC, Skene JHP (1992) The 25 Kda Synaptosomal-Associated Protein SNAP-25 is the major methionine-rich polypeptide in rapid axonal-transport and a major substrate for palmitoylation in adult CNS. Journal of Neuroscience 12:4634-4641.

Heuser JE, Reese TS (1973) Evidence for recycling of synaptic vesicle membrane during transmitter release at the frog neuromuscular junction. J Cell Biol 57:315-344.

Hughes BW, Kusner LL, Kaminski HJ (2006) Molecular architecture of the neuromuscular junction. Muscle Nerve 33:445-461.

Hurlbut WP, Ceccarelli B (1974) Transmitter release and recycling of synaptic vesicle membrane at the neuromuscular junction. Adv Cytopharmacol 2:141-154.

Inoue K, Fujinaga Y, Watanabe T, Ohyama T, Takeshi K, Moriishi K, Nakajima H, Inoue K, Oguma K (1996) Molecular composition of Clostridium botulinum type A progenitor toxins. Infect Immun 64:1589-1594.

Jahn R, Grubmuller H (2002) Membrane fusion. Curr Opin Cell Biol 14:488-495.

Jahn R, Scheller RH (2006) SNAREs--engines for membrane fusion. Nat Rev Mol Cell Biol 7:631-643.

Jahn R, Lang T, Sudhof TC (2003) Membrane fusion. Cell 112:519-533.

Janz R, Goda Y, Geppert M, Missler M, Sudhof TC (1999) SV2A and SV2B function as redundant Ca2+ regulators in neurotransmitter release. Neuron 24:1003-1016.

Jockusch WJ, Praefcke GJ, McMahon HT, Lagnado L (2005) Clathrin-dependent and clathrin-independent retrieval of synaptic vesicles in retinal bipolar cells. Neuron 46:869-878.

Johnstone SR, Morrice LM, van Heyningen S (1990) The heavy chain of tetanus toxin can mediate the entry of cytotoxic gelonin into intact cells. FEBS Letters 265:101-103.

Jongeneel CV, Bouvier J, Bairoch A (1989) A unique signature identifies a family of zinc-dependent metallopeptidases. FEBS Letters 242:211-214.

Jung HH, Lauterburg T, Burgunder JM (1997) Expression of neurotransmitter genes in rat spinal motoneurons after chemodenervation with botulinum toxin. Neuroscience 78:469-479.

Juzans P, Comella JX, Molgo J, Faille L, Angaut-Petit D (1996) Nerve terminal sprouting in botulinum type-A treated mouse levator auris longus muscle.

Neuromuscul Disord 6:177-185.

Kalandakanond S, Coffield JA (2001) Cleavage of intracellular substrates of botulinum toxins A, C, and D in a mammalian target tissue. J Pharmacol Exp Ther 296:749-755.

Kang Y, Stein CS, Heth JA, Sinn PL, Penisten AK, Staber PD, Ratliff KL, Shen H, Barker CK, Martins I, Sharkey CM, Sanders DA, McCray PB, Jr., Davidson BL (2002) In vivo gene transfer using a nonprimate lentiviral vector pseudotyped with Ross River Virus glycoproteins. J Virol 76:9378-9388.

Kaspar BK, Llado J, Sherkat N, Rothstein JD, Gage FH (2003) Retrograde viral delivery of IGF-1 prolongs survival in a mouse ALS model. Science 301:839-842.

Katz B, Miledi R (1968) The role of calcium in neuromuscular facilitation. J Physiol 195:481-492.

Kay MA, Glorioso JC, Naldini L (2001) Viral vectors for gene therapy: the art of turning infectious agents into vehicles of therapeutics. Nat Med 7:33-40.

Keir SD, Mitchell WJ, Feldman LT, Martin JR (1995) Targeting and gene expression in spinal cord motor neurons following intramuscular inoculation of an HSV-1 vector. J Neurovirol 1:259-267.

Keith RK, Poage RE, Yokoyama CT, Catterall WA, Meriney SD (2007) Bidirectional modulation of transmitter release by calcium channel/syntaxin interactions in vivo. J Neurosci 27:265-269.

Keller JE, Neale EA, Oyler G, Adler M (1999) Persistence of botulinum neurotoxin action in cultured spinal cord cells. FEBS Lett 456:137-142.

Kitamura M, Takamiya K, Aizawa S, Furukawa K (1999) Gangliosides are the binding substances in neural cells for tetanus and botulinum toxins in mice. Biochimica et Biophysica Acta-Molecular and Cell Biology of Lipids 1441:1-3.

Kitamura M, Igimi S, Furukawa K, Furukawa K (2005) Different response of the knockout mice lacking b-series gangliosides against botulinum and tetanus toxins. Biochim Biophys Acta 1741:1-3.

Koenig JH, Ikeda K (1996) Synaptic vesicles have two distinct recycling pathways. J Cell Biol 135:797-808.

Kordower JH, Emborg ME, Bloch J, Ma SY, Chu Y, Leventhal L, McBride J, Chen EY, Palfi S, Roitberg BZ, Brown WD, Holden JE, Pyzalski R, Taylor MD, Carvey P, Ling Z, Trono D, Hantraye P, Deglon N, Aebischer P (2000) Neurodegeneration prevented by lentiviral vector delivery of GDNF in primate models of Parkinson's disease. Science 290:767-773.

Koriazova LK, Montal M (2003) Translocation of botulinum neurotoxin light chain protease through the heavy chain channel. Nat Struct Biol 10:13-18.

Koticha DK, McCarthy EE, Baldini G (2002) Plasma membrane targeting of SNAP-25 increases its local concentration and is necessary for SNARE complex formation and regulated exocytosis. J Cell Sci 115:3341-3351.

Kozlovsky Y, Chernomordik LV, Kozlov MM (2002) Lipid intermediates in membrane fusion: formation, structure, and decay of hemifusion diaphragm. Biophys J 83:2634-2651.

Kurazono H, Mochida S, Binz T, Eisel U, Quanz M, Grebenstein O, Wernars K,

Poulain B, Tauc L, Niemann H (1992) Minimal essential domains specifying toxicity of the light chains of tetanus toxin and botulinum neurotoxin type A. J Biol Chem 267:14721-14729.

Lacy DB, Stevens RC (1999) Sequence homology and structural analysis of the clostridial neurotoxins. Journal of Molecular Biology 291:1091-1104.

Lacy DB, Tepp W, Cohen AC, DasGupta BR, Stevens RC (1998) Crystal structure of botulinum neurotoxin type A and implications for toxicity. Nat Struct Biol 5:898-902.

Lalli G, Schiavo G (2002) Analysis of retrograde transport in motor neurons reveals common endocytic carriers for tetanus toxin and neurotrophin receptor p75NTR. J Cell Biol 156:233-239.

Lalli G, Bohnert S, Deinhardt K, Verastegui C, Schiavo G (2003) The journey of tetanus and botulinum neurotoxins in neurons. Trends Microbiol 11:431-437.

Lalli G, Herreros J, Osborne SL, Montecucco C, Rossetto O, Schiavo G (1999) Functional characterisation of tetanus and botulinum neurotoxins binding domains. Journal of Cell Science 112:2715-2724.

Lambeng N, Gillard M, Vertongen P, Fuks B, Chatelain P (2005) Characterization of [(3)H]ucb 30889 binding to synaptic vesicle protein 2A in the rat spinal cord. Eur J Pharmacol 520:70-76.

Lane SR, Liu YC (1997) Characterization of the palmitoylation domain of SNAP-25. Journal of Neurochemistry 69:1864-1869.

Lauer JM, Dalal S, Marz KE, Nonet ML, Hanson PI (2006) SNARE complex zero layer residues are not critical for N-ethylmaleimide-sensitive factor-mediated disassembly. J Biol Chem 281:14823-14832.

Lawrence G, Wang J, Chion CK, Aoki KR, Dolly JO (2007) Two protein trafficking processes at motor nerve endings unveiled by botulinum neurotoxin e. J Pharmacol Exp Ther 320:410-418.

Lawrence GW, Dolly JO (2002) Ca2+-induced changes in SNAREs and synaptotagmin I correlate with triggered exocytosis from chromaffin cells: insights gleaned into the signal transduction using trypsin and botulinum toxins. J Cell Sci 115:2791-2800.

Lawrence GW, Foran P, Dolly JO (1996) Distinct exocytotic responses of intact and permeabilised chromaffin cells after cleavage of the 25-kDa synaptosomal-associated protein (SNAP-25) or synaptobrevin by botulinum toxin A or B. Eur J Biochem 236:877-886.

Li C, Ullrich B, Zhang JZ, Anderson RGW, Brose N, Sudhof TC (1995) Ca^{2+}-dependent and Ca^{2+}-independent activities of neural and nonneural synaptotagmins. Nature 375:594-599.

Lin RC, Scheller RH (1997) Structural organization of the synaptic exocytosis core complex. Neuron 19:1087-1094.

Lin S, Landmann L, Ruegg MA, Brenner HR (2008) The role of nerve- versus muscle-derived factors in mammalian neuromuscular junction formation. J Neurosci 28:3333-3340.

Linden RM, Berns KI (2000) Molecular biology of adeno-associated viruses. Contrib Microbiol 4:68-84.

Linden RM, Ward P, Giraud C, Winocour E, Berns KI (1996) Site-specific integration by adeno-associated virus. Proc Natl Acad Sci U S A

93:11288-11294.

Littleton JT, Chapman ER, Kreber R, Garment MB, Carlson SD, Ganetzky B (1998) Temperature-sensitive paralytic mutations demonstrate that synaptic exocytosis requires SNARE complex assembly and disassembly. Neuron 21:401-413.

Livett BG (1984) Adrenal-medullary chromaffin cells-*in vitro*. Physiological Reviews 64:1103-1161.

Livett BG, Mitchel-Hill KI, Dean DM, eds (1987) Adrenal chromaffin cells their isolation and culture.

Lonart G (2002) RIM1: an edge for presynaptic plasticity. Trends Neurosci 25:329-332.

Lynch BA, Lambeng N, Nocka K, Kensel-Hammes P, Bajjalieh SM, Matagne A, Fuks B (2004) The synaptic vesicle protein SV2A is the binding site for the antiepileptic drug levetiracetam. Proc Natl Acad Sci U S A 101:9861-9866.

Mahrhold S, Rummel A, Bigalke H, Davletov B, Binz T (2006) The synaptic vesicle protein 2C mediates the uptake of botulinum neurotoxin A into phrenic nerves. FEBS Lett 580:2011-2014.

Mannes AJ, Caudle RM, O'Connell BC, Iadarola MJ (1998) Adenoviral gene transfer to spinal-cord neurons: intrathecal vs. intraparenchymal administration. Brain Res 793:1-6.

Mars T, Yu KJ, Tang XM, Miranda AF, Grubic Z, Cambi F, King MP (2001) Differentiation of glial cells and motor neurons during the formation of neuromuscular junctions in cocultures of rat spinal cord explant and human muscle. J Comp Neurol 438:239-251.

Martinov VN, Sefland I, Walaas SI, Lomo T, Nja A, Hoover F (2002) Targeting functional subtypes of spinal motoneurons and skeletal muscle fibers in vivo by intramuscular injection of adenoviral and adeno-associated viral vectors. Anat Embryol (Berl) 205:215-221.

Marxen P, Erdmann G, Bigalke H (1991) The translocation of botulinum A neurotoxin by chromaffin cells is promoted in low ionic strength solution and is insensitive to trypsin. Toxicon 29:181-189.

Marz KE, Lauer JM, Hanson PI (2003) Defining the SNARE complex binding surface of alpha-SNAP: implications for SNARE complex disassembly. J Biol Chem 278:27000-27008.

Matveeva EA, Vanaman TC, Whiteheart SW, Slevin JT (2008) Levetiracetam prevents kindling-induced asymmetric accumulation of hippocampal 7S SNARE complexes. Epilepsia.

Mazarakis ND, Azzouz M, Rohll JB, Ellard FM, Wilkes FJ, Olsen AL, Carter EE, Barber RD, Baban DF, Kingsman SM, Kingsman AJ, O'Malley K, Mitrophanous KA (2001) Rabies virus glycoprotein pseudotyping of lentiviral vectors enables retrograde axonal transport and access to the nervous system after peripheral delivery. Hum Mol Genet 10:2109-2121.

McConville J, Vincent A (2002) Diseases of the neuromuscular junction. Curr Opin Pharmacol 2:296-301.

McLaughlin SK, Collis P, Hermonat PL, Muzyczka N (1988) Adeno-associated virus general transduction vectors: analysis of proviral structures. J Virol 62:1963-1973.

McMahon HT, Ushkaryov YA, Edelmann L, Link E, Binz T, Niemann H, Jahn R, Südhof TC (1993) Cellubrevin is a ubiquitous tetanus-toxin substrate homologous to a putative synaptic vesicle fusion protein. Nature 364:346-349.

McNew JA, Parlati F, Fukuda R, Johnston RJ, Paz K, Paumet F, Sollner TH, Rothman JE (2000) Compartmental specificity of cellular membrane fusion encoded in SNARE proteins. Nature 407:153-159.

Meinrenken CJ, Borst JG, Sakmann B (2003) Local routes revisited: the space and time dependence of the Ca2+ signal for phasic transmitter release at the rat calyx of Held. J Physiol 547:665-689.

Meldolesi J, Chieregatti E (2004) Fusion has found its calcium sensor. Nat Cell Biol 6:476-478.

Meunier FA, Lisk G, Sesardic D, Dolly JO (2003) Dynamics of motor nerve terminal remodeling unveiled using SNARE-cleaving botulinum toxins: the extent and duration are dictated by the sites of SNAP-25 truncation. Mol Cell Neurosci 22:454-466.

Miller CE, Busath DD, Strongin B, Majewski J (2008) Integration of Ganglioside GT1b Receptor into DPPE and DPPC Phospholipid Monolayers: An X-ray Reflectivity and Grazing Incidence Diffraction Study. Biophys J.

Misura KM, Scheller RH, Weis WI (2000) Three-dimensional structure of the neuronal-Sec1-syntaxin 1a complex. Nature 404:355-362.

Misura KM, Scheller RH, Weis WI (2001) Self-association of the H3 region of syntaxin 1A. Implications for intermediates in SNARE complex assembly. J Biol Chem 276:13273-13282.

Misura KM, Bock JB, Gonzalez LC, Jr., Scheller RH, Weis WI (2002) Three-dimensional structure of the amino-terminal domain of syntaxin 6, a SNAP-25 C homolog. Proc Natl Acad Sci U S A 99:9184-9189.

Montal MS, Blewitt R, Tomich JM, Montal M (1992) Identification of an ion channel-forming motif in the primary structure of tetanus and botulinum neurotoxins. FEBS Lett 313:12-18.

Montecucco C, Schiavo G (1994) Mechanism of action of tetanus and botulinum neurotoxins. Molecular Microbiology 13:1-8.

Moore JP, McKeating JA, Weiss RA, Sattentau QJ (1990) Dissociation of gp120 from HIV-1 virions induced by soluble CD4. Science 250:1139-1142.

Neiman AM (1998) Prospore membrane formation defines a developmentally regulated branch of the secretory pathway in yeast. Journal of Cell Biology 140:29-37.

Nicolopoulos-Stournaras S, Iles JF (1983) Motor neuron columns in the lumbar spinal cord of the rat. J Comp Neurol 217:75-85.

Nishiki T, Tokuyama Y, Kamata Y, Nemoto Y, Yoshida A, Sato K, Sekiguchi M, Takahashi M, Kozaki S (1996) The high-affinity binding of *Clostridium botulinum* type B neurotoxin to synaptotagmin II associated with gangliosides G(T1b)/G(D1a). FEBS Letters 378:253-257.

O'Sullivan GA, Mohammed N, Foran PG, Lawrence GW, Oliver Dolly J (1999) Rescue of exocytosis in botulinum toxin A-poisoned chromaffin cells by expression of cleavage-resistant SNAP-25. Identification of the minimal essential C-terminal residues. J Biol Chem 274:36897-36904.

Ojeda AM, Kolmakova NG, Parsons SM (2004) Acetylcholine binding site in the

vesicular acetylcholine transporter. Biochemistry 43:11163-11174.

Osen-Sand A, Staple JK, Naldi E, Schiavo G, Rossetto O, Petit-Pierre S, Malgaroli A, Montecucco C, Catsicas S (1996) Common and distinct fusion proteins in axonal growth and transmitter release. Journal of Comparative Neurology 367:222-234.

Pahler A, Hendrickson WA, Kolks MA, Argarana CE, Cantor CR (1987) Characterization and crystallization of core streptavidin. J Biol Chem 262:13933-13937.

Park JG, Sill PC, Makiyi EF, Garcia-Sosa AT, Millard CB, Schmidt JJ, Pang YP (2006) Serotype-selective, small-molecule inhibitors of the zinc endopeptidase of botulinum neurotoxin serotype A. Bioorg Med Chem 14:395-408.

Peden CS, Burger C, Muzyczka N, Mandel RJ (2004) Circulating anti-wild-type adeno-associated virus type 2 (AAV2) antibodies inhibit recombinant AAV2 (rAAV2)-mediated, but not rAAV5-mediated, gene transfer in the brain. J Virol 78:6344-6359.

Pellegrini LL, O'Connor V, Lottspeich F, Betz H (1995) Clostridial neurotoxins compromise the stability of a low energy SNARE complex mediating NSF activation of synaptic vesicle fusion. Embo J 14:4705-4713.

Perrais D, Merrifield CJ (2005) Dynamics of endocytic vesicle creation. Dev Cell 9:581-592.

Pestronk A, Drachman DB (1978a) A new stain for quantitative measurement of sprouting at neuromuscular junctions. Muscle Nerve 1:70-74.

Pestronk A, Drachman DB (1978b) Motor nerve sprouting and acetylcholine receptors. Science 199:1223-1225.

Pestronk A, Drachman DB, Griffin JW (1980) Effects of aging on nerve sprouting and regeneration. Exp Neurol 70:65-82.

Pluta K, Luce MJ, Bao L, Agha-Mohammadi S, Reiser J (2005) Tight control of transgene expression by lentivirus vectors containing second-generation tetracycline-responsive promoters. J Gene Med 7:803-817.

Poulain B, Mochida S, Weller U, Hogy B, Wadsworth JDF, Dolly JO, Tauc L (1991) Heterologous combinations of heavy and light chains from botulinum neurotoxin inhibit neurotransmitter release in *Aplysia*. Journal of Biological Chemistry 266:9580-9585.

Poulain B, Wadsworth JD, Shone CC, Mochida S, Lande S, Melling J, Dolly JO, Tauc L (1989) Multiple domains of botulinum neurotoxin contribute to its inhibition of transmitter release in Aplysia neurons. J Biol Chem 264:21928-21933.

Powell JA, Rieger F, Blondet B, Dreyfus P, Pincon-Raymond M (1984) Distribution and quantification of ACh receptors and innervation in diaphragm muscle of normal and mdg mouse embryos. Dev Biol 101:168-180.

Preston DC, Shapiro EB (2005) Electromyography and neuromuscular disorders.

Quetglas S, Iborra C, Sasakawa N, De Haro L, Kumakura K, Sato K, Leveque C, Seagar M (2002) Calmodulin and lipid binding to synaptobrevin regulates calcium-dependent exocytosis. Embo J 21:3970-3979.

Qureshi MH, Wong SL (2002) Design, production, and characterization of a

monomeric streptavidin and its application for affinity purification of biotinylated proteins. Protein Expr Purif 25:409-415.

Qureshi MH, Yeung JC, Wu SC, Wong SL (2001) Development and characterization of a series of soluble tetrameric and monomeric streptavidin muteins with differential biotin binding affinities. J Biol Chem 276:46422-46428.

Ravichandran V, Chawla A, Roche PA (1996) Identification of a novel syntaxin- and synaptobrevin/VAMP-binding protein, SNAP-23, expressed in non-neuronal tissues. Journal of Biological Chemistry 271:13300-13303.

Regazzi R, Sadoul K, Meda P, Kelly RB, Halban PA, Wollheim CB (1996) Mutational analysis of VAMP domains implicated in Ca2+-induced insulin exocytosis. Embo J 15:6951-6959.

Richards DA, Guatimosim C, Rizzoli SO, Betz WJ (2003) Synaptic vesicle pools at the frog neuromuscular junction. Neuron 39:529-541.

Ring RH, Alder J, Fennell M, Kouranova E, Black IB, Thakker-Varia S (2006) Transcriptional profiling of brain-derived-neurotrophic factor-induced neuronal plasticity: a novel role for nociceptin in hippocampal neurite outgrowth. J Neurobiol 66:361-377.

Rizzoli SO, Jahn R (2007) Kiss-and-run, collapse and 'readily retrievable' vesicles. Traffic 8:1137-1144.

Rizzoli SO, Richards DA, Betz WJ (2003) Monitoring synaptic vesicle recycling in frog motor nerve terminals with FM dyes. J Neurocytol 32:539-549.

Rohll JB, Mitrophanous KA, Martin-Rendon E, Ellard FM, Radcliffe PA, Mazarakis ND, Kingsman SM (2002) Design, production, safety, evaluation, and clinical applications of nonprimate lentiviral vectors. Methods Enzymol 346:466-500.

Rossetto O, Gorza L, Schiavo G, Schiavo N, Scheller RH, Montecucco C (1996) VAMP/synaptobrevin isoforms 1 and 2 are widely and differentially expressed in nonneuronal tissues. Journal of Cell Biology 132:167-179.

Ruegg MA, Bixby JL (1998) Agrin orchestrates synaptic differentiation at the vertebrate neuromuscular junction. Trends Neurosci 21:22-27.

Ruitenberg MJ, Eggers R, Boer GJ, Verhaagen J (2002) Adeno-associated viral vectors as agents for gene delivery: application in disorders and trauma of the central nervous system. Methods 28:182-194.

Rummel A, Mahrhold S, Bigalke H, Binz T (2004a) The HCC-domain of botulinum neurotoxins A and B exhibits a singular ganglioside binding site displaying serotype specific carbohydrate interaction. Mol Microbiol 51:631-643.

Rummel A, Karnath T, Henke T, Bigalke H, Binz T (2004b) Synaptotagmins I and II act as nerve cell receptors for botulinum neurotoxin G. J Biol Chem 279:30865-30870.

Rummel A, Eichner T, Weil T, Karnath T, Gutcaits A, Mahrhold S, Sandhoff K, Proia RL, Acharya KR, Bigalke H, Binz T (2007) Identification of the protein receptor binding site of botulinum neurotoxins B and G proves the double-receptor concept. Proc Natl Acad Sci U S A 104:359-364.

Salaun C, James DJ, Greaves J, Chamberlain LH (2004) Plasma membrane targeting of exocytic SNARE proteins. Biochim Biophys Acta 1693:81-89.

Salpeter MM (1999) Neurobiology. The constant junction. Science 286:424-425.

Salpeter MM, Marchaterre M, Harris R (1988) Distribution of extrajunctional acetylcholine receptors on a vertebrate muscle: evaluated by using a scanning electron microscope autoradiographic procedure. J Cell Biol 106:2087-2093.

Salpeter MM, Andreose J, O'Malley JP, Xu R, Fumagalli G, Lomo T (1993) Degradation of acetylcholine receptors at vertebrate neuromuscular junctions. Ann N Y Acad Sci 681:155-164.

Samulski RJ (2000) Expanding the AAV package. Nat Biotechnol 18:497-498.

Sandvig K, van Deurs B (2005) Delivery into cells: lessons learned from plant and bacterial toxins. Gene Ther 12:865-872.

Sanes JR, Lichtman JW (1999) Development of the vertebrate neuromuscular junction. Annu Rev Neurosci 22:389-442.

Sano T, Pandori MW, Chen X, Smith CL, Cantor CR (1995) Recombinant core streptavidins. A minimum-sized core streptavidin has enhanced structural stability and higher accessibility to biotinylated macromolecules. J Biol Chem 270:28204-28209.

Schaffer DV, Koerber JT, Lim KI (2008) Molecular engineering of viral gene delivery vehicles. Annu Rev Biomed Eng 10:169-194.

Schantz EJ, Kautter DA (1978) Microbiological methods: Standardized assay for Clostridium botulinum toxins. AOAC.

Schantz EJ, Johnson EA (1990) Dose standardisation of botulinum toxin. Lancet 335:421.

Schiavo G, Matteoli M, Montecucco C (2000) Neurotoxins affecting neuroexocytosis. Physiological Reviews 80:717-766.

Schiavo G, Rossetto O, Santucci A, DasGupta BR, Montecucco C (1992a) Botulinum neurotoxins are zinc proteins. J Biol Chem 267:23479-23483.

Schiavo G, Poulain B, Benfenati F, DasGupta BR, Montecucco C (1993a) Novel targets and catalytic activities of bacterial protein toxins. Trends Microbiol 1:170-174.

Schiavo G, Shone CC, Rossetto O, Alexander FC, Montecucco C (1993b) Botulinum neurotoxin serotype F is a zinc endopeptidase specific for VAMP/synaptobrevin. J Biol Chem 268:11516-11519.

Schiavo G, Shone CC, Bennett MK, Scheller RH, Montecucco CM (1995) Botulinum neurotoxin type C cleaves a single Lys-Ala bond within the carboxyl-terminal region of syntaxins. Journal of Biological Chemistry 270:10566-10570.

Schiavo G, Poulain B, Rossetto O, Benfenati F, Tauc L, Montecucco C (1992b) Tetanus toxin is a zinc protein and its inhibition of neurotransmitter release and protease activity depend on zinc. Embo J 11:3577-3583.

Schiavo G, Benfenati F, Poulain B, Rossetto O, Polverino de Laureto P, DasGupta BR, Montecucco C (1992c) Tetanus and botulinum-B neurotoxins block neurotransmitter release by proteolytic cleavage of synaptobrevin. Nature 359:832-835.

Schiavo G, Rossetto O, Catsicas S, Polverino de Laureto P, DasGupta BR, Benfenati F, Montecucco C (1993c) Identification of the nerve terminal targets of botulinum neurotoxin serotypes A, D, and E. J Biol Chem 268:23784-23787.

Schiavo G, Santucci A, Dasgupta BR, Mehta PP, Jontes J, Benfenati F, Wilson

MC, Montecucco C (1993d) Botulinum neurotoxins serotypes A and E cleave SNAP-25 at distinct COOH-terminal peptide bonds. FEBS Lett 335:99-103.

Schmid MF, Robinson JP, DasGupta BR (1993) Direct visualization of botulinum neurotoxin-induced channels in phospholipid vesicles. Nature 364:827-830.

Schmidt JJ, Bostian KA (1995) Proteolysis of synthetic peptides by type A botulinum neurotoxin. J Protein Chem 14:703-708.

Schmidt JJ, Bostian KA (1997) Endoproteinase activity of type A botulinum neurotoxin: substrate requirements and activation by serum albumin. J Protein Chem 16:19-26.

Schmidt JJ, Stafford RG (2005) Botulinum neurotoxin serotype F: identification of substrate recognition requirements and development of inhibitors with low nanomolar affinity. Biochemistry 44:4067-4073.

Schmidt JJ, Stafford RG, Bostian KA (1998) Type A botulinum neurotoxin proteolytic activity: development of competitive inhibitors and implications for substrate specificity at the S1' binding subsite. FEBS Lett 435:61-64.

Schmiedl A, Breitling F, Winter CH, Queitsch I, Dubel S (2000) Effects of unpaired cysteines on yield, solubility and activity of different recombinant antibody constructs expressed in E. coli. J Immunol Methods 242:101-114.

Schneggenburger R, Neher E (2000) Intracellular calcium dependence of transmitter release rates at a fast central synapse. Nature 406:889-893.

Schoch S, Gundelfinger ED (2006) Molecular organization of the presynaptic active zone. Cell Tissue Res 326:379-391.

Schoch S, Deak F, Konigstorfer A, Mozhayeva M, Sara Y, Sudhof TC, Kavalali ET (2001) SNARE function analyzed in synaptobrevin/VAMP knockout mice. Science 294:1117-1122.

Shapiro RL, Hatheway C, Swerdlow DL (1998) Botulism in the United States: a clinical and epidemiologic review. Ann Intern Med 129:221-228.

Sheng ZH, Yokoyama CT, Catterall WA (1997) Interaction of the synprint site of N-type Ca^{2+} channels with the C2B domain of synaptotagmin I. Proceedings of the National Academy of Sciences of the United States of America 94:5405-5410.

Shone CC, Roberts AK (1994) Peptide substrate specificity and properties of the zinc-endopeptidase activity of botulinum type B neurotoxin. Eur J Biochem 225:263-270.

Shone CC, Tranter HS (1995) Growth of clostridia and preparation of their neurotoxins. Curr Top Microbiol Immunol 195:143-160.

Shyng SL, Salpeter MM (1989) Degradation rate of acetylcholine receptors inserted into denervated vertebrate neuromuscular junctions. J Cell Biol 108:647-651.

Sieburth D, Ch'ng Q, Dybbs M, Tavazoie M, Kennedy S, Wang D, Dupuy D, Rual JF, Hill DE, Vidal M, Ruvkun G, Kaplan JM (2005) Systematic analysis of genes required for synapse structure and function. Nature 436:510-517.

Simpson LL (1982) The interaction between aminoquinolines and presynaptically acting neurotoxins. J Pharmacol Exp Ther 222:43-48.

Simpson LL (1983) Ammonium chloride and methylamine hydrochloride antagonize clostridial neurotoxins. J Pharmacol Exp Ther 225:546-552.

Simpson LL (2004) Identification of the major steps in botulinum toxin action. Annu Rev Pharmacol Toxicol 44:167-193.

Simpson LL, Rapport MM (1971) Ganglioside inactivation of botulinum toxin. J Neurochem 18:1341-1343.

Sloop RR, Cole BA, Escutin RO (1997) Human response to botulinum toxin injection: type B compared with type A. Neurology 49:189-194.

Sobel J (2005) Botulism. Clin Infect Dis 41:1167-1173.

Sobel J, Tucker N, Sulka A, McLaughlin J, Maslanka S (2004) Foodborne botulism in the United States, 1990-2000. Emerg Infect Dis 10:1606-1611.

Sollner T, Whiteheart SW, Brunner M, Erdjument-Bromage H, Geromanos S, Tempst P, Rothman JE (1993) SNAP receptors implicated in vesicle targeting and fusion. Nature 362:318-324.

Söllner T, Bennett MK, Whiteheart SW, Scheller RH, Rothman JE (1993) A protein assembly-disassembly pathway *in vitro* that may correspond to sequential steps of synaptic vesicle docking, activation, and fusion. Cell 75:409-418.

Son YJ, Thompson WJ (1995) Nerve sprouting in muscle is induced and guided by processes extended by Schwann cells. Neuron 14:133-141.

Son YJ, Trachtenberg JT, Thompson WJ (1996) Schwann-cells induce and guide sprouting and reinnervation of neuromuscular-junctions. Trends in Neurosciences 19:280-285.

Squire, Bloom, McConnell, Roberts, Spitzer, Zigmond (2003) Fundamental Neuroscience.

Steegmaier M, Yang B, Yoo J-S, Huang B, Shen M, Yu S, Luo Y, Scheller RH (1998) Three novel proteins of the syntaxin/SNAP-25 family. Journal of Biological Chemistry 273:34171–34179.

Steffens S, Tebbets J, Kramm CM, Lindemann D, Flake A, Sena-Esteves M (2004) Transduction of human glial and neuronal tumor cells with different lentivirus vector pseudotypes. J Neurooncol 70:281-288.

Stein CS, Martins I, Davidson BL (2005) The lymphocytic choriomeningitis virus envelope glycoprotein targets lentiviral gene transfer vector to neural progenitors in the murine brain. Mol Ther 11:382-389.

Stenmark P, Dupuy J, Imamura A, Kiso M, Stevens RC (2008) Crystal structure of botulinum neurotoxin type A in complex with the cell surface co-receptor GT1b-insight into the toxin-neuron interaction. PLoS Pathog 4:e1000129.

Stevens CF, Sullivan JM (2003) The synaptotagmin C2A domain is part of the calcium sensor controlling fast synaptic transmission. Neuron 39:299-308.

Stoeckel K, Schwab M, Thoenen H (1977) Role of gangliosides in the uptake and retrograde axonal transport of cholera and tetanus toxin as compared to Nerve Growth Factor and wheat germ agglutinin. Brain Research 132:273-285.

Sudhof TC (2000) The synaptic vesicle cycle revisited. Neuron 28:317-320.

Sudhof TC (2004) The synaptic vesicle cycle. Annu Rev Neurosci 27:509-547.

Sudhof TC, De Camilli P, Niemann H, Jahn R (1993) Membrane-fusion machinery - insights from synaptic proteins. Cell 75:1-4.

Sutton RB, Fasshauer D, Jahn R, Brunger AT (1998) Crystal structure of a SNARE complex involved in synaptic exocytosis at 2.4 A resolution. Nature 395:347-353.

Swaminathan S, Eswaramoorthy S (2000) Structural analysis of the catalytic and binding sites of Clostridium botulinum neurotoxin B. Nat Struct Biol 7:693-699.

Tacket CO, Shandera WX, Mann JM, Hargrett NT, Blake PA (1984) Equine antitoxin use and other factors that predict outcome in type A foodborne botulism. Am J Med 76:794-798.

Takamori S, Holt M, Stenius K, Lemke EA, Gronborg M, Riedel D, Urlaub H, Schenck S, Brugger B, Ringler P, Muller SA, Rammner B, Grater F, Hub JS, De Groot BL, Mieskes G, Moriyama Y, Klingauf J, Grubmuller H, Heuser J, Wieland F, Jahn R (2006) Molecular anatomy of a trafficking organelle. Cell 127:831-846.

Tam SL, Gordon T (2003) Mechanisms controlling axonal sprouting at the neuromuscular junction. J Neurocytol 32:961-974.

Teng FY, Wang Y, Tang BL (2001) The syntaxins. Genome Biol 2:REVIEWS3012.

Thakker-Varia S, Alder J, Crozier RA, Plummer MR, Black IB (2001) Rab3A is required for brain-derived neurotrophic factor-induced synaptic plasticity: transcriptional analysis at the population and single-cell levels. J Neurosci 21:6782-6790.

Toonen RF, Verhage M (2007) Munc18-1 in secretion: lonely Munc joins SNARE team and takes control. Trends Neurosci 30:564-572.

Tsukamoto K, Kohda T, Mukamoto M, Takeuchi K, Ihara H, Saito M, Kozaki S (2005) Binding of Clostridium botulinum type C and D neurotoxins to ganglioside and phospholipid. Novel insights into the receptor for clostridial neurotoxins. J Biol Chem 280:35164-35171.

Tsukamoto K, Kozai Y, Ihara H, Kohda T, Mukamoto M, Tsuji T, Kozaki S (2008) Identification of the receptor-binding sites in the carboxyl-terminal half of the heavy chain of botulinum neurotoxin types C and D. Microb Pathog 44:484-493.

Ullian EM, Harris BT, Wu A, Chan JR, Barres BA (2004) Schwann cells and astrocytes induce synapse formation by spinal motor neurons in culture. Mol Cell Neurosci 25:241-251.

Ullrich B, Li C, Zhang JZ, McMahon H, Anderson RG, Geppert M, Sudhof TC (1994) Functional properties of multiple synaptotagmins in brain. Neuron 13:1281-1291.

Ungermann C, Wickner W (1998) Vam7p, a vacuolar SNAP-25 homolog, is required for SNARE complex integrity and vacuole docking and fusion. EMBO Journal 17:3269-3276.

Union E Monograph on Botulinum toxin preparations. In: The European pharmacopoeia 5th Edition.

Unwin N (2005) Refined structure of the nicotinic acetylcholine receptor at 4A resolution. J Mol Biol 346:967-989.

Vaidyanathan VV, Puri N, Roche PA (2001) The last exon of SNAP-23

regulates granule exocytosis from mast cells. J Biol Chem 276:25101-25106.

Vaidyanathan VV, Yoshino K, Jahnz M, Dorries C, Bade S, Nauenburg S, Niemann H, Binz T (1999) Proteolysis of SNAP-25 isoforms by botulinum neurotoxin types A, C, and E: domains and amino acid residues controlling the formation of enzyme-substrate complexes and cleavage. J Neurochem 72:327-337.

Veit M, Sollner TH, Rothman JE (1996) Multiple palmitoylation of synaptotagmin and the t-SNARE SNAP-25. FEBS Letters 385:119-123.

Verderio C, Rossetto O, Grumelli C, Frassoni C, Montecucco C, Matteoli M (2006) Entering neurons: botulinum toxins and synaptic vesicle recycling. EMBO Rep 7:995-999.

Verdu E, Ceballos D, Vilches JJ, Navarro X (2000) Influence of aging on peripheral nerve function and regeneration. J Peripher Nerv Syst 5:191-208.

Verhage M, Maia AS, Plomp JJ, Brussaard AB, Heeroma JH, Vermeer H, Toonen RF, Hammer RE, van den Berg TK, Missler M, Geuze HJ, Sudhof TC (2000) Synaptic assembly of the brain in the absence of neurotransmitter secretion. Science 287:864-869.

Vigna E, Naldini L (2000) Lentiviral vectors: excellent tools for experimental gene transfer and promising candidates for gene therapy. J Gene Med 2:308-316.

Volchuk A, Mitsumoto Y, He LJ, Liu Z, Habermann E, Trimble W, Klip A (1994) Expression of Vesicle Associated Membrane Protein 2 (VAMP-2) synaptobrevin II and cellubrevin in rat skeletal muscle and in a muscle cell line. Biochemical Journal 304:139-145.

von Euler US, Floding I (1959) A fluorometric micromethod for differential estimation of adrenaline and noradrenaline. Acta Physiology Scandinavia Supplement 118:45-56.

Wang P, Yang G, Mosier DR, Chang P, Zaidi T, Gong YD, Zhao NM, Dominguez B, Lee KF, Gan WB, Zheng H (2005) Defective neuromuscular synapses in mice lacking amyloid precursor protein (APP) and APP-Like protein 2. J Neurosci 25:1219-1225.

Wang Y, Tang BL (2006) SNAREs in neurons--beyond synaptic vesicle exocytosis (Review). Mol Membr Biol 23:377-384.

Washbourne P, Cansino V, Mathews JR, Graham M, Burgoyne RD, Wilson MC (2001) Cysteine residues of SNAP-25 are required for SNARE disassembly and exocytosis, but not for membrane targeting. Biochem J 357:625-634.

Washbourne P, Thompson PM, Carta M, Costa ET, Mathews JR, Lopez-Bendito G, Molnar Z, Becher MW, Valenzuela CF, Partridge LD, Wilson MC (2002) Genetic ablation of the t-SNARE SNAP-25 distinguishes mechanisms of neuroexocytosis. Nat Neurosci 5:19-26.

Weber T, Zemelman BV, McNew JA, Westermann B, Gmachl M, Parlati F, Söllner T, Rothman JE (1998) SNAREpins: minimal machinery for membrane fusion. Cell 92:759-772.

Weihe E, Tao-Cheng JH, Schafer MK, Erickson JD, Eiden LE (1996) Visualization of the vesicular acetylcholine transporter in cholinergic

nerve terminals and its targeting to a specific population of small synaptic vesicles. Proc Natl Acad Sci U S A 93:3547-3552.

Weller U, Dauzenroth ME, Gansel M, Dreyer F (1991) Cooperative action of the light chain of tetanus toxin and the heavy chain of botulinum toxin type A on the transmitter release of mammalian motor endplates. Neuroscience Letters 122:132-134.

WHO (2002) Botulism. In: Fact sheet N°270 (centre WM, ed), p Fact sheet N°270: World Health Organisation.

Wilson DW, Wilcox CA, Flynn GC, Chen E, Kuang WJ, Henzel WJ, Block MR, Ullrich A, Rothman JE (1989) A fusion protein required for vesicle-mediated transport in both mammalian cells and yeast. Nature 339:355-359.

Wojcik SM, Brose N (2007) Regulation of membrane fusion in synaptic excitation-secretion coupling: speed and accuracy matter. Neuron 55:11-24.

Wong LF, Azzouz M, Walmsley LE, Askham Z, Wilkes FJ, Mitrophanous KA, Kingsman SM, Mazarakis ND (2004) Transduction patterns of pseudotyped lentiviral vectors in the nervous system. Mol Ther 9:101-111.

Wright MC, Son YJ (2007) Ciliary neurotrophic factor is not required for terminal sprouting and compensatory reinnervation of neuromuscular synapses: re-evaluation of CNTF null mice. Exp Neurol 205:437-448.

Wu SC, Wong SL (2005) Engineering soluble monomeric streptavidin with reversible biotin binding capability. J Biol Chem 280:23225-23231.

Xie Q, Bu W, Bhatia S, Hare J, Somasundaram T, Azzi A, Chapman MS (2002) The atomic structure of adeno-associated virus (AAV-2), a vector for human gene therapy. Proc Natl Acad Sci U S A 99:10405-10410.

Xu T, Bajjalieh SM (2001) SV2 modulates the size of the readily releasable pool of secretory vesicles. Nat Cell Biol 3:691-698.

Yoshihara M, Montana ES (2004) The synaptotagmins: calcium sensors for vesicular trafficking. Neuroscientist 10:566-574.

Zhang B (2003) Genetic and molecular analysis of synaptic vesicle recycling in Drosophila. J Neurocytol 32:567-589.

Zhou LQ, de Paiva A, Liu D, Aoki R, Dolly JO (1995) Expression and purification of the light chain of botulinum neurotoxin A: A single mutation abolishes its cleavage of SNAP-25 and neurotoxicity after reconstitution with the heavy chain. Biochemistry 34:15175-15181.

Zolotukhin S, Byrne BJ, Mason E, Zolotukhin I, Potter M, Chesnut K, Summerford C, Samulski RJ, Muzyczka N (1999) Recombinant adeno-associated virus purification using novel methods improves infectious titer and yield. Gene Ther 6:973-985.

Zufferey R, Dull T, Mandel RJ, Bukovsky A, Quiroz D, Naldini L, Trono D (1998) Self-inactivating lentivirus vector for safe and efficient in vivo gene delivery. J Virol 72:9873-9880.

Appendix 1

Buffers and Solutions:

Locke's buffer: 154 mM NaCl; 2.55 mM KCl; 2.13 mM $K_2HPO_4.2H_2O$; 0.88 mM $KH_2PO_4.2H_2O$; 10 mM glucose; 15 mM HEPES pH 7.4; 1x Antibiotic/Antimycotic mix from Invitrogen

Phosphate buffered Saline (PBS): 0.17 mM $NaH_2PO_4.2H_2O$, 1.76 mM Na_2HPO_4, 150 mM NaCl, 2.6 mM KCl

Chromaffin growth medium: DMEM with 2 mM L-glutamine; 2 mM Na pyruvate; 25 mM HEPES pH7.4; 1x Antibiotic/Antimycotic mix from Invitrogen; 10 µM cytosine arabinofurinoside; 8 µM fluorodeoxyuridine; 10 µM dibutyryl cAMP; 5 µM dexamethasone-2-1 phosphate; 50 µg / ml sodium ascorbate; 10% (v/v) heat-inactivated FCS

Low ionic strength media (LISM): 5 mM NaCl; 4.8 mM KCl; 2.2 mM $CaCl_2.2H_2O$; 1.2 mM KH_2PO_4; 1.2 mM $MgSO_4$; 5.6 mM glucose; 220 mM sucrose; 0.5% (w/v) BSA; 20 mM HEPES pH 7.4; 1x Antibiotic/Antimycotic mix from Invitrogen

Laemlli gel loading buffer: 8% SDS; 20% glycerol; 0.012% (w/v) bromophenol blue; 4% 2-mercaptoethanol; 0.5 M Tris HCl; pH 6.8

Western transfer buffer: 25 mM Tris HCl; 192 mM glycine

Tris buffered saline (TBS): 150 mM NaCl; 25 mM Tris-HCl pH 7.0

KGH media for permeabilisation: 140mM Potassium glutamate; 1mM $MgCl_2$; 6mM Glucose; 20mM HEPES; pH 7.2

Pre-Scission buffer: 50mM Tris-HCl; 150mM NaCl; 1mM EDTA; 1mM DTT; pH 7.0

Cerebellar mix: 40mM HEPES-NaOH; 20mM NaCl; 80mM KCl; 3.7mM d-Glucose; 2.8mM $CaCl_2.2H_2O$; 1.6mM $MgSO_4$; 1mM $NaH_2PO_4.2H_2O$; pH 7.4

HEPES basal buffer for glutamate release (HBB): 40mM HEPES; 240mM NaCl; 10mM KCl; 4mM $MgCL_2.6H_2O$; 2.5mM $CaCl_2.2H_2O$; 10mM d-Glucose; pH 7.4; 300-310mOSM

HEPES stimulation buffer for glutamate release (HSB): 40mM HEPES; 110mM NaCl; 140mM KCl; 4mM $MgCL_2.6H_2O$; 2.5mM $CaCl_2.2H_2O$; 10mM d-Glucose; pH

7.4; 300-310mOSM

Partial cerebellar growth media (PCGM): 375 ml Basal Media Eagle (Sigma); 125ml cerebellar mix; 5ml N2 supplement (Invitrogen); 5ml 100xAntibiotic/Antimycotic solution (Invitrogen); 10ml dialysed Horse serum; 5ml Glutamax (Invitrogen)

Complete cerebellar growth media (CCGM): PCGM with 40 µM Ara-C (Cytosine β-D-arabinofuranoside)

Western stripping buffer: 4.9g Tris-HCl (pH 6.7); 3.52ml 2-β-mercaptoethanol; 10g SDS; Make upto 500ml with dH_2O

TBS/Tween: 50mM Tris; 138mM NaCl; 2.7mM KCl; 0.05% Tween-20

Protease buffer: 20mM Hepes; 100mM NaCl; 10µM $ZnSO_4$

PCR master mix 2x: 10µl NEB Taq polymerase; 10µl 25mM dNTP mix; 100µl NEB PCR buffer; 50µl 50mM $MgCl_2$; 330µl dH_2O

SDS for colony blot: 100g SDS in 1000ml dH_2O

Denaturing buffer for colony blot: 500mM NaOH; 1.5M NaCl

Neutralisation buffer for colony blot: 1.5M NaCl; 500mM Tris-HCl; pH 7.4

20xSSC for colony blot: 87.65g NaCl; 50.25g TriSodium.Citrate.$2H_2O$; 500ml dH_2O

2xHBS for transfection: 50mM HEPES; 280mM NaCl; 1.5mM Na_2HPO_4

$CaCl_2$ for transfection: 300mM $CaCl_2$.$2H_2O$

1X PBS for transfection: NaCl 8.05g; KCl 0.195g; Na_2HPO_4 1.42g; KH_2PO_4 0.245g; 1000ml dH_2O; pH 7.4

10xTE: 100 mM Tris pH 7.5; 10 mM EDTA pH 8.0

10x TAE: 400 mM Tris-acetate; 10 mM EDTA

HEPES-NaCl buffer: 50mM HEPES; 150mM NaCl

Appendix 2 – Published material

Brief Communications

Adeno-Associated Virus Transfer of a Gene Encoding SNAP-25 Resistant to Botulinum Toxin A Attenuates Neuromuscular Paralysis Associated with Botulism

Arvind Raghunath,[1] **Francesc Perez-Branguli,**[1] **Leonard Smith,**[2] **and J. Oliver Dolly**[1]

[1]International Centre for Neurotherapeutics, Dublin City University, Dublin 9, Ireland, and [2]Integrated Toxicology Division, United States Army Medical Research Institute of Infectious Diseases, Fort Detrick, Maryland 21702-5011

Advances in viral gene therapy have opened new possibilities for treating a range of motor neuron diseases, but these have not yet been translated into clinically applicable therapies because of difficulties in delivery to susceptible/damaged neurons, ambiguities in the identity of gene(s) implicated, and a paucity of means to quantify any physiological improvement. Most of these hurdles can be overcome by using the neuromuscular paralysis induced by botulinum neurotoxin type A (BoNT/A) as a prototype disease. Furthermore, because human botulism, occasionally fatal, causes prolonged muscle disablement as a result of the intraneuronal persistence of the toxin's SNAP-25 (S25)-cleaving protease, development of a genetic approach could lead to a potential treatment for this debilitating disease. Adeno-associated viral delivery of a cleavage-resistant S25 gene (S25-R198T) to chromaffin cells *in vitro* yielded exocytotically active S25-R198T that diminished subsequent blockade by BoNT/A of evoked catecholamine release. Evaluation *in vivo*, by administering this virus into rat spinal cord before injecting BoNT/A, showed a decreased inhibition of acetylcholine release as reflected in elevated retention of neuromuscular transmission. A similar, although smaller, protection of synaptic transmission from the toxin was seen after peripherally injecting the therapeutic virus. Such therapy also curtailed nerve sprouting normally induced by BoNT/A. This first demonstration of the utility of a DNA-based therapy for botulism paves the way for further advances in its treatment and for application to genetic disorders of motor neurons.

Key words: botulinum; gene transfer; neuromuscular junction; motor neuron; SNARE proteins; sprouting

Introduction

A major challenge facing gene therapy for motor neuron disorders, a group of rare yet debilitating and ultimately fatal diseases affecting spinal motor neurons, is targeted, minimally traumatic delivery. Because of the limited number of motor neurons (e.g., rat sciatic nerve has only ~2000 efferents) (Nicolopoulos-Stournaras and Iles, 1983), insults that are merely sublethal in other cells can be extremely deleterious [e.g., in superoxide-dismutase mutant mice, which ubiquitously express the damaged protein, motor neurons are the most affected (Bruijn et al., 2004)]. Their anatomical structure, with a relatively inaccessible cell body in the spinal column and an elongated axon, complicates therapies including gene transfer by viral vectors. Those that transfect motor neurons [adeno-associated virus (AAV), lentivirus, and herpes virus] do so most efficiently when in direct contact with the cell body (Mannes et al., 1998). Because intraspinal injection is difficult under clinical conditions, the use of periph-

erally deliverable vectors would be desirable; moreover, such an advance requires a model that allows accurate measurement of the graded improvements currently achievable.

An ideal system to evaluate such therapies is the blockade of neuromuscular transmission by botulinum neurotoxin type A (BoNT/A). Its light chain Zn^{2+}-dependent endoprotease causes irreversible blockade of acetylcholine (ACh) exocytosis by specific cleavage of SNAP-25 (S25), a protein essential for this fundamental process (Blasi et al., 1994). Importantly, protection from inhibition by BoNT/A can be achieved by expression of a toxin-resistant S25 mutant gene (O'Sullivan et al., 1999). Furthermore, because current treatments are ineffective in combating botulism, it is imperative that a refined therapy is designed with the ability to abrogate the prolonged convalescence and high mortality and morbidity associated with this condition.

Herein, sustained neuromuscular paralysis by BoNT/A was attenuated using AAV vectors that give long-term expression of a cleavage-resistant S25 mutant (S25-R198T), having all the properties of the wild type, including ability to substitute for truncated S25 and recover exocytosis in intoxicated chromaffin cells (O'Sullivan et al., 1999). AAV vectors provide an efficient and relatively safe way to ensure prolonged expression of genes in neurons (Burger et al., 2005), and botulism in rats provides a much more valid model for evaluating this gene therapy. Injection of AAVs encoding S25-R198T into the spinal anterior horn

innervating the soleus muscle protected neuromuscular transmission from subsequent inhibition by BoNT/A. Moreover, muscles treated in this way showed a decreased amount of nerve sprouting compared with unprotected controls. Finally, administering the therapeutic AAVs directly into the soleus muscle resulted in their retrograde transport to motor cell bodies and a consequential reduction of BoNT/A-mediated blockade of neurotransmission at peripheral synapses. These findings provide the first evidence for the potential applicability of gene therapy to the intractable problems posed by botulism and, possibly in the longer-term, genetic disorders of motor neurons.

Materials and Methods

Construction, production, and purification of recombinant AAVs expressing BoNT-resistant S25. PCR, using the S25BamH1His$_6$-For and S25XhoI-Rev primer pair, generated a His$_6$-tagged S25 from a mouse S25 gene; this was inserted into the pAAV-MCS plasmid to generate the pAAV-His$_6$-S25 plasmid [~96% homologous to human S25 (for primer sequences, see supplemental material, available at www.jneurosci.org)]. A similar technique, with the substitution of S25RTXhoI-Rev for S25XhoI-Rev, created pAAV-His$_6$-S25-R198T encoding a BoNT/A-resistant S25. These different plasmids, along with AAV-hrGFP, were used to create their respective replication-deficient AAVs and purified on heparin-agarose, as described previously (Zolotukhin et al., 1999). Viral (protein) yield and purity were assessed on Coomassie-stained SDS-PAGE gels by comparing the surface proteins (VP1, VP2, and VP3) to a bovine serum albumin (BSA) standard. Real-time quantitative PCR, with appropriate primers, quantified the number of genomic copies (GCs) per preparation, and a dilution series applied to HEK-293 cells yielded the number of transducing units.

Culture of chromaffin cells, infection with recombinant AAVs, intoxication with BoNT/A, and assay of catecholamine release. Bovine adrenal chromaffin cells were isolated as described previously (Lawrence et al., 1996), infected with AAVs, and 7 d later exposed for 24 h to 10 nM BoNT/A under conditions that promote its uptake. Ba^{2+}-evoked catecholamine release was measured after different viral treatments and normalized to that in the presence of the toxin alone and presented as mean ± SD ($n = 4$), from two or more sets of experiments. t tests were used to determine the statistical significance.

Stereotaxic intraspinal administration of AAVs for transfection of anterior horn neurons supplying the soleus muscle. Rats were anesthetized with medetomidine/fentanyl citrate, and the T10-L2 vertebrae were exposed and positioned in a stereotaxic frame using spinal adapters (Stoelting, Wood Dale, IL). After careful penetration of the vertebral lamina over the T13 spinal level using a microdrill, known quantities of the virus were injected over 5 min with a Hamilton microsyringe attached to a 30 ga beveled needle. After a further 5 min, the needle was withdrawn and the procedure repeated at L1 and L2 levels; twitching of the lower limb muscles confirmed the accurate placement of the needle. The paraspinal muscles and the superficial fascia, reinforced with a polypropylene mesh, were sutured with vicryl sutures, and the skin was closed with Prolene sutures before injection of atipamazole/nalbuphine and carprofen/bupivacaine.

In situ recording of neuromuscular transmission after BoNT/A administration. Three weeks after the intraspinal injection, ~1 mouse LD$_{50}$ of BoNT/A in 10 µl of normal saline (NS)/BSA was injected into the soleus muscle. After a 16–25 d recovery, the rats were anesthetized, and the soleal contribution to the Achilles tendon was isolated and ligated to a sensitive force transducer (FORT10 and PowerLab 4/20T; ADInstruments, Castle Hill, New South Wales, Australia). The sciatic nerve, exposed at midthigh level, and the belly of the soleus muscle were stimulated at 1 Hz/200 mV/0.2 ms and 1 Hz/5 V/2 ms, respectively; 60 Hz stimulation provided the response at tetanic frequencies.

Immunohistochemical detection of S25, His$_6$-S25, His$_6$-S25-R198T, and GFP expression. Serial 25 µm muscle and spinal cord sections were permeabilized before exposure to the primary antibody (1:50 for anti-NF200 and anti-His$_6$) diluted in PBS with 0.05% Tween 20/1% BSA/2% goat serum and, after washing, to the relevant secondary antibodies (1:50

Alexa-488 or 1:100 A546/phycoerythrin-labeled goat anti-mouse) with or without 1:500 fluorescently tagged α-bungarotoxin (α-BuTx; with Alexa 488 or rhodamine). These were visualized with an Olympus (Tokyo, Japan) IX51 inverted fluorescent microscope or, when appropriate, a Zeiss (Thornwood, NY) confocal microscope (LSM510).

Determination of the distribution of ACh receptors at neuromuscular junctions using fluorophore-conjugated α-BuTx. Random soleal sections from rats injected with BoNT/A alone, AAV-His$_6$-S25-R198T, and then BoNT/A and untreated controls were stained with an α-BuTx–Alexa-488 conjugate; for determination of muscle parameters, see supplemental material (available at www.jneurosci.org). Staining with anti-NF200 and fluorescently tagged α-BuTx allowed visual monitoring of sprouting at neuromuscular junctions (NMJs) protected by viral-mediated production of BoNT/A-resistant S25.

Results

Protection of stimulated exocytosis from BoNT/A-induced blockade by prior expression of His$_6$-S25-R198T, but not wild-type S25, in chromaffin cells

AAV helper-free vector system based on a nonpathogenic parvovirus was used to construct recombinant type-2 AAVs incorporating different genes. Initially, control viruses expressing the hrGFP marker protein were produced; heparin affinity chromatography yielded pure viruses containing only viral surface proteins (Fig. 1*A*,*B*). Their activity was established from expression of hrGFP fluorescence in infected chromaffin cells (Fig. 1*C*). Later, wild-type or mutated S25, engineered to be nonsusceptible to cleavage by BoNT/A, were introduced into this vector. In some cases, the proteins were coexpressed with an hrGFP marker using an IRES segment (AAV-His$_6$-S25-R198T-IRES-hrGFP); coexpression was demonstrated by immunodetection of His$_6$, S25, and hrGFP in lysed cells (Fig. 1*D*).

Their protective abilities were demonstrated in chromaffin cells exposed for 7 d to various concentrations of the recombinant viruses before challenge with 10 nM BoNT/A (the 150 kDa neurotoxin free of accessory proteins was used throughout). AAV-His$_6$-S25-R198T viruses gave a dose-dependent relative increase in exocytosis of ~55% compared with the level recorded for cells treated with toxin alone (Fig. 1*E*). The highest concentration of viral particles tested, equivalent to a multiplicity of infection = 50, infected ~90% of the cells. The AAV-His$_6$-S25-R198T-IRES-hrGFP virus yielded a lower, yet significant, relative protection (~23%), whereas overexpression of wild-type S25 failed to show any effect (Fig. 1*E*). This extent of prophylaxis, despite using large numbers (>10^6 cells per well) of postmitotic neuroendocrine cells, justified progression to *in vivo* testing of this gene therapy paradigm. Moreover, infection of chromaffin cells with viral particles expressing toxin-resistant, but not wild-type, S25 gave appreciable rescue of evoked catecholamine exocytosis that had been inhibited by preexposure to BoNT/A (see supplemental material, available at www.jneurosci.org).

Efficient expression of cleavage-resistant S25 in peripheral nerve terminals of rats after intraspinal administration of AAVs protects against the neuroparalytic effects of BoNT/A

Published data (Adler et al., 2001) determined the choice of rat soleus muscle as an *in vivo* system to study the effects of viral vector-induced BoNT prophylaxis. The efficiency of neuromuscular transmission (ENT; the ratio of the force of contraction elicited by nerve stimulation to that elicited by direct muscle stimulation) provides an accurate and sensitive means to determine the progress of, and recovery from, toxin-induced paralysis. Stereotaxic injection of AAVs expressing marker hrGFP and/or His$_6$-S25-R198T into the right anterior T12, L1, and L3 spinal
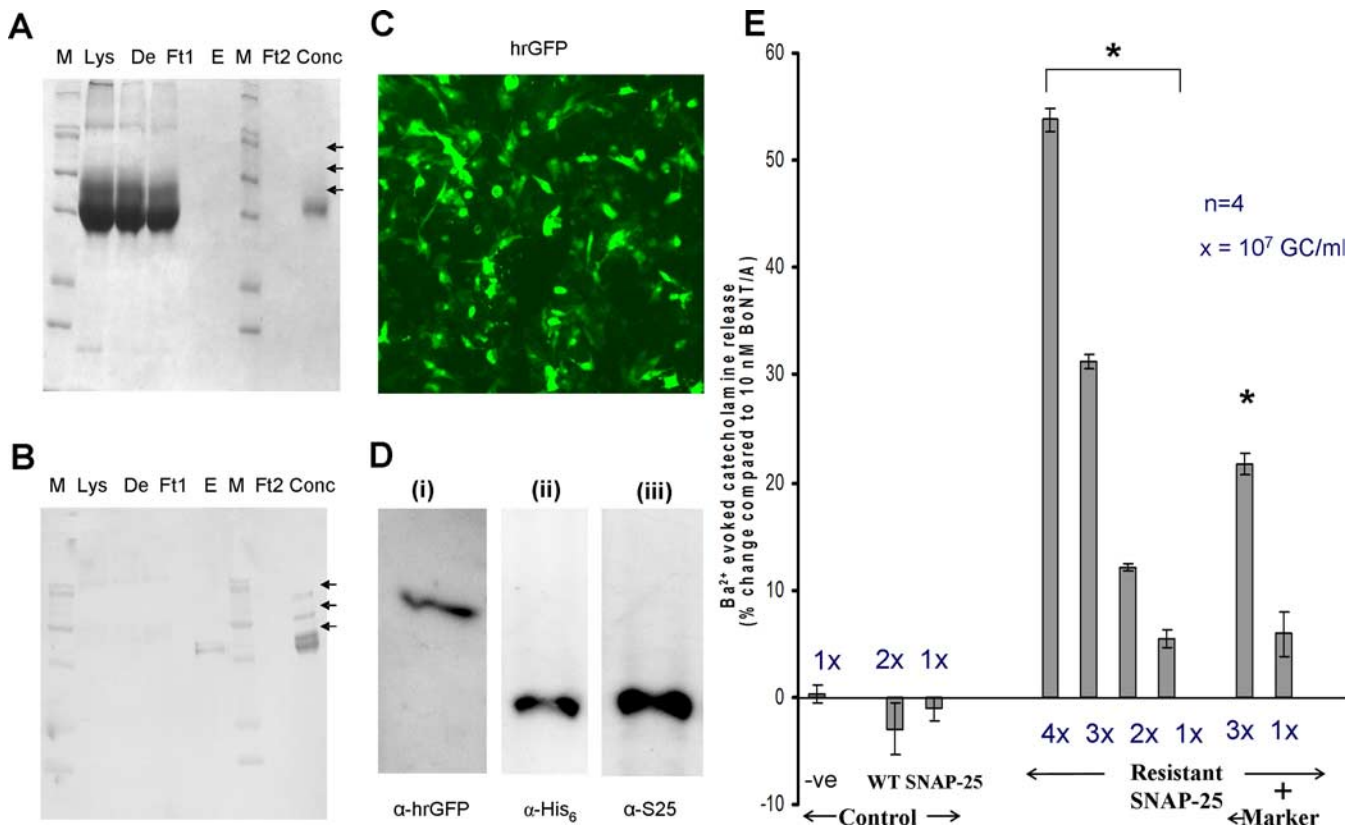
Figure 1. AAV-mediated expression in chromaffin cells of cleavage-resistant S25, but not wild-type, antagonizes inhibition of catecholamine release by BoNT/A. *A, B*, Coomassie-stained gel (*A*) and Western blot (*B*) of aliquots from stages of the production of AAV-hrGFP. M, Markers; Lys, lysate; De, deoxycholate extract; Ft1, flow-through from heparin-agarose column; E, eluate; Ft2, flow-through from concentrator; Conc, concentrated AAV-hrGFP. Arrows show surface proteins VP1, VP2, and VP3 with $M_r = 87,000, 73,000$, and $62,000$, respectively. *C*, Fluorescent microscopy demonstrated extensive infection by AAVs. *D*, Western blotting confirmed coexpression of hrGFP and His$_6$-S25-R198T. *E*, Chromaffin cells were infected with AAVs (10^7 GCs per well or multiples expressing His$_6$-S25WT, His$_6$-S25-R198T, or His$_6$-S25-R198T plus hrGFP) or vehicle and 7 d later exposed to 10 nM BoNT for 24 h before quantifying Ba^{2+}-evoked catecholamine release. Averaged relative release from virus-treated and control cells ± SD is plotted ($n = 4$). Cells expressing cleavage-resistant S25 showed a significant increase in catecholamine release (*$p < 0.01$, as determined by a *t* test) compared with controls.

horns, containing the cell bodies of neurons supplying the soleus, resulted in a localized coexpression of hrGFP and His$_6$-S25-R198T, confirming the accuracy of the microsurgical procedure (Fig. 2*A*). After 6–7 weeks, the expressed proteins were also seen in the periphery at NMJs, identified by colocalization with α-BuTx (hrGFP and α-BuTx in Fig. 2*B* and His$_6$-S25-R198T and α-BuTx in Fig. 2*C*). The functional effectiveness of this cleavage-resistant S25 was established by bilateral injection of ∼1 mouse LD$_{50}$ of BoNT/A in NS/BSA into the soleus 21 d after viral injection, followed by ENT measurements after a further 16 d. The expected reduction in transmitter release after injecting BoNT/A alone was confirmed, whereas the maintenance of near-normal neurotransmission in synaptic junctions overexpressing hrGFP or S25-R198T demonstrates purity of the preparations and the minimal trauma caused by the stereotaxic technique (Fig. 2*Di,Dii*). Animals preinjected with AAV-His$_6$ S25-R198T showed a significantly greater retention of neuromuscular transmission (Fig. 2*Div*) compared with the unprotected (contralateral) side after a BoNT/A challenge (Fig. 2*Diii*) ($p < 0.05$); summarized data from four animals for each group are depicted in Figure 2*E*. This attenuation of BoNT/A-induced neuroparalysis is the first ever demonstration of a nonimmunological protective therapy in whole animals and establishes the functional effectiveness of the peripherally delivered cleavage-resistant S25.

BoNT/A-induced synapse remodeling is reduced by protection of neuromuscular transmission with a spinal injection of AAV-His$_6$-S25-R198T

Sections of soleal muscles from BoNT/A-treated and control rats were stained with α-BuTx-A488 and the anti-NF200 antibody to visualize the postsynaptic and presynaptic parts of the NMJ, respectively. Comparison of images from control and those treated 16 or 25 d earlier with BoNT/A revealed a much greater number of sprouts in the latter (Fig. 3, compare *A* with *B–F*). Additionally, in agreement with published results (Brown et al., 1980), it was observed that axonal and endplate sprouting frequently coexisted in the same muscle and, sometimes, in the same endplate (Fig. 3*F*). After characterizing BoNT/A-induced sprouting, the effect of protection on this process was determined. Immunostaining of soleal sections treated with toxin for 16 d showed less extensive sprouting at NMJs of rats that received BoNT/A-resistant S25 than those given toxin alone (Fig. 3*G,H*). To quantify these changes, the amount of sprouting in "protected (by AAV-His$_6$-S25-R198T) and challenged (by BoNT/A)" muscles were compared with "unprotected and challenged" or "unprotected and unchallenged" muscles. Because changes in ACh receptor density and distribution are highly sensitive to perturbations of synaptic transmission, an automated quantitation of α-BuTx–fluorophore conjugate binding to the postsynaptic part of the NMJ was chosen (Pestronk and Drachman, 1978; Wang et
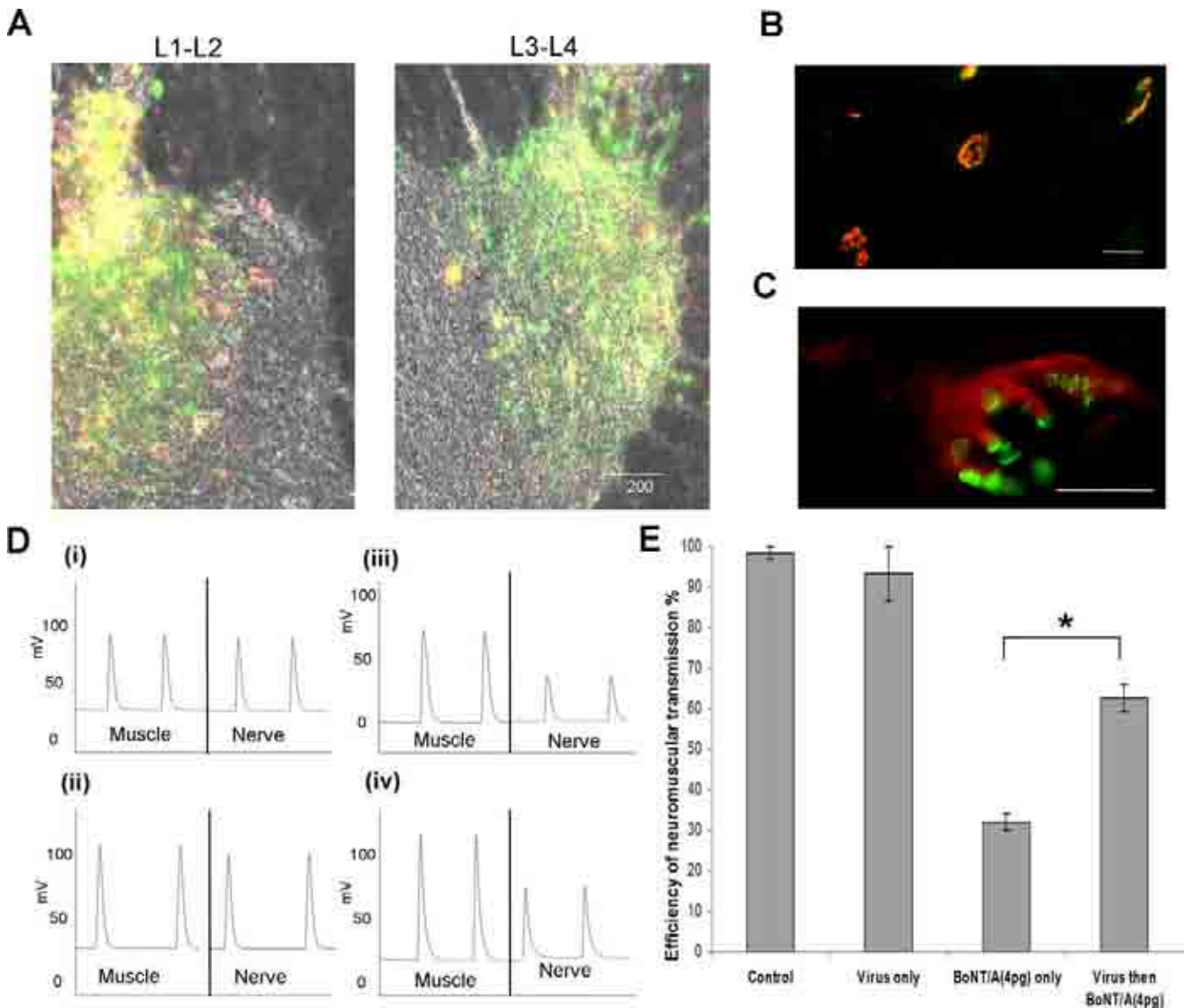
Figure 2. Treatment with AAV-His$_6$-S25-R198T protects against neuromuscular paralysis induced by BoNT/A. **A**, Spinal cord sections from rats injected with AAVs (5 μl of 10^{11} GC/ml) expressing hrGFP (green) and His$_6$-S25-R198T (red) show colocalization in the right L1/L2 and L3/L4 anterior horns. Scale bar, 200 μm. **B**, **C**, Delivery of hrGFP (green; **B**) and His$_6$-S25-R198T (red; **C**) to presynaptic terminals demonstrated by colocalization with the postsynaptic ACh receptor (α-BuTx, red in **B**, green in **C**), in soleal sections from rats injected with AAV-hrGFP (**B**) or AAV-His$_6$-S25-R198T (**C**). Scale bars, 20 μm. **D**, Effect on ENT of spinal injection of AAV-hrGFP (**i**) and AAV-His$_6$-S25-R198T (**ii, iv**) or vehicle (**iii**) into animals, some of which were challenged with BoNT/A 21 d later (**iii, iv**). Representative contractions after a further 16 d from single supramaximal stimulation of the sciatic nerve (right) and direct stimulation of the muscle (left) are shown. **E**, Summarized data showing that viral pretreatment protects ENT from subsequent paralysis by BoNT/A; each bar represents the mean $\pm$ SD of values from four animals (*$p < 0.05$).

al., 2005). Relative to untreated muscles, significant increases were found after BoNT/A treatment in the mean endplate area, the area of the largest endplates and, probably because of the muscle wasting that accompanies paralysis, the endplate space occupied per muscle section (Fig. 3I). However, interestingly, the average endplate area was significantly reduced in those endplates expressing S25 R198T compared with controls [treated with the toxin alone (Fig. 3J)]. A lesser, nonsignificant reduction was seen in the maximum endplate and in the ratio of endplate to muscle areas (Fig. 3J).

Partial protection against BoNT/A-induced neuroparalysis in rats by neuronal expression of His$_6$-S25-R198T after peripheral injection of its AAV construct

Although intraspinal AAV injection achieved efficient transduction and protection of motor neurons against BoNT/A, a periph-

erally deliverable therapy is still preferable. The control AAV-hrGFP virus underwent retrograde transport to the spinal cord, as confirmed by expression of the marker protein in motor neurons of the anterior horn supplying the soleus muscle (Fig. 4A). Having confirmed the utility of such an approach, the ability of AAV-His$_6$-S25-R198T to protect the motor neurons from BoNT/A-mediated paralysis was next evaluated by its injection into the soleus muscle, followed a week later by toxin administration; the contralateral muscle was injected with the toxin alone. When tested 3 weeks after the viral injection, the protected NMJs in the best responding animals showed a fourfold to sixfold higher retention of synaptic transmission [18.5 vs 3.2% for single stimulation (Fig. 4Bi) and 62.5 vs 15.3% for tetanic stimulation (Fig. 4Bii)]. The combined results, from six animals for each treatment, showed that the side injected with the virus gave a >2.5-fold increased retention of muscle strength in response to tetanic
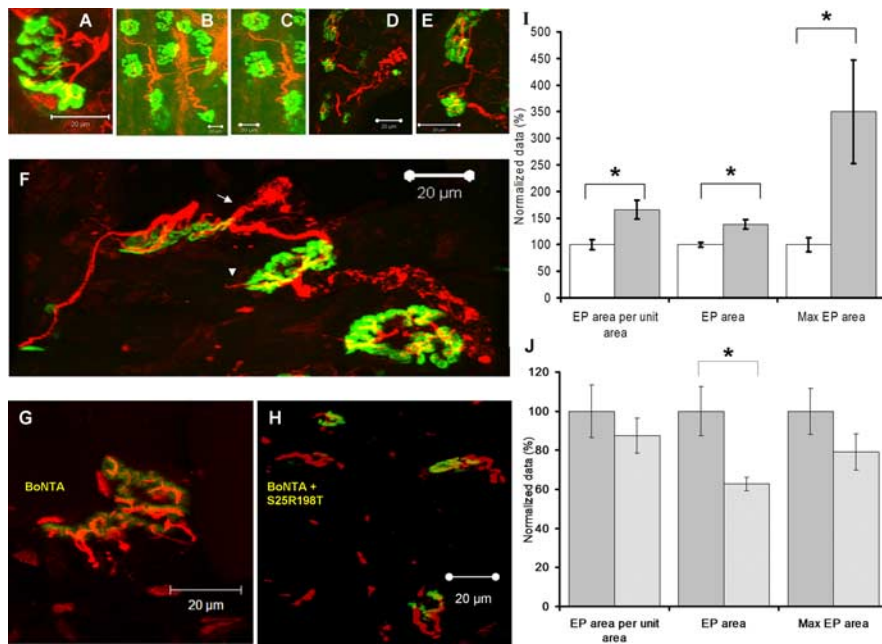
Figure 3. Influence of virally expressed His$_6$-S25-R198T on synaptic remodeling in rat soleus muscles induced by BoNT/A. **A–F,** Immunofluorescent images from control (**A**) and muscles injected with ∼2 LD$_{50}$ units of BoNT/A (**B–F**) showing axonal sprouting (**B**, magnified in **C**), terminal sprouting (**D**, magnified in **E**), and mixed sprouting [**F**; axonal sprouting (arrow) and terminal sprouting (arrowhead)]. Scale bars, 20 μm. α-NF200 is shown in red with α-BuTx-A488 in green. **G, H,** The effect of having administered AAV-His$_6$-S25-R198T 21 d before BoNT/A injection (**H**) compared with the muscle given the toxin only (**G**). **I, J,** An automated quantitation of sprouting determined the various parameters plotted (as average ± SEM) in **I** for muscle treated with BoNT/A (shaded) or vehicle (open) and in **J** those receiving BoNT/A alone (shaded) or BoNT/A plus AAV-His$_6$-S25-R198T (hatched) (*$p \leq 0.005$ by unpaired t test).

stimulation (27.5 vs 10.5%) (Fig. 4B). These investigations provide an encouraging demonstration of the potential of minimally invasive paths to a gene therapy for botulism.

Discussion

To prevent the prolonged convalescence associated with human botulism caused by BoNT/A, a clinically effective therapy needs to act at multiple stages by antagonizing the toxin's binding or uptake, inhibiting its breakdown of S25, and/or hastening recovery by replenishing truncated S25 with a functional, BoNT-resistant form (O'Sullivan et al., 1999). Although progress toward the first two goals is being achieved by pharmacological means using inhibitors of the toxin's protease, a novel gene therapy approach is necessary to attain the final stages, especially in light of the extraordinary persistence of BoNT/A protease at nerve terminals (Keller et al., 1999; Foran et al., 2003; Meunier et al., 2003). The applicability of gene therapy was initially revealed by demonstrating the attenuation of this toxin's inhibition of secretion from chromaffin cells after overexpression of a cleavage-resistant S25 (O'Sullivan et al., 1999). Because the classical gene transfection used in that earlier study gave very low efficiency, much more effective gene delivery is a prerequisite for *in vivo* therapeutic purposes. To this end, the gene encoding S25-R198T was inserted into an AAV vector yielding a highly efficient, nonpathogenic virus for transferring genes into nondividing neurons.

Initial experiments confirmed that overexpression of a His$_6$-tagged cleavage-resistant S25 in eukaryotic cells does not overwhelm the posttranslational processes, especially palmitoylation, as revealed by the membrane association of this protein (see supplemental results, available at www.jneurosci.org as supplemental material). This is important in light of the failure of free cytoplasmic S25 to take part in productive exocytosis (Washbourne et

al., 2001) and because of the necessity for toxin-resistant S25 to antagonize disabled S25 at the membrane (O'Sullivan et al., 1999). The administered viruses infected 90% of ∼10^6 chromaffin cells and produced enough BoNT/A-resistant S25 to overcome the toxin's inhibitory effects.

Although the *in vitro* results validated this therapeutic strategy, it was necessary to establish its applicability to the more complex *in vivo* system. BoNT/A-induced paralysis can be measured by decrease in force of contraction evoked by stimulation of the sciatic nerve in rat limb muscles (Adler et al., 2001). The synaptic remodeling of rat soleal NMJs after neuroparalysis (Pestronk and Drachman, 1978; Brown et al., 1980) was another reason for choosing this muscle. Direct injection into the spinal anterior horn was used initially because it gives a more intense infection of motor neurons and, consequently, recombinant protein production than intrathecal administration (Mannes et al., 1998). Intraspinal injection of cleavage-resistant S25-expressing AAVs resulted in a localized expression of this protein in the lumbar anterior horns and, subsequently, peripheral transport to their synaptic terminals (Fig. 2). Significantly, the expressed and peripherally transported transgenic protein successfully substituted for native cleavage-susceptible S25, as demonstrated by enhanced retention of nerve-stimulated muscle contractility in preprotected animals later challenged with BoNT/A (Fig. 2), detected by single supramaximal stimuli or tetanic pulses with protection being more marked with the latter. Only AAVs expressing His$_6$-S25-R198T, and not those that produce hrGFP or wild-type His$_6$-S25, proved effective. This is the first report on successful antagonism of BoNT/A action in live animals using viral-mediated gene delivery. The protection seen demonstrates that the recombinantly produced protein cannot only overcome the persistent protease activity of the toxin at motor neuron terminals, but also any probable inhibition by the truncated native S25 (Dolly and Aoki, 2006). A combination of such gene delivery with effective inhibitors of the protease should help provide both immediate and prolonged therapy.

Published data suggested that AAVs undergo successful retrograde transport from mouse NMJs and can efficiently infect the supplying motor neurons, with ∼1 in 1000 reaching the cell body (Kaspar et al., 2003). Although injection of >5 × 10^{11} AAVs into soleal muscle proved necessary to detect infected motor neurons, this mode of administration offers advantages of minimal trauma and faster recovery from the operating procedure; most notably, in terms of possible clinical application, it allows easier access to important muscles. The potential of peripheral application is reflected by the promising protection obtained.

It is believed that synaptic remodeling after BoNT/A-induced paralysis plays an important role in the early recovery (de Paiva et al., 1999; Meunier et al., 2003). The quantity of sprouts is thought to depend strongly on the amount of toxin, the kind of muscle [fast muscles have lower amounts of mostly axonal sprouting, compared with slow muscles, which show a higher percentage of
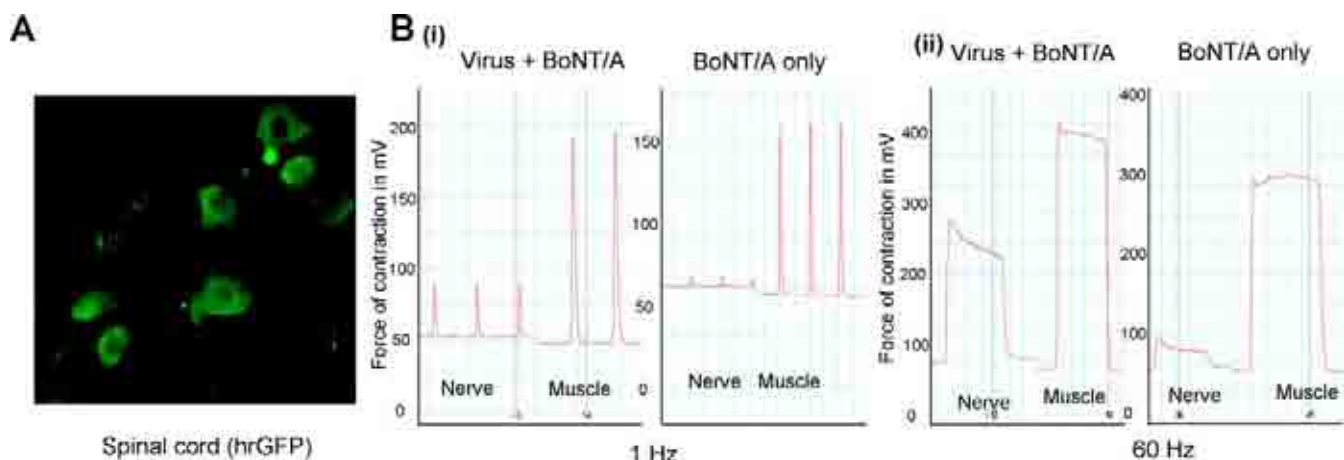
Figure 4. Peripheral administration of therapeutic AAVs results in their retrograde transport and partial protection against subsequently administered BoNT/A. **A**, Fluorescent microscopic detection of hrGFP in rat spinal lumbar motor neurons after peripheral administration of AAV-hrGFP. **B**, Rats were injected three times with 50 μl of 10^{11} GCs/ml AAV-His$_6$-S25-R198T into the right soleus muscle; after 7 d, $\sim2 \times$ LD$_{50}$ of BoNT/A was injected bilaterally. Single (**i**) and tetanic (**ii**) stimulation from best-responding rats show the improvement resulting from viral preinjection.

terminal sprouts (Pestronk and Drachman, 1978; Brown et al., 1980)], and the duration of paralysis (Meunier et al., 2003). The data herein revealed a reduction in synaptic remodeling when paralysis is limited by overexpression of cleavage-resistant S25 in nerve endings, substantiating the hypothesis that the extent of neurotransmission blockade, along with the duration, are strong determinants of synapse remodeling. The changes in sprouting seen after treatment with the same dose of BoNT/A toxin in the presence or absence of viral protection seem to confirm that the differential effects on sprouting seen previously with the different toxin serotypes are a property of the duration of paralysis and not of the substrate cleaved.

This study attained an important milestone in devising a peripherally deliverable gene therapy that can counteract the prolonged paralysis by BoNT serotypes. The proof of principle obtained provides an encouraging foundation on which to build more versatile vectors based on lentiviruses that could allow the simultaneous transfection of neurons with multiple-toxin-resistant S25, VAMP-2, and syntaxin for combating several serotypes and even novel chimera. Furthermore, botulinization solves problems associated with using murine models of human motor neuron diseases. The ability to control the extent/severity of "disease" combined with the availability of a sensitive assay for measuring peripheral neurotransmission and knowledge of the gene required to protect against the toxin's effects, ought to allow meaningful assessment of successful delivery. Such elimination of these multiple variables should enable a more focused and successful optimization of a peripherally administered viral vector that can target therapeutic genes into motor neurons.

References

Adler M, Keller JE, Sheridan RE, Deshpande SS (2001) Persistence of botulinum neurotoxin A demonstrated by sequential administration of serotypes A and E in rat EDL muscle. Toxicon 39:233–243.

Blasi J, Binz T, Yamasaki S, Link E, Niemann H, Jahn R (1994) Inhibition of neurotransmitter release by clostridial neurotoxins correlates with specific proteolysis of synaptosomal proteins. J Physiol (Paris) 88:235–241.

Brown MC, Holland RL, Ironton R (1980) Nodal and terminal sprouting from motor nerves in fast and slow muscles of the mouse. J Physiol (Lond) 306:493–510.

Bruijn LI, Miller TM, Cleveland DW (2004) Unraveling the mechanisms involved in motor neuron degeneration in ALS. Annu Rev Neurosci 27:723–749.

Burger C, Nash K, Mandel RJ (2005) Recombinant adeno-associated viral vectors in the nervous system. Hum Gene Ther 16:781–791.

de Paiva A, Meunier FA, Molgo J, Aoki KR, Dolly JO (1999) Functional repair of motor endplates after botulinum neurotoxin type A poisoning: biphasic switch of synaptic activity between nerve sprouts and their parent terminals. Proc Natl Acad Sci USA 96:3200–3205.

Dolly JO, Aoki KR (2006) The structure and mode of action of different botulinum toxins. Eur J Neurol 13 [Suppl 4]:1–9.

Foran PG, Mohammed N, Lisk GO, Nagwaney S, Lawrence GW, Johnson E, Smith L, Aoki KR, Dolly JO (2003) Evaluation of the therapeutic usefulness of botulinum neurotoxin B, C1, E, and F compared with the long lasting type A. Basis for distinct durations of inhibition of exocytosis in central neurons. J Biol Chem 278:1363–1371.

Kaspar BK, Llado J, Sherkat N, Rothstein JD, Gage FH (2003) Retrograde viral delivery of IGF-1 prolongs survival in a mouse ALS model. Science 301:839–842.

Keller JE, Neale EA, Oyler G, Adler M (1999) Persistence of botulinum neurotoxin action in cultured spinal cord cells. FEBS Lett 456:137–142.

Lawrence GW, Foran P, Dolly JO (1996) Distinct exocytotic responses of intact and permeabilised chromaffin cells after cleavage of the 25-kDa synaptosomal-associated protein (SNAP-25) or synaptobrevin by botulinum toxin A or B. Eur J Biochem 236:877–886.

Mannes AJ, Caudle RM, O'Connell BC, Iadarola MJ (1998) Adenoviral gene transfer to spinal-cord neurons: intrathecal vs. intraparenchymal administration. Brain Res 793:1–6.

Meunier FA, Lisk G, Sesardic D, Dolly JO (2003) Dynamics of motor nerve terminal remodeling unveiled using SNARE-cleaving botulinum toxins: the extent and duration are dictated by the sites of SNAP-25 truncation. Mol Cell Neurosci 22:454–466.

Nicolopoulos-Stournaras S, Iles JF (1983) Motor neuron columns in the lumbar spinal cord of the rat. J Comp Neurol 217:75–85.

O'Sullivan GA, Mohammed N, Foran PG, Lawrence GW, Oliver Dolly J (1999) Rescue of exocytosis in botulinum toxin A-poisoned chromaffin cells by expression of cleavage-resistant SNAP-25. Identification of the minimal essential C-terminal residues. J Biol Chem 274:36897–36904.

Pestronk A, Drachman DB (1978) Motor nerve sprouting and acetylcholine receptors. Science 199:1223–1225.

Wang P, Yang G, Mosier DR, Chang P, Zaidi T, Gong YD, Zhao NM, Dominguez B, Lee KF, Gan WB, Zheng H (2005) Defective neuromuscular synapses in mice lacking amyloid precursor protein (APP) and APP-like protein 2. J Neurosci 25:1219–1225.

Washbourne P, Cansino V, Mathews JR, Graham M, Burgoyne RD, Wilson MC (2001) Cysteine residues of SNAP-25 are required for SNARE disassembly and exocytosis, but not for membrane targeting. Biochem J 357:625–634.

Zolotukhin S, Byrne BJ, Mason E, Zolotukhin I, Potter M, Chesnut K, Summerford C, Samulski RJ, Muzyczka N (1999) Recombinant adeno-associated virus purification using novel methods improves infectious titer and yield. Gene Ther 6:973–985.